

AGARD

ADVISORY GROUP FOR AEROSPACE RESEARCH & DEVELOPMENT
7 RUE ANCELLE, 92200 NEUILLY-SUR-SEINE, FRANCE

AGARD CONFERENCE PROCEEDINGS 568

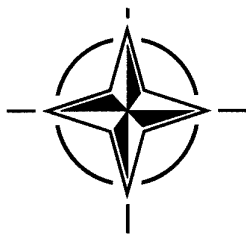
Widespread Fatigue Damage in Military Aircraft

(L'endommagement en fatigue des avions militaires)

Papers presented at the 80th Meeting of the AGARD Structures and Materials Panel, held in Rotterdam, The Netherlands, 10-11 May 1995.

19960202 028

DISTRIBUTION STATEMENT A
Approved for public release
Distribution Unlimited



NORTH ATLANTIC TREATY ORGANIZATION

1995 OCTOBER 1995

AGARD

ADVISORY GROUP FOR AEROSPACE RESEARCH & DEVELOPMENT

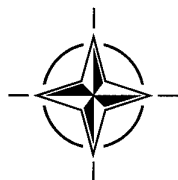
7 RUE ANCELLE, 92200 NEUILLY-SUR-SEINE, FRANCE

AGARD CONFERENCE PROCEEDINGS 568

Widespread Fatigue Damage in Military Aircraft

(L'endommagement en fatigue des avions militaires)

Papers presented at the 80th Meeting of the AGARD Structures and Materials Panel, held in Rotterdam, The Netherlands, 10-11 May 1995.



North Atlantic Treaty Organization
Organisation du Traité de l'Atlantique Nord

The Mission of AGARD

According to its Charter, the mission of AGARD is to bring together the leading personalities of the NATO nations in the fields of science and technology relating to aerospace for the following purposes:

- Recommending effective ways for the member nations to use their research and development capabilities for the common benefit of the NATO community;
- Providing scientific and technical advice and assistance to the Military Committee in the field of aerospace research and development (with particular regard to its military application);
- Continuously stimulating advances in the aerospace sciences relevant to strengthening the common defence posture;
- Improving the co-operation among member nations in aerospace research and development;
- Exchange of scientific and technical information;
- Providing assistance to member nations for the purpose of increasing their scientific and technical potential;
- Rendering scientific and technical assistance, as requested, to other NATO bodies and to member nations in connection with research and development problems in the aerospace field.

The highest authority within AGARD is the National Delegates Board consisting of officially appointed senior representatives from each member nation. The mission of AGARD is carried out through the Panels which are composed of experts appointed by the National Delegates, the Consultant and Exchange Programme and the Aerospace Applications Studies Programme. The results of AGARD work are reported to the member nations and the NATO Authorities through the AGARD series of publications of which this is one.

Participation in AGARD activities is by invitation only and is normally limited to citizens of the NATO nations.

The content of this publication has been reproduced directly from material supplied by AGARD or the authors.

Published December 1995

Copyright © AGARD 1995
All Rights Reserved

ISBN 92-836-1021-0



Printed by Canada Communication Group
45 Sacré-Cœur Blvd., Hull (Québec), Canada K1A 0S7

Widespread Fatigue Damage in Military Aircraft

(AGARD CP-568)

Executive Summary

A structure potentially susceptible to Widespread Fatigue Damage (WFD) is defined by the Industry Committee on Widespread Fatigue Damage, as a structure which has the characteristics of similar features operating at similar stresses where structural capability could be affected by similar cracking.

The well-publicised 1988 incident of the Aloha Airlines Boeing 737, which lost a large section of fuselage structure in flight, ushered in the era of research into ageing aircraft. This incident was caused by a collinear series of fatigue cracks which suddenly linked to form a single critical crack, leading to the catastrophic failure. At the time of the Aloha incident, a large number of relatively high-life military aircraft were in service, mainly in the roles of air transport, air-to-air refuelling and maritime reconnaissance.

Maintaining the structural integrity of these aircraft in prolonged service requires consideration to be given to inspections for detecting possible multiple damage in its various forms:

“Multi-site” damage (MSD) occurs mainly on neighbouring elements (lines of attachment holes, for example) or as a result of a fabrication surface damage (a long, continuous, scratch, for example). Their coalescence can lead to a sudden loss of residual strength.

The concept of “resistance to damage” implies structures which are able to tolerate the presence of cracked elements by ensuring that cracks are slowly propagated and to tolerate the presence of broken elements by providing load path redundancy. On this basis, the strength of the remaining undamaged structure must be sufficient to ensure safety in flight during a specified operating period.

The role of Damage Tolerance is to assure structural integrity through in-service directed inspections of critical structures. The aircraft should be designed not to crack within one lifetime but may still crack due to damage caused during manufacture or during service.

To operate safely, the structural components must be subjected to an in-service inspection program that will ensure the detection of a crack before it reaches the critical size (the size at which it will not support the in-service limit loads). Detection requirements in-use are extremely difficult to satisfy.

Full-scale fatigue testing until a lifetime which is a multiple of the target life would be an obvious solution. The frequently suggested twice the target life should be regarded as a bare minimum. Full-scale fatigue testing of new aircraft fuselages does not cover, however, the deterioration of fatigue strength of lap joints due to corrosion effects.

Recommendations for the further development of models to compare theoretical predictions with test data on a range of laboratory specimens (representative of pressurized fuselage structures) have been formulated by the Meeting participants.

Contents

	Page
Executive Summary	iii
Preface	vii
Préface	viii
Structures and Materials Panels	ix
Technical Evaluation Report by R. SUNDER	T
	Reference
SESSION I: TECHNICAL ISSUES AND METHODS	
Overview of Widespread Fatigue Damage: Risk Assessment Methodology by J.W. LINCOLN	1
A Special Uniaxial Coupon Test Specimen for the Simulation of Multiple Site Fatigue Crack Growth and Link-up in Fuselage Skin Splices by G.F. EASTAUGH, D.L. SIMPSON, P.V. STRAZNICKY and R.B. WAKEMAN	2
Fracture Analysis of Stiffened Panels Under Biaxial Loading with Widespread Cracking by J.C. NEWMAN, Jr. and D.S. DAWICKE	3
Widespread Fatigue Damage and Single Member Failure Prediction of Military Jet Trainers of Czech Design and Production by J. FIDRANSKY and J. FIALA	4
Analysis of Aircraft Panels with WFD, Based on the Elastic Plastic Finite Element Alternating Method (EPFEAM) and $T^*\epsilon$ Integral by C.R. PYO, H. OKADA and S.N. ATLURI	5
SESSION II: ANALYSIS AND RISK ASSESSMENT	
A Concept for the Evaluation of MSD Based on Probabilistic Assumptions by P. HORST and H.J. SCHMIDT	6
Statistical Property of Widespread Fatigue Damage by M. SHINOZUKA, G. DEODATIS, S.G. SAMPATH and H. ASADA	7
Risk Analysis in the Presence of Corrosion Damage by A.P. BERENS and J.G. BURNS	8
Risk Assessment of an Aging Military Trainer Aircraft by J.W. LINCOLN	9
Destructive Teardown of a C-141 Lower Inner Wing Surface by J.B. COCHRAN, R.P. BELL, G.M. WEITZ and R.E. ALFORD	10

SESSION III: DESIGN METHODOLOGIES AND EXPERIENCES

Multiple Site Fatigue Damages of Aircraft Structures by G.I. NESTERENKO	11
Avoiding WFD — A Guide to the Fatigue Design Regulations for British Military Aircraft by A. CARDRICK	12
Living with Wide Spread Fatigue Damage by R. JONES, E.S. WILSON and S. HAMMOND	13
Damage Tolerance to WFD on Combat Aircraft an Application to a Metallic Wing Lower Panel by R.J. CAZES and F. GOERUNG	14
Fatigue Damages During Tornado MAF Test by W. BRÖCKER and M. BUDERATH	15
Damage Tolerance Evaluation on the A7-P Aircraft Considering the PoAF Usage by M. de FREITAS, A. FONSECA, H. GONÇALO and C. PIRES	16
Widespread Fatigue Damage in Combat Aircraft by H. ANSELL and T. JOHANSSON	17
The Effect of Proof Pressure Testing on the Retardation of Multi-site Damage by E. BITTEL	18
Paper 19 WITHDRAWN	

Preface

Several NATO member countries have been experiencing aging aircraft related problems in their military fleets, particularly among their military transport aircraft. The most troubling aging aircraft structure-related issue is widespread fatigue damage, sometimes termed as multiple site damage, whose onset due to fatigue causes a dramatic structural strength reduction.

WFD is characterized by small cracks emanating from similar, contiguous structural details which are subjected to near-uniform stress cycling—a direct result of improved understanding of loads and optimum utilization of material by the aircraft designer, but also due to either manufacturing induced anomalies or continued operation beyond the original intended lifetime. Due to the difficulty in detecting WFD, an inspection-based maintenance program is usually not an option for preservation of the ability of the structure to additionally sustain credible battle damage and damage due to other sources.

WFD has been found in several high time military aircraft. Moreover, as the several planned life extension programs are implemented in the NATO fleets, it is probable that several more aircraft models will experience WFD at some point in time. Invariably, when WFD occurs, the affected model in the fleet is subjected to an extensive modification program which is almost always expensive and time-consuming.

The motivation for a Specialist Meeting on the subject is tied to the need for a methodology to quantitatively predict structural degradation on account of WFD as a function of usage, and when WFD is likely to occur. If the need is met, the NATO member nations will be able to make tactical adjustments to the schedule of fatigue consumption for each aircraft, and, thus, avoid impairment of fleet readiness.

The subject has held a fascination for me since my involvement in the Federal Aviation Administration's (FAA) Aging Aircraft Research Program. Even after the intervening years, I cannot improve on the fatherly advice that the FAA's Technical Oversight Group on Aging Aircraft have for a young aircraft designer who should worry about WFD: verify the design loads, keep the stresses low, pay attention to manufacturing quality, and build-in a Maginot Line (fail-safe design) that will not be overwhelmed or outflanked.

I thank all the authors and those that attended the Meeting. It made for interesting presentations, punctuated by stimulating discussions. Thanks are also offered to the four session chairpersons: my colleague in the FAA, Mr. Thomas Swift, Professor J. Schijve of Delft University, Dr. John Bristow of the Civil Aviation Authority in the U.K., and Dr. Jan Achenbach of Northwestern University. Particular thanks go to Dr. R. Sunder who acted as the rapporteur and to Dr. Wolf Elber, whose idea it was to convene the meeting.

S.G. Sampath, Chairman
SMP Sub-Committee —
Widespread Fatigue Damage

Préface

Aujourd'hui, différents pays membres de l'OTAN font état de problèmes relatifs au vieillissement des aéronefs faisant partie de leurs flottes militaires, et en particulier des avions de transport militaires. Le phénomène le plus inquiétant dans ce domaine est l'endommagement en fatigue généralisé (WFD), appelé parfois l'endommagement multi-foyers, dont l'apparition, due à la fatigue, entraîne une diminution spectaculaire de la résistance structurale.

L'endommagement en fatigue généralisé est caractérisé par des petites fissures émanant d'éléments structuraux contigus similaires, qui sont soumis à une alternation répétitive de contraintes quasi-uniformes, qui est le résultat direct d'une meilleure compréhension des charges et de l'utilisation optimale des matériaux par les concepteurs d'aéronefs, mais qui est dû soit aux anomalies introduites lors de la fabrication, soit à l'exploitation de l'aéronef au-delà de la durée de vie préconisée. Vu les problèmes posés dans la plupart des cas par la détection du WFD, un programme de maintenance basé sur des inspections ne représente pas une solution acceptable et apte à garantir l'intégrité de la structure résultant aux dommages infligés sur le champ de bataille ou par d'autres sources.

Des cas d'endommagement en fatigue généralisé ont été constatés sur un certain nombre d'avions militaires ayant comptabilisés beaucoup d'heures de vol. En outre, au fur et à mesure de la mise en œuvre des différents programmes d'extension de vie des flottes de l'OTAN, il est probable que d'autres catégories d'aéronef manifestent aussi des signes de WFD à un moment donné. Invariablement, lors de l'apparition du WFD, l'appareil atteint fait l'objet d'un programme de modifications très complet, qui s'avère, dans la plupart des cas, long et coûteux.

L'incitation pour organiser une réunion de spécialistes sur ce sujet est directement liée à la nécessité d'une méthodologie permettant la prévision quantitative de la dégradation structurale due au WFD en fonction de l'utilisation de l'aéronef, et du moment le plus probable où apparaîtra le début du WFD. Si ce besoin est satisfait, les pays membres de l'OTAN pourront opérer les ajustements tactiques au niveau du planning de l'attrition par l'usure de chaque avion, évitant ainsi toute perturbation de la disponibilité opérationnelle de la flotte.

Il s'agit d'un sujet qui me fascine depuis l'époque où je participais au programme de recherche de l'administration fédérale d'aviation (FAA) sur le vieillissement des aéronefs. Même aujourd'hui, malgré toutes les années qui me séparent de ce projet, je me rappelle très bien des conseils paternels qu'avait le groupe de veille technique de la FAA pour un jeune concepteur d'aéronefs, censé s'occuper des problèmes WFD : vérifier les charges de calcul, réduire au minimum les contraintes, faire attention à la qualité de la fabrication et incorporer une «ligne Maginot» (conception à sûreté intégrale), qui ne pourra être ni franchie ni contournée (sic).

Je tiens à remercier tous les auteurs et tous les participants à la réunion. Les présentations étaient intéressantes et les discussions stimulantes. Je remercie également les quatre présidents de session : mon collègue du FAA, M. Thomas SWIFT, le Professeur J. SCHIJVE de l'Université de Delft, le Dr John BRISTOW de la Direction générale de l'aviation civile au Royaume-Uni, et le Dr Jan ACHENBACH de la Northwestern University. Enfin, je tiens à exprimer mes remerciements tout particuliers au Dr R. SUNDER, qui a exercé les fonctions de rapporteur et au Dr Wolf ELBER, qui a eu la bonne idée de convoquer cette assemblée.

Structures and Materials Panel

Chairman: Prof. O. Sensburg
Chief Engineer
DASA
Militaerflugzeuge LM2
Postfach 80 11 60
81663 Munich
Germany

Deputy Chairman: Prof. S. Paipetis
Prof. of Applied Mechanics
School of Engineering
Dept. of Mechanical Engineering
University of Patras
26110 Patras
Germany

SUB-COMMITTEE MEMBERS

Chairman: Dr. S. Sampath
Federal Aviation Administration Technical Center
Atlantic City Inter'n'l Airport
Code ACD-200
Atlantic City, NJ 08405
USA

Members:	T. Akyurek	—	TU	H.H. Ottens	—	NE
	P. Armando	—	FR	G. Papakonstantinou	—	GR
	D. Chaumette	—	FR	C. Perron	—	CA
	M. Curbillon	—	FR	N. Sandsmark	—	NO
	E.E. Gdoutos	—	GR	D.L. Simpson	—	CA
	H. Goncalo	—	PO	E.A. Starke	—	US
	P. Heuler	—	GE	A. Turkdogan	—	TU
	A. Humble	—	UK			
	C. Moura Branco	—	PO			

PANEL EXECUTIVE

Dr. Jose M. CARBALLAL, Spain

Mail from Europe:
AGARD-OTAN
7, rue Ancelle
92200 Neuilly-sur-Seine
France

Mail from US and Canada:
From USA and Canada
AGARD-NATO/SMP
PSC 116
APO AE 09777

Tel: 33 (1) 4738 5790 & 5792
Telefax: 33 (1) 4738 5799
Telex: 610176F

TECHNICAL EVALUATION REPORT

by

R. Sunder
Technical Director, BiSS (P) Ltd
BANGALORE 560 003, India

This report summarises the proceedings of the Specialists' Meeting on "Widespread Fatigue Damage in Military Aircraft" held during the 80th meeting of the AGARD Structures and Materials Panel, Rotterdam, May 10-11, 1995. The objective of the meeting was to ascertain from the research community the methodologies that NATO air fleet commanders can use to predict, and thus avoid, occurrence of widespread fatigue damage (WFD) in ageing aircraft. Eighteen papers were presented during the course of two days. Broadly, the scope of these papers may be classified as follows:

Methodological aspects - Authors from the United States, Australia and Sweden provided accounts of methodologies, including case studies, describing how WFD in specific aircraft types was dealt with. A paper was presented from the United Kingdom on fatigue design regulations that are recommended to avoid WFD in British military aircraft.

Service experience - Two papers from the United States described studies on a trainer and transport aircraft, respectively, whose continued safe and economical operation was based upon tear down inspection and risk assessment.

Full-scale fatigue testing - Papers from the Czech Republic, Russia and Germany addressed the issue of full-scale fatigue testing and consequent structural reinforcement to preclude WFD over the expected or extended service lives.

Research on WFD - Papers from several countries discussed ongoing research, describing both analytical and experimental studies on the deterministic and probabilistic aspects of WFD.

A brief description of individual papers in each category is given below and the report concludes with a discussion on what can be concluded from the proceedings of the meeting.

Dr. J.W. Lincoln, in the opening paper, provided an overview of a probabilistic approach, developed and implemented by the U.S. Air Force, to manage ageing aircraft susceptible to WFD. The methodology equates WFD to loss of damage tolerance capability. Risk assessment proceeds on the premise that continued (uninspected) operation of a structure susceptible to WFD progressively increases the probability of failure due to fatigue crack growth and associated reduction in residual strength. Prior research had indicated that a one in 107 (or less) single flight probability of failure is adequate for long term operations. A major requirement for risk assessment is the development of a data base from tear down inspections and its correlation with operational usage measured from the Individual Airplane Tracking Program

(IATP), implemented on USAF aircraft. Tear down inspections involve the painstaking effort of total disassembly, clean-up and inspection of thousands of fastener holes and other stress raisers to detect and measure damage. However, the process is cost-effective, as indicated by the USAF experience. This methodology evolved over a period of about twenty years from experience with several aircraft types, including the B-52, KC-135, C-5A, C-141B, F-5, T-37 and T-38. The risk assessment methodology discussed by Dr. Lincoln appears to provide an objective assessment of all possible cracking scenarios because it is based on real data from tear down inspections. It has been applied to a number of operational problems of the USAF, including determination of service life potential (retirement for cause), calibration of inspection intervals and for deciding on structural modifications for life extensions without high risk of consequent WFD. Finally, risk assessment provides the proper perspective to management for decision making in the light of substantial expenditures associated with available options along with their implications related to flight safety. The paper by Prof. R. Jones et al provided a stimulating overview of the Australian experience in dealing with WFD in military aircraft. The accent of this paper was on the application of finite element (FEM) stress analysis and repair techniques to fatigue critical structural components. The paper describes case studies including the fairly complex problem of interaction of multiple three dimensional flaws. Graphite and boron epoxy patches and doublers were used in repair. Problems described in the paper include multiple cracks in the Mirage III wing lower skin rivet holes, fuselage frame flange, webbing and outer strap plate, Macchi wing rivet hole cracking, centre plane lower spar boom cracking, fuselage corrosion and stress corrosion in empennage. The composite repair technology was also applied to highly stressed wing pivot fitting on the F-111 fleet that experienced premature failures during proof testing. Based on the experience with several aircraft types including the Mirage III, Macchi, F111C and F/A-18, the Royal Australian Air Force (RAAF) have formulated a policy and methodology that covers design and certification of repairs including the interaction of multiple repairs, consequent inspection intervals and their impact on structural integrity management. The authors stress the significance of robust but accurate techniques for structural integrity assessment that can be used for WFD assessment as well as for design and qualification of the repair procedure. They also emphasise the importance for ASIP qualification of a repair solution, including its damage tolerance in the presence of one or more growing flaws. Dr. H. Ansell and Mr. T. Johansen described the SAAB-Scania experience in developing combat aircraft with consideration of WFD observed during full-scale fatigue tests. The Swedish aircraft industry with a background of 40 years has developed a number of military aircraft. Current structural design philosophy revolves around ASIP compliance. Satisfaction of damage tolerance requirements is verified through FEM analysis in the design stage, followed by full-scale testing including residual strength tests. The analysis covers residual life estimates for critical locations to

determine inspection periods. The paper describes the experience with the wing structure of four aircraft types: 32 Lansen, 35 Draken, SK60 and 37 Viggen. The first two of these were designed for lower stress levels and saw no signs of WFD during testing over the factored design lifetime. The latter models however indicated the possibility of WFD while the larger fastener pitch in the SK60 resulted in a lower probability of WFD. Dr. A.W. Cardrick, in his paper, introduces the United Kingdom approach to avoiding WFD as given in the Fatigue Regulations for British Military Aeroplanes (DefStan00-970). The salient feature of the paper is the introduction of the 'Perceptible Distress' concept, whereby, the design process ensures there is only one fatigue critical component in the structure (all others are suitably stressed to ensure a much larger safe life). This component is then monitored using damage tolerance approach for signs of 'perceptible distress'. It would follow that IATP as described in the USAF ASIP document can be effectively replaced by special instrumentation to track the condition of the single fatigue critical component. Safe life design requirements for other components are described, along with the lifing conditions that would need to be satisfied. The substance of the paper appears to be in conflict with the idea of pre-existing flaws (rogue defects) that forms the basis for ASIP. However, there was little discussion, probably because the author was not present. It is felt that the ingenious concept of perceptible distress may lead to unforeseen situations in service in the event certain loading actions were overlooked in the full-scale fatigue test. Also, the approach may not be adequate for aircraft types that may see considerable stress redistribution due to variation in their mission profile and to structural components whose stressing is affected by conditions other than those that control the stress response of the perceptible distress component.

In a second paper that Dr. John Lincoln presented during the meeting, he examines the adequacy of the USAF damage tolerance inspection criterion for the specific case of an ageing trainer aircraft. The study involved risk assessment on the basis of data generated from tear down inspections of retired wings with tracked service history. Crack size and stress probability distributions along with the inspection performance related probability of detection (POD) function constitute the inputs for risk assessment. Thereby, a probabilistic component is superposed on the deterministic fracture mechanics function relating crack size to service usage. This component is now sensitive to the inspection technique used on specific aircraft, scatter in structural response as well as the intrinsic probabilistic sensitivity of residual strength to continued operation after the n-th inspection. The major conclusion of the study was that inspection frequency established from deterministic conditions while being adequate in early life can become unconservative with ageing because, as the population of cracks grows, the risk of failure to detect a crack that may become critical before the next inspection increases. The conventional damage tolerance method had indicated an inspection period of 430 hours. Based on the

results of the study that was reported however, the inspection interval was corrected to 300 hours to ensure an acceptably low risk of structural failure. Mr. Cochran et al provide a detailed description of a tear down inspection C-141 lower inner wing surface. The effort involved the inspection of some 8000 fastener as well as non-fastener holes. The results of the study formed inputs for risk assessment that lead to the establishment of service life limit, retirement of certain tail numbers deemed to have exhausted safe and economic service life potential and repair schemes for the remaining fraction of the fleet. A remarkable feature of the study was the time involved in the exercise: the tear down inspection was completed within six months, subsequent inspections of the fleet completed in three months and implementation of repair schemes within 12 months of completion of fleet inspection. Thus, the effort found practical application across the fleet within a short span of some 18 months after initiation!

Dr. J. Fidransky and Mr. J. Fiala of Aero Vodochody provided a brief overview of the Czech experience in handling the problem of WFD in military jet trainers. A detailed description is provided on the L39/L59 aircraft which are in operation in several countries, with a cumulative 4.5 million flight hours of service experience. Though no catastrophic in-service structural failures have been reported, a number of problems including WFD in the fuselage - empennage area were encountered during full-scale testing. Mixed success was reported in the application of FEM analysis to WFD, particularly in the case of large built up structure. A fracture mechanics approach and cumulative damage concepts were used to design repair schemes, including composite repair patches for cracked skin areas. The analyses account for both manoeuvre loads as well as acoustic loading in the engine duct area which had caused WFD during prototype flights of the L59. Through full-scale testing under flight-by-flight loading and design retrofits, service life of the L39/L59 aircraft was extended from the initial 3,000 hours in the 70s to 15,000 hours. The authors noted the application of ASIP concepts in the design and certification of structural modifications and also the implementation of IATP for tracking service usage. Prof. G.I. Nesterenko described the experience with WFD on the Soviet AN-10A passenger transport. This aircraft type was prematurely withdrawn from service after catastrophic failures in the early seventies traced to WFD in the wing centerplane area not subject to routine inspection. Uniform distribution of high local stresses was responsible for the almost simultaneous initiation of multiple fatigue cracks leading to catastrophic failure of the centerplane. The aircraft was designed according safe-life principles but the full-scale test did not accurately simulate service loading. A research effort was launched to study fatigue and fracture of structural subassemblies and full-scale structure using aircraft withdrawn from service. The author concludes that conservative analyses using a mix of safe-life and fail-safe design concepts combined with experimental evaluation of damage tolerance is essential for reliable assessment of residual

strength in the presence of WFD. Drs. W. Broecker and M. Buderath described observation of WFD on engine inlet duct panels during the Tornado full-scale fatigue testing. These were caused by simulated service loading (manoeuvre spectrum) applied in the test. Analysis of the problem did not reveal the possibility of WFD, thus indicating that testing is needed to evaluate the significance of WFD. Dr. Broecker clarified that WFD in the inlet duct was not due to acoustic loading and indeed no such failures have been reported from service.

Of the nine papers which appear to fall in the category of research, four describe experimental efforts, while five address analytical techniques to handle the deterministic and probabilistic aspects of WFD. Mr. G.F. Eastaugh et al describe the development of a laboratory test coupon to simulate MSD development and linkup in fuselage skin splices similar to those on narrow body jet transports. Though the coupon does not totally simulate the biaxial stress state and out of plane bending effects (pillowing), typical of a fuselage panel, MSD type cracking was observed on all tested coupons, with test results comparable to those in the literature from tests on fuselage panels. Also, a companion computer program was developed to predict MSD crack growth with results that appear to match experimental data. The design of the test coupon allows tailoring of geometry and fastener details to resemble a particular aircraft. Mr. R.J. Cazes and Mr. F. Goerung describe a Dassault Aviation study on the structural integrity of lower wing panels subject to long term corrosion damage that acts in a similar way as MSD (multiple-site damage) or even MED (multi-element damage). Such damage had been observed on the centerplane and wing lower panel of the Mercure jet transport after some 15 years of service. The problem was also studied on the Mirage 2000 combat aircraft wing panels assuming reduced material thickness due to corrosion. Microbial corrosion was indicated in the case of the Mercure, apart from the well known effect of aggressive environment like sea water. The authors point out the danger of gradual reduction in material thickness on inner surfaces that may remain unnoticed in service. As the damage is nonperforating, it may not be noticed early, even in fuel tank and fuselage panels. Studies of residual life and strength in the presence of corrosion damage indicate severe reduction in these values. Preventive action through periodic surface protection is recommended as a solution to the problem. Prof. M. de Freitas et al describe an exercise in instrumented flight data acquisition including mechanical strain readings on an A7-P Corsair aircraft of the Portuguese Air Force. Available analytical techniques for fatigue analysis were then used to track simulated single and multiple site cracks as a function of service usage. The research study indicated a more severe load spectrum when compared to the same aircraft type in service with the US Navy and USAF. Also, the parametric coefficients relating g-level to local stresses were found to be different from those established by the manufacturer. This was attributed to differences in stores configuration. Sqn. Ldr. E. Bittel describes a Royal Air Force study on the feasibility of proof pressure

testing as a means to qualify a structure susceptible to MSD. The study was performed on test coupons with an array of (unloaded) holes simulating a string of rivets in the fuselage. A single 30% overload simulating proof pressure was applied in the experiments. Both the experiments as well as analytical predictions using the Wheeler model indicate negligible retardation potential of proof testing. During the discussion following the paper, reservations were expressed about the efficacy of proof pressure testing for purpose of MSD retardation considering its meagre potential after a 30% proof load (larger proof load being unacceptable). Also, it was suggested that a specimen with multiple holes may not be adequate for a realistic simulation. Drs. J.C. Newman and D. S. Dawicke describe a NASA research effort to develop an analytical package backed up with experimental results for a local fracture criterion based on Crack Tip Opening Angle (CTOA). It was shown to provide consistent results as indicated by microphotographically measured CTOA values of about six degrees for a given material (2024T3), independent of loading conditions and crack geometry. The technique was also found to work with MSD situations and biaxial loading. An inconsistency observed in CTOA measurements during NLR studies on panels was attributed by Dr. Newman to conditions of local buckling. Prof. S. N. Atluri provides an overview of analyses of aircraft panels with MSD based on elastic-plastic finite element alternating method (EPFEAM) and the T^* integral for residual strength estimates. The salient feature of the EPFEAM technique is a detailed FEM consideration of the uncracked 3D body for stress analysis, followed by a coarse mesh analysis of flaws in the body using analytical solutions. The first part of the calculations is involved but is performed only once, while the second part can be rapidly repeated as required. The EPFEAM technique and the T^* criterion are found to provide an efficient solution to study the MSD link-up phenomenon. Drs. P. Horst and H.J. Schmidt introduce a mixed approach for the consideration of MSD and consequent WFD, whereby probabilistic aspects govern crack formation, while subsequent growth and reduction in residual strength are controlled by deterministic parameters. Standard deviation of initial crack formation affects MSD potential and therefore, the required inspection intervals corresponding to an MSD situation become highly random in nature. The method allows for the simulation of the effects of POD, scatter in initial quality and in fatigue life, and can be used to predict best and worst case scenarios. Dr. M. Shinozuka et al performed a Bayesian reliability analysis to determine non-periodic inspection schedules from data collected during in-service inspections. The analysis quantifies uncertainty of individual parameters determined during inspections. In contrast to the previous paper, probabilistic aspects are attributed to both crack formation and growth. A salient feature of the procedure is its adaptability to multi-site as well as multi-element damage. As the technique relies on data collected from service, the quality of reliability (risk) estimates are likely to improve as more in-service inspection data become available. Mr. A.P. Berens and Mr. J.G. Burns extend the USAF risk assessment procedure described in earlier papers at

the meeting to the problem of corrosion risk analysis. The study assumes that risk is affected by reduced thickness of the material and associated increase in crack growth rates and decrease in residual strength. Time histories of probability of single flight failure were calculated using a risk analysis computer code specially developed for the study. Probability of detection of corrosion participates in the analytic scheme. The results of the study indicate that if inspection intervals were initially determined from damage tolerance criteria, both safety and durability can be adversely affected by corrosion.

SUMMARY: This AGARD meeting provided a unique forum for sharing the experience of a number of NATO as well as non-NATO countries in the area of structural integrity management of ageing aircraft. Tear down inspections accompanied by risk analysis appear to have established themselves as reliable and cost-effective methodologies to handle the continued operation of a number of ageing USAF aircraft. These methodologies can be readily applied to other aircraft types, provided ASIP compliance was ensured in their development and certification. Advances in materials development and in both deterministic and probabilistic analyses of residual life and strength appear to have found immediate applications. The Australian experience is an example of how quickly such advances can be applied (through to certification) to ensure continued safe operation of ageing military aircraft. Prof. R. Jones presentation on repair technology included the application of the alternating method for FEM analysis described in another paper at this meeting by Prof. S.N. Atluri. During discussions at the conclusion of the meeting, Mr. T. Swift (FAA) emphasised the special significance of MSD and MED, which from a design viewpoint, needs to be avoided altogether, in view of the unacceptably precipitous fall in residual strength and short residual life after its onset. Prof. J. Schijve noted that glass fibre reinforced laminate (Glare) would be a potential deterrent to MSD situations in fuselage splices. This, combined with improved riveting quality are likely to provide substantial increase in crack free (safe) life. Mr. Swift underlined the importance at this time of harmonising the three basic philosophies in structural design: Safe Life, Fail Safety and Damage Tolerance. It would appear that studies on the growth and merger of multiple cracks in an MSD situation are unlikely to provide results of practical value in view of: (a) the short duration of their growth to failure, and more importantly (b) the need for the structure to always tolerate a long lead crack caused by uncontained engine fragment or battle damage, accidental damage or a crack that escapes detection during its infancy. One may suggest therefore that future work concentrate instead on strategies to ensure crack arrest through properly designed fail-safe elements. Also, an understanding of crack formation or very early crack growth in an MSD situation (an essentially safe-life approach) is essential for the designer to ensure that WFD is avoided during the service life of the component. The emphasis may have to shift to stressing and technological aspects that determine crack formation kinetics in the case of new aircraft

and to repair or reinforcement technology in the case of ageing aircraft. ASIP design guidelines assume that materials and material combinations used in the design will be generally highly resistant to corrosion. As indicated by the proceedings of this meeting, corrosion can sometimes affect durability and residual strength significantly. It would therefore follow that IATP should incorporate tracking of environmental conditions also. These are also expected to have a significant impact on the endurance of composite structures and repair schemes. The ASIP approach and its evolution through risk assessment and incorporation of MSD/WFD aspects appears to be widely accepted although contrasting views were expressed in a few papers. For a more comprehensive exposure to the rich world-wide experience of aircraft development and operation, it is recommended that future meetings continue to include specialists from a variety of countries including non-NATO regions. One example is Russia, with its variations in concepts behind lifing, inspections, residual strength assessment and certification as applied to several generations of military aircraft. If suitably documented, the Russian experience may present a useful contribution to future AGARD proceedings.

OVERVIEW OF WIDESPREAD FATIGUE DAMAGE: RISK ASSESSMENT METHODOLOGY

John W. Lincoln
ASC/ENF BLDG 125
2335 Seventh Street STE 6
Wright-Patterson Air Force Base, Ohio 45433-7809
USA

1. SUMMARY

The United States Air Force has used the probabilistic method to determine the onset of widespread fatigue damage in its aircraft for the past twenty years. They have focused their efforts on the loss of damage tolerance capability for both monolithic and fail-safe structures. The application of the probabilistic method requires that the appropriate data bases be established. The USAF generated these data bases through teardown inspections and from the operational usage tracking programs. The purpose of this paper is to provide an overview of the methodology for the probabilistic approach through risk assessments performed on USAF aircraft. These risk assessments provided the basis to make the appropriate aircraft modifications for elimination of this problem. In addition, a sample problem illustrating some of the essential data requirements for these analyses and the consequences of the results will be discussed.

2. INTRODUCTION

The determination of the time of onset of widespread fatigue damage (WFD) in a structure may be made from either deterministic or probabilistic approaches. For the deterministic approach, it may be defined as a condition where the simultaneous cracks at multiple structural details are of sufficient size and density whereby the structure will no longer meet its damage tolerance requirement (e.g., maintaining required residual strength after partial structural failure). For the probabilistic approach, the onset of widespread fatigue cracking is that point in the operational life of an aircraft when the damage tolerance or fail-safe capability of a structure has been degraded such that the probability of failure of the intact structure or the structure with discrete source damage has been reduced below the thresholds specified by the procuring (or certification) agency. The USAF has used the probabilistic approach for its assessment of the time of onset of WFD for its aircraft.

The definitions above apply equally well to WFD in the form of multiple element damage or multiple site damage. Multiple element damage is typically characterized by cracking in multiple adjacent elements of a structure. Multiple site damage is typically characterized by multiple cracks in a single element. A case where only a single element is involved is found only rarely.

Since the early seventies, the basic approach for maintaining safety of operational aircraft in the United States Air Force has been through the damage tolerance approach as required by the Aircraft Structural Integrity Program (ASIP), which is described in detail in MIL-STD-1530A. This document, which was released in 1975, specifies that the deterministic damage tolerance approach will be used to establish inspection intervals and modification times. This approach has been used successfully and it is planned that it will be used as the basis for design of future conventional aircraft. There are cases, however, for older aircraft where the damage tolerance alone is not adequate to protect the safety of aircraft. This paper discusses some of the applications of the probabilistic approach for the determination of the time of onset of WFD. The term "risk assessment" will mean the determination of the probability of failure of an aircraft selected at random from a population of similar aircraft. The primary result of the calculations is the single flight probability of failure. This is the probability that failure will occur on a single flight of an aircraft selected randomly from the population. The probability of failure after a given time and the expected number of losses may be easily determined from this calculation.

Over the past twenty years, risk assessments have been made on numerous USAF aircraft. This list includes the B-52 wing, KC-135 wing, C-5A wing, C-141B fuselage and wing, F-5 fuselage, T-38 fuselage and wing, and the T-37 complete aircraft. The KC-135 wing, the C-5A wing, C-141 wing, and the T-38 wing assessments were motivated by the potential for WFD. The procedure that has been used is developed in Reference [1], and an example of the application to the T-38 wing is shown in Reference [3]. The question on an acceptable level of risk is discussed in References [2] and [3]. It was concluded that for military aircraft that a single flight probability of 10^{-7} or less is adequate for long term operations. This risk, for most weapon systems, results in an expected number of losses that is less than one. For risks greater than this, the exposure should be limited. For the case of WFD in fail-safe structures, the question of the probability of the threat of discrete source damage must also be considered. An example of this is discussed below for the C-5A. The F-5 fuselage, the T-38 fuselage and the T-37 aircraft are examples of a situation where the damage tolerance assessment revealed critical areas

that were not readily inspectable and also were beyond their deterministically derived damage tolerance limits. For these cases, a risk assessment was used to provide a basis for continued flight until the inspections could be performed. The using command was advised of the risks involved and there was an agreement to accept the risk as quantified.

The risk assessment that was performed on the T-38 wing has historical significance in that it is the first time that the risk assessment was used to shorten the inspection interval that was derived from the damage tolerance assessment. The previous risk assessments were typically performed to permit an extension of the damage tolerance derived inspection interval to permit continued operation of the aircraft. The T-38 wing is an example of a structure that has no fail-safety. The inspection program on the wing was derived from a damage tolerance assessment based on maintaining safety through slow crack growth. An inspection interval of 1350 flight hours was originally derived from this assessment. Later, it was found that the usage severity had increased such that the inspection interval needed to be reduced to 430 hours. The question was: "Does the original deterministically derived inspection interval need to be reduced to 430 hours to protect the safety of these aircraft?" To answer this question, a risk assessment was performed. It was known through teardown inspections that there were numerous small cracks in these wings. Nineteen wings that had been subjected to a teardown inspection revealed that, in the critical areas, twenty-eight percent of the fastener holes were cracked. The upper bound of these cracks was approximately 2.5 millimeters. This assessment showed that the inspection interval of 430 flight hours was unconservative and the interval should be reduced to 300 hours to maintain a desired level of safety for these wings until they could be replaced. The single flight probability of failure, for an aircraft that is inspected by the original 1350 flight hour inspection interval, was found to be completely ineffective for protecting the safety of these aircraft. A reduction in risk from the inspections performed at 300 hour intervals, although the single flight probability of failure of 10^{-7} was exceeded, was judged to be acceptable because of limited exposure to higher than desired risk. The results of the T-38 study showed that the deterministic damage tolerance analysis may be complemented by the risk assessment for an aircraft in an advanced stage of cracking.

The wings of the KC-135, C-5A, and C-141B do have fail-safe capability. The risk assessment that was performed on the KC-135 is significant in that it was the first USAF aircraft where the loss of fail safety was quantified based on this process. As discussed in Reference [4], the loss of fail-safety of the KC-135 wing was a result of widespread fatigue cracking. The fact that the wings were in this state was the motivation for the replacement of their lower surface. These aircraft were

originally manufactured with 7178-T6 aluminum lower wing skins that were operating at stresses approximately fifty percent higher than would be typically accepted for a damage tolerant design. Finite element analyses of the wing had shown that approximately twenty fastener holes are subjected to significantly higher stresses in the event of failed skin element. If there was a crack of one millimeter in one of these fastener holes then the residual strength could have been reduced to a level considerably below limit load. In 1972 there were several KC-135 wings that had been subjected to a teardown inspection. These inspections provided the basic data from which a judgment could be made on when the lower wing skins needed to be replaced. A risk analysis for the wing was used to help make this judgment. The data base included 245 cracks, each of which were 1.27 millimeters or longer in length. Also, 29 crack pairs were found which for the purposes of this study were defined as 1.27 millimeters in length for the primary crack and 0.254 millimeters in length for the secondary crack. The most critical crack pair from each aircraft was used for this evaluation. The results of this study showed that the mean time for a crack pair to develop was 10,709 to 15,441 flight hours with ninety-five percent confidence. On the basis of these results, a risk assessment showed that by the time the fleet of aircraft had reached its anticipated life of 13,000 flight hours, it would be expected that there would be, at best, one loss and, at worst, fourteen losses. This assessment was performed by the Oklahoma Air Logistics Center and was completed in 1975. On the basis of these results and other complementary information, a decision was made to establish 8,500 flight hours as the threshold for replacement of the lower wing surface with the more tolerant 2024-T3 aluminum. The KC-135 risk assessment focused management attention on the problems with the 7178-T6 lower wing skins, and provided the basis for the successful resolution of these problems.

In 1972, a damage tolerance assessment of the wing structure of the C-5A was made and from these results a safety limit of 8,000 Representative Mission Profile (RMP) was established on 15 January 1975. The safety limit, which is defined as the time in flight hours from an initial flaw to critical, was the life of the wing structure since the small critical crack size precluded an inspection to extend its life. In 1973, there was a concern about the loss of fail-safety because of cracking in the 7075-T6 aluminum wing. This concern was partially based on the observation of the nature of the cracking in the full-scale fatigue test article. It was found that cracking which occurred in the spanwise splices often developed in a hole common to a fastener. Another reason for the concern is that nonlinear finite element analyses performed for the case of a broken panel showed that there were many fastener holes in the adjacent panel subjected to a stress that approached ultimate strength of the material. Approximately fifty to sixty fastener holes were in this

category. Consequently, a small crack on the order of one millimeter in one of these holes could significantly degrade fail-safety. However, the crack size data base for determination of the statistics of the crack population did not exist at that time and the subject was not pursued.

Another damage tolerance assessment of the C-5A wing was initiated in September of 1977 to reevaluate all actions necessary for the protection of structural safety until the wing could be modified. As a part of the effort of the 1977 assessment, a wing was torn down that had been on an operational aircraft (Lockheed number 68-0214) [4]. This aircraft had accumulated approximately 6,700 RMP flight hours. The teardown inspection was performed on the left wing including the entire center section. A total of 44,641 fastener holes was examined in detail. This inspection revealed 1,361 cracks of which 931 were considered significant. The results from the teardown inspection were extensive enough such that they could be used to assess the risk of failure of the intact structure from fatigue cracking and also could be used to assess the degradation of fail-safety from this cracking.

A risk assessment was made to determine the failure probabilities for two cases. The first case was for the situation where the aircraft was assumed to have a failed panel. This assessment was made to evaluate the loss of fail-safety in the structure due to cracking in the adjacent panels. The second case was for the situation where the structure was assumed to be intact. The assessment for the latter case was aimed at providing an upper bound on the number of hours that the aircraft could be flown before a modification of the wing would be required. The analyses determined the single flight probability of failure. The United States Air Force Scientific Advisory Board (SAB) in September of 1977 endorsed the following statement regarding fail-safety: "If a structural member fails due to an external source, then the risk of catastrophic structural failure on a single flight of no more than one in ten thousand is acceptable." This means that there was a perception that the threat of discrete source damage was one in one thousand per flight. This is believed to be quite conservative for peacetime operations, but may be realistic for battle damage.

For the C-5A, the discrete source damage was assumed to be the loss of a wing panel. It was found that the failure probability of one in ten thousand was reached at approximately 4300 RMP flight hours. Additional analyses for the intact structure showed that the single flight failure probability of one in ten million was reached at approximately 7000 RMP flight hours. The damage tolerance derived safety limit (i.e., 8000 RMP flight hours) was found to be slightly larger than the time when the risk crossed the one in ten million threshold. Typically, the safety limit derived from the damage tolerance assessment is reached in less time than that

required for the risk to become unacceptable. The damage tolerance assessment on the C-5A did not address the issue of loss of fail-safety. These analyses were completed in 1979. The usage of the C-5A operational aircraft was carefully monitored until the wing box change was accomplished. The aircraft were successfully flown until the wing boxes were removed and replaced with a considerably more robust structure.

The risk assessment method used on the C-5A was considerably different from that used on the KC-135. The approach used on the C-5A quantified the risk of catastrophic failure on a single flight of an aircraft selected at random from the population. From this calculation, the expected number of aircraft losses may be determined.

In 1991, a risk assessment [5] was performed on the C-141 wing. In particular, the assessment was on Wing Station 405, which is the location of the wing joint connecting the inner wing and the outer wing. Inspections of in-service aircraft had revealed numerous failures of members of the front and rear beams at this location. In addition, there were cracks found in the skins and splice plates of the chordwise joint. To answer the question on the presence of fatigue cracking, a teardown inspection was conducted on a wing from a crash damaged aircraft. This inspection confirmed the potential for WFD that could degrade fail-safety. Subsequently, a risk assessment was conducted based on the findings from in-service aircraft inspections. From the discussion above, a single flight probability of failure of one in ten million was considered acceptable. The reason for this is that the failure scenario started with the structure intact rather than partially failed from an external source such as engine disintegration or battle damage. In this case there was a high likelihood that there would be a first element failure. It is important to recognize this possibility when assessing fail-safe structure. This assessment showed that the C-141 aircraft had been flying with a higher than desired risk of catastrophic failure. The assessment was also invaluable in that it showed that the chordwise splice was the element of the structure that was protecting the aircraft from failure and that it must be inspected to maintain flight safety. As in the case of other aircraft, the risk assessment on the C-141 focused management attention on the problem. An inspection program was immediately implemented on the aircraft and a modification program to strengthen this joint was established.

In many cases, the development of the damage tolerance derived inspection program does not include the cracking scenarios that are representative of widespread fatigue cracking. If this possibility was included, the inspection costs would be significantly more since the scope of the inspection program would have to be increased significantly. In many situations, even increasing the scope of the inspection program may not result in an

acceptable risk of catastrophic failure. Therefore, it is essential that the flight time be determined at which the onset of WFD has occurred. It is at this time that a modification program should be initiated to eliminate the problem. In some cases, however, an interim inspection program must be established to provide for continued operational service of the aircraft until the modification can be implemented.

3. RISK ASSESSMENT METHODOLOGY

As discussed in Reference [1], the approach is based on the assumption that the crack length function at a given location and the maximum stress occurrence on a randomly selected flight at that location are known through their probability distribution functions. It is also assumed that the crack length at a given location is independent of the applied stress at that location, such that the joint probability density function for crack length and stress is the product of the respective marginal density functions. The procedure identified in Reference [1] assumes that the crack growth function is not random and it depends only on flight time. Further, the critical stress function (i.e., the stress at which a crack will propagate by rapid fracture) is not random and it depends only on stress. The procedure may be generalized such that the crack growth and the critical stress functions are only known through their probability distributions.

The methodology may be applied to the case of the structure remaining intact or to the case where the structure has suffered a partial failure. Both of these cases are important and the approach to obtaining a solution of these problems is quite similar. For this discussion, the emphasis will be on the case where the structure has been subjected to a partial failure from a specified threat. It is essential to specify the threat since the calculation is made for the conditional probability of failure given that the structure has suffered a partial failure.

For each location in the structure that has an effect on the probability of failure, the following functions must be determined:

Probability distribution for crack length at a reference time

Probability distribution for stress

The critical stress

Crack growth

Inspection probability of detection

The probability distribution for crack length could be determined from the results of a teardown inspection of a durability test article or from a teardown inspection of an in-service aircraft. As indicated in the introduction, for

the C-5A wing, there was a teardown inspection of an in-service aircraft to provide the crack length probability distribution. The teardown data was used to generate a Weibull distribution that was used to obtain the probability of exceeding a given crack length in the interval $[10^{-6}, 1.0]$. It was found that there is a Weibull slope (shape parameter) for the small cracks that is different from the Weibull slope found for the large cracks. The large cracks are the only ones that contribute to the risk, and consequently, the small cracks may be ignored.

An alternate method of obtaining the probability distribution for crack length was used on the A-7D. For this aircraft, strips were taken out of the wing skin of an essentially new aircraft that had been crash damaged. These strips were placed in a cyclic test machine. Cracks were propagated with a spectrum that consisted of 5000 cycles of a stress of 137.93 MPa and 100 cycles of a stress of 206.90 MPa. The 206.90 MPa stress acted as marker cycles for the fractographic examination, which in combination with analysis, was used to trace these cracks back to zero time. A total of eighty-five cracks was traced from open holes, of which some were countersunk and some were not. These experimentally derived equivalent initial cracks were used to generate a log normal distribution function.

It is noted that the crack length probability distribution function may not contain the possibility of the remote or "rogue flaw" that is used as a basis for the initial flaw in the damage tolerance assessment. Consequently, there is an unquantified risk associated with this process. It is believed, however, that for the purpose of identifying the onset of WFD that this omission is not significant.

Another data item required for the analysis is the probability of exceeding a given stress in a single flight of a particular mission of the aircraft. The data base from which this is derived is the stress exceedance function, which is the number of times a given stress is exceeded for the mission under consideration. The stress exceedance function for the intact structure is normally used in design for durability or damage tolerance analyses and it is subsequently modified based on in-service usage of the aircraft. Consequently, it is available to the analyst. The stress exceedance function for the partially failed structure, however, is not usually available to the analyst. The analysis of the partially failed structure is difficult because it typically requires that the structure and its fastener system be treated as being nonlinear. This was the case with the analysis of the C-5A wing. For that wing, with a failed panel, the stresses in the structure adjacent to the failure are elevated to near the ultimate stress capability of the material. The analysis also showed that the stress remained high for a considerable distance along the splice. The calculations, which were correlated with fail-safe tests on the C-5A wing, showed that approximately

fifty to sixty fastener holes were subjected to significantly elevated stresses when a panel failed. Therefore, it was possible that a small number of cracks in the adjacent structure could, if large enough, cause degradation of fail-safety. In other words, a small population of cracks could increase the probability of failure to an unacceptable level.

The cumulative probability for stress is derived in the following manner. First, the exceedance function ordinate is transformed to exceedances per flight by multiplying the number of exceedances per hour by the number of hours per flight. Second, the exceedances per flight greater than one are made equal to one. Finally, if it is assumed that there is no more than one counted exceedance per flight, then the resulting function defines the fraction of flights for which a given stress is exceeded. This function is, therefore, the probability distribution function for exceeding a given stress in a single flight. Typically, the data from which the data was derived is not extensive enough for the calculation of the failure probability. Therefore, a probability distribution function is used to provide for the calculation of the probability of exceeding a given stress within the interval $[10^{-6}, 1.0]$. The Weibull and the Gumbel distribution functions have proven useful for this purpose.

As with the rogue flaw, the stress probability distribution function may not contain the remote or rogue loading occurrences. Again, since the emphasis is on the onset of WFD, the omission of these rogue loads is not believed to be significant.

The risk assessment approach defined in Reference [1] utilizes a critical stress function. This function is used to define the limit on the integration of the joint density function for crack length and stress. The volume of the joint density function outside of this limit is the single flight probability of failure. As indicated above, it is supposed that this function is not random and depends on the stress for a particular geometry and material fracture toughness. This function, which for the intact structure is dependent on the fracture toughness, is typically available from the calculations performed in support of the conventional damage tolerance assessment. The fracture toughness is known only through its probability distribution function. In the Reference [1] approach, the fracture toughness was supposed to be the mean value of this probability distribution function. It is believed that the error associated with this assumption is negligible. It is recommended that the implication of this assumption be assessed through sensitivity studies. For cases where the fracture toughness variability is judged to be significant, the problem can be solved by the technique described in Reference [6].

For the case of the partially failed structure, however, the problem of establishing the critical stress function is more difficult because the high stresses cause strains that

may exceed the limits of the applicability of linear fracture mechanics. In this case, additional testing is needed to determine the critical stress function over the required range of stress. An example of this is illustrated in Reference [7]. For a given crack length, the ordinate of this function is known only through its probability distribution function. As indicated above for the lower stresses, the implication of the assumption of the use of the mean of this distribution should be assessed.

The crack growth function is derived from a linear fracture mechanics analysis for each mission that is to be considered in the analysis. This function is used to revise the crack length probability distribution function to represent the crack population at a given number of flight hours. This function is derived from the crack growth function that is typically available from the damage tolerance assessment. It needs to be extended to smaller cracks than those in the damage tolerance assessment to accommodate the range of cracks in the crack length probability distribution function. This extension should be able to be accomplished based on linear fracture mechanics. The "small crack effect" need not be considered in the analysis unless this effect is significant for those crack lengths for which the risk of failure is unacceptable. The crack growth function is actually only known through its probability distribution function. The implication on the risk from using only the mean crack growth function should be addressed by a sensitivity analysis. Reference [6] describes a study that indicated that the variability of the crack growth function had a second order influence on the risk calculation.

As indicated in the introduction, an inspection program may play an important role in the maintenance of safety until a structural modification can be implemented to remove the potential of WFD. The influence on failure probability from inspections can be incorporated into the risk assessment through the use of a probability of detection function. This function defines the probability of finding a crack of a given size or larger. It is typically extremely difficult to determine this function. One of the main reasons for this difficulty is that the service conditions under which the inspection is performed are usually different from the laboratory conditions. A probability of detection function developed in the laboratory should be considered an upper bound of the probability of detection function that would be expected to be representative of in-service inspections. These differences are minimized for systems where the skill of the technician is not a major factor in the inspection process.

4. EXAMPLE PROBLEM

The following example problem is provided to illustrate some of the essential features of the risk analysis process. The risk of catastrophic failure is to be found for both the intact and partially failed structure of a hypothetical aircraft that has been designed for a 30,000 hour life. It

is assumed that the aircraft is to fly only one mission. It is supposed that the mission is two hours in length. It is further supposed that there is only one area of the structure required for this calculation and the only significant contribution to the risk from that area is 500 fastener holes. It will also be assumed that for each of these holes the initial crack distribution may be represented by the A-7D crack probability distribution function as shown in Figure 1. For the intact structure, the stress exceedance function for each of these holes is shown in Figure 2, and the corresponding stress probability distribution function, derived from the exceedance function, is shown in Figure 3. For the partially failed structure, it is supposed that only ten of the 500 fastener holes are subjected to an increased stress equal to 1.5 times the stress for the intact structure. It is further supposed that the shape of the stress probability distribution function remains the same. The critical stress function is described by Figure 4. This function is an adequate description for both the intact and the partially failed structure cases. It is assumed that the fracture toughness is not a random function. The crack growth function for each of the 500 fastener holes in the intact structure is given in Figure 5. The initial flaw size for this function was selected to permit the determination of the incremental crack growth of the flaws in the crack distribution function. The final function that is needed for the calculation of risk is the inspection probability of inspection function shown in Figure 6.

The single flight probability of failure for the intact structure without inspections is shown in Figure 7. From this figure, it is seen that the risk exceeds the one in ten million threshold of acceptability at about 22,000 flight hours. On the basis of the crack growth function shown in Figure 5, the critical stress function shown in Figure 4, and the inspection probability of detection function shown in Figure 6, the damage tolerance inspections may be determined. The first inspection is at 7600 flight hours and the inspection interval following the first inspection is 5000 hours. The single flight probability of failure for the intact structure with inspections is shown in Figure 8. It is seen that these inspections are quite effective in reducing the risk of failure and the risk is contained within acceptable limits to 30,000 flight hours. It is clear from this figure that based on the inspection capability assumed and the inspection interval derived from the damage tolerance methodology, the risk is increasing significantly. Therefore, a reduction of the inspection period must be made if it is intended to fly the aircraft significantly beyond its originally intended life of 30,000 flight hours.

The single flight probability of failure for the partially failed structure without the effect of inspections is shown in Figure 9. This is the conditional probability given that the structure has been damaged from an external source. It is seen that the threshold of acceptability for this case (i.e., one in ten thousand) is crossed at approximately

16,000 flight hours. The aircraft has degraded fail-safe capability long before the time the intact structure has reached the unacceptable risk threshold. The influence of inspections on the probability of failure is shown in Figure 10. It is seen that the inspections are essentially ineffective in reducing the risk for this case. This example clearly illustrates that the damage tolerance derived inspection program may not adequately protect the fail-safety of an aircraft in the presence of widespread fatigue cracking.

5. CONCLUSIONS

Risk assessments that have been made for USAF aircraft have shown that they are useful for assessment of the time of the onset of WFD. As demonstrated by the T-38 aircraft, it provided a tool for assessing the time when the damage tolerance derived inspection program may be unconservative. However, by far, the most important application of the risk assessment is to determine when the damage tolerance or fail-safe capability of the structure will be degraded by the onset of widespread fatigue cracking. The risk assessment appears to be the only viable method for the evaluation of all of the possible cracking scenarios that provides a common understanding of the implication of such cracking. The data base for the assessment may be derived by several approaches. However, the USAF experience has demonstrated that a teardown inspection of an operational aircraft is quite effective for achieving it. The data base from the teardown inspection of the durability test article is also extremely useful in assessing the time of onset of widespread fatigue cracking. Further, the USAF experience has shown that the risk assessment has been a vital tool to communicate to management the criticality of a given situation and compare the risk with recommended levels of acceptability. This information has been the basis for management actions in all cases evaluated.

There is no process today or likely to be in the future that will provide a completely accurate determination of the time of onset of WFD. The probabilistic approach will, however, provide an adequate estimate of this time to permit it to be confirmed by special nondestructive inspections. When its presence has been confirmed, then the problem must be removed by appropriate structural modification. This has been the approach used in the past for both military and commercial aircraft and is believed to be the approach of choice for the future.

6. REFERENCES

1. Lincoln, J.W.: "Method for Computation of Structural Failure Probability for an Aircraft," ASD-TR-80-5035, 1980.
2. Lundberg, B., "Fatigue Life of Airplane Structures," The Eighteenth Wright Brothers Lecture, Journal of Aeronautical Sciences, Volume 22, Number 6, June 1955.

3. Lincoln, J.W., "Risk Assessment of an Aging Military Aircraft," *Journal of Aircraft*, Volume 22, Number 8, 1985.

4. Lincoln, J.W., "Life Management Approach for USAF Aircraft," AGARD Conference Proceedings 506, Fatigue Management, December, 1991.

5. Alford, R.E., Bell, R.P., Cochran, J.B. and Hammond, D.O., "C-141 Wing Station 405 Risk Assessment," Proceedings of the 1991 USAF Structural Integrity Program Conference, December, 1991.

6. Berens, A, Hovey, P. and Skinn, D., "Risk Analysis for Aging Aircraft Fleets," Volume 1: Analysis. UDR-TR-91-43, 1991.

7. Swift, T., "The Influence of Slow Growth and Net Section Yielding on the Residual Strength of Stiffened Structure," Proceedings of the 13th Symposium of the International Committee on Aeronautical Fatigue, Pisa, Italy, 1985.

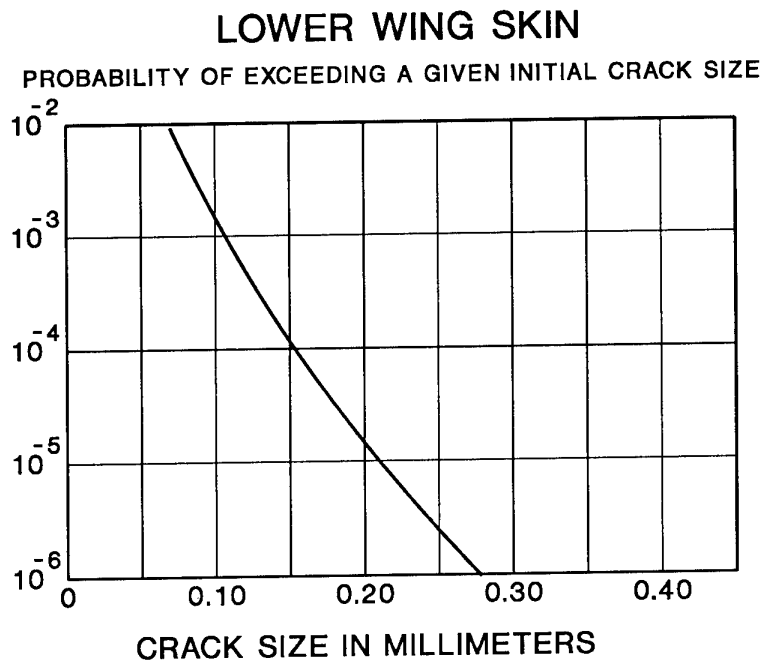


Figure 1 Crack length probability distribution function

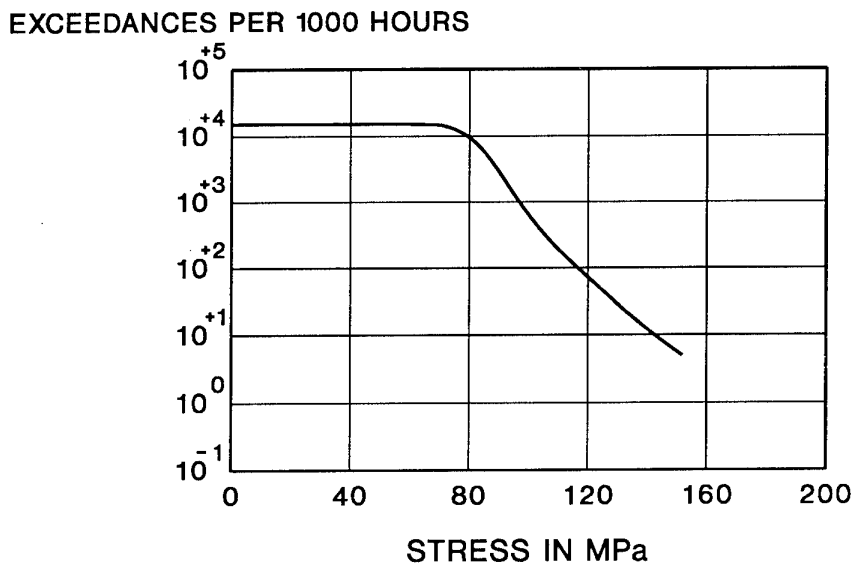


Figure 2 Stress exceedance function

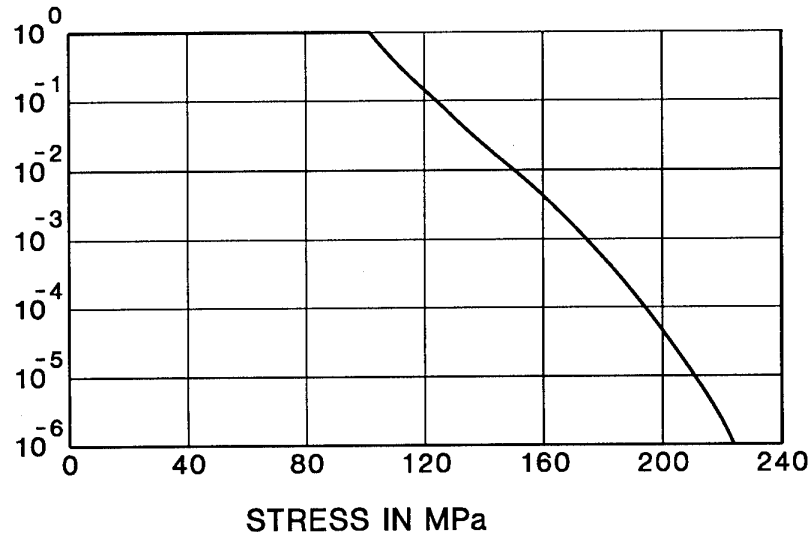


Figure 3 Stress probability distribution function

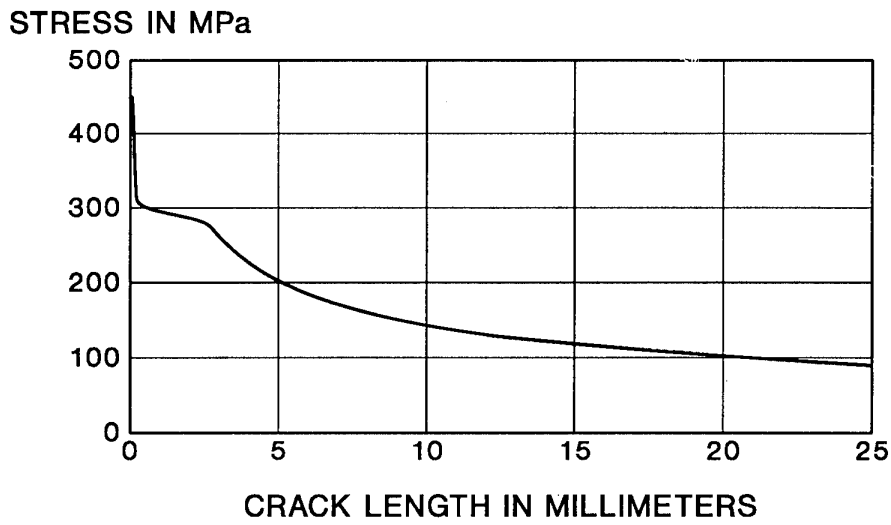


Figure 4 Critical stress function

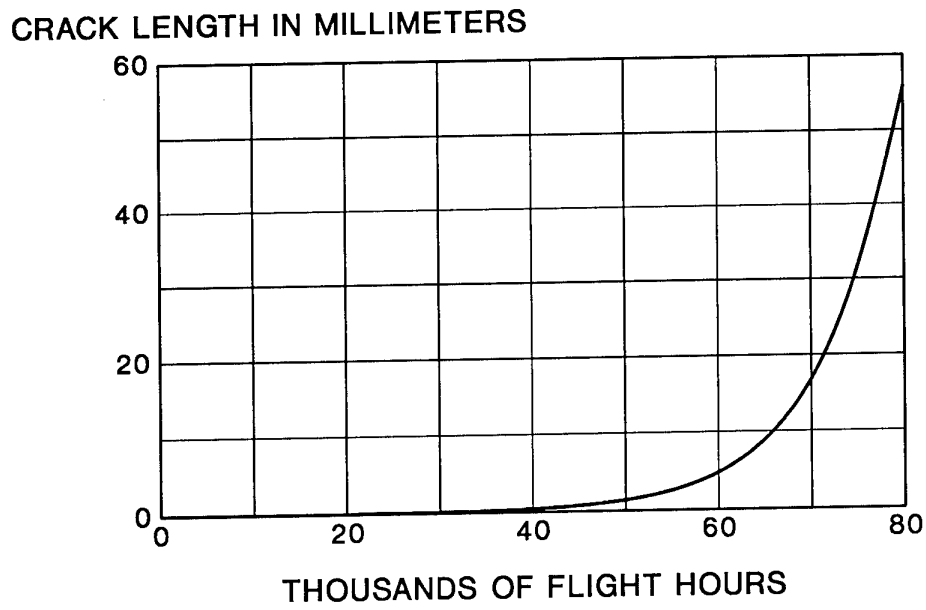


Figure 5 Crack growth function

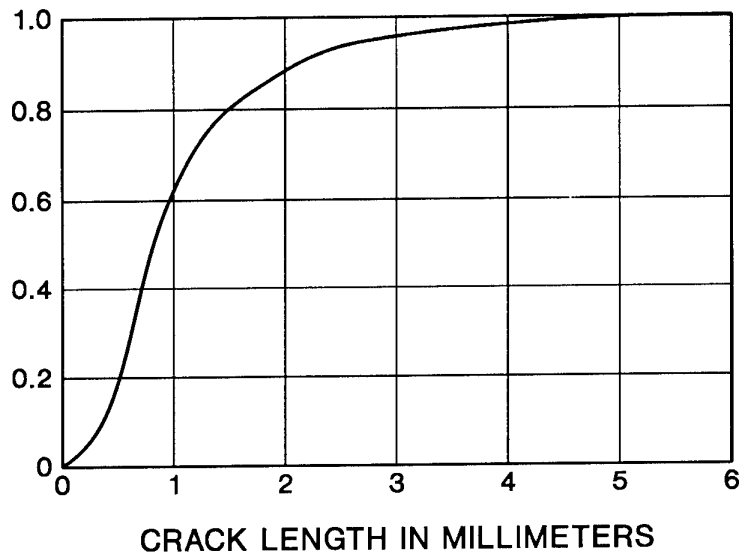


Figure 6 Probability of detection function

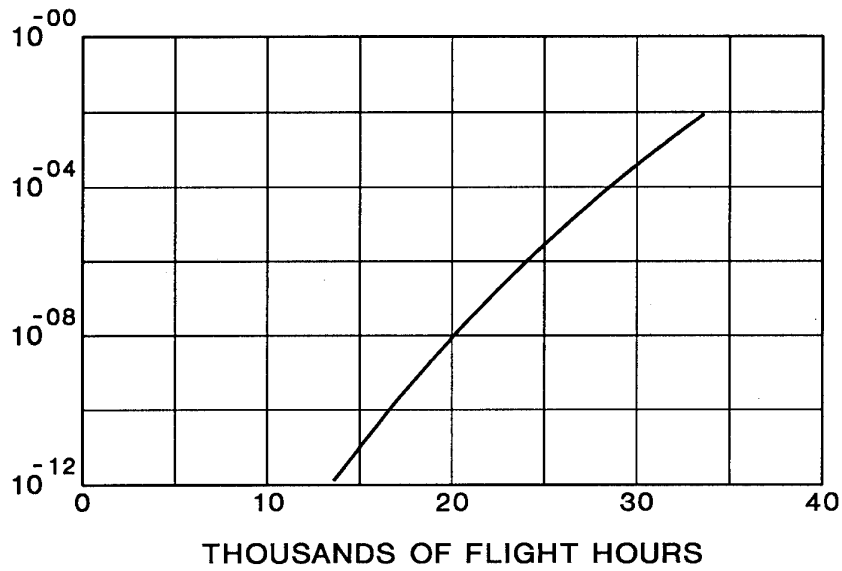


Figure 7 Single flight probability of failure without inspections - intact

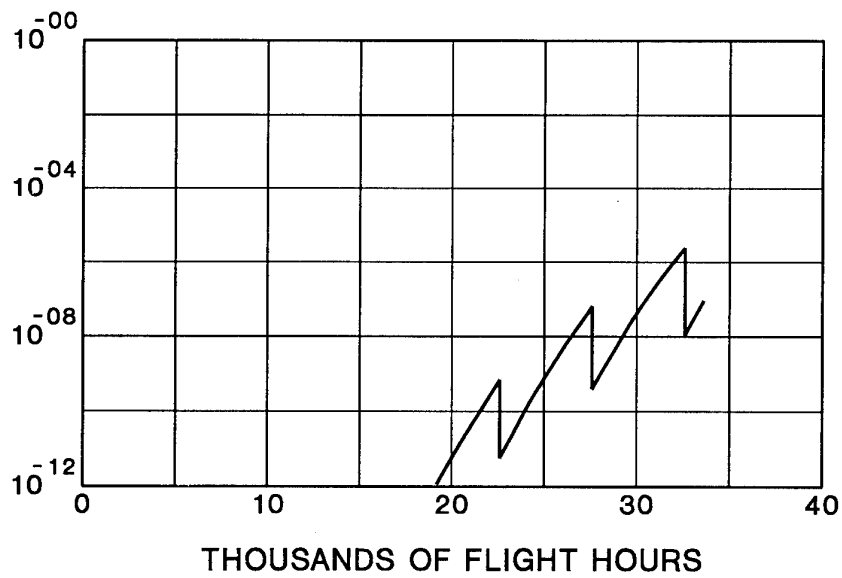


Figure 8 Single flight probability of failure with inspections - intact

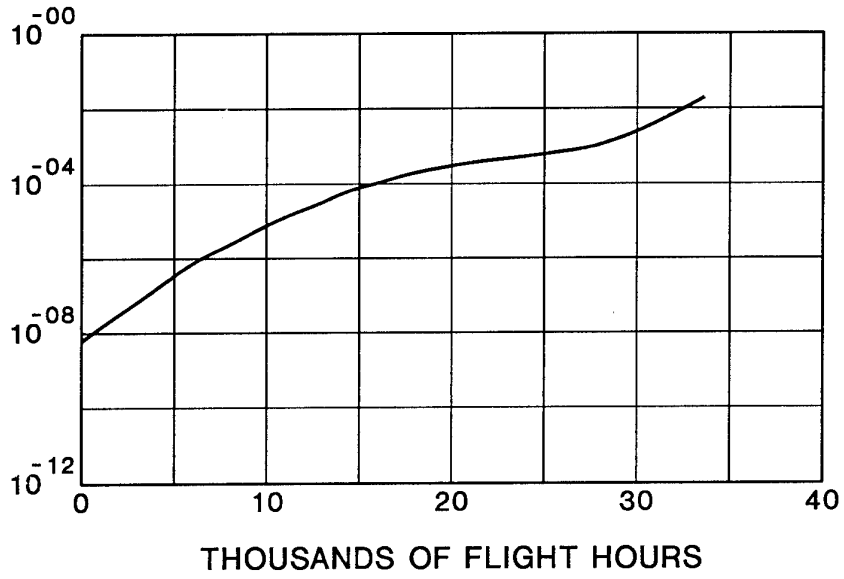


Figure 9 Single flight probability of failure without inspections - damaged

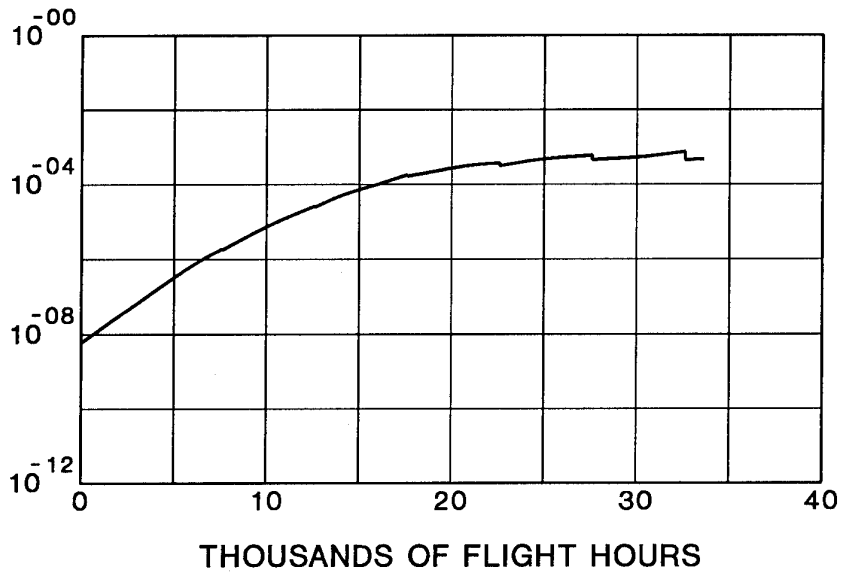


Figure 10 Single flight probability of failure with inspections - damaged

**A SPECIAL UNIAXIAL COUPON TEST SPECIMEN FOR THE SIMULATION OF
MULTIPLE SITE FATIGUE CRACK GROWTH AND LINK-UP
IN FUSELAGE SKIN SPLICES**

G.F. Eastaugh and D. L. Simpson

Structures Materials and Propulsion Laboratory, Institute for Aerospace Research,
National Research Council, Montreal Road, Ottawa, Ontario, Canada K1A 0R6

P.V. Straznicky and R.B. Wakeman

Department of Mechanical and Aerospace Engineering
Carleton University, 1125 Colonel By Drive, Ottawa, Ontario, Canada K1S 5B6

SUMMARY

This paper reviews the loading and fatigue characteristics of longitudinal fuselage splices, and presents a specification and design concept for a uniaxial coupon test specimen that is intended to simulate these characteristics at low cost relative to full-scale panel and fuselage test articles. In particular, the specimen is intended to simulate the initiation, growth and link-up of multiple site fatigue damage (MSD). This simulation cannot be done with conventional coupon splice specimens. For proof-of-concept testing, the MSD specimen was tailored to be roughly representative of current narrow-body jet transport aircraft, using limited aircraft stress and other data available in the open literature. The results indicate that the specimen concept can fulfill its intended purpose. It would now be appropriate to apply the MSD specimen concept to a specific aircraft, in collaboration with the aircraft manufacturer. A procedure for tailoring the MSD specimen to a particular aircraft is proposed.

1 INTRODUCTION

Testing to determine the multiple site fatigue damage (MSD) crack growth characteristics of fuselage splices has hitherto been done only on expensive full-scale panel and fuselage test articles, because available coupon specimens, while suitable for determining the fatigue crack initiation life of splices, are not suitable for crack growth testing. The main shortcoming of conventional coupon specimens was noted by the Industry Committee on Widespread Fatigue Damage in 1992 [1], which observed that in coupon specimens there is "no representative crack growth after the occurrence of initial damage, due to the unrealistic increase of net stress". Because the ligament stresses between cracks are not limited by load transfer to the surrounding structure, the crack growth rates in a standard specimen become progressively more atypical as crack lengths increase.

The loading, stress distribution and fatigue characteristics of longitudinal fuselage splices are not widely understood, and relevant data are dispersed throughout the literature. This data has been studied and some preliminary tests have been performed, to arrive at a specification and design concept for a coupon specimen that can be used to study realistically the initiation, growth and link-up of MSD cracks in these splices. The results of this work are presented in this paper. The loading and fatigue characteristics of a longitudinal splice are presented in some detail, though the data should not be regarded as comprehensive. The capabilities and limitations of the specimen concept are subsequently presented with reference to these characteristics. Five specimens have been designed and manufactured to match criteria that are roughly representative of current narrow-body jet transport aircraft. These specimens have been tested to prove the specimen concept as far as is possible without applying it to a particular aircraft. The test results are presented and discussed, and a

procedure is proposed for tailoring the specimen to an aircraft. In addition, these test results are compared with multiple crack growth curves generated using a computer model of MSD.

2 LOADING AND STRESS DISTRIBUTION OF A LONGITUDINAL FUSELAGE SPLICE

2.1 External Loading

The primary fatigue load on a longitudinal fuselage splice is fuselage pressurization to an approximately constant amplitude of around 55 kPa (8 psi) once per flight. During a lifetime of 20 years, a long range transport aircraft might be subjected to 20,000 pressurization cycles, while a medium range aircraft might be subjected to 80,000 pressurization cycles. This pressure subjects a splice to a combination of hoop tension, longitudinal tension, and out-of-plane bending. The out-of-plane bending is associated with two effects. The first is pillowing of the skin between stiffeners. The second is the distortion, known as secondary bending, caused by the action of hoop tension on the eccentricity inherent in single-shear lap or butt splices. Splices, like other structure, can also be significantly affected by aerodynamic and inertial loads. These modify the local hoop, out-of-plane bending and longitudinal stresses, and may generate in-plane shear stresses.

The schematic diagram in **Figure 1** illustrates the loads on a longitudinal splice due to fuselage pressurization. It shows a circumferential cross-section through two skin panels and the associated stringers. The displacements in the figure are exaggerated for illustrative purposes. The splice is a single shear lap splice, and is rivetted to a stringer. This general configuration is used in many transport aircraft, although the detailed design varies: there may be two to four rows of rivets; there may be pad-up doublers of various sizes and profiles; and the faying surfaces may be bonded, coated with sealant, or just chemically treated.

2.2 Stress Distribution Within a Splice

The skin at the two extreme rivet rows of a splice tends to be more highly stressed than elsewhere in the splice. This is because the hoop stress, rivet load, and out-of-plane bending stress are generally all higher at the extreme rows than at other rows. The first rivet row in the countersunk sheet is usually the critical row. On an aircraft, this is the upper row in the outer sheet. The primary reason why fatigue cracking tends to start here rather than in the lower row of the inner sheet is that the countersink increases the stress concentration at the holes. An important contributory factor is that the out-of-plane bending due to skin pillowing reinforces secondary bending in the outer sheet, while opposing it in the inner sheet. This effect can be seen in **Figure 1**.

Within a splice, load is transferred from one sheet to the other primarily through rivet shear, but also through friction

between the sheets. A combination of uneven load transfer, stress concentrations due to holes, and out-of-plane bending gives rise to a complex, 3-dimensional stress distribution. The complexity is clearly illustrated in **Figure 2** by the contours of maximum shear strain for the surface of a preliminary two-row lap splice specimen. This is a photoelastic image, which was obtained by coating the splice with 0.25 mm (0.010 in) thick birefringent plastic and viewing it under load through a standard polariscope. The camera image was then processed on a personal computer using special software developed by Komorowski [2]. The regions of low stress between the rivets result from out-of-plane bending, and the associated contours suggest that the bending stress is greatest along a line roughly tangential to the rivet holes.

It is difficult to measure the stress distribution within a splice. Photoelastic images like the one in **Figure 2** only indicate the difference between the principal strains or stresses, and the technique can only be used on easily accessible and visible surfaces. Therefore, strain gauges are also used. These are placed on both sides of a sheet, to distinguish between membrane and bending stresses. In the rivetted area, one of each pair of strain gauges must be installed within the splice before it is assembled. A groove must be machined in the opposite sheet to provide the necessary clearance for gauge and wiring. An alternative to placing gauges on both sides of the sheet is to create a laminated strain gauge assembly comprising two strain gauges separated by a "beam" of some suitable material. The laminated gauge need only be placed on one side of the sheet, but is less accurate than the previous approach. Measurements of bending ratio (bending stress/local membrane stress) on actual fuselage splices made by Schutz and Lowak [3] using a laminated strain gauge range from 0.2 to 1.8. No other published data has been found on bending stress in actual fuselage splices.

Finite element modelling can be used to estimate the general stress distribution within a splice. However, it must be used cautiously when modelling rivet and hole details, since the estimates of stress underneath a rivet head cannot be validated directly.

An analytical solution has been proposed by Hartman and Schijve [4] for the out-of-plane bending stress at the outer rivet rows in a lap splice under tensile load, but some test data by Schutz and Lowak [3] suggests that the approach overestimates the bending stress by 60% to 100%. Schutz and Lowak found evidence that yielding at the rivet/sheet interface effectively reduces the eccentricity in the splice, and might be partly responsible for the discrepancy.

Since fatigue cracks start in or close to the rivet hole, the stress distribution in the immediate vicinity of a rivet hole is of particular interest. It is the result of several superimposed loading conditions:

- biaxial tension in the sheet;
- pin-loading at the hole due to load transfer through rivet shear;
- clamping load applied by the rivet;
- surface shear within the clamping zone of the rivet due to load transfer through friction;
- internal pressure in the hole due to expansion of the rivet, possibly causing yielding;
- out-of-plane bending due to skin pillowing and joint eccentricity.

The relative importance of each of these loading conditions varies with the design of the splice and the fuselage. It is likely that, in some aircraft, the amplifying effects of out-of-plane bending and stress concentration at a hole are creating hole-edge stresses close to or above the yield strength under normal operating conditions.

3 FATIGUE CRACK INITIATION IN A LONGITUDINAL FUSELAGE SPLICE

3.1 Crack Initiation Characteristics of Interest

The fatigue crack initiation characteristics outlined in this paper are based on published in-service and full-scale test data, notably data in References [5] to [13]. The discussion of parameters influencing these characteristics also draws on data from laboratory experiments and theoretical studies, including published data in References [3], [4], and [14] to [19].

For the purposes of this paper, crack initiation is defined as the development of a dominant micro-crack. The period of growth until this crack becomes economically detectable will vary with the initiation site, the geometry of the splice, and the inspection technique. Cracks typically initiate at hidden locations - at the edge of a rivet hole, or at the faying surface of the sheets. Visual and high frequency eddy current techniques are currently used for inspecting fuselage skin splices. These techniques cannot reliably detect cracks until they are through the sheet and clear of the rivet head. Consequently, it is useful to refer to the first appearance of a crack beyond a rivet head as "visible initiation".

The initiation characteristics of interest in the context of MSD in longitudinal splices are the initiation site, the initiation life, and the distribution in initiation life. The initiation site is of interest because it influences the choice of inspection method and frequency. The initiation life, together with the undetectable growth period, determines the inspection threshold. The distribution in initiation life determines the size and uniformity of a cluster of MSD, and hence the detectable period of crack growth prior to fuselage failure.

3.2 Initiation Site

In an aircraft splice, fatigue cracking usually starts in the upper rivet row in the outer sheet, for the reasons discussed earlier. However, with a dome-head rivet, such as might be used on lower speed transport aircraft or in repairs, the critical row might be in either sheet. With a skin thickness typical of narrow-body fuselages, cracking may occur in the inner sheet, where it is difficult to inspect. With the thicker skin used in wide-body fuselages, cracking is more likely to occur in the outer sheet. The reason why skin thickness seems to determine the outcome is probably related to the net bending stress realized at the edges of the clamped area. If both heads of the rivet were identical, the bending stress due to splice eccentricity and skin pillowing would be higher in the outer sheet. However, differences between the machined and driven heads of the rivet cause the bend radius to be tighter in the inner sheet, and can reverse the situation. This effect is more pronounced in thinner sheet.

The exact location of the initiation site relative to the rivet depends on the extent of the clamped area around the rivet, on the magnitude of the bending stress, and on the type of rivet (countersunk or dome-head):

- a. If there is firm clamping over a finite area, such as would occur with a well driven dome-head rivet, cracks will tend to initiate at the edge of this area, which may be along a line well forward of the rivet holes. Fretting seems to play an important role, and so several initiation sites may be seen before a dominant crack develops. High out-of plane bending effects at the edge of the clamped area may be the cause of this fretting.
- b. If there is weak clamping, such as occurs with most countersunk rivets, cracks will tend to initiate at or close to the edge of the rivet hole. Bending will promote initiation outboard of the centre-line of the rivet row, while the distribution of membrane stress around the hole will counteract this tendency.

Initiation in the outer sheet of a splice is beneficial from an inspection standpoint, and can be further assured by appropriate detailed design of the splice. For example, in the DC-10, the pad-up doublers are given a finger-shaped profile to ensure that any fatigue cracking will start in the outer skin.

3.3 Initiation Life

Published data indicate that crack initiation in splices may be occurring early in the airframe life of some aircraft. Striation counts on the Aloha 737 provided evidence of crack growth underneath rivet heads for at least 25% of the total airframe fatigue life [5], while cracks have appeared beyond rivet heads during full scale tests after less than 50% of airframe life [6].

The fatigue crack initiation life of a splice is highly dependent on the detailed design of the splice. Minor changes in the geometry, rivet and hole details, or faying surface treatments can make major differences in initiation life. Some important splice parameters and associated design details are as follows:

- a. *Local Membrane Stress.* Influenced by the thickness, profile and method of attachment (rivets or adhesive) of local pad-up doublers.
- b. *Local Bending Stress.* Influenced by the same design details as a. plus the spacing of the extreme two rivet rows, the position of the underlying stringer, the degree to which the stringer attenuates secondary bending at the critical rivet row, and whether the splice is bonded.
- c. *Load Transfer at the Rivet.* Influenced by the number of rivet rows, the diameter, pitch and shear stiffness of the rivets in all rows, and whether the splice is bonded.
- d. *Location and Magnitude of Peak Stresses in and Around the Rivet Hole.* Influenced by hole shape, surface finish, rivet clamping force and area in conjunction with faying surface friction, rivet shank expansion relative to the hole, whether the hole or skin has been cold worked (eg, shot peening, FTI split sleeve technique, and Douglas stress-coining), and whether the splice is bonded.
- e. *Susceptibility to Fretting.* The relative motion associated with fretting is difficult to avoid in practical fuselage splices. Even in bonded splices some relative movement occurs between rivets and hole surfaces. Fretting and fretting

corrosion products tend to be retained within the splice, thereby aggravating the condition. Fretting affects initiation life by affecting d. above. The nature of fretting suggests that it could be reduced by increasing the overall stiffness of the splice, minimizing out-of-plane bending stress, and reducing load transfer at the rivets per a., b., and c. above. However, research is needed in this area.

- f. *Susceptibility to the Environment.* Fatigue cracks tend to initiate earlier and crack growth tends to be faster in moist environments. Moisture also promotes pitting and intergranular corrosion, thereby creating stress concentrations. Faying surfaces and rivet/hole interfaces promote this type of attack through the mechanisms of crevice corrosion. Sealant applied to the faying surfaces and rivets prior to assembly can be effective in keeping moisture out of the splice. Surface chemical treatments, inhibitors, paints, drainage, ventilation, and effective maintenance can help to slow its effects.

Another damaging effect of corrosion in splices arises from the fact that corrosion products occupy several times the volume of the original metal, and cause the splice to pillow between the rivets [20]. This pillowing creates static stresses that could affect fatigue characteristics.

In view of the number of parameters that affect crack initiation life in a splice, and the uncertainties as to how they might interact, the fatigue initiation life of a splice is usually verified by tests. A combination of coupon tests and full scale panel and fuselage tests is used. Although damage tolerance regulations require that environmental effects be taken into account [21], there are not yet any realistic procedures for environmental fatigue testing. Large scale environmental fatigue testing is impractical, and so a coupon specimen that simulates aircraft loading and fatigue characteristics is needed. Also, a realistic accelerated corrosion fatigue test procedure is needed.

3.4 Distribution in Initiation Life

There is some evidence from full-scale tests that the uniformity of cracks within a MSD cluster determines the length of the growth period from first link-up to critical length. In the 747, this period seems to vary from about 10,000 pressurization cycles for a small, non-uniform cluster of cracks down to 1,000 cycles for a larger, more uniform cluster spanning most of a frame-bay.

The number and uniformity of cracks that develop in a given frame-bay prior to the first link-up probably depend on the uniformity of the stress distribution and the scatter in initiation life. For uniform cracks to develop, this initiation scatter must be low relative to the period of growth from first appearance of a crack to first link-up. It would be useful to determine which parameters affect the scatter in initiation life.

4 FATIGUE CRACK GROWTH IN LONGITUDINAL FUSELAGE SPLICES

Based on published in-service and test data, notably [5] to [13], the general characteristics of crack growth in fuselage splices appear to be as follows:

- a. There is a period of relatively slow growth under the rivet heads followed by faster growth beyond the rivet heads. In 737 splices, the hidden growth period is roughly similar in magnitude to the visible growth period to first link-up.

b. Clusters of cracks develop in one or more frame-bays, away from frames and straps. The cracks may be uniform or non-uniform to varying degrees. The clusters may be broad, ie, stretch across most of the width of a frame-bay, or they may be narrow, ie, consist of only 2 or 3 cracked rivet holes in close proximity.

c. Eventually 2 adjacent cracks link up to form a lead crack. This lead crack grows much faster than other, unlinked cracks, and tends to dominate subsequent crack growth within a frame-bay. The link-up of the remaining cracks and uncracked holes proceeds one ligament at a time until there is a linked crack spanning most of the frame-bay.

d. Cracks grow longitudinally, along the rivet row, in most cases. In some cases they grow obliquely, indicating the presence of in-plane shear stress. In either case, cracks that have overlapped generally curve towards and eventually intersect the opposing crack.

e. The combination of a large MSD cluster and uniform crack lengths results in a relatively short period between the first link-up and the development of a linked crack across the full frame-bay.

f. On the other hand, either small clusters or non-uniform cracks will result in a relatively long growth period after first link-up. On the 747 the growth period from first link-up to critical length is between 1,000 and 10,000 cycles depending on cluster size and uniformity.

g. A linked lead crack is slowed down temporarily by circumferential frames and straps, but otherwise grows rapidly until it reaches critical length, which is typically one to two frame bays for a single crack.

h. If there are cracks in the next frame-bay, the lead crack may grow faster and its critical length may be shorter. If the intervening frame is still intact, the cracks may have to be close for these interaction effects to be significant.

i. In narrow-body aircraft, the lead crack may turn in a circumferential direction and form a skin flap. The flap may initiate before or after the crack has become unstable, and may occur at either the first or second frame encountered. The change in crack direction may occur abruptly, close to the frame, or it may be gradual. Narrow-body fuselages are designed to promote this type of fail-safe crack behaviour, but it is less likely to occur if the crack is in a splice, particularly if there are cracks ahead of the lead crack.

The effect of longitudinal stress due to pressurization on crack growth in splices is not known for certain. Extrapolating from theory on the stress intensity factors of cracked holes in biaxial stress fields [22], it appears that longitudinal stress is likely to slow down initiation and crack growth underneath the rivet head, but that its effect might be negligible for longer cracks. Some recent comparative uniaxial/biaxial test data for splices [23] tends to support this extrapolation with regard to initiation and early growth, but further test data is needed.

While higher out-of-plane bending is known to reduce the overall fatigue life of splices, its specific effect on crack growth rates beyond the rivet head are not known. It is possible that bending is more significant in reducing initiation life than in promoting faster crack growth. Research in this area is needed.

Load redistribution limits crack growth rates at all stages of MSD crack growth. For small MSD cracks the load is transferred to the surrounding skin. For cracks several inches long, there is evidence [13] of significant load transfer to frames and tear straps.

5 GENERAL DESIGN CONCEPT FOR THE MSD TEST SPECIMEN

5.1 Essential and Desirable Requirements for a MSD Test Specimen

The characteristic dangers of fatigue cracking in longitudinal fuselage splices can be summarized as follows:

a. The cracking tends to occur as MSD, which implies that the period of growth of the lead crack from detectable length to critical length can be much shorter than in the case of a single crack.

b. The presence of cracks in adjacent frame-bays can either prevent the arrest of the lead crack at the frame or promote explosive decompression rather than the flapping mode of failure.

The MSD specimen is intended to address the first of these issues, by providing an effective yet inexpensive means of investigating early crack growth and link-up in existing aircraft splices, and of performing parametric studies to improve the durability and damage tolerance characteristics of future designs and repairs. It is considered that these objectives can be achieved using a design concept that meets the essential requirements listed in *Table 1*.

Table 1. Essential Requirements for MSD Specimen

-
- Inexpensive to manufacture and test relative to full-scale panel and fuselage test specimens.
 - Physically representative of the critical rivet row for a length of up to one frame-bay.
 - Simulates hoop tension and out-of plane bending loads at the critical rivet row (dominant fatigue loads).
 - Simulates load transfer from cracked areas to surrounding structure.
 - Produces MSD crack initiation, growth and link-up as observed on aircraft.
 - Reliable for statistical studies - no premature failures due to nuisance cracks.
 - Easily adaptable to a variety of aircraft or research applications.
-

It is desirable that the specimen concept also accommodate biaxial and in-plane shear loading. Biaxial loading is not considered an essential requirement, since the specimen is intended to be used as a component of a wider test programme that includes full-scale biaxial panel and fuselage tests. Moreover, the added cost and complexity of biaxial testing argue in favour of using uniaxial testing whenever it will give

adequate results. As indicated earlier in connection with splice fatigue characteristics, uniaxial testing might be conservative with regard to early crack growth rates, while giving fairly accurate results for growth beyond the rivet heads. This performance could be adequate for many applications. Shear loading, while also not considered a priority for the MSD specimen, could be simulated in a uniaxial specimen by applying the load obliquely.

5.2 Chosen Specimen Concept

The chosen solution consists of a pin-loaded uniaxial specimen with continuous straps bonded along each edge, and with profiled doublers bonded across its width above and below the splice. This concept has been implemented as the 25.4 cm (10 in) wide specimen shown in **Figure 3**. The width was dictated by available equipment and facilities, and should be considered as the minimum for MSD tests. For full simulation of a frame-bay without mid-bay tear straps, a 51 cm (20 in) wide specimen would be used.

The bonded side straps fulfill several functions:

- They moderate the increase in net section stress as cracks grow, and thereby simulate the load transfer characteristics of a fuselage. The stiffness of the straps can be adjusted to achieve the desired results.
- They avoid the development of nuisance cracks at the edges of the specimen.
- They prevent cracks growing through to the edge of the specimen and causing premature failure.
- They make it unnecessary to load the specimen through rigid clamps in a rigid load-frame. A pin-joined mounting scheme and a locally assembled load-frame can be used, to minimize equipment costs.

The profiled doublers have two functions. Their main function is to control the hoop stress distribution across the width of the splice. Their position, profile and stiffness can be adjusted in conjunction with the edge straps to produce the required stress distribution. Secondly, they provide extra thickness of material under the clamping plates, and thereby minimize the possibility of nuisance fatigue cracks in this area.

The out-of-plane bending stress experienced by the sheet at the critical rivet row can be adjusted by changing the spacing between the two outer rivet rows of the splice. A decrease in spacing will increase the bending stress, and vice versa. In this context it should be borne in mind that the main objective is to simulate conditions at the critical rivet row - not necessarily to simulate the whole splice.

The concept is adaptable to biaxial loading, should the need arise. One method of introducing the longitudinal load, would be through unidirectional composite laminates bonded to the edge straps. A generally similar technique has already been used by Vlieger on a splice specimen [23].

The concept is suitable for combined corrosion and fatigue testing of splices. Techniques similar to those used in a previous AGARD corrosion fatigue research programme [24] could be used for pre-exposure and concurrent exposure to accelerated corrosion.

6 PROOF-OF-CONCEPT TEST SPECIMEN

6.1 Splice Geometry and Materials for Proof-of-concept

The specimen illustrated in **Figures 3 and 4** was used for proof-of-concept testing. The materials, geometry, hoop stress distribution, and load transfer characteristics of the specimen were selected to be roughly representative of current commercial transport aircraft, but there was no attempt to simulate any particular aircraft exactly. This approach was considered to be sufficient for proving the concept, design methodology and manufacturing procedures, and was also expected to yield useful test data on the characteristics of MSD. The specimen comprised two sheets of 1 mm (0.040 in) thick aluminium alloy 2024-T3 alclad held by three rows of 4 mm (5/32 in) diameter rivets of aluminium alloy 2117-T4. The edge straps and profiled doublers were of the same material as the spliced sheets. To avoid unnecessary complexity at the proof-of-concept stage, it was decided to omit pad-up doublers and interfaying sealant or adhesive in the splice itself.

6.2 Loading System and Instrumentation

The specimen was subjected to constant amplitude sinusoidal loading with a maximum load of 32.1 kN (7,219 lb) and a fatigue ratio of 0.02. This load had been estimated to produce a maximum nominal hoop stress of 93 kPa (13.5 ksi). The mounting scheme is shown in **Figure 4**. It comprised two pairs of reusable clamping plates and close tolerance loading pins held by fork-ends. The specimen was loaded using a single hydraulic actuator, and a standard load cell provided load feedback to the electronic control system.

A typical strain gauge installation is shown in **Figure 5**. A row of strain gauges was positioned 2.54 cm (1 in) from the critical rivet row, to measure the hoop stress distribution. Pairs of gauges were placed back to back on each side of the sheet at each location, to distinguish between membrane stress and bending stress. On some specimens another row of back-to-back gauges was placed along a line tangential to the rivet holes of the critical row. This is the approximate location of maximum out-of-plane bending stress in non-bonded lap splices. It was also a standard location for strain gauges chosen by the AGARD panel on fatigue rated fastener systems [25]. The panel's choice was based on work by Schutz and Lowak on secondary bending in splices [3]. One gauge of each pair of the bending strain gauges was located at the faying surface of the applicable sheet, and had to be installed before the splice was rivetted. A 0.5 mm (0.020 in) deep groove was milled in the opposite sheet, to provide clearance for the gauge and wiring. The groove was located in a low-stressed area, and so was unlikely to affect the stress distribution significantly in other areas of the splice.

A typical strain gauge installation for measuring nominal hoop stress can be seen in **Figure 6**. In this case, the strain gauges at the rivet row were omitted. The specimen in the figure is fully cracked and under the maximum fatigue load of 32.1 kN (7,219 lb). It illustrates the stability of the specimen, even when MSD has linked up to form a long lead crack.

6.3 Hoop Stress Distribution in Non-cracked Specimen

The non-cracked hoop stress distribution in the test specimen is shown in **Figure 7**. It was relatively flat over the central 4 inches of the specimen, and then curved gradually downwards to a value at the outer rivets which was 90% of the maximum

value. The graph applies to a line 2.54 cm (1 in) ahead of the critical rivet row, and was obtained by placing strain gauges as shown in **Figures 5 and 6**. The stress distribution along this line in the non-cracked condition is referred to in this paper as the *nominal stress distribution* applied to the splice.

The stress distribution was representative of those published by Miller et al. in References [13] and [26] for Boeing narrow-body and wide-body aircraft. These show a relatively flat stress distribution over most of the frame bay, with a fairly sharp reduction in stress towards the frames and straps. The value of the skin hoop stress at the frames and straps varies in the Boeing data between 60% and 90% of mid-bay stress. Since the specimen was only 25.4 cm (10 in) wide, the flat portion of the hoop stress distribution applied to fewer rivets than in an uninterrupted frame-bay 51 cm (20 in) wide. In this respect, the specimen more closely represented those narrow-body aircraft that have tear straps every 25.4 cm.

The desired hoop stress distribution was achieved with the help of a finite element model of the specimen. The design of the straps and profiled doublers was adjusted iteratively until the desired stress distribution was achieved on the finite element model. When the first proof-of-concept specimen was manufactured and tested, the measured hoop stress distribution corresponded closely with the predicted one, as can be seen in **Figure 7**.

6.4 Out-of-plane Bending

The lower graph in **Figure 8** compares the membrane and bending stresses at the rivet row with those at the nominal stress location one inch ahead of the rivet row in the third specimen. The upper graph gives both the Secondary Bending Ratio (SBR) and the Secondary Bending Factor (SBF). These are defined as follows:

$SBR = \text{bending stress/local membrane stress.}$

$SBF = \text{bending stress/nominal stress*}$

(*one inch from the critical rivet row)

Unfortunately, no published data on out-of-plane bending for narrow-body aircraft has been found that can be compared directly with the data in **Figure 8**. As mentioned earlier, Schutz and Lowak obtained SBR values ranging from 0.2 to 1.8 on a variety of fuselage splices. The proof-of-concept specimen had a measured SBR of 0.45, which was within this range.

During the design of the proof-of-concept specimen, the SBF was estimated using the approximate theory mentioned earlier. In future, a quasi three-dimensional finite element model will be developed for this purpose.

6.5 Hoop Stress Distribution and Load Transfer in Cracked Specimen

Figure 9 shows the hoop stress distribution in the proof-of-concept specimen for an advanced MSD situation, comprising a linked lead crack 7.04 cm (2.77 in) long through three rivets approaching a second crack 1.07 cm (0.42 in) long through one rivet. The stress distribution predicted using a finite element model is also shown. No similar data could be found in the literature for an actual aircraft, and so no attempt was made to design the specimen to produce a particular cracked stress distribution. Instead, the specimen was designed so that the stress in the side straps would approximately double in a fully cracked specimen. Based on the limited data found in

the literature, this approach was judged to give roughly representative load transfer characteristics, and was considered sufficient for proof of concept.

The predicted stress distribution matched the measured stress distribution except in the region of the shorter crack, where it was lower by 12%. The difference was probably due in part to the coarseness of the finite element mesh, which is discussed further in the next subsection.

6.6 Finite Element Model of MSD Test Specimen

To minimize computing time, the finite element model of the specimen was kept as simple as possible, consistent with obtaining agreement within 5% between predicted and measured values of hoop stress in a non-cracked specimen. Further refinement of the model has not yet been attempted. It was implemented in NISA2 commercial finite element code, as a two-dimensional model, in which the two sheets were joined by omni-directional spring elements at the rivet locations, as shown in **Figure 10**. The stiffness of the spring elements was set to represent the apparent shear stiffness of rivets in a similar splice. This information is available from empirically based formulae, such as those published by Swift [27] or Niu [28]. The model used 8-noded thin shell elements with 6.4 mm (1/4 in) sides to represent the sheets in the splice area. A graded mesh of larger elements was used elsewhere. The bond lines were assumed to be rigid, and the presence of straps and doublers was represented by increasing the thickness of the elements.

Figure 11 is a contour plot of the hoop stress distribution under a nominal 44.5 kN (10,000 lb) load. The graph of predicted hoop stress in **Figure 7** was constructed from this data. The nominal stress location was chosen to be along a line 2.54 cm (1 in) from the critical rivet row. This location was close to the splice, but was relatively free from the stress perturbations caused by the presence of the splice.

Cracks in the specimen were modelled by leaving nodes in adjacent elements in the same sheet disconnected (unmerged). The mesh was not refined at the crack tips, because accurate crack tip stresses were not required. The results are illustrated by the contours of hoop stress in **Figure 12**. There is one long crack, 7.00 cm (2.75 in) long, through 3 rivet holes and one short one, 1.27 cm (0.5 in), through 1 rivet hole. This was the model for the advanced MSD situation discussed earlier (**Figure 9**). The coarseness of the mesh limited the accuracy with which crack length and tip position could be represented. The main discrepancy was in the length of the smaller crack, which was 1.27 cm in the model and 1.07 cm in reality. This would account at least partly for the 12% underestimate of hoop stress in the vicinity of the small crack. Elsewhere, agreement was good. In future, a generally finer mesh will be developed for modelling cracks.

7 PROOF-OF-CONCEPT TEST RESULTS

7.1 Crack Growth Curves

Five specimens have been tested for initial proof-of-concept, and all developed crack patterns comparable to those in published cases of MSD. An overview of the crack growth curves plotted for the first of these specimens is in **Figure 13**. The graph plots crack length against load cycles at each rivet position. The vertical grid indicates the centers of the 8 rivets across the specimen, and the curves are oriented in the actual direction of crack growth.

Cracks were first observed on each side of rivet #3. Subsequently, cracks were observed at rivets #2 (left), #5 (left and right) and #4 (left), in that sequence. The first link-up occurred between rivets #3 and #4. At approximately the same time, cracks from #2 (right) and #3 (left) overlapped, as can be seen from the crossing of the two crack growth curves. The sudden accelerations evident in some of the crack growth curves occurred because link-ups elsewhere had increased the local stress intensity factor. The gaps between opposing curves represent the sizes of the ligaments between approaching crack tips one cycle before link-up, except in the case of #3-#4, where the last measurement was taken up to 50 cycles prior to link-up.

Similar overviews of multiple crack growth curves are shown for the second to fifth specimens in **Figure 14**. In these cases, the gaps between curves generally do not represent the final ligament sizes, because measurements of crack tip position were not taken immediately prior to link-up. As before, the crossing of opposing curves indicates that the approaching cracks overlapped. In some cases, these overlapped cracks subsequently linked up.

Cracks appeared in the third specimen much earlier than in the other four. This specimen had become contaminated with oil during manufacture. The oil probably reduced the load transfer through friction between the faying surfaces, and increased the load transfer at the rivets. The results provide evidence that the rate of initiation and early crack growth in splices are sensitive to the coefficient of friction between faying surfaces.

7.2 General MSD Characteristics in Specimen Tests

The crack patterns in all five specimens tested show a mixture of relatively uniform and non-uniform MSD typical of published cases of MSD. Despite pronounced asymmetric crack development in some cases, all specimens remained directionally stable on the load-frame until cracks had linked up across the full width of the specimen. The periods of growth between the first appearance of a crack, the first link-up, and the link-up of cracks across the specimen were as listed in **Table 2**.

Although there was no attempt to simulate closely the splice

geometry, manufacturing processes, stress level or interfaying surface treatments of any particular aircraft, it is interesting to compare the specimen test data in **Table 2** with the summary of published in-service and test data for Boeing aircraft, also shown in the table. This comparison indicates that early crack growth under the rivet heads in the specimen was significantly slower overall than on Boeing aircraft, except in one case. Subsequent crack growth rates were closer to those on Boeing aircraft, but still generally slower. These results confirm the need for close simulation of actual design and conditions, if useful results for a particular aircraft are to be obtained.

The proof-of-concept tests demonstrated the same general MSD characteristics as observed in published in-service and full-scale test data (listed earlier). In this context, the main observations and conclusions from the tests were as follows:

- a. The specimen test results confirmed that after the first link-up the aggregate crack growth rate of MSD within a frame-bay is very fast, possibly allowing less than two years at average utilization until the lead crack reaches critical proportions - typically a length of one to two frame-bays. It seems that, for some aircraft, inspection policy might have to be geared to detecting cracks before the first link-up.
- b. Comparison of the first two specimens with the remaining three confirmed that greater uniformity in the initiation pattern of MSD tends to reduce the growth period from first crack to first link-up, and from first link-up to a major lead crack. Clearly, the initiation pattern is important in this context, and should be assessed carefully for each aircraft type. The MSD specimen could be a cost-effective means of obtaining statistical data to support such an assessment.
- c. In light of the previous two observations, and the fact that striation counts on the Aloha aircraft indicated a long growth period under the rivet heads [5], it is highly desirable to find an economical means of detecting cracks under rivet heads.

7.3 The Mechanism of Link-up

During testing of the first specimen, the mechanism of link-up was studied closely. It appeared to involve a complex pattern of plastic distortion and necking across the full width of the ligament prior to fracture. Fast fracture prior to yielding was not observed. Link-up occurred at fairly small crack

Table 2. Crack Growth Statistics from First Five Specimens

	<i>First Crack</i>	<i>First Link-up</i>	<i>Fully Cracked*</i>	<i>Total Life</i>
<i>First specimen</i>	336,500 cycles	+70,000	+6,000	412,500
<i>Second specimen</i>	292,000 cycles	+70,500	+5,800	368,300
<i>Third specimen</i>	48,700 cycles	+28,000	+4,400	81,100
<i>Fourth specimen</i>	175,000 cycles	+52,500	+3,500	231,000
<i>Fifth specimen</i>	195,000 cycles	+60,500	+4,900	260,400
<i>Boeing (various)**</i>	21,000 to 79,000 cycles	+ 9,000 to +42,000	+1,000 to +10,000	

Notes: * "Fully cracked" here means continuously cracked through 8 rivet holes on the specimen and about 18 rivet holes across most of a frame-bay on Boeing aircraft.
 ** The data for Boeing aircraft is for published cases of MSD on several different narrow-body and wide-body aircraft having differences in fuselage and splice design, stress levels and planned life. The data are intended only to convey the order of magnitude of crack growth periods.

separations of 1.5 to 4.5 mm (0.06 to 0.18 in), and the size of the final ligament prior to link-up increased with crack size. Plastic failure of the ligaments of longer cracks occurred over 2 or 3 cycles in the specimen, as illustrated in **Figure 16**, indicating that the surrounding structure was providing a measure of displacement control. The changes in stress distribution and crack growth rates leading up to and following an overlap suggested that overlapped cracks could be modelled as linked cracks when the vertical separation is small (< 2 mm). No conclusions were drawn for larger vertical separations.

As a result of these observations link-up was defined in the computer model of MSD crack growth as occurring when the cracks, with Irwin plastic zone correction added, touch each other. This criterion was developed from ideas put forward by Swift in 1987 [29], and is logical for two reasons. Firstly, the crack tip plastic zone size in thin sheet is relatively large. Secondly, the criterion predicts larger final ligaments for longer cracks, as was observed on the test specimen.

When used in the computer model the link-up criterion produced accurate results. For the first proof-of-concept test specimen, the measured and predicted crack tip separations just prior to link-up are given in **Table 3**. The validity of the link-up criterion has not yet been studied at overload stress levels.

Table 3. Measured and Predicted Crack Tip Separations One Cycle Before Link-up (First MSD Test Specimen)

Linking Cracks.	Crack Tip Separation in mm (in)	
	Measured	Predicted*
#3Right/#4Left	< 2 (0.08)	1.5 (0.06)
#4Right/#5Left	1.5 (0.06)	2.8 (0.11)
#5Right/#6Left	2.5 (0.10)	2.8 (0.11)
#6Right/#7Left	4.5 (0.18)	3.5 (0.14)

* Using computer model of MSD crack growth

7.4 Comparison of Test Results with Computer Model of MSD Crack Growth in a Fuselage Splice

The computer program for predicting MSD crack growth can produce graphical output of multiple crack growth curves for the critical row of rivets in a splice in a few minutes on a personal computer. This computational speed has been achieved by using Rooke's technique [30] of compounding known stress intensity factor solutions to calculate the stress intensity factor for each crack tip. The interaction of all cracks and rivet holes in the row are taken into account.

The program requires inputs of splice geometry, initial hoop stress distribution, initial rivet loads, fatigue stress ratio, Young's modulus, and empirical data on crack growth rate (da/dN) vs. stress intensity factor range (ΔK). The timing of the visible initiation of each crack can be pre-defined by the user. This approach is appropriate for parametric studies and for comparisons between computed and experimental crack growth curves. If a probabilistic analysis is required, the user can add a subprogram to define visible initiation statistically based on experimental S-N curves for a comparable splice.

Computed crack growth curves for the first proof-of-concept test, are compared with the experimental curves in **Figure 17**.

For this computation, the pattern of visible initiation of the cracks was made to correspond to the pattern observed in the test specimen by gearing the visible initiation of each new crack to the length of an existing, adjacent crack. Good agreement between the measured and computed curves has been achieved, and so further development of this form of MSD analysis seems warranted. More detail on the computer program is included in Reference [31].

The program was used to predict the outcome of simultaneous visible initiation at all rivets in the proof-of-concept specimen. On an aircraft, this would be close to a worst case MSD scenario. The resulting crack growth curves are in **Figure 18**. The computer model indicated that the period from first crack to fully cracked would be 30,000 cycles. This is slightly shorter than measured for the third specimen, which had the most uniform cracking of the five specimens. It is less than 50% of the period measured for most of the other specimens. The results confirm earlier observations that the degree of uniformity in the crack pattern is of considerable significance from a damage tolerance standpoint.

7.5 Conclusions Regarding Proof-of-concept

The specification for a MSD specimen in **Table 1** addresses the shortcomings of conventional coupon specimens used for the fatigue testing of longitudinal fuselage splices. It is intended to result in an effective yet inexpensive means of investigating early crack growth and link-up in existing aircraft splices, and of performing parametric studies to improve the durability and damage tolerance characteristics of future designs and repairs. Though the proof-of-concept test specimen did not represent a particular aircraft exactly, the results of the five tests described herein give confidence that the specification can be met fully by the specimen concept described in this paper:

- The specimen produced MSD initiation patterns and link-up characteristics comparable to those described earlier for published cases of MSD in in-service aircraft and full-scale fuselage tests. Initiation lives were generally higher, and crack growth rates were generally slower than on Boeing aircraft. These data confirm that splice details and stress conditions will have to be simulated closely when tailoring the specimen to a particular aircraft.
- Specimens remained intact and directionally stable, even with asymmetric crack distributions. In every test, the growth and link-up of cracks could be monitored until the lead crack had grown through all rivets across the specimen. There were no premature failures or nuisance cracks.
- Effective and efficient strain gauge, photoelastic and finite element modelling techniques for adapting the MSD test specimen to different aircraft or research applications have been demonstrated.
- The specimens were inexpensive to design, manufacture and test relative to full-scale panel and fuselage test specimens.

It would now be appropriate to apply the MSD test specimen concept to a particular aircraft, in collaboration with the aircraft manufacturer. This process would be used to determine how closely the specimen can simulate the stresses and fatigue characteristics of the aircraft, and to explore how the specimen might be integrated into a fuselage damage tolerance test programme.

8 TAILORING THE MSD SPECIMEN TO A PARTICULAR AIRCRAFT

Based on experience gained with the design and testing of the proof-of-concept specimen, the following steps are proposed for tailoring the MSD test specimen to a specific aircraft in the future:

- a. Obtain the nominal frame-bay hoop stress distribution on the aircraft (2.54 cm from the upper rivet row) for a non-cracked splice. Repeat the measurements for one or more crack configurations, including an advanced MSD situation, in which there is a long lead crack and one or more smaller cracks in the same frame-bay. Optional methods are:
 - standard strain gauges on each side of the skin of an aircraft or full-scale test (FST) article, placed similarly to typical specimen instrumentation for nominal stress in **Figure 5**; or
 - a finite element model of the fuselage, like the one discussed in Reference [13].
- b. Obtain the out-of-plane bending stress distribution on the aircraft along a line making a tangent to the rivet holes. Optional methods are:
 - laminated strain gauges on the external skin of an aircraft or FST article, like the one discussed in connection with splice loading and stresses; or
 - standard strain gauges on the external skin and within the splice on a FST article, installed similarly to typical specimen instrumentation for bending in **Figure 5**; or
 - a finite element model of the fuselage, including a local model of the splice.
- c. Obtain a photoelastic image from the aircraft of maximum shear strain contours in the external surface of the same non-cracked splice and surrounding skin as in a. above, using the special image processing technique discussed in connection with splice loading and stresses.
- d. Tailor the MSD specimen to simulate as closely as possible the stress distributions obtained in steps a., b., and c. above. For this purpose, use a finite element model like the one described in the last section.
- e. Manufacture two prototype specimens with full instrumentation per **Figure 5**. Insert simulated cracks in one specimen that match the crack configuration on the aircraft, FST article or fuselage finite element model as used in step a. above. Perform static tests on the two specimens to confirm that the non-cracked and cracked hoop stress distributions match those of the aircraft at the nominal location 2.54 cm (1 in) from the critical rivet row. Also confirm that the non-cracked bending stress distribution at the critical rivet row matches that of the aircraft.
- f. Manufacture one prototype specimen for photoelastic analysis. Test it to confirm that the image of maximum shear stress contours matches the one taken from the aircraft.

9 CONCLUSION

The uniaxial coupon test specimen concept described in this paper will allow fairly realistic fatigue crack growth testing of longitudinal fuselage splices to be done inexpensively relative to full-scale panel and fuselage test articles. In this respect, the specimen fills a gap in test capability noted by the Industry Committee on WSFD. The specimen concept has been implemented as a 25.4 cm (10 in) wide specimen for proof-of-concept testing, using a design and stress distribution that are roughly comparable to those of longitudinal fuselage splices in current narrow-body jet transport aircraft. The design and proof-of-concept testing of this specimen have been outlined in a way that illustrates how the specimen simulates the dominant fatigue loading of a fuselage splice, and how the concept would be tailored to simulate a splice within a frame-bay of a specific aircraft.

All five specimens tested to date produced typical MSD cracks. The visual initiation, growth and link-up characteristics of these cracks can be seen in crack growth curves presented in this paper. The specimen concept, together with its design and manufacturing methodologies, has been validated as far as is possible using the limited aircraft stress and other data in the open literature. It would now be appropriate to apply the MSD test specimen concept to a specific aircraft, in collaboration with the aircraft manufacturer. This process would provide a full assessment of the specimen concept, together with useful data in support of fuselage damage tolerance analysis and future splice design.

A computer program that predicts MSD crack growth has been developed as a companion to the specimen. Crack growth curves predicted with this program compare favourably with test results from the MSD specimen. The computer model will be useful for preliminary parametric studies and in the determination of efficient test matrices.

ACKNOWLEDGEMENTS

This work was funded by the National Research Council of Canada, Carleton University, the Natural Sciences and Engineering Research Council of Canada, and the Canadian Department of National Defence (FA 220794NRC08).

REFERENCES

1. Schmidt, H.J., and Brandecker, B., "Results of the AAWG Committee on Widespread Fatigue Damage", in "Durability of Metal Aircraft Structures", Atlanta Technology Publications, 1992.
2. Foster, M. and Komorowski, J.P., "Image Processing System with Special Routines for Automated Analysis of Photoelastic Images - User Manual", Institute for Aerospace Research, National Research Council, ST-613 31 January 1991.
3. Schutz, D. and Lowak, H., "The Effect of Secondary Bending on the Fatigue Strength of Joints", Laboratorium für Betriebsfestigkeit Report FB-113 (1974), RAE library translation No. 1858 August 1975.
4. Hartman, A. and Schijve, J., "The Effect of Secondary Bending on the Fatigue Strength of 2024-T3 Alclad Rivetted Joints", NLR TR 69116U December 1969.

5. Part 2 of the U. S. National Transportation Safety Board Report on the Fuselage Failure of an Aloha Airlines Boeing 737-200 in April 1988, published in Aviation Week and Space Technology 4 September - 15 September 1989.
6. Maclin, J.R., "Performance of Fuselage Pressure Structure", in "1991 International Conference on Aging Aircraft and Structural Airworthiness", NASA CP 3160, p67-74.
7. Tong, P., "Multiple Site Damage", in "2nd Annual International Conference on Aging Aircraft October 1989", report DOT/FAA/CT-89/39, p90-98.
8. Goranson, U., "Continuing Airworthiness of Aging Jet Transports", in "2nd Annual International Conference on Aging Aircraft October 1989", report DOT/FAA/CT-89/39, p61-89.
9. Bobo, S.N., "Non-destructive Testing of Aging Aircraft", in "FAA Aging Aircraft NDT Workshop", October 1989, p18-33.
10. Mayville, R.A. and Warren, T.J., "A Laboratory Study of Fracture in the Presence of Lap splice Multiple Site Damage", in "Structural Integrity of Aging Airplanes", Springer Verlag 1991, p 263-273.
11. Swift, T., letter to P.V.Straznicky, Carleton University, 1991.
12. Piascik, R.S., Scott, A.W. and Miller, M., "The Characterization of Widespread Fatigue Damage in Fuselage Structure", in "FAA/NASA International Symposium on Advanced Structural Integrity Methods for Airframe Durability and Damage Tolerance", NASA CP 3274 September 1994, p563-579.
13. Miller, M., Gruber, M.L., Wilkins, K.E. and Worden, R.E., "Full-scale Testing and Analysis of Fuselage Structure", in "FAA/NASA International Symposium on Advanced Structural Integrity Methods for Airframe Durability and Damage Tolerance", NASA CP 3274 September 1994, p481-496.
14. Jarfall, L., "Shear Loaded Fastener Installations", SAAB-SCANIA report KH R-3360 15 April 1983.
15. Schijve, J., "Multiple-Site-Damage Fatigue of Riveted Joints", in "Durability of Metal Aircraft Structures", Atlanta Technology Publications, 1992.
16. Lee, E.U., "Effect of Load Transfer on Fatigue of Mechanically Fastened Joints", in "Fatigue and Mechanically Fastened Composite and Metallic Joints", J. Potter, Ed., ASTM STP 927, 1986.
17. Ozleton, M.W. and Coyle, T.G., "Fatigue Life Improvement by Cold Working Fastener Holes in 7050 Aluminium", in "Fatigue and Mechanically Fastened Composite and Metallic Joints", J. Potter, Ed., ASTM STP 927, 1986.
18. Speakman, E.R., "Advanced Fastener Technology for Composite and Metallic Joints", in "Fatigue and Mechanically Fastened Composite and Metallic Joints", J. Potter, Ed., ASTM STP 927, 1986.
19. Pelloux, R., Warren, A. and O'Grady, J., "Fractographic Analysis of Initiation and Growth of Fatigue Cracks at Rivet Holes", in "Structural Integrity of Aging Airplanes", Springer Verlag 1991, p293-308.
20. Bellingier, N.C., Krishnakumar, S. and Komorowski, J.P., "Modelling of Pilling Due to Corrosion in Fuselage Lap Joints", Canadian Aeronautics and Space Journal, Vol. 40, No. 4, December 1994, p125-130.
21. US Department of Transportation advisory Circular "Damage-tolerance and Fatigue Evaluation of Structure", AC 25.571-1A, 3 May 1986.
22. Broek, D., "Elementary Engineering Fracture Mechanics", Kluwer 1986.
23. Vlieger, H., "Results of Uniaxial and Biaxial Tests on Riveted Fuselage Lap Joint Specimens", in "FAA/NASA International Symposium on Advanced Structural Integrity Methods for Airframe Durability and Damage Tolerance", NASA CP 3274 September 1994, p911-931.
24. Wanhill, R.J.H., De Luccia, J.J. and Russo, M.T., "The Fatigue in Aircraft Corrosion Testing (FACT) Programme", AGARD Report No. 713, February 1989.
25. van der Linden, H.H., Ed., "Fatigue Rated Fastener Systems", AGARD-R-721 November 1985.
26. Miller, M., Kaelber, K. and Worden, R.E., "Finite Element Analysis of Pressure Vessel Panels", in "Durability of Metal Aircraft Structures", Atlanta Technology Publications, 1992.
27. Swift, T., "The Application of Fracture Mechanics to the Development of the DC-10 Fuselage", AGARD-AG-176 January 1974, p226-287.
28. Niu, M.C.Y., "Airframe Structural Design", Conmillit Press, 1988.
29. Swift, T., "Damage Tolerance in Pressurized Fuselages - 11th Plantema Memorial Lecture", 14th Symposium of the International Committee on Aeronautical Fatigue (ICAF) June 1987.
30. Rooke, D.P., "Compounding Stress Intensity Factors - Applications to Engineering Structures", The Parthenon Press 1986.
31. Eastaugh, G.F., Straznicky, P.V. and Simpson, D.L., "Multiple Site Damage in Fuselage Skin Splices - Experimental Simulation and Theoretical Prediction", Canadian Aeronautics and Space Journal, Vol. 40, No. 4, December 1994, p151-157.

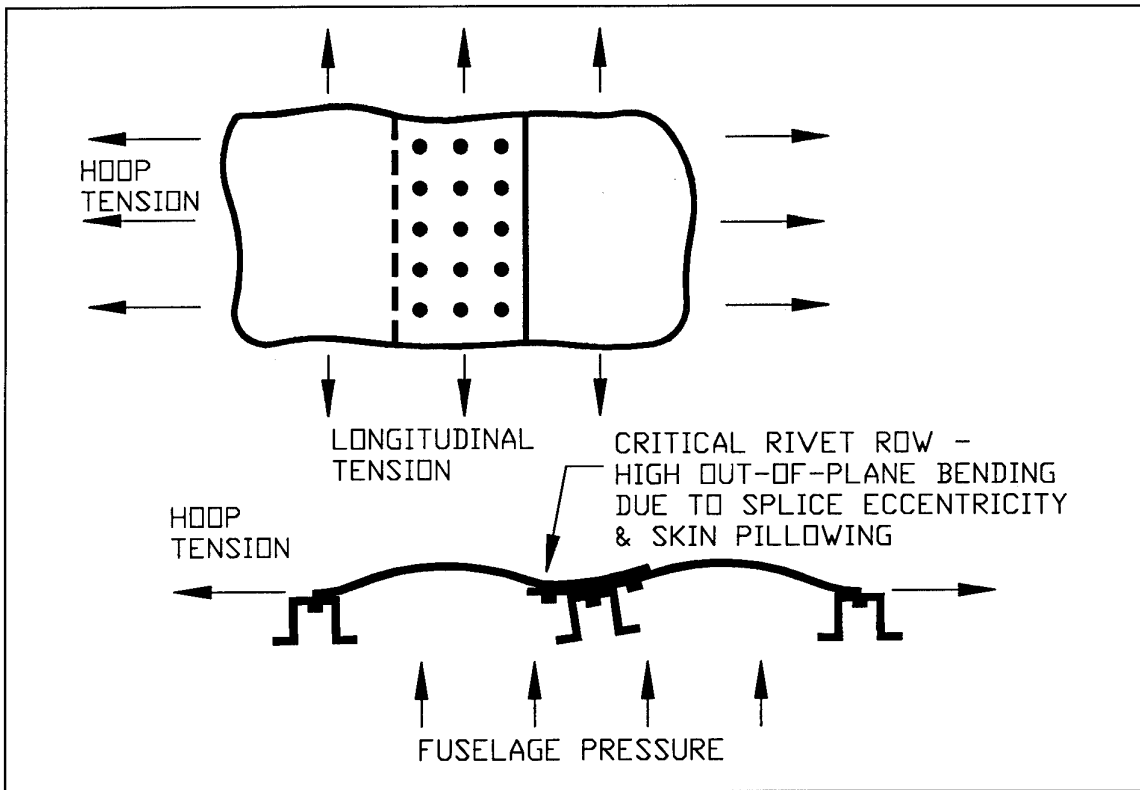


Figure 1 Loads on a longitudinal splice due to fuselage pressurization.

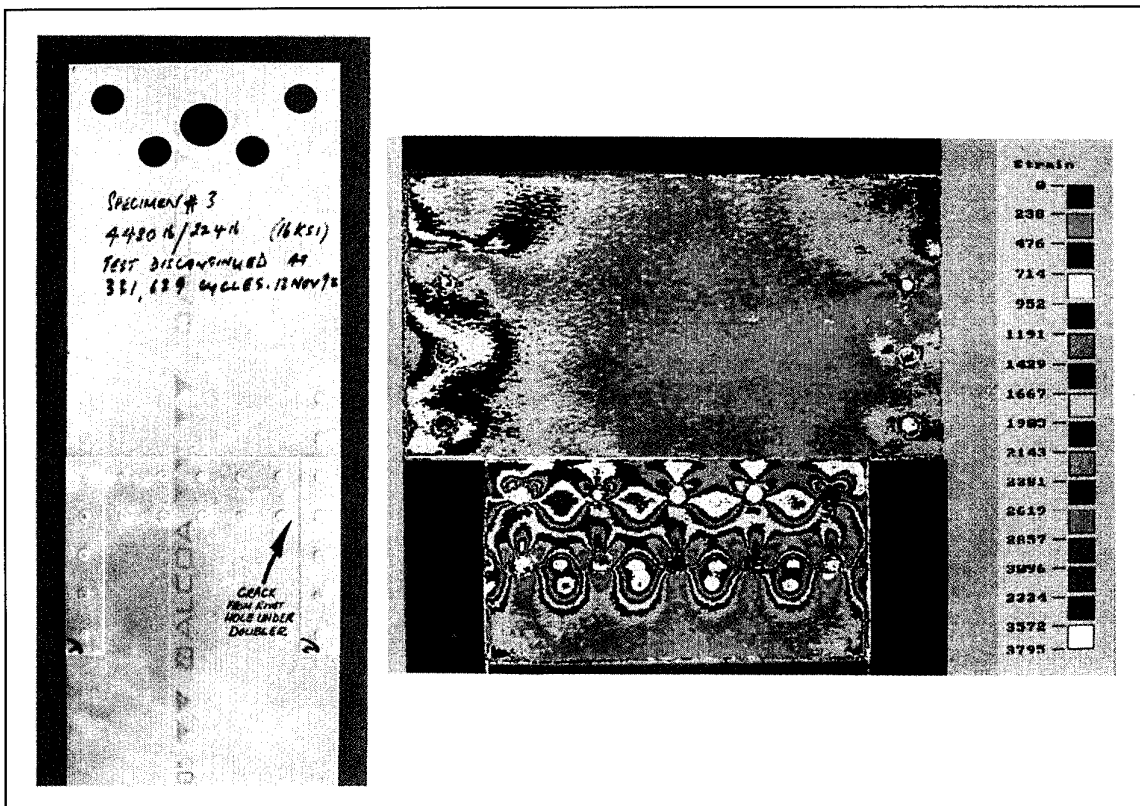
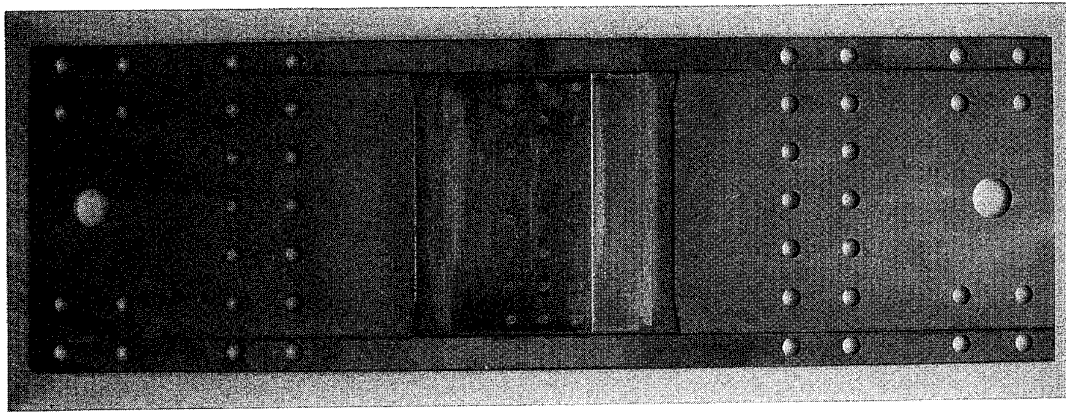


Figure 2 Photoelastic contours of maximum shear strain for a preliminary two-row lap splice specimen under tension. (Specimen has rivetted doublers at its edges)

Countersunk Side



Driven Side

BONDED DOUBLER

BONDED SIDE STRAP

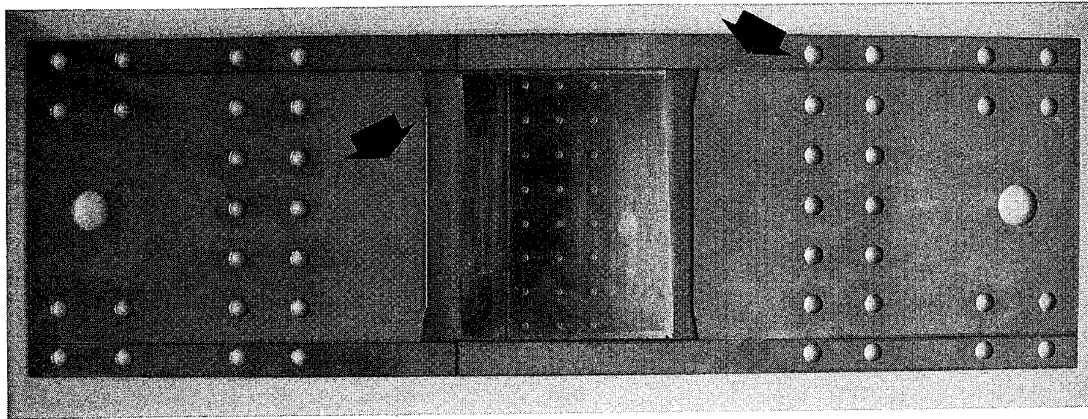


Figure 3 Optimum MSD test specimen concept - full length bonded side straps and full width bonded doublers - implemented here as 25.4 cm (10 in) wide specimen for proof-of-concept testing.

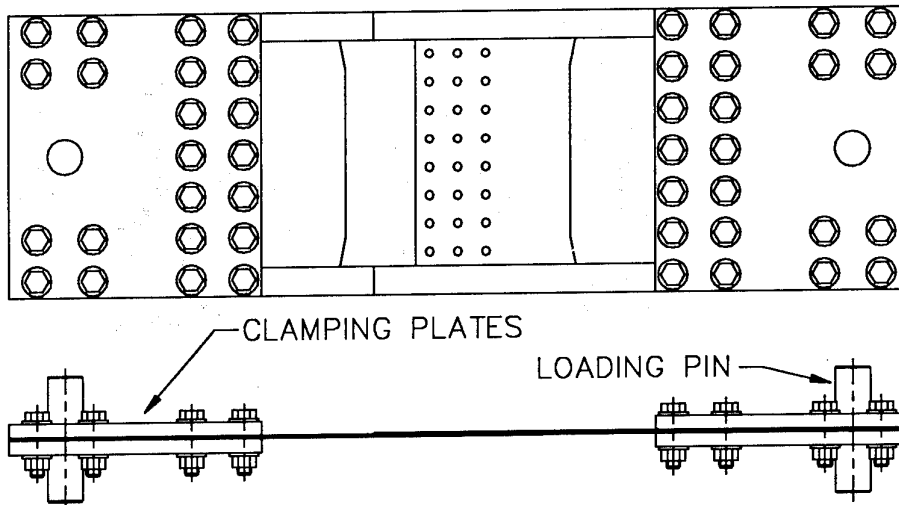


Figure 4 Concept for mounting MSD test specimen in load-frame.

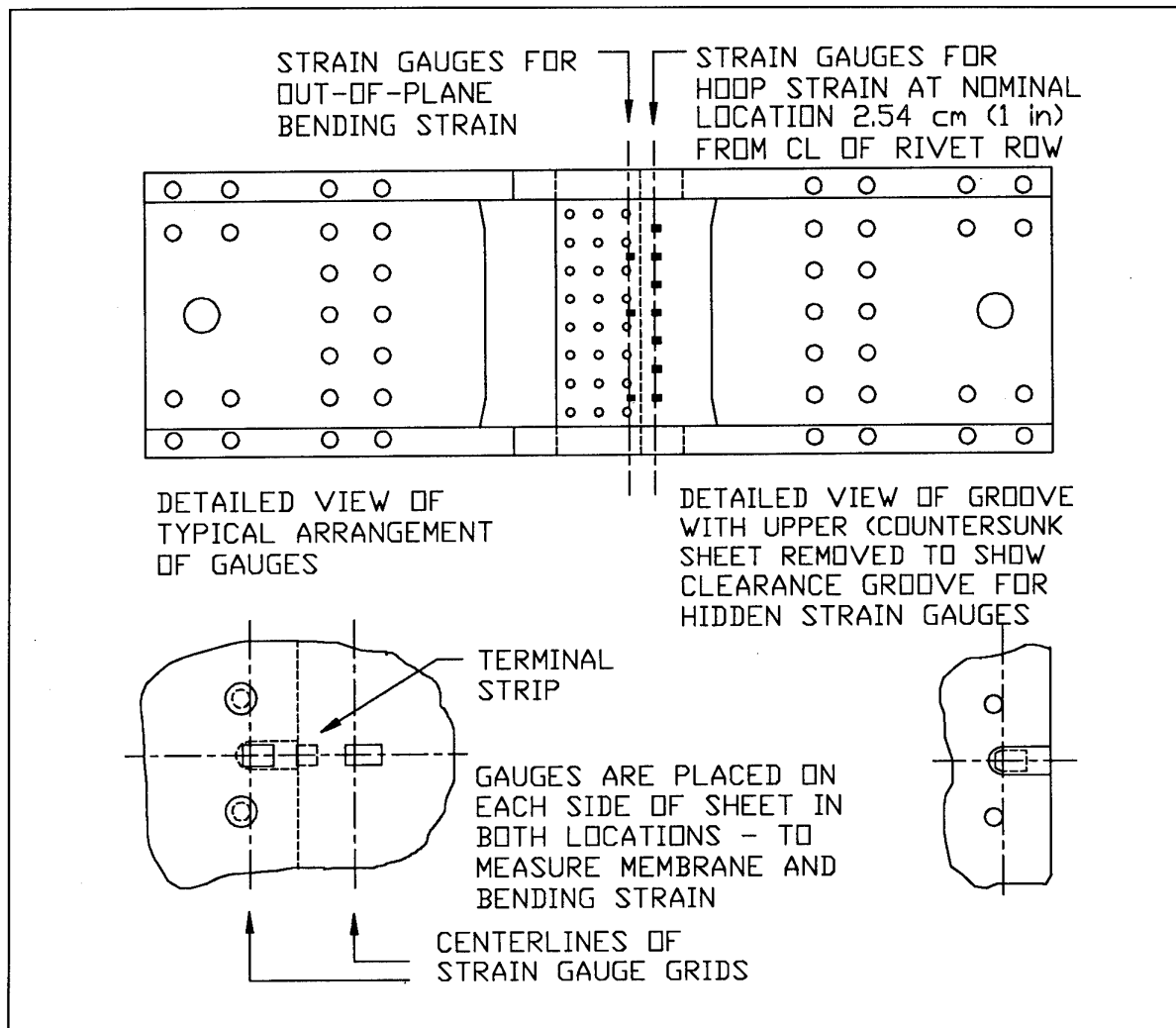


Figure 5 Typical strain gauge installation for MSD test specimen.

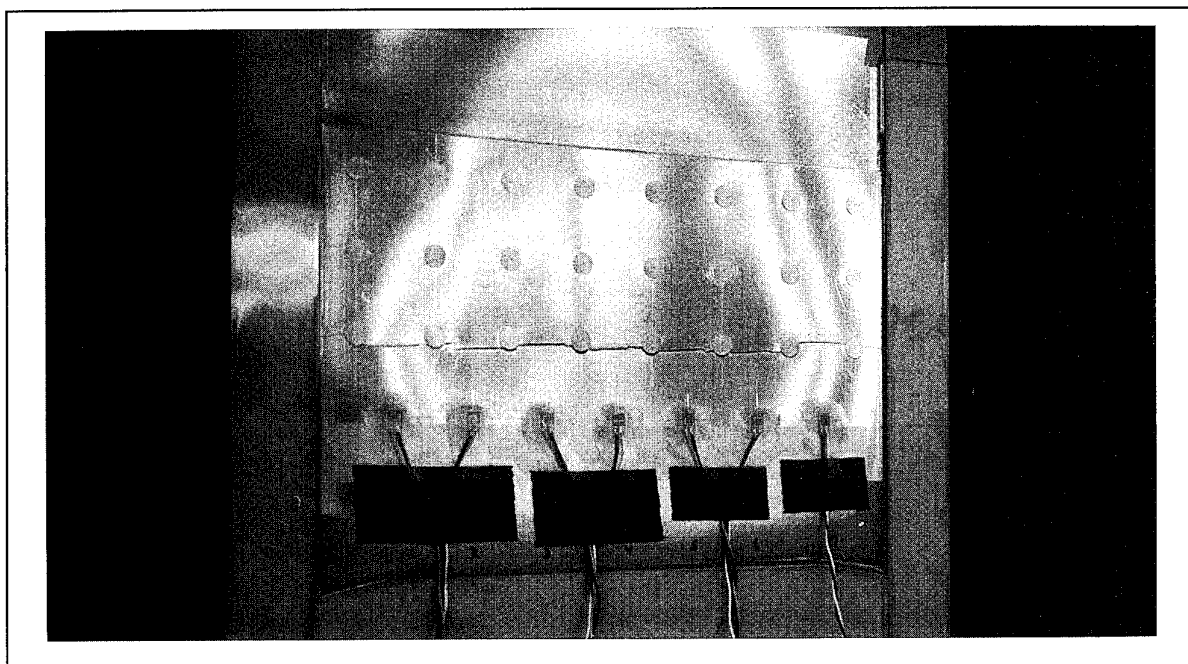


Figure 6 Fully cracked MSD test specimen under 32.1 kN (7,219) lb load.

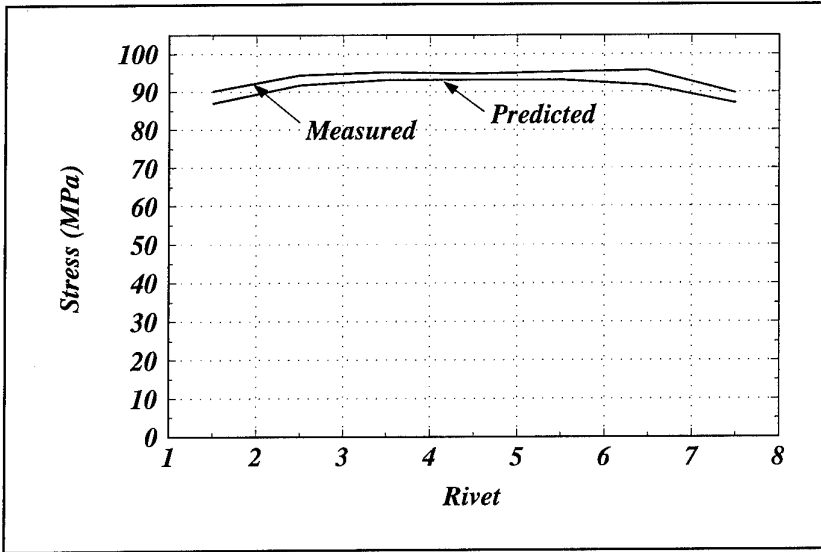


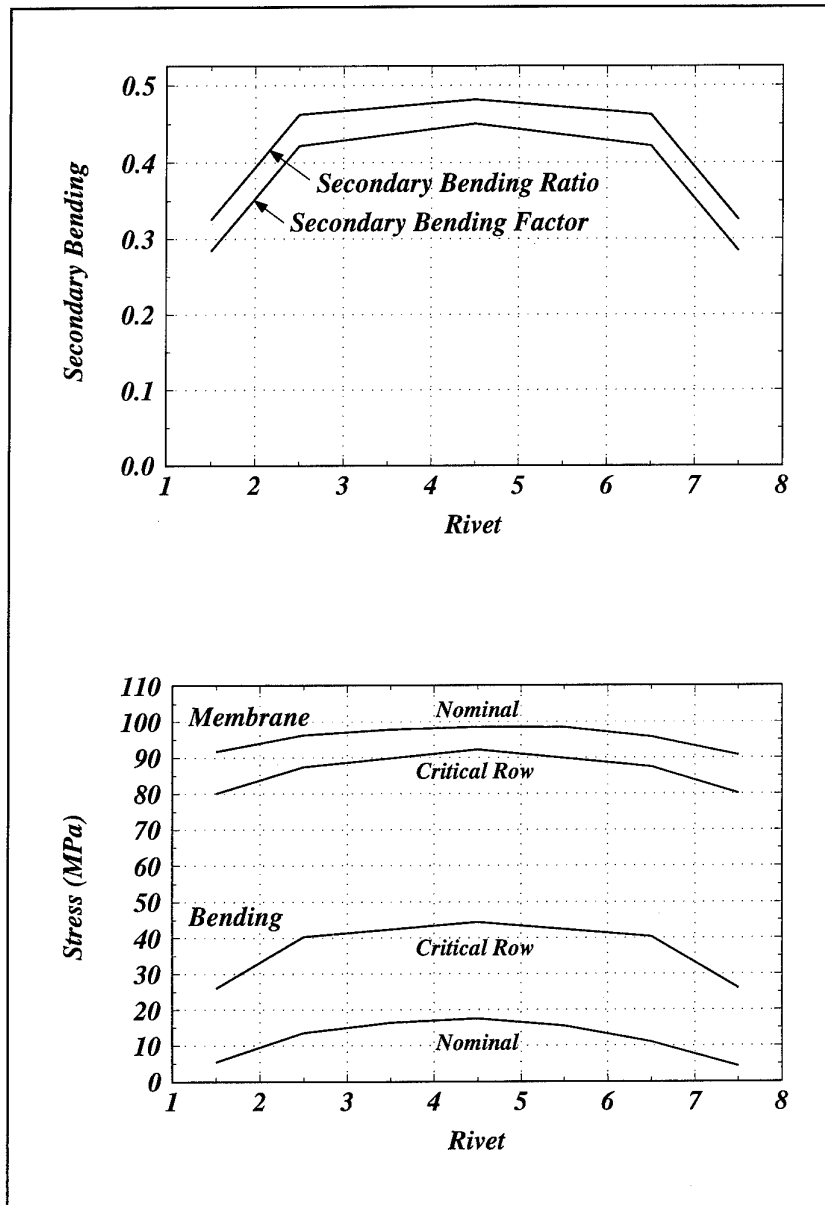
Figure 7

Measured and predicted non-cracked hoop stress distributions across the first MSD test specimen at the nominal location 2.54 cm (1 in) from the critical rivet row.

Figure 8

Measured non-cracked membrane (hoop) stress and secondary bending stress distributions across the fourth MSD test specimen: at the nominal location 2.54 cm (1 in) from the critical rivet row; and along a tangent to the critical row of rivet holes. Upper graph shows secondary bending ratio and factor at critical rivet row derived from lower graph.

(Bending ratio = bending stress/local membrane stress.
Bending factor = bending stress/nominal membrane stress)



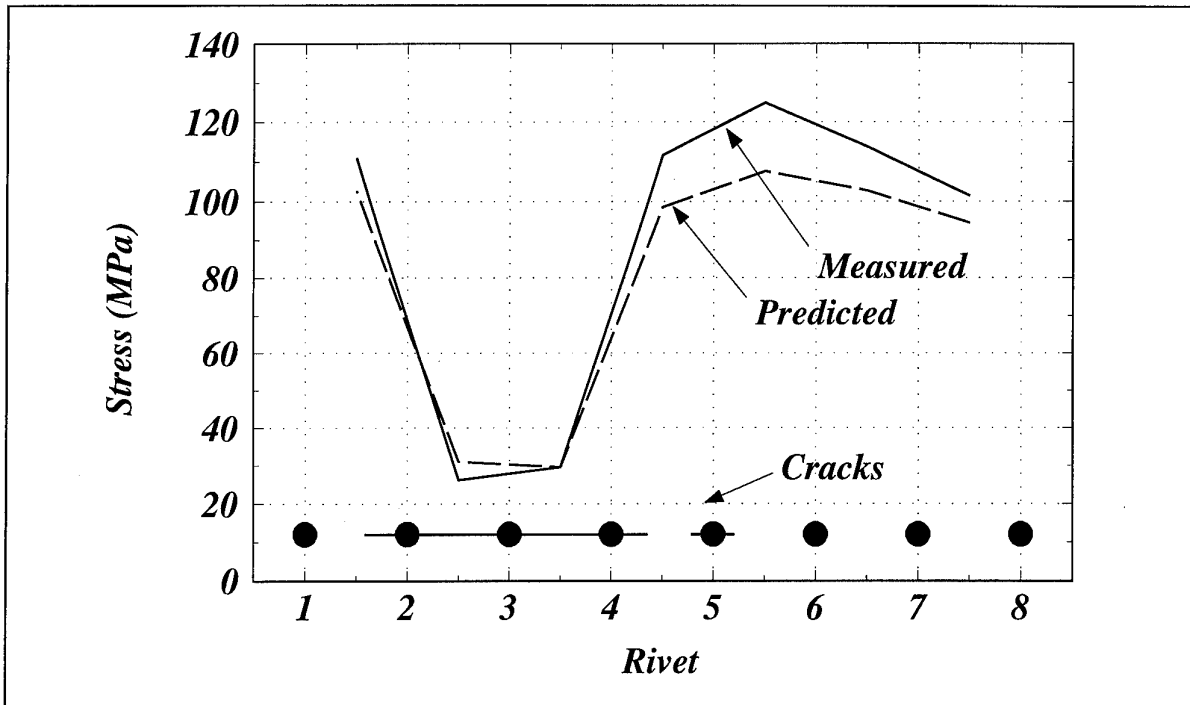


Figure 9 Measured and predicted hoop stress distributions across the first MSD test specimen with a lead crack 7.04 cm (2.77 in) long approaching a smaller crack 1.07 cm (0.42 in) long.

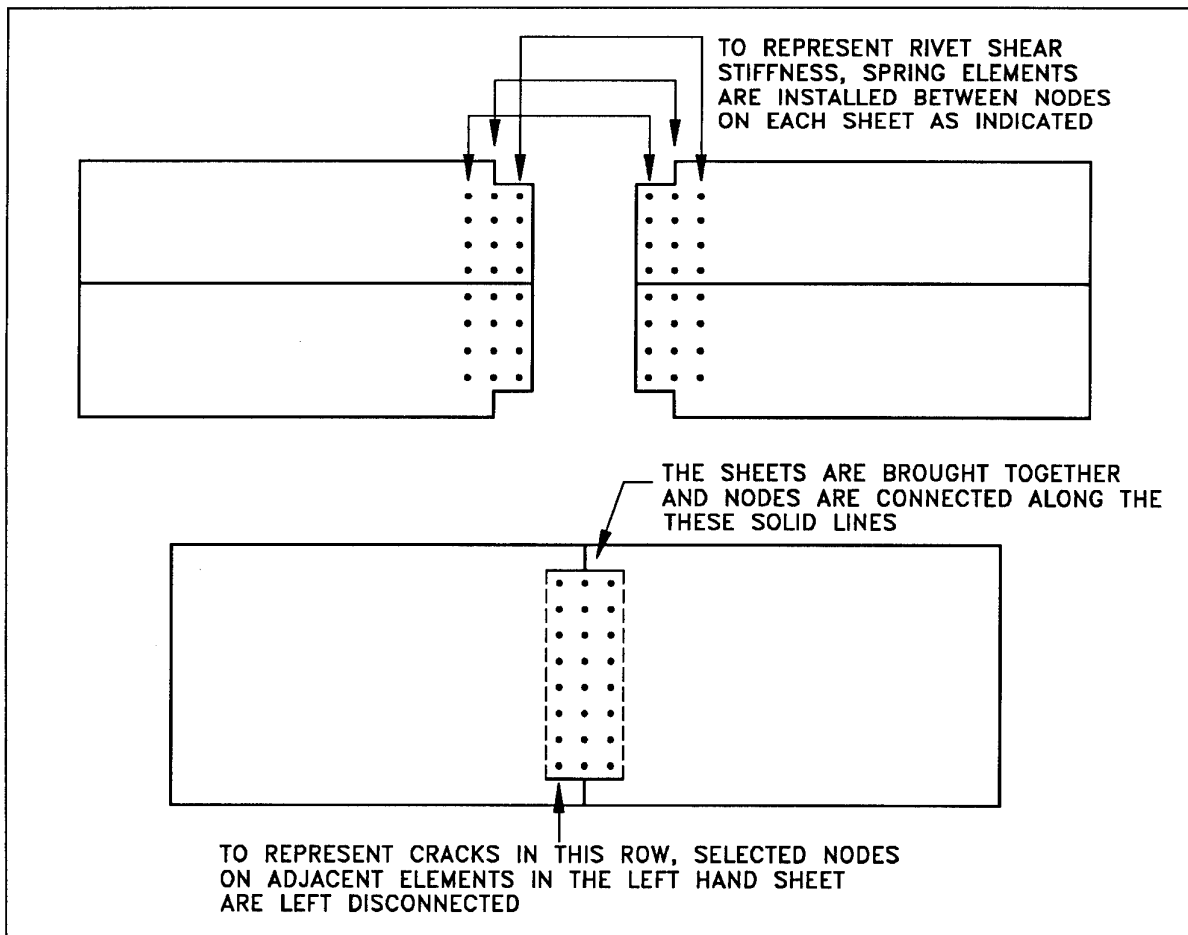


Figure 10 Process of constructing the finite element model of the MSD test specimen.

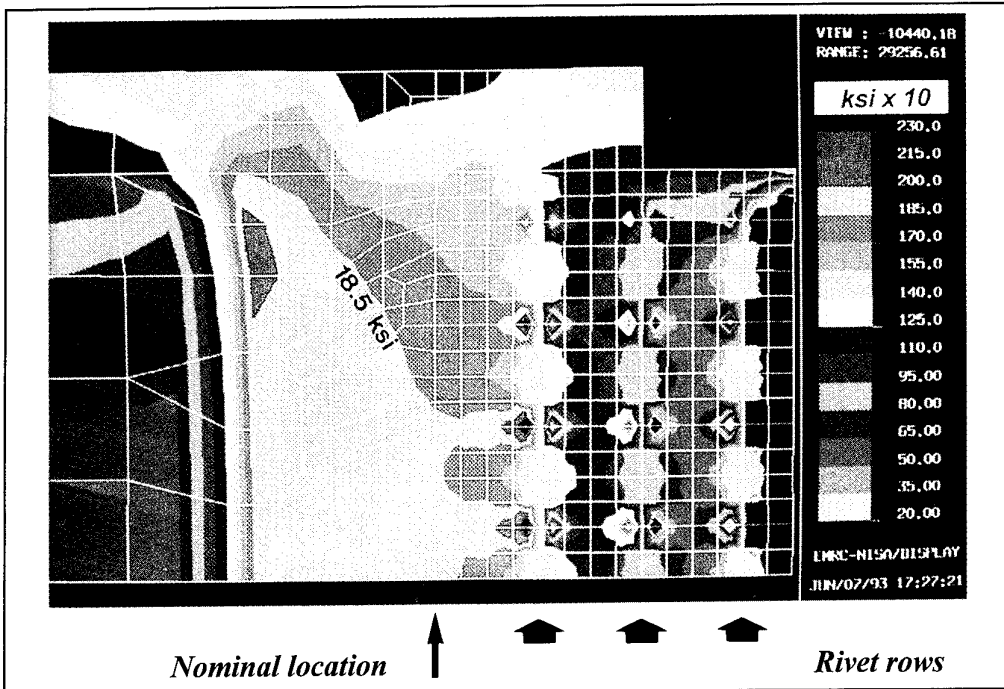


Figure 11 Hoop stress contours in half-width finite element model of MSD test specimen without cracks loaded to 44.5 kN (10,000 lb) - contours steps 10 MPa (1.5 ksi).

Figure 12

Hoop stress contours in finite element model of MSD test specimen with cracks loaded to 44.5 kN (10,000 lb) - contour steps 24 MPa (3.5 ksi).

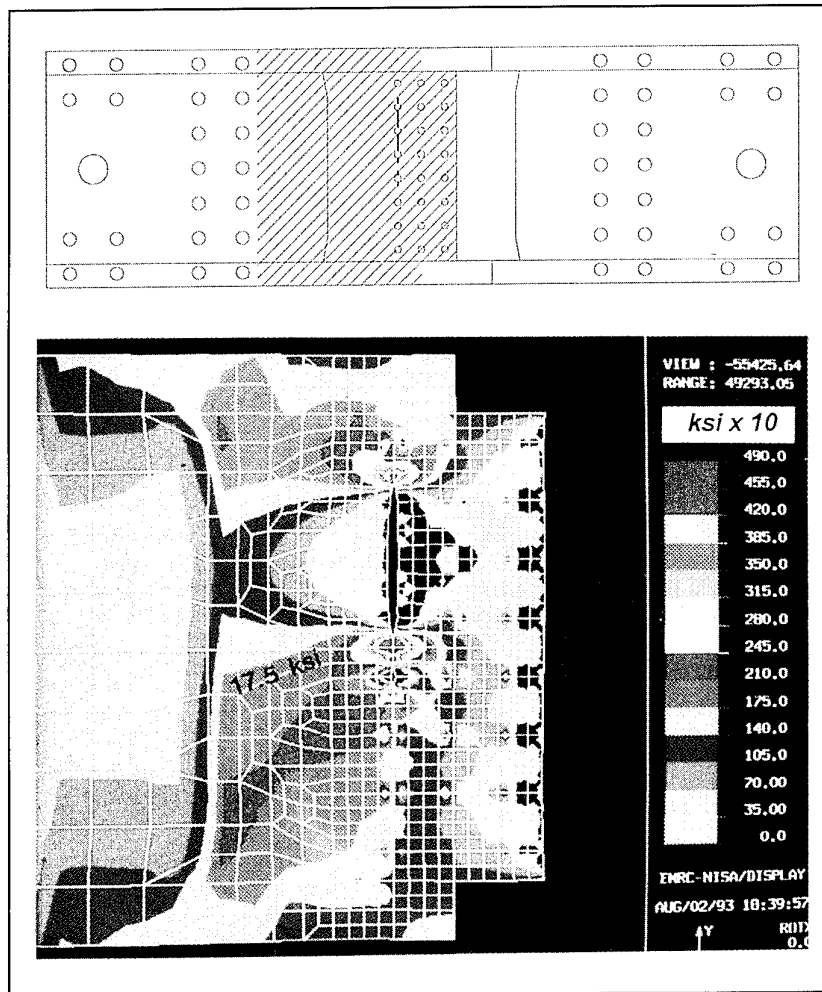


Figure 13

Overview of all crack growth curves measured on the first MSD test specimen - actual rivet spacing 2.54 cm (1 in).

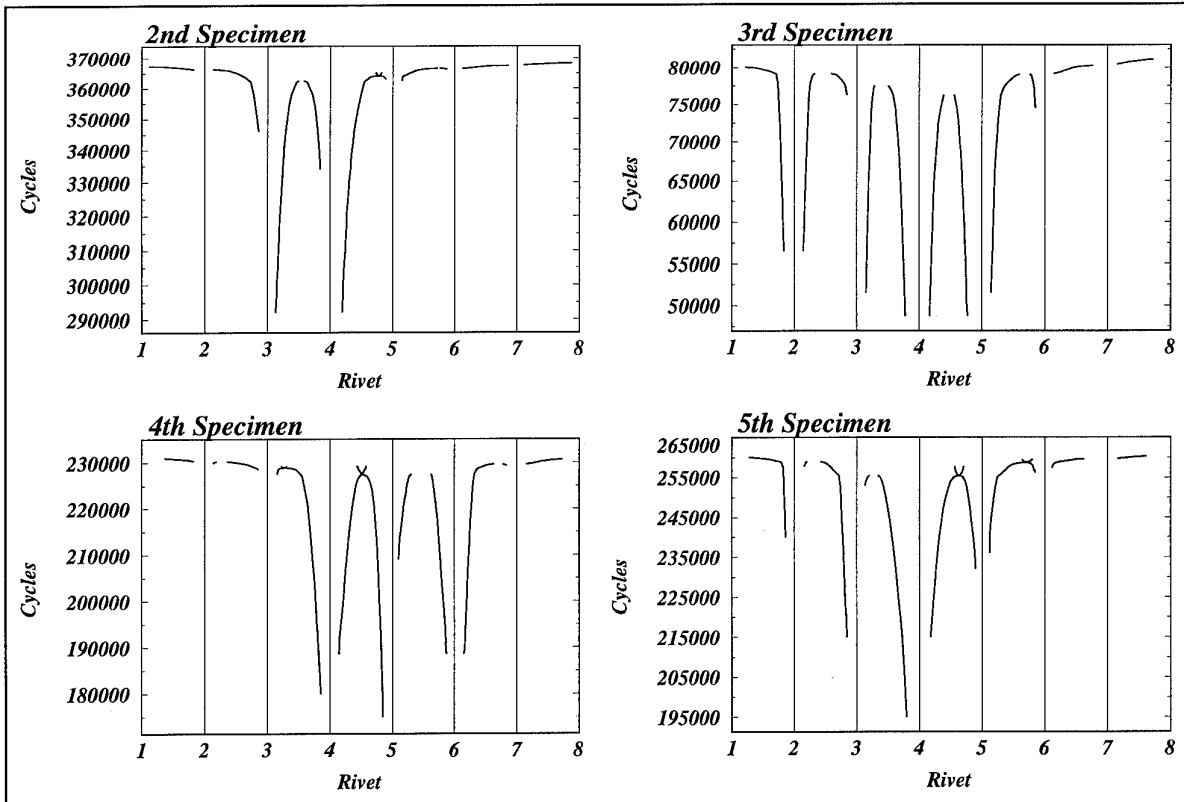
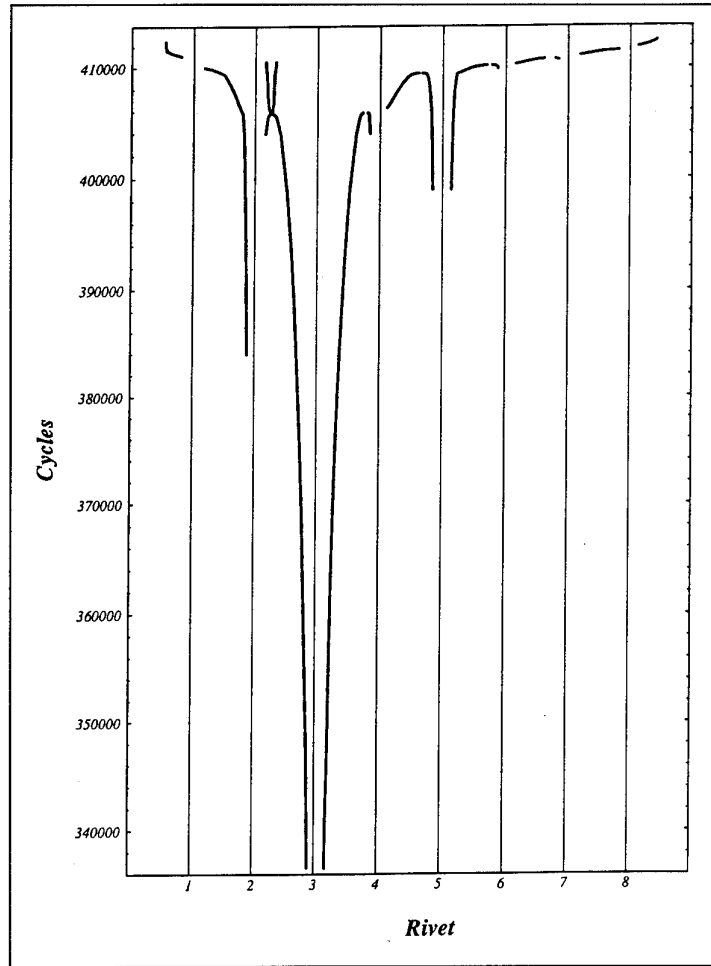


Figure 14 Crack growth curves measured on the second to fifth MSD test specimens.

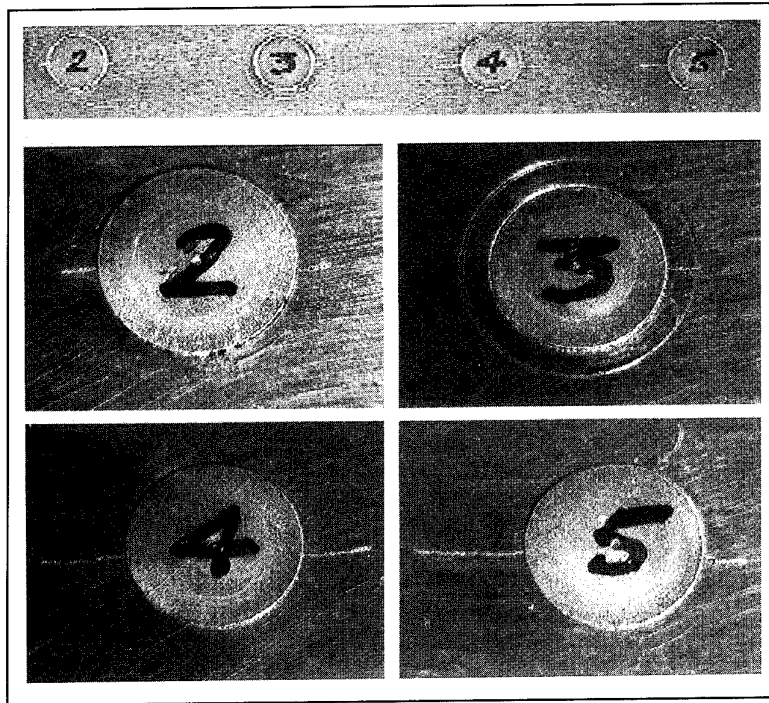


Figure 15

Photograph of fatigue cracks in the third MSD test specimen during proof-of-concept testing.

Figure 16

Microscope photographs of the progressive failure over three load cycles of a ligament during link-up of a 10.7 cm (4.2 in) lead crack (left) and a 0.8 cm (0.3 in) crack (right) in the first MSD test specimen - scale approximate and not exactly the same in each photograph.

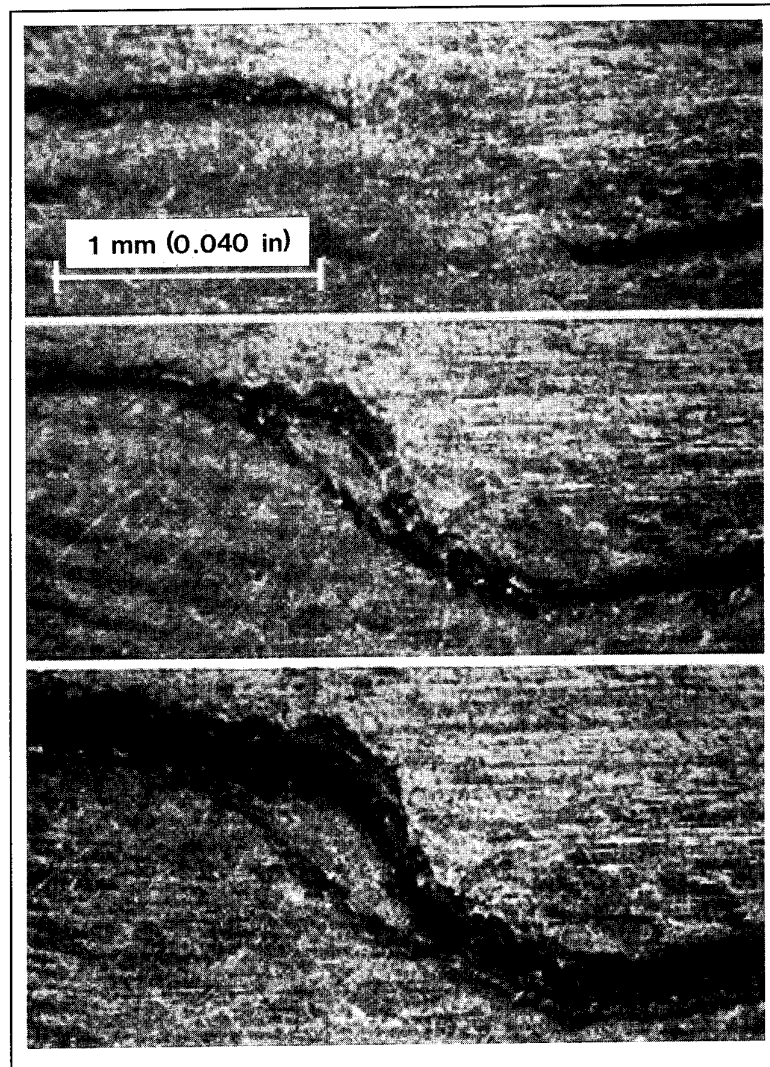


Figure 17

Comparison of measured and predicted crack growth curves for the first proof-of-concept test of the MSD test specimen.

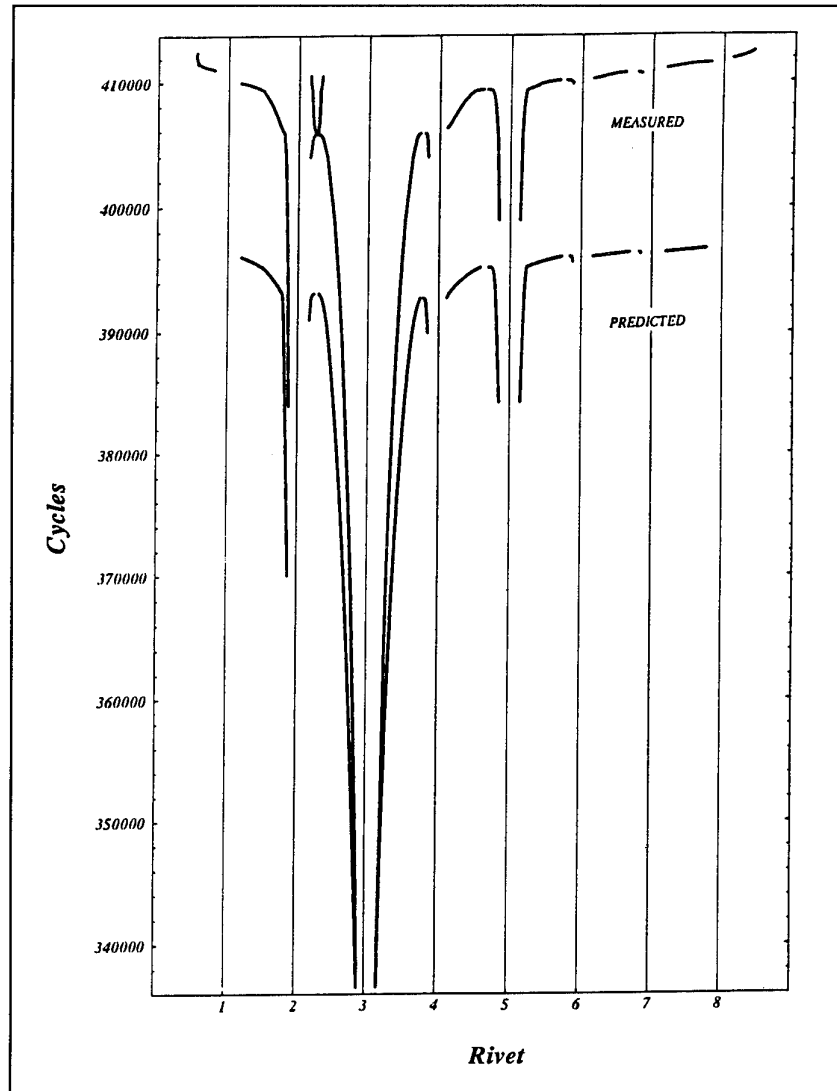
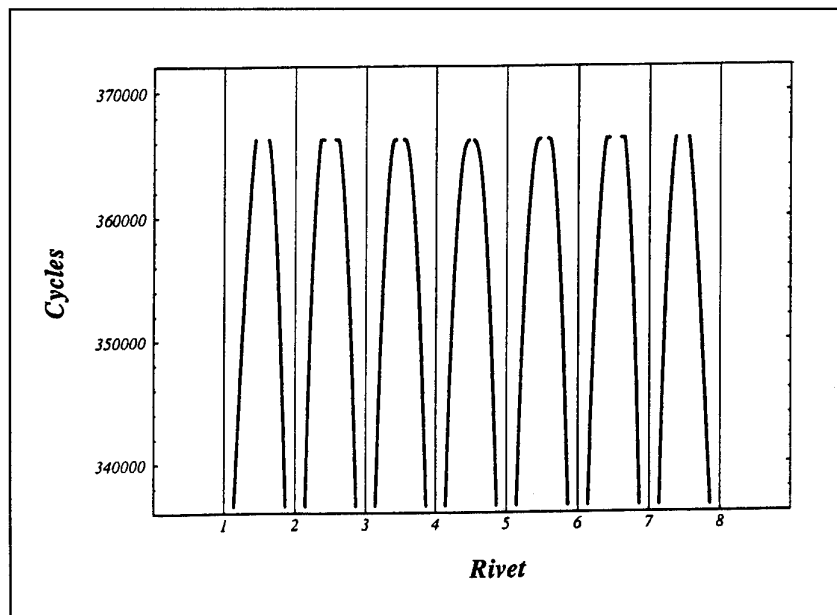


Figure 18

Overview of predicted crack growth curves assuming simultaneous visible initiation of cracks at all rivets.



FRACTURE ANALYSIS OF STIFFENED PANELS UNDER BIAXIAL LOADING WITH WIDESPREAD CRACKING

J.C. Newman, Jr.
NASA Langley Research Center
Hampton, Virginia, 23681-0001
USA

and

D.S. Dawicke
Analytical Services and Materials, Inc.
Hampton, Virginia, 23681-0001
USA

1. SUMMARY

An elastic-plastic finite-element analysis with a critical crack-tip-opening angle (CTOA) fracture criterion was used to model stable crack growth and fracture of 2024-T3 aluminum alloy (bare and clad) panels for several thicknesses. The panels had either single or multiple-site damage (MSD) cracks subjected to uniaxial or biaxial loading. Analyses were also conducted on cracked stiffened panels with single or MSD cracks. The critical CTOA value for each thickness was determined by matching the failure load on a middle-crack tension specimen. Comparisons were made between the critical angles determined from the finite-element analyses and those measured with photographic methods. Predicted load-against-crack extension and failure loads for panels under biaxial loading, panels with MSD cracks, and panels with various number of stiffeners were compared with test data, whenever possible. The predicted results agreed well with the test data even for large-scale plastic deformations. The analyses were also able to predict stable tearing behavior of a large lead crack in the presence of MSD cracks. The analyses were then used to study the influence of stiffeners on residual strength in the presence of widespread fatigue cracking. Small MSD cracks were found to greatly reduce the residual strength for large lead cracks even for stiffened panels.

2. INTRODUCTION

Aging of the commercial transport fleets around the world increases the possibility of a reduction or loss of structural integrity through fatigue cracking. Widespread fatigue damage (cracks developing at several adjacent locations) is of great concern because the residual strength of a stiffened structure with a single long crack may be significantly reduced by the existence of adjacent smaller cracks as postulated by Swift [1]. Whereas a single long crack in a fuselage structure may produce flapping, a process by which a cracked fuselage would peel open in a small local region and lead to safe decompression, a fuselage with a long lead crack and multiple-site or multiple-element damage (MSD or MED) cracking may not flap. Tests on panels with long lead cracks and MSD are showing that residual strengths are strongly degraded [2]. Current fuselage designs must rely upon periodic inspections to assure safe operation [3]. One of the objectives in the NASA Aging Aircraft Research Program [4] is to develop the methodology to predict flapping or failure in damaged fuselage structures in the presence of MSD or MED. The approach is to use a finite-element shell code with global-local, adaptive mesh capabilities and appropriate local fracture criteria to predict progressive failure in complex structures. In the future, fuselage structures may be designed by analysis, and verified by tests, to produce flapping or improved crack arresting capability under MSD or MED conditions.

Stable crack growth in metallic materials have been studied extensively using elastic-plastic finite-element methods [5-15]. These studies were conducted to develop efficient techniques to simulate crack extension and to examine various local and global fracture criteria. These criteria included crack-tip stress or strain, crack-tip-opening displacement or angle, crack-tip force, energy release rates, J-integral, and the tearing modulus. Of these, the crack-tip-opening angle (CTOA) or displacement (CTOD) was shown to be the most suited for modeling stable crack growth and instability during the fracture process. deKoning [7] showed that CTOA was nearly constant from initiation in an aluminum alloy. Shih et al [10] and Kanninen et al [11], in fracture analyses of both steel and aluminum alloys, showed that CTOA at initiation was much larger than the value needed for stable crack growth. Newman [12] used critical CTOD (or CTOA) values obtained from compact specimens to predict failure loads for several other crack configurations (two aluminum alloys and a very ductile steel) within 10 percent. Brocks and Yuan [13], Newman et al [14], and Demofonti and Rizzi [15] found that CTOD or CTOA was nearly constant after a small amount of crack growth for various materials and thicknesses. In some cases, the region of stable tearing where CTOD or CTOA was not constant appeared to be related to thickness but this region has not been defined quantitatively and its sensitivity to numerical calculations needs to be studied further.

Numerous investigators have also experimentally measured CTOA or CTOD during fracture. Luxmoore et al [16] showed that CTOA was constant from the onset of stable crack growth in two aluminum alloys, but found different values for different configurations. Paleebut [17], using a laser-interferometric displacement technique, measured CTOD (δ_i) at the initiation of stable tearing in compact specimens made of two aluminum alloys; these results agreed well with numerical values that Newman [12] used to model initiation, stable tearing and instability. Reuter et al [18], using microtopography [19], measured CTOD at the initial crack-front location and found a nearly linear relationship

with crack extension for low-strength steel. These results would imply that CTOA was nearly constant from initiation for some materials. Newman et al [20] and Dawicke et al [21,22] using a high-resolution camera with a video system, have measured the critical angles during stable crack growth in aluminum alloys. These results also indicate that CTOA was constant after a small amount of tearing (greater than the sheet thickness) for several crack configurations. The non-constant CTOA region was associated with severe tunneling during the initiation of stable tearing.

To develop the fracture methodology to predict the influence of widespread fatigue cracking on fuselage structures, the behavior of multiple cracks in thin-sheet materials subjected to biaxial loading with various stiffener conditions, typical of fuselage structure, must be tested and analyzed. Recent tests, sponsored by the U.S. Federal Aviation Administration (FAA) Technical Center, were conducted by Broek et al [23] and deWit et al [24] on flat panels made of 2024-T3 aluminum alloy sheet with a wide variety of MSD crack configurations. These tests provided a large database on the effects of MSD cracking on residual strength. Newman et al [25], using the elastic-plastic finite-element analysis, has demonstrated that the CTOA criterion can accurately model the stable tearing behavior of multiple cracks. Donne and Doker [26], recently conducted fracture test on 2024-T3 cruciform specimens subjected to biaxial loading. Many years ago, Leybold [27] and Vlieger [28] conducted fracture tests on 2024-T3 sheet panels with either 2024 or 7075 aluminum alloy stiffeners (intact or broken). These types of tests form the framework for establishing the creditability of the CTOA fracture criterion for predicting stable tearing and fracture of complex structure.

The objective of the present paper was to use the critical CTOA fracture criterion to study stable tearing and failure of 2024-T3 aluminum alloy panels (bare and clad) under a wide variety of loading conditions. Analyses were conducted on panels with single cracks under either uniaxial or biaxial loading, panels with multiple-site damage

(MSD) cracking, and cracked stiffened panels. A two-dimensional, elastic-plastic (incremental flow theory, small strain), finite-element analysis (FEA) was used to model the fracture process. The critical CTOA value for each material thickness was determined by matching the failure load on a middle-crack tension specimen.

Comparisons were then made between measured and predicted load-against-crack extension and failure loads for panels under biaxial loading, panels with MSD cracks, and panels with various number of stiffeners. The analyses were then used to study the influence of stiffeners on residual strength in the presence of widespread fatigue cracking.

3. NOMENCLATURE

A_C	Cross-sectional area of crack or notch, mm ²
A_S	Cross-sectional area of stiffener, mm ²
B	Specimen thickness, mm
c	Crack length (see Fig. 1), mm
c_i	Initial crack length, mm
D	Rivet diameter, mm
d	Minimum element size along crack line, mm
d_T	Spacing between multiple cracks, mm
E	Young's modulus, MPa
L	Total length of all cracks, mm
L_C	Initial length of lead crack, mm
L_T	Length of each small MSD crack, mm
P	Applied load, kN
p	Rivet pitch, mm
S	Applied stress, MPa
S_k	Peak stress during crack linkup ($k = 1$ to 3), MPa
S_n	Net-section stress, MPa
S_f	Gross failure stress, MPa
W	Specimen width, mm
W_s	Stringer width, mm
β	Biaxial load or stress ratio
Δc	Crack extension, mm
δ_i	Critical sawcut displacement at initiation of crack, mm
λ	Stiffener ratio defined by A_S/A_C
μ	Stiffener ratio defined by A_S to total panel cross-sectional area
σ_{ys}	Uniaxial yield stress (0.2% offset), MPa
σ_u	Uniaxial tensile strength, MPa
ψ_C	Critical crack-tip-opening angle, degrees

4. MATERIALS AND CRACK CONFIGURATIONS

Several 2024-T3 aluminum alloy material thicknesses were analyzed. Four materials were the bare alloy (1 to 6 mm-thick) and the other materials were the clad alloy (1 or 2 mm-thick). These materials are summarized in Table 1. For all material thicknesses, middle-crack tension specimen test results, with either sawcuts or cracks (see Fig. 1), were used to determine the fracture parameters to simulate sawcuts (δ_i) and cracks (ψ_C) in the finite-element analysis. Guide plates were used to help prevent buckling in all tests.

Table 1.- Critical CTOA determined from 2024-T3 M(T) specimens using the FEA.

Condition	B, mm	δ_i , mm	ψ_C , degs.	Ref.
Alclad	1	0.075	5.1	23
Bare	1	0.2	3.4 (a)	24
Bare	1.6	0	6.0	27
Alclad	2	0.2	6.5	28
Bare	2.3	0	6.0	20-22
Bare	6	0	5.0	26

(a) Buckling may have occurred during test (measured ψ_C was 5.5 degs.).

Tests on the 2.3-mm thick bare alloy were conducted at NASA Langley on three specimen types: middle-crack tension M(T), compact tension C(T), and three-hole-crack tension (THCT) specimens, as shown in Figure 1. The M(T) specimens were 76 and 305 mm-wide, the C(T) specimens were 152.4 mm-wide, and the THCT specimens were 305 mm-wide. All specimens were fatigue precracked at a low stress level to produce a sharp fatigue crack. The THCT specimen simulates a crack growing in a stiffened panel, in that, the stress-intensity factor solution [12] is quite similar. Test results are reported in references 20-22.

Fracture tests were conducted by Broek et al [23] and deWit et al [24] on M(T) and multiple-site damage (MSD) specimens made of the

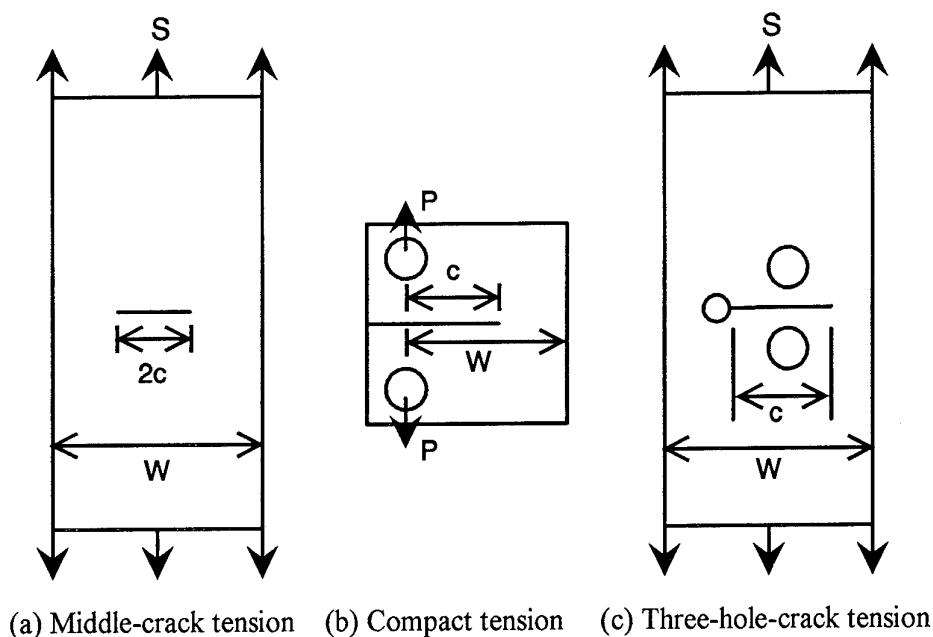


Fig. 1 - Laboratory fracture specimens tested and analyzed.

1 mm-thick clad and bare alloy, respectively. A typical MSD specimen is shown in Figure 2. The clad specimens were 508 mm-wide and the bare specimens were 2300 mm-wide. In both test programs, sawcuts were used instead of fatigue cracks. The MSD specimens contained a large lead sawcut (such as Sawcut #3) and anywhere from 2 to 20 MSD sawcuts.

Donne and Doker [26] conducted fracture tests on M(T) and cruciform (biaxial) specimens made of 6 mm-thick material. The M(T) specimen was 250 mm-wide and the biaxial specimens were 300 mm-wide in the test section. The biaxial specimen is shown in Figure 3. Both specimen types had fatigue cracks.

Leybold [27] and Vlieger [28] conducted fracture tests on 2024-T3 sheet panels with either 2024 or 7075 aluminum alloy stiffeners. The stiffened panel tests by Leybold had a single intact 2024 stringer, as shown in Figure 4(a). The stiffener width, W_s , and thickness was varied to give a stiffness ratio (λ) of 0.2 or 1. The stiffness ratio was defined as the ratio of stringer cross-sectional area to notch area. The panels had a very sharp notch of various lengths. The tests by Vlieger [28] had a central sawcut in a sheet with five 7075 stringers with the central stringer broken, as shown in Figure 4(b). In

both test programs, the specimen widths were about 300 mm.

5. FINITE-ELEMENT ANALYSIS OF STABLE TEARING

An elastic-plastic finite-element code, ZIP2D, was used in the current study [12,25,29]. The elastic-plastic analysis employed the initial-stress concept of Zienkiewicz et al [30] which is based on incremental flow theory and the small-strain assumption. A multi-linear representation of the uniaxial stress-strain curve for 2024-T3 (and 7075-T6 for stringers) was used in the analyses with the von Mises yield criterion.

The finite-element models for all crack configurations analyzed were composed of two-dimensional, constant-strain, triangular elements. All sawcuts and cracks were located along a straight line, defined as the X-axis (see Fig. 4a). Symmetry was employed whenever possible to reduce the number of degrees-of-freedom. The minimum element size (d) along the line of crack extension was about 0.5 mm. This value has been found to be adequate for analyzing stable tearing in a wide variety of materials, as shown by Newman [12]. Equal-lateral triangles were used along the crack line so that cracks moving in either the positive or negative X-direction, such as in MSD crack configurations, would

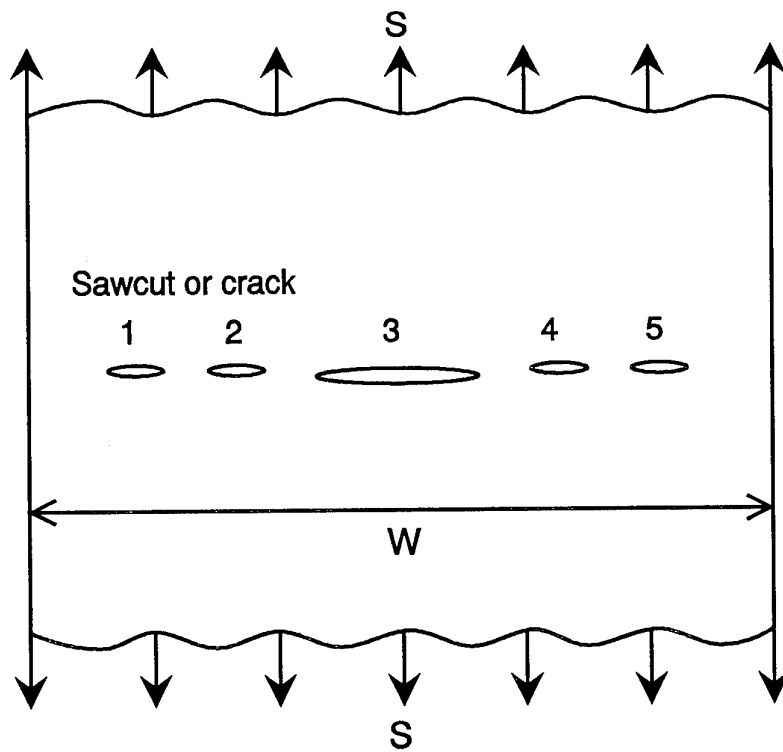


Fig. 2 - Multiple-site damage (MSD) crack configuration.

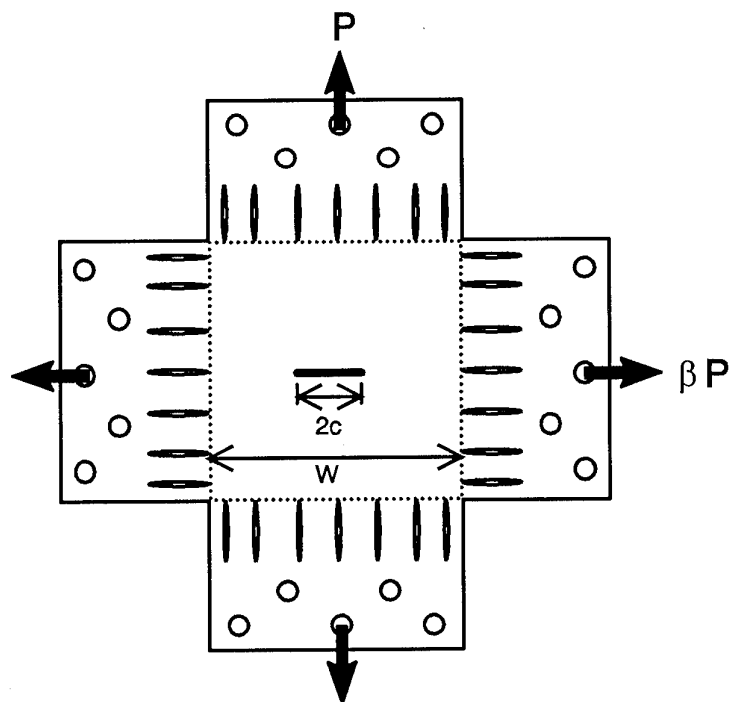


Fig. 3 - Cracked panel subjected to biaxial loading.

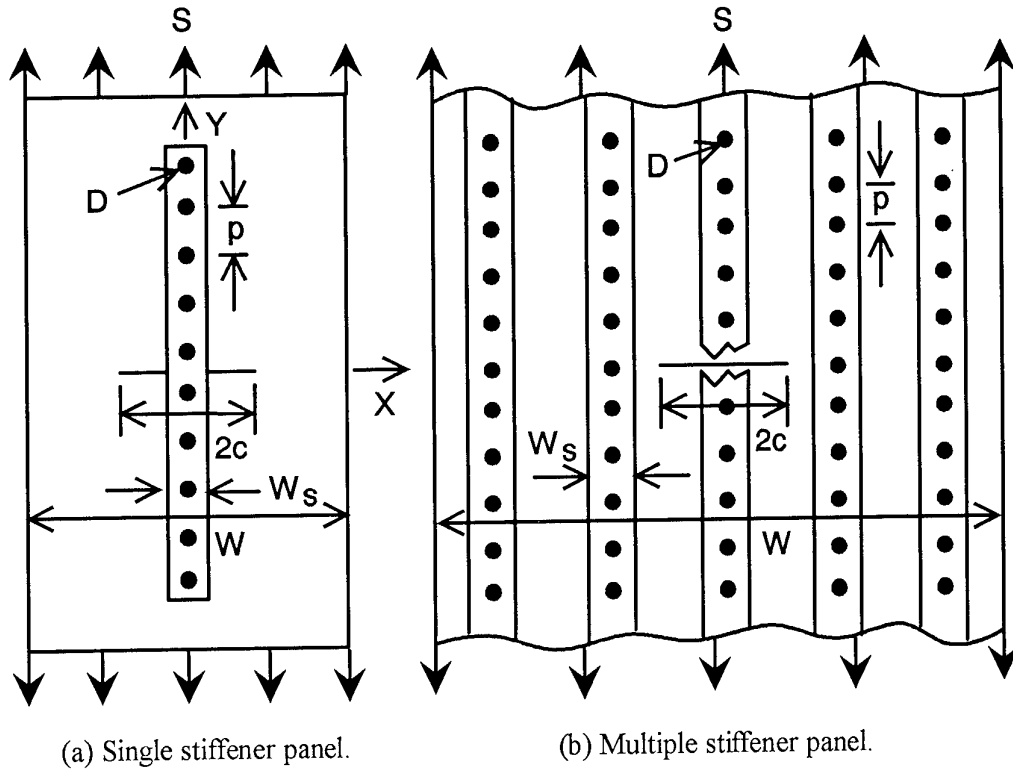


Fig. 4 - Types of cracked stiffened panels analyzed.

experience the same local mesh pattern. This pattern was found to be necessary to maintain nearly symmetric crack extension for the MSD crack configurations. Fictitious springs were used to fix displacement boundary conditions along the X-axis and to change boundary conditions associated with crack extension. For free nodes along the crack line, the spring stiffness were set equal to zero; for fixed nodes, the stiffness were assigned extremely large values. See reference 12 for details on the elastic-plastic finite-element analysis with crack extension and reference 25 for crack extension of multiple cracks.

In the FEA, a critical value of CTOA (ψ_c) was chosen as the fracture criterion for stably tearing cracks. Whenever the CTOA equaled or exceeded a preset critical value (ψ_c) during incremental loading, the crack-tip node was released and the crack advanced to the next node. This process was repeated until crack growth became unstable under load control or the crack reached the desired length under displacement control. The critical ψ_c value was

selected by trial-and-error to match the average failure load measured on several M(T) specimens.

To simulate the effects of a sawcut, a critical sawcut displacement, δ_i , was selected to model the deformations that take place at a sawcut before a crack would initiate. Again, the critical value was selected to match the load require to initiate a crack at the sawcut. Once a crack had initiated, the critical angle was used to grow the crack. Table 1 gives a summary of the critical fracture parameters determined from various thickness 2024-T3 aluminum alloy M(T) specimens. These fracture parameters were used to predict stable crack extension and failure of the MSD crack configurations, the biaxially-loaded specimens, and the cracked stiffened panels.

6. CRITICAL CTOA MEASUREMENTS

Photographic techniques have been developed to measure critical CTOA values during crack initiation and stable tearing on several different types of laboratory specimens. In one method, a

high-resolution optical microscope connected to a video system was used to record images of the deformed crack surfaces [21,22]. In each frame, the critical value of CTOA was measured at several locations behind the crack tip. For consistency, a standard distance from 0.5 to 1.5 mm was selected. In the second method, a digital-imaging correlation (DIC) method [31] was used to record digitized images of speckle patterns around the crack-tip location. These two methods produced essentially the same CTOA values during stable tearing. A detailed description of these methods are given in Dawicke and Sutton [21].

Stable crack growth experiments were conducted on three specimen types: middle-crack tension M(T), compact tension C(T), and three-hole-crack tension (THCT) specimens, see Newman et al [20]. The standard laboratory specimens, M(T) and C(T), were selected to illustrate the influence of specimen type and loading on critical CTOA values. The THCT specimen was selected to measure CTOA in a structurally-configured specimen. The THCT specimen has a stress-intensity factor solution similar to a cracked stiffened panel [12]. The critical CTOA was measured during the fracture process on these three specimens. The results are shown in Figure 5. The critical angle ψ_c is plotted against crack extension, Δc . For each increment of crack extension, several values of ψ_c were measured and the average is plotted. The initial fatigue crack surfaces were flat and showed a small amount of tunneling in the interior. During the early stage of stable tearing, however, the crack front exhibited severe tunneling in the interior and the crack surfaces were still relatively flat [21,22]. The vertical line indicates the approximate location where the crack surfaces had completed the transition from flat to shear mode fracture (45 deg. slant through the thickness). The ψ_c values measured during crack initiation were high but dropped sharply during crack extensions equal to about the sheet thickness. Afterwards, the critical angle appeared to level off between 5 to 7 degrees. The solid horizontal line is the ψ_c value (6 degs.) determined from the FEA to fit the failure loads on several M(T) test specimens.

Newman et al [20] and, later, Dawicke and Sutton [21] traced the reason for the high CTOA values during crack initiation to severe crack-front tunneling and the large plastic deformations on the specimen surface (recorded with the photographic methods).

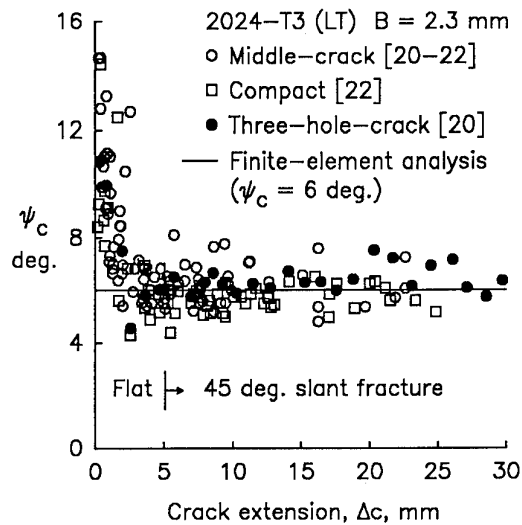


Fig. 5 - Measured and calculated critical CTOA.

7. DETERMINING CRITICAL CTOA FROM MIDDLE-CRACK TENSION SPECIMENS

The method used to determine the critical CTOA from a fracture test on a 6 mm-thick M(T) specimen is illustrated in Figure 6. The applied load is plotted against crack extension (measured by electrical potential [26]). From the FEA using the full stress-strain curve of the material, a trial-and-error procedure was used to select a critical angle such that the analysis would match the test maximum load. The critical angle, ψ_c , was found to be 5 degrees assuming plane-stress conditions. Results from the FEA are shown by the solid curve. The analysis tended to overestimate crack extension in the early stages of crack growth. However, this is believed to have been caused by severe crack tunneling during crack initiation. Tunneling is expected to be nearly equal to the plate thickness. A comparison between the measured and predicted crack-opening displacements (COD) measured at the centerline of the M(T) specimen is shown in Figure 7. The predicted displacements were in excellent agreement with the test results.

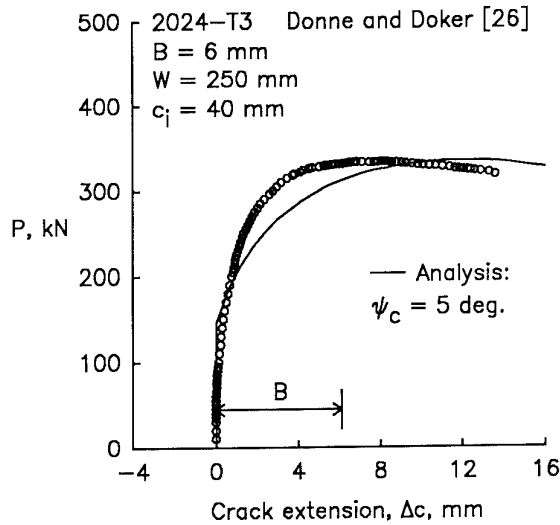


Fig. 6 - Measured and calculated stable tearing for M(T) specimen.

8. PREDICTING FAILURE OF MULTIPLE-SITE DAMAGE SPECIMENS

The critical CTOA (ψ_c) for cracks and δ_i for sawcuts determined from the M(T) specimens made of the 2024-T3 Alclad and bare materials were used to predict the stable crack growth behavior of the MSD panels tested by Broek et al [23] and deWit et al [24]. A crack-mouth-opening displacement gage was placed at the centerline of the large lead sawcut (like Sawcut #3 in Fig. 2) to record the load-displacement record during the tests. In general, the displacement record gave several peak stresses (S_k) during stable tearing and crack linkup, in addition to the maximum failure stress (S_f). Comparisons are made between measured and predicted peak stresses during crack linkup. In reference 24, videos were also taken of each test to record stable crack extension and crack linkup. Comparison are also made between measured and predicted crack initiation, crack extension, and failure loads on the panels.

A comparison of measured and predicted results for all of the MSD panels test by Broek et al [23] is given in reference 25. The results for only one of the panels will be shown here. The test had a large sawcut in the center with two smaller MSD sawcuts on either side of the large sawcut, like than shown in Figure 2. Figure 8 shows applied stress plotted against the total

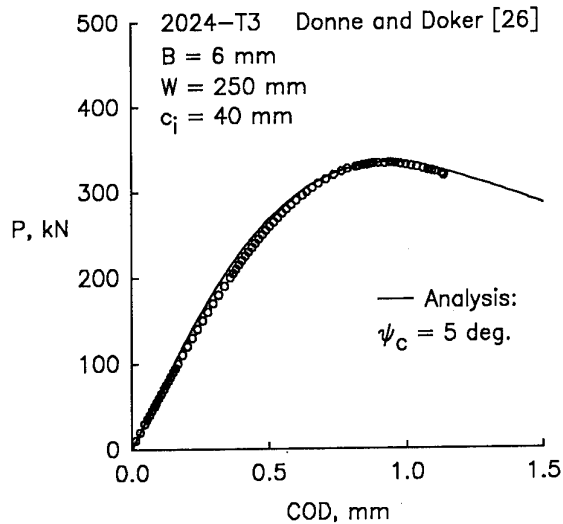


Fig. 7 - Measured and calculated crack-opening displacements for M(T) specimen.

crack length, L , of all sawcuts and cracks. The tests results indicated three peak stresses S_1 , S_2 and S_3 . The maximum stress, S_f , corresponded to the second peak stress. These stresses are plotted as horizontal lines because they could not be related to any particular crack length. Predicted results are shown as the solid curve ($\delta_i = 0.075$ mm; $\psi_c = 5.1$ degs.). The first and second peak stresses from the analysis were within 2 percent of the test results, while the final peak stress (S_3) was about 5 percent lower than the test result. Final failure with a single large crack corresponded to nearly net-section stress $S_n = \sigma_{ys}$ (dotted line). A comparison between the test and FEA results for the other panels demonstrated that the analysis with a critical CTOA could predict crack linkup and failure within about 5 percent.

The objective of the test program conducted by the National Institute of Standards and Technology (NIST) [24] was to study the fracture behavior of very large-scale, thin-sheet aluminum alloy specimens with MSD crack configurations. The test program consisted of ten fracture tests on 2300 mm-wide, 1 mm-thick, 2024-T3 aluminum alloy panels with a single large sawcut and 6 to 20 MSD sawcuts of various size and location. A summary of the panels tested is shown in Table 2. All but one of the panels were restrained from buckling.

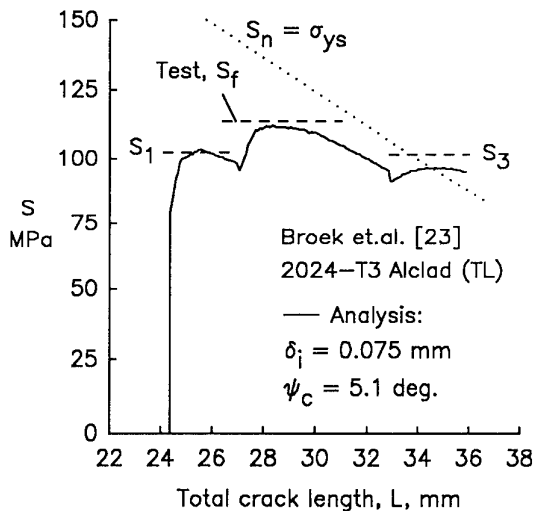


Fig. 8 - Measured and predicted crack linkup and failure for specimen with five MSD cracks.

At the beginning of the test program, the FEA method developed at NASA Langley was used to predict the load-crack-extension behavior of tests from MSD #2 to #10 based only on the results from the first test (MSD #1). The only exception was test MSD #6 which was conducted without anti-buckling guides. In order to calibrate the finite-element analysis (before any CTOA measurements were made on the material), the critical CTOA was evaluated from test MSD #1. This panel was tested with a total sawcut of 355 mm. The load-crack-extension results from this tests were used to find the two fracture parameters (δ_i , ψ_c) that are required to simulate fracture of panels with sawcuts. The critical displacement at the sawcut tip was selected as 0.2 mm based on the crack-initiation load. The critical CTOA value was found to be 3.4 degrees. The calculated load-against-crack extension agreed well with the test results. These two parameters were used to predict the behavior of all other panels before the tests were conducted. These results were provided to NIST prior to the tests.

Again, the results for only one of the panels will be shown here. The test had a large sawcut in the center with six smaller MSD sawcuts on either side of the large sawcut. Figure 9 shows applied stress plotted against the length of the

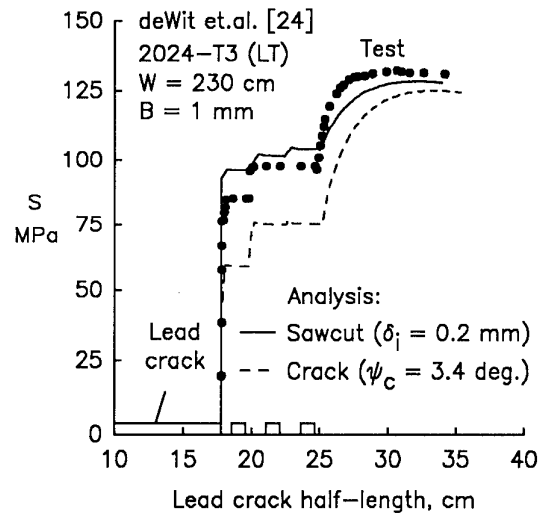


Fig. 9 - Measured and predicted crack linkup and failure for panel with seven MSD cracks.

large lead crack as it grows and links up with the other sawcuts or cracks. The boxes at the bottom of the figure show a schematic of the tip of the lead sawcut and the placement of the three MSD sawcuts. The test results from the video camera are shown by the symbols. Again, the predicted results are shown as the solid curve ($\delta_i = 0.2$ mm; $\psi_c = 3.4$ degs.). The predicted results agreed well with the test, especially the maximum failure load. To demonstrate the influence of sawcuts on crack linkup and failure, a prediction was also made with the sawcut parameter δ_i set to zero, as shown by the dashed curve. Although the maximum failure load was only slightly affected, the crack linkup behavior was greatly influenced, being 30 percent lower than the test with sawcuts. Table 2 gives a comparison between the maximum test loads and those predicted from the finite-element analyses. With the exception of test #5, all predictions were within about 6 percent of the test loads. The predicted results for loads at crack linkup also agreed reasonable well with the test results recorded on movie and video systems used by NIST.

During the test program, the photographic method [21] was used on several occasions to make measurement of the critical CTOA during stable tearing. The long-focal length, high

resolution camera and video system was used to record the crack-surface profile during stable tearing. Material from the first test (MSD #1) was also provided to NASA to make CTOA measurements on small laboratory M(T) specimens (75 mm-wide). Several hundred measurements were made on the large and small specimens. After cracks had initiated from the sawcuts and grown for about one thickness, the critical CTOA value approached a constant of about 5.5 degrees. The CTOA values were basically the same for the small laboratory test specimens and the wide panel tests. This observation is crucial in the verification of the critical CTOA fracture criterion.

Table 2.- Comparison of measured and predicted failure loads on NIST multiple-site damage (MSD) fracture tests.

MSD Panel (a)	Number of sawcuts	Test load, kN	Predicted load, kN	Percent error
1	1	342.5	341.6 (b)	-0.3
2	1	428.4	427.0	-0.3
3	1	288.7	291.8	1.1
4	7	307.4	298.0	-3.0
5	7	405.7	359.9	-11.3
7	11	214.4	221.5	3.3
8	21	211.3	225.1	6.5
9	21	352.3	332.7	-5.6
10 (c)	11	232.2	221.5	-4.6

(a) MSD #6 was tested without anti-buckling guides.

(b) Fitted to test ($\delta_1 = 0.2$ mm, $\psi_c = 3.4$ deg.).

(c) MSD #10 was a repeat of MSD #7.

The most striking difference between the CTOA values measured on the test specimens and that used in the analyses was the large difference between the angles. The average of the tests was 5.5 degrees and the computed value was 3.4 degrees. The large discrepancy is believed to be due to buckling of the panels above and below the anti-buckling guides. Observations of the test panels during fracture clearly showed severe buckling of the unrestrained panel. But further

study is required to resolve the discrepancy.

9. PREDICTING FAILURE OF BIAXIALLY-LOADED SPECIMENS

Donne and Doker [26] conducted fracture tests on cruciform specimens made of 6 mm-thick material. The biaxial specimen with a fatigue crack is shown in Figure 3. Tests were conducted under displacement control for the load perpendicular to the crack and load control in the other direction to maintain a constant biaxial ratio (β). Guide plates were used in the tests with negative β .

A comparison between measured and predicted load-against-crack extension is shown in Figure 10. The applied load is plotted against crack extension (again measured by electrical potential [26]). The analyses were conducted under load control to maintain a constant β ratio. The predicted results (solid curves) tended to greatly overestimate crack extension in the early stages of crack growth, similar to that observed for the M(T) specimen. But here the discrepancies were much larger. The reason for the large differences is unknown but, again, they may be related to severe tunneling. A comparison between the measured and predicted crack-opening displacements (COD) measured at the centerline of the biaxial specimen is shown in Figure 11. The predicted displacements agreed well with the test results for all biaxial ratios. The analyses

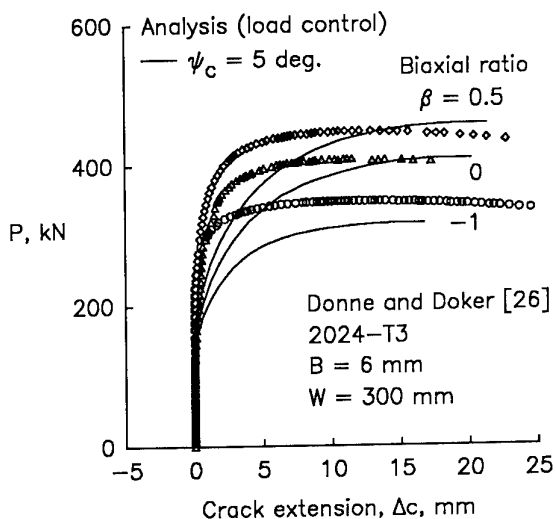


Fig. 10 - Measured and predicted stable tearing for biaxial specimens.

using the CTOA method was able to predict failure loads within 10 percent of the test loads for all biaxial ratios.

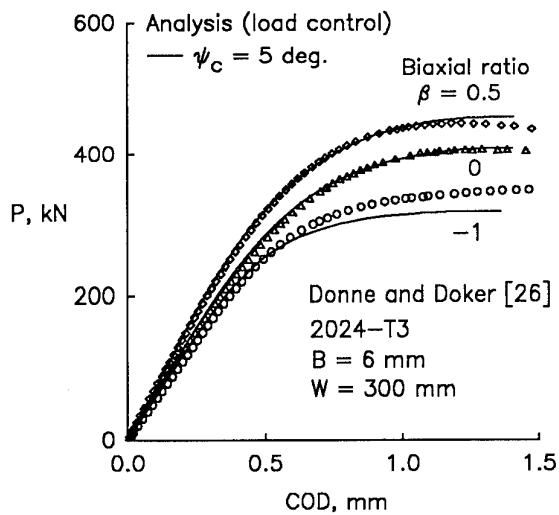


Fig. 11 - Measured and predicted crack-opening displacements for biaxial specimens.

10. PREDICTING FAILURE OF CRACKED STIFFENED PANELS

To predict stable crack growth and failure of cracked stiffened panels, the finite-element method was used to model both the sheet and stiffeners, as shown in Figure 12. The stiffener model lies in the same plane as the sheet and is connected to the sheet at the rivet locations. Both the sheet and stringers are modeled with constant-strain elements and have multiple-linear stress-strain curves for the respective materials. The rivet connection was modeled by an elastic-perfectly plastic shear spring with an elastic modulus of 70,000 MPa, Poisson's ratio of 0.3, and a shear yield of 200 MPa. Because constant-strain elements were used to model the stringers, analyses were conducted on a simulated stringer with rivet loading, as shown in Figure 13. Mesh A (not shown) had 826 elements modeling the stringer and rivet (rivet and sheet were tied together). Mesh B had 16 elements, as shown, and this type of mesh was used to model all stringers. Figure 14 shows a comparison between the rivet displacements calculated from Mesh A and B. As expected, Mesh B (dashed curves) was too stiff and gave smaller displacements than Mesh A for a given

rivet load (solid curves). Altering the elastic modulus of the material for Mesh B ($E' = 0.5E$) gave elastic displacements that matched well with displacements from Mesh A. The yield properties of the materials were not changed. Thus, in the panel analyses, the elastic modulus of the stringer material was set to $0.5E$.

Leybold [27] conducted fracture tests on 2024-T3 sheet panels with a single stiffener, as shown in Figure 4(a). The stiffener width, W_s , and thickness was varied to give a stiffness ratio (λ) of 0.2 or 1. The stiffness ratio was defined as the ratio of stringer cross-sectional area to notch area. The panels had a very sharp notch of various lengths. Figure 15 shows a comparison of measured and predicted failure stresses on panels with no stiffener [32] and those with $\lambda = 0.2$ and 1 [27]. The symbols show the test results and the curves show the predicted results using a critical angle of 6 degrees. The test results and predicted failure stresses agreed well.

Vlieger [28] conducted fracture tests on 2024-T3 sheet panels with multiple stiffeners. The tests had a central sawcut in a sheet with five 7075 stringers with the central stringer broken, as shown in Figure 4(b). Figure 16 shows a comparison of measured and predicted stable crack extension on panels with different initial sawcuts. The symbols show the test results and the curves show the predicted results using fracture parameters (δ_i, ψ_c) determined from $M(T)$ specimen tests. Again, the test results and predictions agreed fairly well.

11. INFLUENCE OF MSD CRACKING ON BIAXIALLY-LOADED STIFFENED PANELS

Swift [1] had postulated that small MSD cracks may have a large influence on the residual strength for a large lead crack. This phenomenon has been demonstrated using the FEA and the critical CTOA fracture criterion on flat panels [25]. How stiffeners impact the influence of MSD cracks on lead-crack behavior needs to be studied. The FEA and the CTOA criterion was used to study this behavior for the 2024-T3 thin-sheet material ($\psi_c = 5.1$ deg.; $\delta_i = 0$). An MSD panel with seven 7075 stringers (central

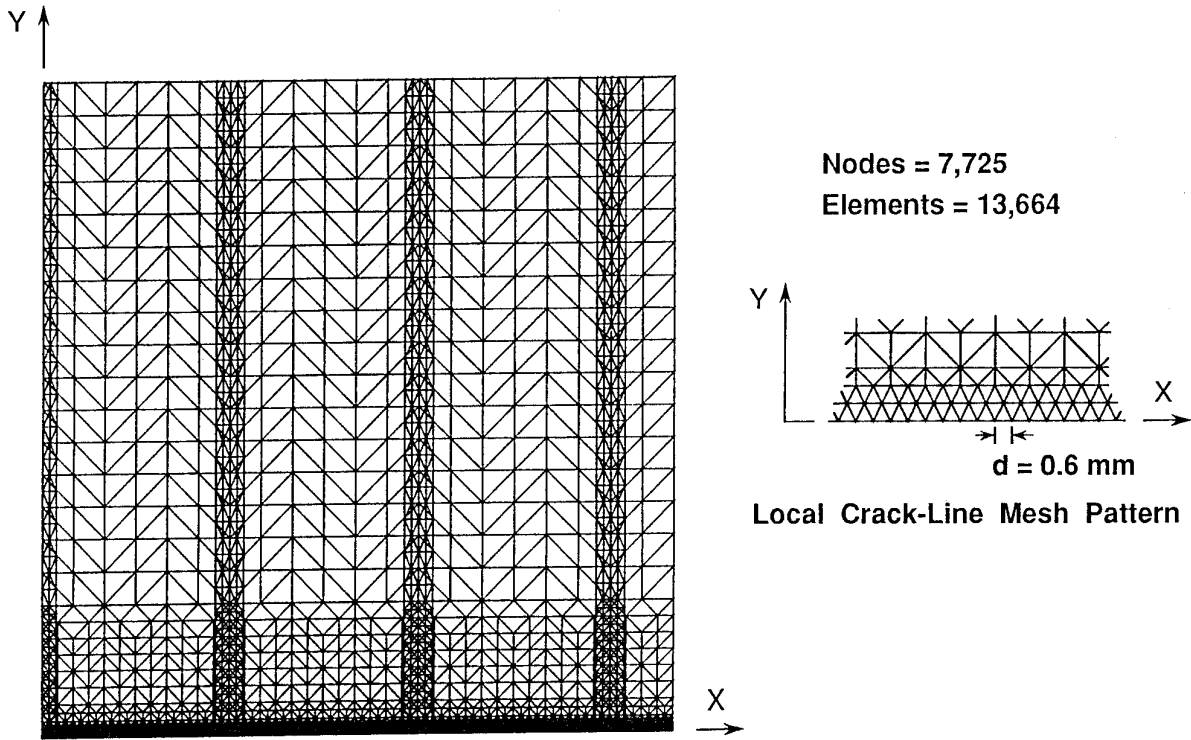


Fig. 12 - Finite-element model for stiffened panel with MSD cracking.

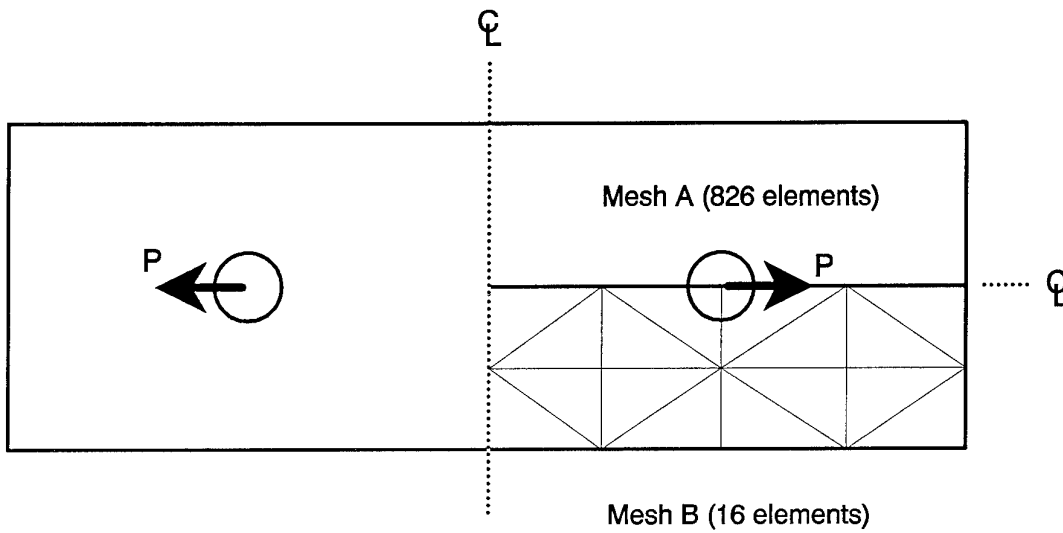


Fig. 13 - Finite-element models for rivetted-loaded stringer.

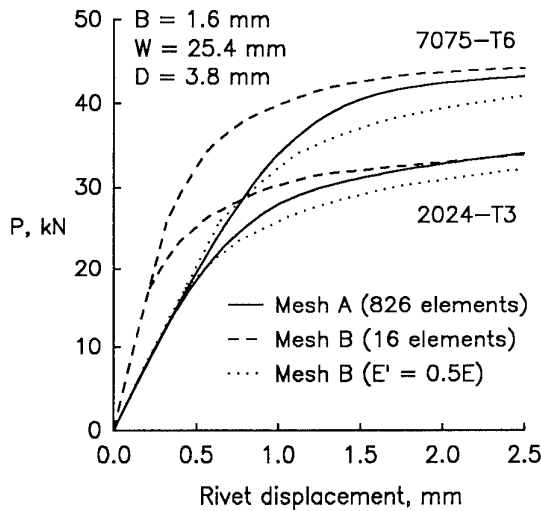


Fig. 14 - Rivet displacements for various finite-element models.

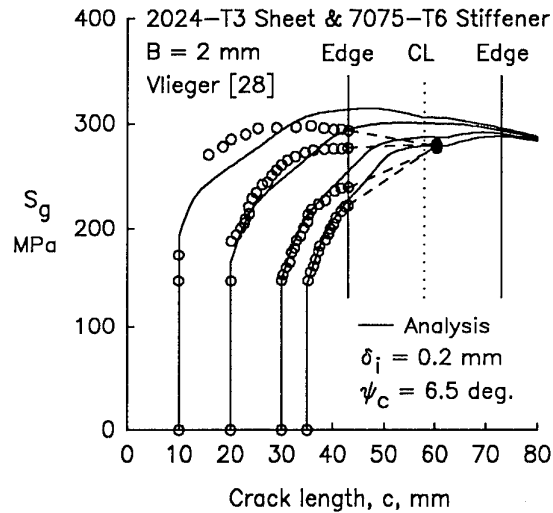


Fig. 16 - Measured and predicted stable tearing in multiple stiffened panels with a broken central stiffener.

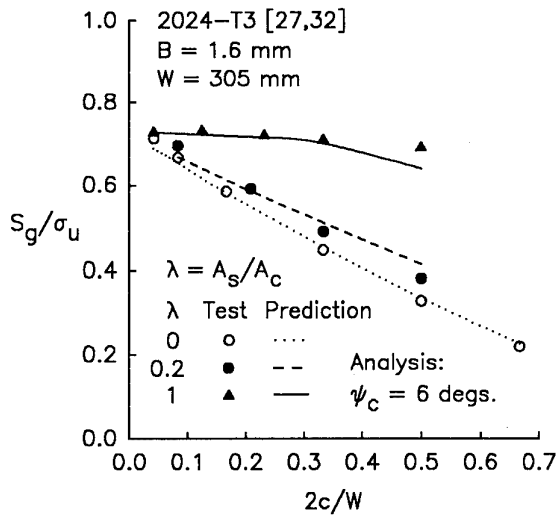


Fig. 15 - Measured and predicted failure stresses for stiffened and unstiffened cracked sheets.

stringer broken), as shown in Figure 17, was analyzed. The finite-element model, shown in Figure 12, was used with symmetry conditions imposed along the X- and Y-axes. The panel had a lead crack ($L_c = 35$ cm) with various number of smaller MSD cracks placed at equal intervals to simulate rivet spacing. The stiffness ratio, cross-sectional area of stringer to total cross-sectional area (μ), was either 0.15 or 0.3.

Figure 18 shows the predicted results for a single crack (dashed curve) and for a lead crack with

15 MSD cracks (solid curve). This figure shows applied stress plotted against lead crack half-length and demonstrates that, even with typical stiffeners, a large number of MSD cracks can cause a large reduction in residual strength. Results shown in Figure 19 are for the identical crack configuration, as shown in Figure 18, except that the stiffener ratio was doubled to 0.3. The final results are quite similar. The increase in the stiffener ratio did not adversely change the influence of MSD on residual strength. The results for only three MSD cracks (located just in front of the lead crack) are also shown. The residual strength is only slightly lowered from the single crack behavior.

A comparison between the relative residual strength ratio from test and analyses for various size MSD cracks are shown in Figure 20. This figure shows the ratio of residual strength with 15 MSD cracks to that with only a single lead crack plotted against MSD crack length. The test results (symbols) were obtained from Goranson [33] for flat sheets (no load transfer) and lap-splice joints (load transfer) with MSD at the rivet locations. The rivet diameter was about 5 mm. (There were no stringers in the tests conducted in reference 33.) The curves were calculated results for a flat panel and panels with seven stringers for $\mu = 0.15$ or 0.3 for various

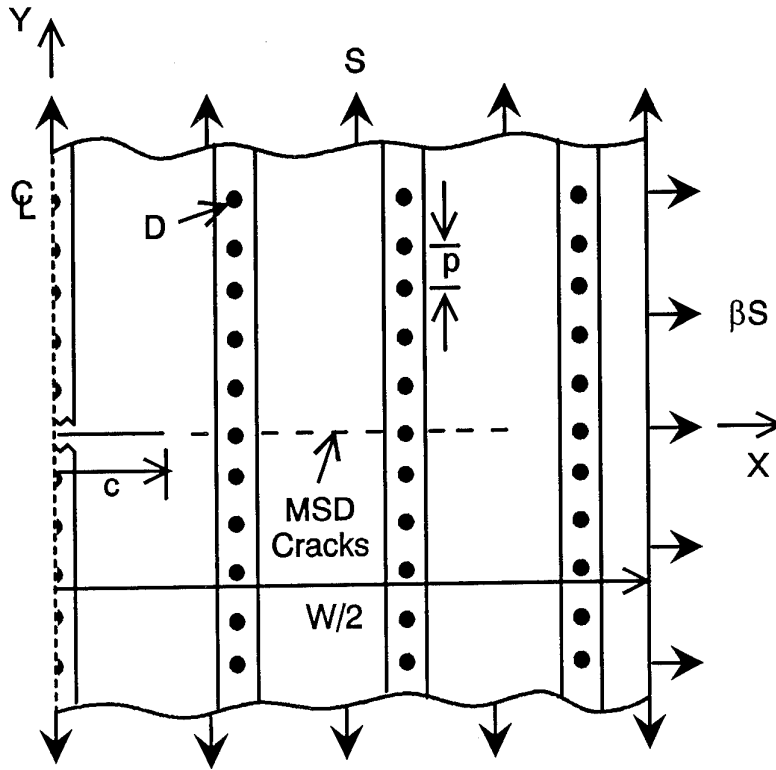


Fig. 17 - Biaxially-loaded cracked stiffened panel with MSD.

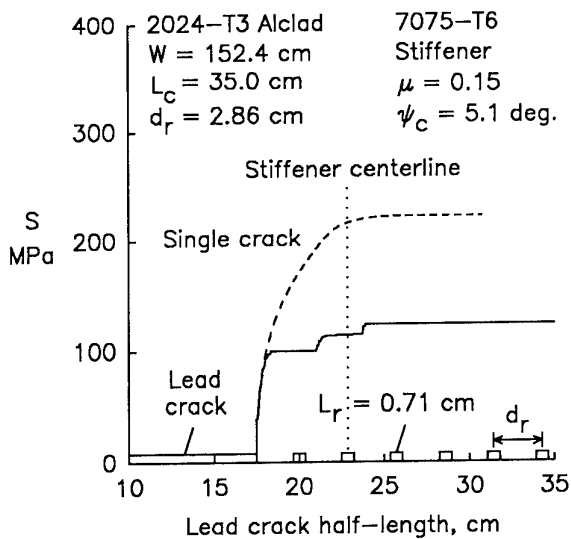


Fig. 18 - Influence of stiffener on lead-crack behavior for single and MSD cracking.

size MSD cracks. For the larger MSD crack sizes, the test and analyses agreed well. However, the results for the smaller MSD cracks did not agree, presumably because rivet holes were not modeled in the analysis.

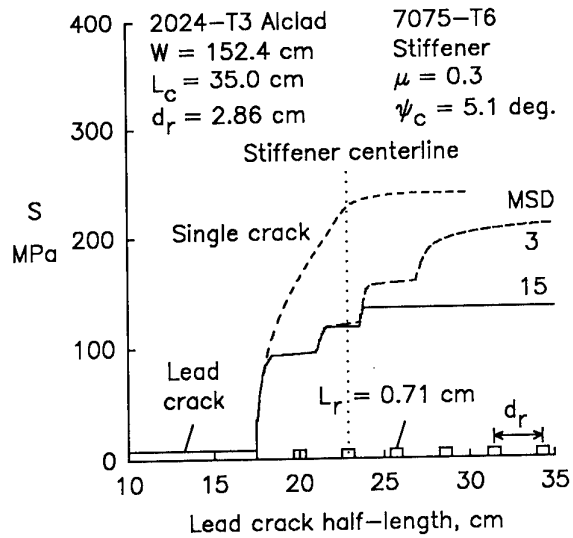


Fig. 19 - Influence of stiffener on lead-crack behavior for various number of MSD cracks.

Further testing and analyses with damaged curved panels with rivets and stringers are necessary to substantiate these results for lap-splice joints and buildup structure.

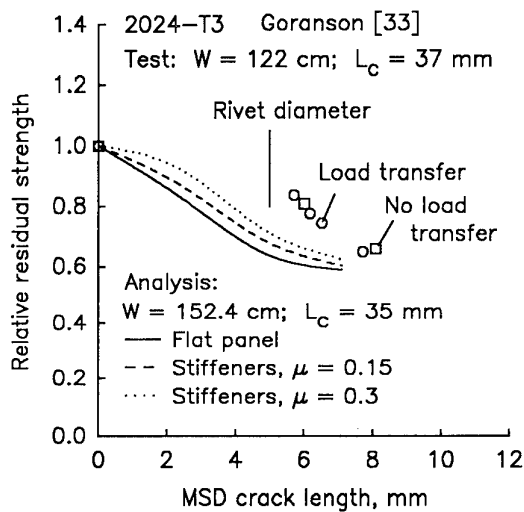


Fig. 20 - Influence of stiffeners and MSD crack size on relative residual strengths.

12. CONCLUSIONS

(1) Critical crack-tip-opening angle (CTOA) is independent of crack configuration and loading for 1 to 6 mm-thick 2024-T3 aluminum alloy material after a small amount of crack extension.

(2) Finite-element fracture simulations using the critical CTOA gives very accurate details of plastic deformation and stable tearing of cracks under complex loading, such as biaxial loading and stiffened panels.

(3) Finite-element analyses predict a significant influence of multiple-site damage (MSD) cracks on lead-crack behavior for both unstiffened and stiffened panels.

(4) Influence of MSD on lead-crack behavior in stiffened panels under biaxial loading is only slightly improved with larger stiffeners.

13. REFERENCES

- [1] Swift, T., "Damage Tolerance in Pressurized Fuselages", *New Materials and Fatigue Resistant Aircraft Design*, 14th International Committee on Aeronautical Fatigue, June 1987.
- [2] Maclin, J., "Performance of Fuselage Pressure Structure", 1991 International Conference on Aging Aircraft and Structural

Airworthiness, C. E. Harris, ed., NASA CP-3160, Washington, D.C., 1992, pp. 67-75.

[3] McGuire, J. F. and Goranson, U. G., "Structural Integrity of Future Aging Airplanes", 1991 International Conference on Aging Aircraft and Structural Airworthiness, C. E. Harris, ed., NASA CP-3160, Washington, D.C., 1992, pp. 33-48.

[4] Harris, C. E., "NASA Aircraft Structural Integrity Program", NASA TM 102637, April 1990.

[5] Kobayashi, A. S.; Chiu, S. T. and Beeuwkes, R., *Engineering Fracture Mechanics*, Vol. 5, No. 2, 1973, pp. 293-305.

[6] Andersson, H., *Journal Mechanics and Physics of Solids*, Vol. 21, 1973, pp. 337-356.

[7] deKoning, A. U., "A Contribution to the Analysis of Slow Stable Crack Growth", National Aerospace Laboratory Report NLR MP 75035U, 1975.

[8] Light, M. F.; Luxmoore, A. and Evans, W. T., *International Journal of Fatigue*, Vol. 11, 1975, pp. 1045-1046.

[9] Rousselier, G., Fourth International Conference on Fracture, Waterloo, Canada, Vol. 3, 1977, pp. 1-6.

[10] Shih, C. F.; de Lorenzi, H. G. and Andrews, W. R., ASTM STP 668, 1979, pp. 65-120.

[11] Kanninen, M. F.; Rybicki, E. F.; Stonesifer, R. B.; Broek, D.; Rosenfield, A. R. and Nalin, G. T., ASTM STP 668, 1979, pp. 121-150.

[12] Newman, J. C., Jr., ASTM STP 833, 1984, pp. 93-117.

[13] Brocks, W. and Yuan, H., ESIS Publication 9, 1991, pp. 19-33.

[14] Newman, J. C., Jr.; Shivakumar, K. N. and McCabe, D. E., ESIS Publication 9, 1991, pp. 117-126.

- [15] Demofonti, G. and Rizzi, L., ESIS Publication 9, 1991, pp. 693-703.
- [16] Light, M. F.; Luxmoore, A. and Evans, W. T., International Journal of Fatigue, Vol. 11, 1975, pp. 1045-1046.
- [17] Paleebut, S., "CTOD and COD Measurements on Compact Specimens of Different Thicknesses", M.S. Thesis, Michigan State University, 1978.
- [18] Reuter, W. G.; Graham, S. M.; Lloyd, W. R. and Williamson, R. L., ESIS Publication 9, 1991, pp. 175-188.
- [19] Kobayashi, T.; Irwin, G. R. and Zhang, X. J., ASTM STP 827, 1989, pp. 234-251.
- [20] Newman, J. C., Jr.; Dawicke, D. S. and Bigelow, C. A., International Workshop on Structural Integrity of Aging Airplanes, Atlanta, GA, March 1992, pp. 167-186.
- [21] Dawicke, D. S. and Sutton, M. A., "Crack-Tip-Opening Angle Measurements and Crack Tunneling under Stable Tearing in Thin Sheet 2024-T3 Aluminum Alloy", submitted to Experimental Mechanics Journal, 1993.
- [22] Dawicke, D. S.; Sutton, M. A.; Newman, J. C., Jr. and C. A. Bigelow, "Measurement and Analysis of Critical CTOA for Thin-Sheet Aluminum Alloy Materials", presented at 25th National Symposium on Fracture Mechanics, Lehigh University, June 1993.
- [23] Broek, D.; Thomson, D. and Jeong, D. Y., NASA Conference Publication 3274, Part I, September 1994, pp. 85-98.
- [24] deWit, R.; Fields, R. J.; Mordfin, L.; Low, S. R. and Harne, D., NASA Conference Publication 3274, Part II, September 1994, pp. 963-984.
- [25] Newman, J. C., Jr.; Dawicke, D. S.; Sutton, M. A. and Bigelow, C. A., Durability and Structural Integrity of Airframes, Vol. I, A. F. Blom, ed., June 1993, pp. 443-468.
- [26] Donne, C. D. and Doker, H., 10th European Conference on Fracture, Berlin, Germany, September, 1994, pp. 891-900.
- [27] Leybold, H. A., "A Method for Predicting the Static Strength of a Stiffened Sheet containing a Sharp Central Notch", NASA TN D-1943, August 1963.
- [28] Vlioger, H., Engineering Fracture Mechanics Journal, Vol. 5, 1973, pp. 447-477.
- [29] Newman, J. C., Jr.: Finite-Element Analysis of Fatigue Crack Propagation--Including the Effects of Crack Closure, Ph.D. Thesis, VPI & State University, Blacksburg, VA, May 1974.
- [30] Zienkiewicz, O. C.; Valliappan, S. and King, I. P., International Journal of Numerical Methods in Engineering, Vol. 1, 1969, pp. 75-100.
- [31] Sutton, M. A.; Bruck, H. A. and McNeill, S. R., Experimental Mechanics Journal, Vol. 29, No. 3, 1989, pp. 261-267.
- [32] Newman, J. C., Jr., ASTM STP-605, 1976, pp. 104-123.
- [33] Goranson, U. G., "Damage Tolerance - Facts and Fiction", Durability and Structural Integrity of Airplanes, Vol. I, A. F. Blom, ed., June 1993, pp. 3-105.

WIDESPREAD FATIGUE DAMAGE AND SINGLE MEMBER FAILURE PREDICTION OF MILITARY JET TRAINERS OF CZECH DESIGN AND PRODUCTION.

Jiří Fidranský
Jiří Fiala
Structural Integrity Department
Aero Vodochody a.s.
250 70 Odolena Voda, Czech Republic

SUMMARY

Military jet trainers originally designed under safe life concept are approaching in a lot of cases their service life estimates, based on 20 years old analyses and tests. The fleet condition and upgraded service spectra evaluation enables a significant life extension, because of safety margins of former approach.

The Czech designed and produced L-39/59 jet trainer has been submitted to the Aircraft Structure Integrity Program (ASIP) with the main goal to extend the service life. As an essential tool for confirmation of the results the full-scale tests have been used. Widespread fatigue damage (WFD) has arisen into existence during the tests on several areas of primary structure, but at least three service lives were without significant damage. In one case there was the phenomenon limiting the fatigue life of the component. In other cases fatigue life was significantly influenced, but widespread fatigue can be used as an indicator of possible damage of a single load path. The acoustic loading was the source of the significant WFD of the engine air intake duct. That is the only WFD occurred in service. Analytical techniques failed in several cases in prediction of WFD so far, but prediction of damage propagation on the stiffened panels still continues. The inspection periods and repair techniques were verified during the tests. To avoid possible structure damage, nondestructive inspection and Individual Aircraft Tracing (IAT) were introduced into maintenance procedures. The skin damage, caused by WFD, was successfully repaired in several cases by composite patches.

1. INTRODUCTION

Aircraft design and production in the Czech Republic has a long tradition. The pioneer work was done before the WW I, but significant development of the aviation industry started in the early twenties. One of the oldest Czech aircraft producers, Aero had been established in 1919. There were about 55 types of indigenous design produced both for military and commercial purposes before the WW II. At the beginning of the jet age, since 1953, licence-built production of MiG fighter had started and when the following decade was over, our indigenous design aircraft came once again into a lot production. The successful jet trainer, designated L-29 Delfin, was built in more than 3,500 units. The production of that type ended in early seventies. As the production of more sophisticated types of jet trainers designated L-39 and L-59 still continues, Aero Vodochody is one of the world biggest jet trainer producers.

The L-39/59 is a subsonic single turbofan two seat basic/advanced trainer developed and produced by Aero Vodochody. Its development started in mid sixties with the goal of producing an effective, low - cost operating and maintenance trainer, suitable for both basic and advanced training. The first L-39 flew in 1968, but the first production aircraft was delivered in 1974. Continuing effort of the development has enabled significant aircraft modifications and the L-39ZA version, with four underwing hardpoints and fuselage gunpod became operational in 1977. Further development of the type culminated in 1993, resulting in the maiden flight of the upgraded L-139 equipped with Allied Signal TFE 731

engine and "western" avionics. There were customer requirements for a low cost advanced trainer with better performance and updated avionics. A redesigned L-59, equipped with more powerful DV2 engine, strengthened airframe, redesigned cockpit and canopy, hydraulically actuated control surfaces and advanced avionics package has been developed, with first operational aircraft in 1990.

Over 2,800 the L-39 aircraft have been built since 1974. Since 1990 the L-59 has followed with over 50 aircraft. The both types have been used in 19 customer countries and the production still continues. The L-39/59 fleet accumulated more than 4.5 million flight hours up to now and there are no aircraft lost due to structural failure and even there is no evidence of any serious fatigue damage on leading aircraft of the fleet.

2. DESCRIPTION OF THE STRUCTURE

A skeleton view of the L-59 is shown in Figure 1. The airframe structure is of a semimonocoque design, made of aluminium alloys and steel. The aircraft was originally designed under safe-life criteria, so there are no multiple load paths in general. The cantilever wing is a three-spar structure manufactured as a one-piece assembly. Most of the structure is made of 2124 aluminium alloys, except for the wing to fuselage attachments and landing gear supporting structure, made of steel.

The main structural elements of the wing are the main spar, with booms made from machined aluminium extrusions. The spar web is machined from a metal sheet. The stringers are extruded and ribs and skin panels are sheet formed. The structure is mostly riveted with a small portion of bonded and bolted joints.

The load path for bending loads is created by the main spar and the skin panel between front and main spars. The main fatigue critical location of the wing is the main spar boom and when the wing structure was tested during full-scale fatigue tests the majority of cracks was initiated by the rivets, joining the lower skin panel to the spar boom.

The fuselage is a predominately semimonocoque structure, with bulkheads made of formed sheet and extruded stringers. The bending load in the fuselage is carried by extruded upper and lower longerons. The most loaded part of the fuselage is the central section, containing the fuel compartments and the engine air intake ducts. The wing structural box is located below the fuel tank floor and air intake ducts. The wing is attached to the fuselage at four points, two points are located at centerline rib and two on main wing spar at the sides. There is a significant cutout for the wing location in the fuselage structure. That is the reason why the dorsal longeron and the fuselage upper panel, being extremely loaded parts, are fatigue critical areas.

The empennage structure is of similar concept as the wing structure. The horizontal stabilizer is of three-spar design of one-piece assembly. The stabilizer is attached to the fuselage at four points. The fin is of two spar design with multiple stringer torsion box. All stringers are attached to the fuselage structure at dorsal longeron and bulkheads intersections.

3. L-39/59 LIFE ASSESSMENT CONCEPT

The aircraft was originally designed under safe-life criteria. The initial service life of the L-39 aircraft in early seventies was established at 3,000 flight hours. The value was valid for the early series of aircraft and it was based on conservative estimates of service spectra as well as preliminary evaluation of constant amplitude full-scale fatigue test of the early prototype. Improved variant of the production version since the early eighties featured 4,500 flight hours of service life, with further extension up to 6,000 flight hours, but analyses were still conservative because there was no demand to extend the life. The life value was sufficient in the past when many former Warsaw Pact operators had very low annual utilization and when military budgets enabled to replace the aircraft after approximately 20 years of service. Under such conditions there was limited threat of fatigue. Tremendous potential for service life extension was obvious. Theoretical analysis and component testing gained important data concerning crack growth in primary structure and last but not least enhance durability of the structure. When the service life extension program started, importance of WFD phenomenon began to be obvious.

The airframe life assessment has been based on analytical work and the evaluation of the test result. The first durability tests of L-39 jet trainer were performed in the seventies. The theoretical durability analysis based on Miner's rule was verified by three fatigue full-scale structure tests - the prototype and two production versions of the aircraft. Both production versions featured design changes and enhanced service life. When the improved L-59 version with strengthened airframe was developed the full-scale fatigue test has been performed. The "flight by flight" method was applied with quasi-random loading using service spectra. Our own software for random loading generation has been developed, reference 1.

Durability test is expected to be finished when the critical crack length is reached. Tests in our case are performed up to the serious damage of primary structure and initial defects are repaired after their significant length is reached. Repairs are designed not to significantly influence the remaining structure. Such approach enables to achieve more than first failure mode. After completion of residual static testing a test article teardown inspection and detailed metallurgical and fractographic evaluations are performed.

4. LIFE EXTENSION PROGRAM

Before the life extension program was started the program goals were established, as described in reference 2. The service life of the L-39/59 aircraft family was expected to be extended up to 15,000 flight hours, or 30,000 missions. Loading spectrum for those figures corresponds to the advanced trainer utilization. Lifetime of the structure has been expected to be over 30 years. The following main threats were expected in that case:

- single member load path failure
- widespread fatigue damage
- corrosion accelerated fatigue
- wear out of movable and dismantlable parts, in coincidence with fretting corrosion
- acoustic fatigue.

The life extension program consists of many Aircraft Structural Integrity Program (ASIP) activities, for instance Load and Environment Spectra Survey measurements, Individual Aircraft Tracing Systems installation, component tests and durability analyses, but the essential tool for durability data acquisition were full-scale tests. As already mentioned, during development and qualification of the L-39/59 aircraft family four full-scale tests

have been performed. The last one, completed on the L-59 airframe, was outstanding by its comprehensive "flight by flight" simulation. In spite of the fact that tested airframe structure was modified during the time and loading sequences were changed even more significantly, the critical areas changed only a little, so that all performed tests can be taken into consideration. The quantitative data are taken from much more realistic "flight by flight" test, where successive damage can be found. Because the data are taken from the in-door tests no environmental degradation or corrosion accelerated damage has been evaluated.

In spite of the fact that WFD is in many cases a much more important phenomenon in transport aircraft structures, there were several important damaged areas of the primary structure influenced by that source of damage.

5. WIDESPREAD FATIGUE OF THE PRIMARY STRUCTURE

The first example of WFD has arisen during the full-scale test, when the rear part of the fuselage and the empennage were tested, see reference 3. The test ran under block of cycles loading and vertical and horizontal surfaces were loaded by both symmetrical and asymmetrical load cases. The significant bending of the fin, in combination with fin torsion caused an important damage in the fin root. There were several damaged areas of the structure, when expected life limit was reached, see Figure 2. Most of the cracks concentrated on stringers and attachment fittings, but one of the most important damage was caused by WFD and eventually limited the life of the component. The intersections of the fin stringers, bulkheads and dorsal longerons were damaged on both sides.

The failure was dangerous because there were a few cracks visible and failed stringer attachments appeared to be under the undamaged skin. The possibility of visual inspection of the critical area was limited. The first short cracks in the outer skin appeared, when the residual strength of the fin had been insufficient. The propagation and link up of the cracks were slow, but critical lengths of the main crack, corresponding to the residual strength requirement, was not proved by the test. Because the depth of the failure was discovered just after teardown inspection, the simulation of the damage propagation on the component was evaluated. The critical intersection is loaded by biaxial loads, that is why simplified component test is not applicable. The analytical simulation of damage propagation at the area failed so far. The importance of the problem decreased a little, because of the fact that the teardown inspection, as well as strain gauge measurement performed during the test, showed that cracks were initiated after the corresponding loading of 13,200 flight hours of safe life were reached. Because there is still a scatter factor in the range between 4.2 to 9.0 applied, in dependence on variability of the results, the margin of safety seems to be close to the requirements for current aircraft versions, but future development potential is fairly limited.

The second important damaged area with significant contribution of WFD was the fuselage upper panel with the dorsal longeron. The comprehensive evaluation has been carried out during the third full-scale fatigue test on the L-39, as described in reference 4. The fuselage upper panel is riveted at the dorsal longeron and prevailing bending of the fuselage caused high tension stresses of the area. The rivet holes and rivets joining the outer skin panel to the dorsal longeron are significant stress concentrators. The stress field surrounding the rivet rows is in Figure 3. During the fatigue test many of the rivets in the area initiated the cracks. Of course, the primary cracks were initiated at the location of the highest stress, see Figure 4. The first

detectable crack was initiated approximately at the number of cycles corresponding to 9,800 hours of the safe life. The cracks propagated and lined up in most cases. The overall length of the longest crack was about 200 mm, but only when the actual simulated life was far beyond our requirements. The strain gauges measurement, as well as the other inspection techniques, proved that in spite of the significant damage of the outer skin the dorsal longeron remained undamaged for a long time. When the strength of the skin panel was reduced more significantly, the cracks at the dorsal longeron were eventually initiated. Because the strength of the upper panel was affected by the redistribution of the load, it accelerated the crack growth rate at the dorsal longeron. The crack initiation in the dorsal longeron started at about 90 % of the total life, but initiation in the outer skin started much earlier, at 60 % of the total life. That is why the WFD of the outer skin can serve as a witness of the possible initiation of the dorsal longeron damage.

The wing features several fatigue critical areas, but the decisive part is the main wing spar lower boom near the wing plane of symmetry. Because of the bending and prevailing positive load factors in the loading spectra, the tension loading dominates. The wing skin is riveted to the boom, the boom cross section differs according to the bending moment. Consequently there is a vast area with the same or very similar stresses. The concentration factors of the rivets are also very similar, so that the damage is often initiated and propagates in the rivet row simultaneously. The mentioned area is a fatigue critical part of the aircraft and it was tested several times. The wing lower panel with the cracks after the test is in Figure 5.

The influence of the design changes was verified by full-scale "flight by flight" component test, where four wing spars with sections of the ribs and the skin were tested, see Figure 6. To have the appropriate bending moment and shear on the component, overall length of the article was 5.0 meters. The test program and results are described in references 5 and 6. The influence of the WFD on crack growth rate and residual stress were evaluated in reference 7.

The components had been loaded until a critical crack length was reached, corresponding to the ability to withstand the maximum limit load. The crack initiation and propagation was traced in detail during the test, as well as followed by fractographic analysis. The cracks were initiated by rivet holes with no exceptions. During the test on every component approximately 45 cracks were initiated and traced. The distance between cracks differed significantly, but there were several cases when the cracks were mutually affected, see Figure 7. The first detectable cracks in the outer skin appeared between 48-60 % of the total life, crack in the spar booms were visually detected between 90-95 % of the total life. According to fractographic analysis, there was a long period between crack initiation and significant crack propagation. The mean value of the life accumulated during the tests corresponded to the 11,500 of the safe flight hours, when scatter factor of 5.8 was applied. Because the further evaluation and the actual scatter of the results showed that scatter factor of 4.2 is sufficient the reached service life is close to our requirements.

In spite of the fact that the near-by cracks were not lined up, because the principal stress was perpendicular to the prevailing crack direction, the WFD significantly affected the crack growth rate and the residual strength. The evaluation of described features was performed for the damaged outer skin. There is no difference in the damage caused by WFD on actual wing or the skin damage on the test article. The data investigated by fractographic analysis and shown in Figure 8 were taken from five

cracks and all four test components. There was a relatively small scatter among crack growth rates of various test articles.

The tests were finished by the residual strength test up to the maximum limit load. The total failure of the component, which limited the strength of the entire wing, was at the locations, where the skin was damaged, without any exceptions. The fracture footprints of the spar boom cracks, where the components were finally broken, were not the largest. The stiff effect of the skin was obvious.

The above mentioned example describes WFD of the major structural member, when the stress field is on the same or very similar level over a large area. Every stress concentrator, for instance the individual joint at rivet row can be a crack initiator and propagation of damage can start almost everywhere. In case that the production quality is poor, the probability of failure is growing up. Consequently the initiation of damage can move along the uniformly stressed area.

The only WFD that emerged during the prototype service of the L-59 were the significant fatigue cracks in the air intake duct. There is a cylindrical ring in front of the engine intake, made of high alloy steel. The structure is made from a steel plate, rolled up and welded. The semi-finished article is heat-treated to relax residual stresses and machined. The final article is of a shell type structure with integral stiffeners. The structure had been examined thoroughly before it entered the service. The overall view on the structure is in Figure 9.

The engine first-stage fan blade tip speed is supersonic for the majority of power settings over the idle. The acoustic energy of the shock waves concentrates in a relatively narrow bandwidth of about 3 kHz. The engine intake in front of the rotor disc has to withstand the acoustic load of about 165 dB. Every part of the air duct has to be high-cycle fatigue durable. The acoustic load was calculated as well as measured before the final intake design entered the service, see reference 8. The structure of the entire air duct was measured to confirm that natural frequencies are different from those of the acoustic excitation. During the ground engine run the nominal stresses on the air intake structure were measured. The maximum nominal stress was about 15 MPa and fatigue endurance of the welded steel, proved by the specimen tests, was above 150 MPa, for 6.10⁶ cycles. Even if we evaluated the still decreasing fatigue endurance for the highest number of cycles, the safety margin was sufficient. There was no evidence of the structural failure during the early prototype service of that design.

The engine control system was modified during the aircraft tests. The pressure probe has been relocated onto the inlet ring. It was necessary for the probe installation to fix the probe pad on the ring wall. The pad was welded to the wall, but it was impossible to perform a heat treatment of the structure, because of thin wall cylindrical structure. After some time of the prototype flight testing a significant damage suddenly arose. The whole crack mesh caused WFD surrounding the probe pad, see Figure 10.

The cracks were fractographically analyzed, as described in reference 9. The primary cracks were initiated by a small defect of the weld. The secondary cracks were initiated afterwards, when the stress field was redistributed. Both systems of the cracks eventually joined. The reason for a very rapid propagation was an extremely high level of residual stresses, caused by welding. The stress field was very complex and consisted of cyclic loading of high frequency and residual stresses. The cracks propagated from the outer surface through the wall and afterwards elongated a little, before the part was withdrawn from service. The propagation was very rapid, because near the whole

length of the crack immediately appeared. The final crack growth rate was about $0.1 \mu\text{m}$ per cycle. The longest measured crack after the part was withdrawn from service was about 100 mm and the thickness of the wall was 2.0 mm. The endurance limit estimates failed, because residual stresses caused by welding process were too high, compared with our former expectations.

The only acceptable solution of the problem was the replacement of the entire inlet ring. The new part has been designed with integral pressure probe pad, machined on the surface of the semi-finished component. The only geometrical stress concentrators remained and the nominal stress level was low enough to be far below the fatigue limit.

6. DAMAGE EVALUATION AND REPAIRS

The WFD evaluation is based in our practice first of all on test results. Analytical prediction of the WFD phenomenon was only partly successful. We were able, by means of stress level study, to predict the areas, where the damage was a most probable one. Prediction of damage propagation is an uneasy task. The WFD was in majority cases initiated by rivets or other stress concentrators as are the welded joints. The detail modelling of the entire structure with rivet joints and all geometrical stress concentrators in MacNeal-Schwendler NASTRAN finite element method (FEM) package failed because of the task complexity. That is why we still rely on test results.

The less complex structural members, with a single fatigue cracks expectation, were successfully analyzed by the MacNeal-Schwendler, P3/FATIGUE program package. Good results were reached when the data of similar component were tested and only design changes were verified analytically. As a good example of such approach the components of the control system and landing gear attachment fittings analyses can be mentioned, but WFD has never been taken into consideration. There was no coincidence of two and more cracks evaluated so far.

Our effort to predict the WFD by analytical tools still continues. The theoretical crack growth and residual stress prediction has been applied for selected fatigue sensitive areas. The different failure modes of the stringers and the skin have been evaluated. The compliance functions of the panels have been found as an input for the crack growth models, regarding the retardation effect of the real service spectra. It seems to be necessary to use FEM for calculation of increasing K-factor along propagating cracks in the stiffened panels. The crack propagation is established among the appropriate increments of K-factors. If two-dimensional calculation of the K-factor is sufficient, the models match well the reality. In thick structural parts, spar booms for instance, the three-dimensional models with the actual footprint of the crack are inevitable. The research of the mentioned problem is still under way.

It is necessary to establish inspection intervals for critical areas of the structure. The test results are frequently used for that purpose in our practice, but different service spectra of individual aircraft can significantly reduce the quality of the assessment. A significant improvement in reliability of the assessment can be reached, if every individual aircraft is traced by multichannel data acquisition system, see reference 10. In general, the fatigue damage can be traced in different ways. According to our experience the direct tracing of damage propagation, based on acoustic emission for instance, is not suitable for operational usage. For different reasons there seems to be an operational proven system based on flight parameters and strain gauge signals tracing. Software for data evaluation can be tuned to actual service or test results. The inspection interval in that case can be based on severity of usage and lifetime intervals will be

auxiliary parameters only. If strain gauges are located near the areas where the damage is expected, the system satisfies the damage tracing requirements. But in case of WFD in service the possible corrosion damage must be taken into consideration, because there are no corrosion sensors available so far, periodical inspection is still necessary.

During the full-scale fatigue tests of the L-39/59 aircraft the WFD of the skin panels occurred in several cases mentioned above. As the effective tool for structure repair, the composite patches were used. The nominal thickness of repaired sheets varied from 1.0 to 2.0 mm the material being the 2024 or 2124 aluminium alloy. Repaired cracks were initiated mostly by rivet holes or seldom by cutouts. The length of cracks was several centimeters in all cases. Unidirectional carbon fibres and carbon fibres fabric were used as a repair material. To reduce additional stresses caused by different thermal expansion coefficients and to avoid possible corrosion problems, a single fibreglass fabric was used. The patch was designed to have an equal stiffness as the repaired skin. That criterion gives better results compared with the rule of the same strength of the patch and the skin. An analytical computer program based on lamination theory equations was used for design of layout of the patch. The fibre strength was seldom critical, but the interlaminar stresses and shear stress of the bond have been carefully checked. The bonding process and the epoxy matrix were modified, for low temperature curing. The efficiency of the patch was proved during the full-scale test. The example can be given for a fuselage skin crack. The crack was initiated during full-scale "flight by flight" test. There were 55,800 simulated flight hours applied up to the moment a crack was found. When the crack reached 25 mm in length, the repair patch was installed. The test continued up to 95,900 simulated flight hours, without any further crack propagation.

7. CONCLUSIONS

The information described above are based mainly on full-scale test results. The accumulated fatigue damage of the L-39/59 aircraft in service is still too low, that is why predicted data have not been proved so far. That is a favourable conclusion in general, but because of possible corrosion acceleration of fatigue damage the actual service damage can be more serious.

The WFD phenomenon is less important in case of safe life structures, because of single load path concept. But the safe life structures can be severely damaged by WFD of structure adjoining the main load paths, the contribution to the entire strength can be significant, because of the crack growth rate acceleration of the main crack in a single load member. The residual strength is affected as well. The damage process of the main structural members is often accelerated when there is WFD of the adjoining structure. In case that it is difficult to inspect the main structural members of safe-life structure the WFD, which is often visible on outer skin, can be used as a good mark for internal and probably more serious damage. There are some exceptions, because the fatigue test of the empennage showed the limited possibility of such indication.

Most of WFD occurred after three service lives were reached at least and such phenomenon is scarcely probable during the safe life of the structure. There are also some exceptions, namely the short cracks at the rivet rows, not lined up, and especially the parts loaded by extreme acoustic loading. The initiation, propagation and link up of such cracks depend heavily on production quality of individual joints. The damaged rivet rows in the skin were successfully repaired by composite patches.

The inspection intervals of the structure in service depends on a lot of circumstances. If the single load path on the primary

structure is influenced by the WFD of the adjoining structure, the occurrence of such kind of damage can be used as one of the symptoms of the necessity immediately to start with the inspection.

8. ACKNOWLEDGMENTS

We would like to emphasize our gratitude to the NATO-AGARD Technology Cooperation Programme representatives, as well as the Structural Material Panels representatives, for their effort to enable us to attend the Conference, in spite of the fact that the country we are coming from is still not among the NATO countries.

We also highly regard the Aero Vodochody company approval to reveal the all valuable data and research results concerning the Widespread Fatigue Damage as presented in the paper.

9. REFERENCES

1. Fidranský, J., "A Brief Description of Random Loading Algorithm for Airframe Test", Aero Vodochody, PP.1-152.86, May 1986, (in Czech).
2. Fidranský, J., "The development Structure Integrity Program description", Aero Vodochody, PP.1-12.93, June 1993, (in Czech).
3. Vrhel, J., "The Full Scale Fatigue Test of the Rear Part of the Fuselage and the Empennage of the L-39MS Aircraft", ARTI, Z-3525/93, November 1993, (in Czech).
4. Vrhel, J., "The Full Scale Fatigue Test of the L-39-X12 Prototype Aircraft", ARTI, Z-2792/83, May 1983, (in Czech).
5. Fidranský, J., Fiala, J., Vrhel, J., "Durability Test of L-39 Wing Spar Booms under Flight by Flight Loading," ARTI, V 1641/89, July 1989, (in Czech).
6. Fidranský, J., Fiala, J., "Full Scale Flight by Flight Wing Spar Fatigue Test", in "The 8th Biennial Conference on Fracture", Torino, Italy, 1990, pp 1670-1673.
7. Běhal, J., "The Feasibility Study of the Residual Strength of the Fatigue Critical Areas of the L-59 Aircraft", ARTI, R-2759/94, December 1994, (in Czech).
8. Šulc, J. et al., "Measurement of the Pressure Fluctuation and Stresses on the Wall of the Air Duct of the L-39MS Prototype during the Engine Run", Czechoslovak Academy of Science, Institute of Thermomechanics, T 429/91, September 1991
9. Siegel, J., Nedbal, I., "Fractographic Analysis of the Air Intake Duct of the L-59 Aircraft", Czech Technical University in Prague, E-KMAT-328/91, September 1991
10. Fidranský, J., Trabert, M., "Aircraft Structural Integrity Program for the Aero Vodochody L-139 Jet Trainer", in 1994 USAF Structural Integrity Program Conference, USAF, December 1994.
11. Aero Company Internal Data of L-39/59 Life Assessment (in Czech).

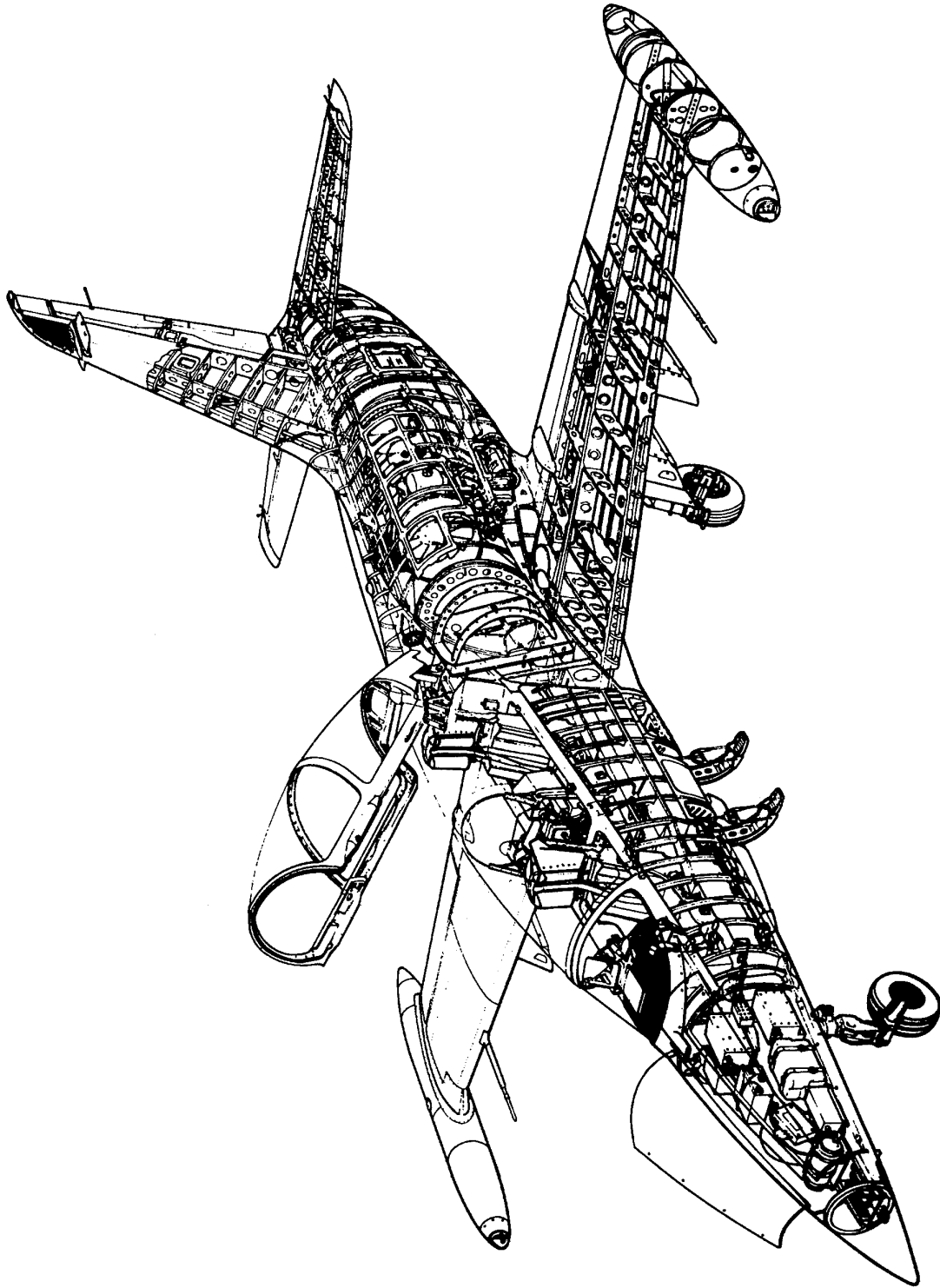


Fig. 1 Skeleton view on L-59 airframe

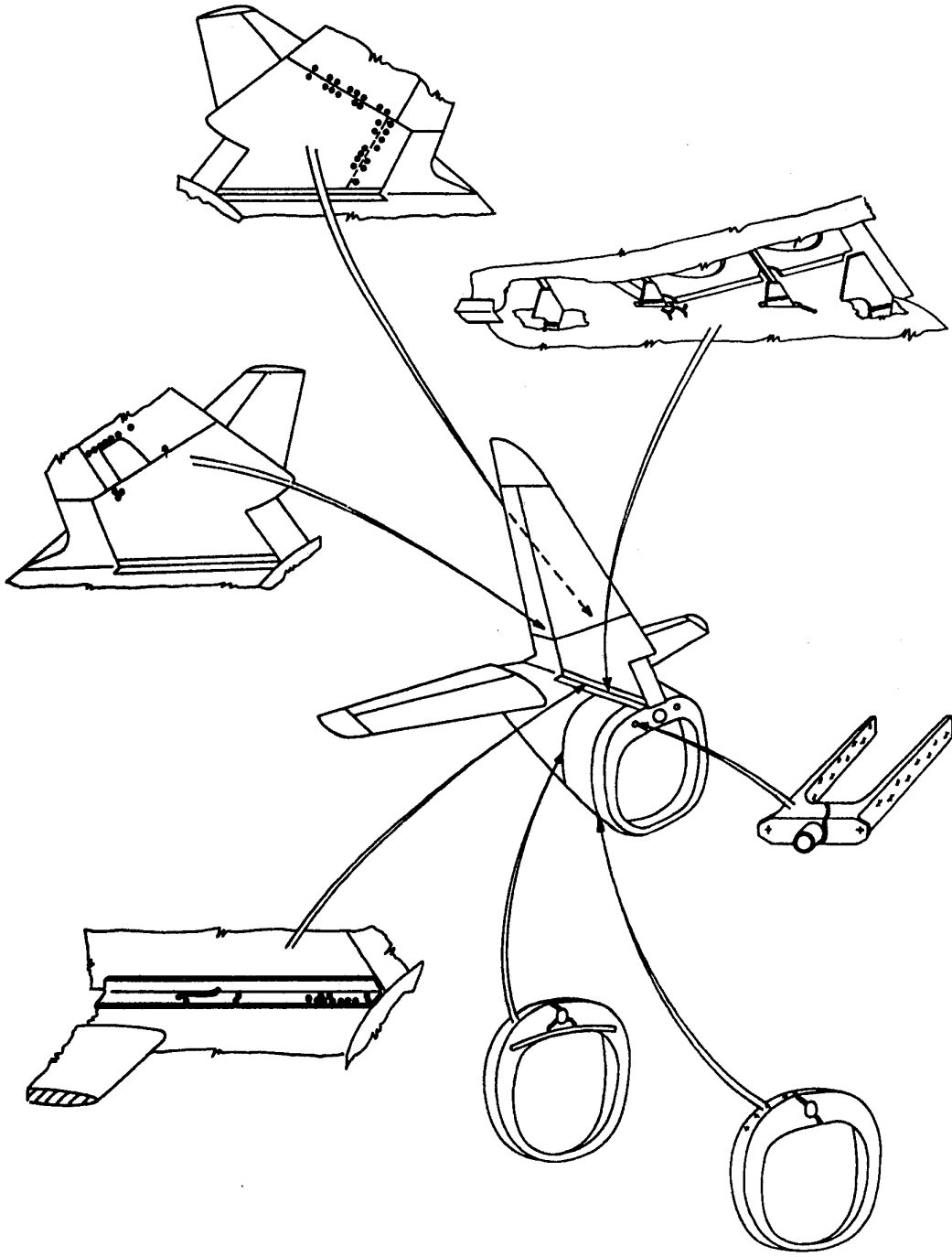


Fig. 2 Empennage structure - damaged area of fin root after the test

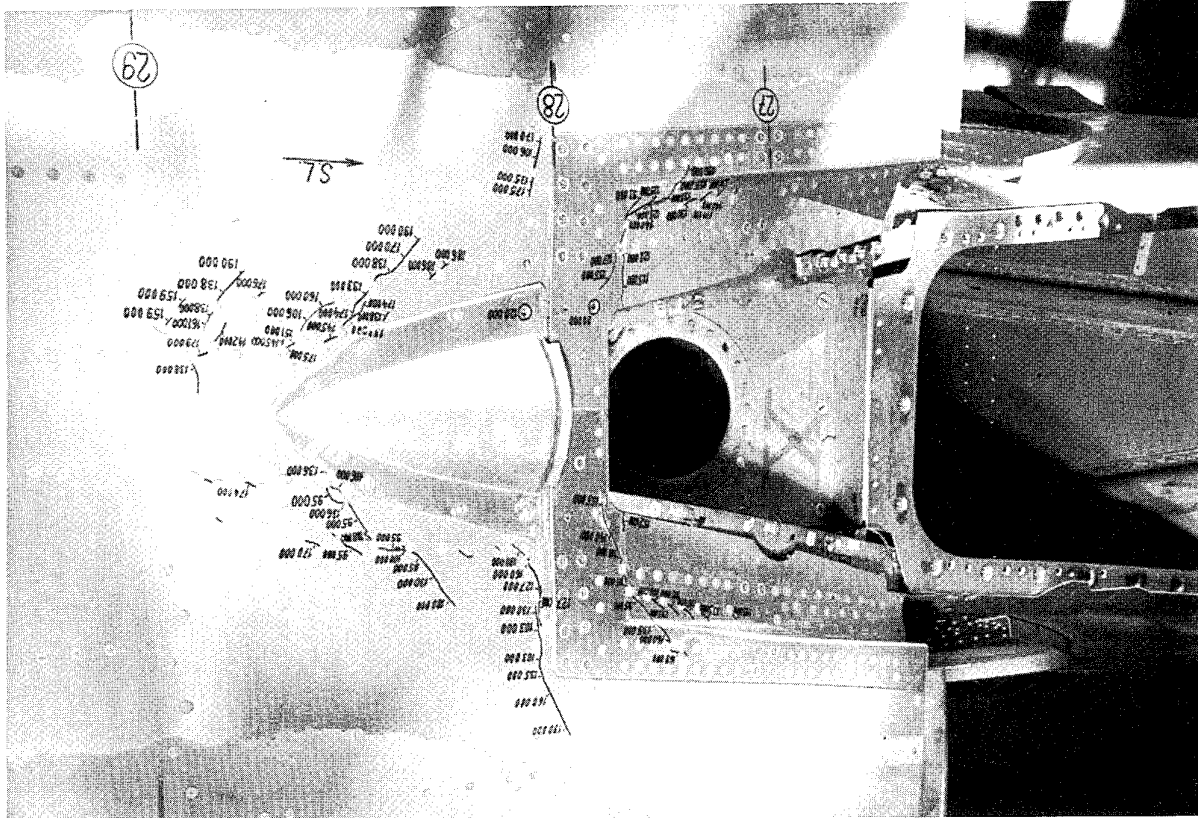


Fig. 3 Fatigue cracks on fuselage upper panel after the test

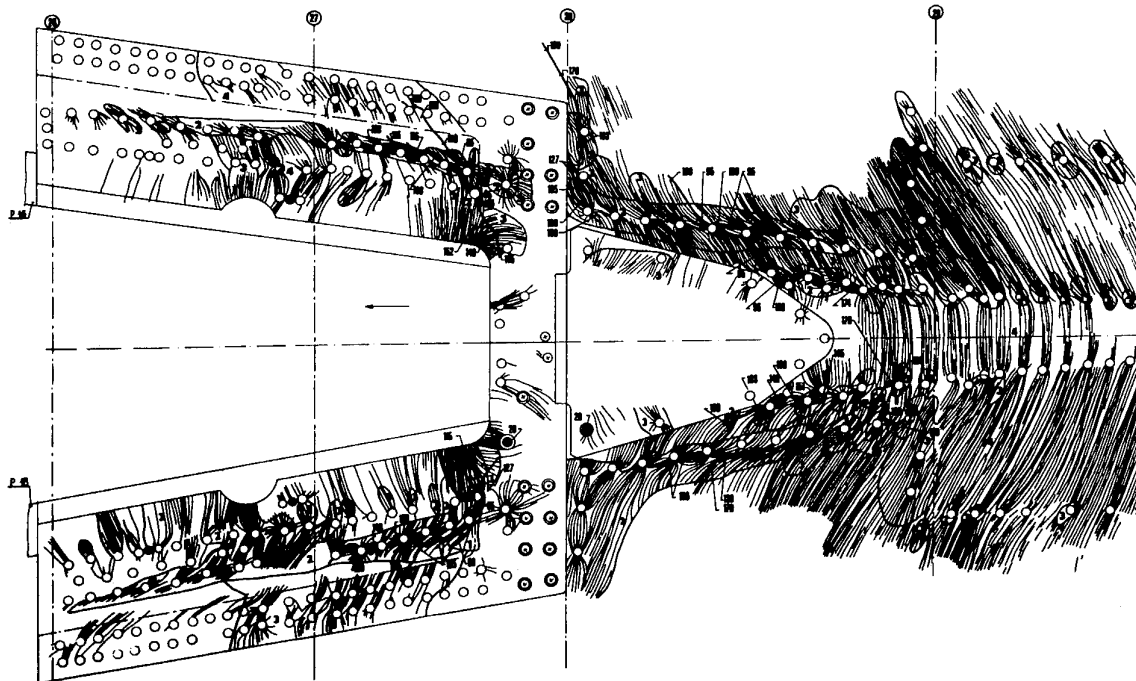


Fig. 4 Stress field on fuselage upper panel - stress coating technique

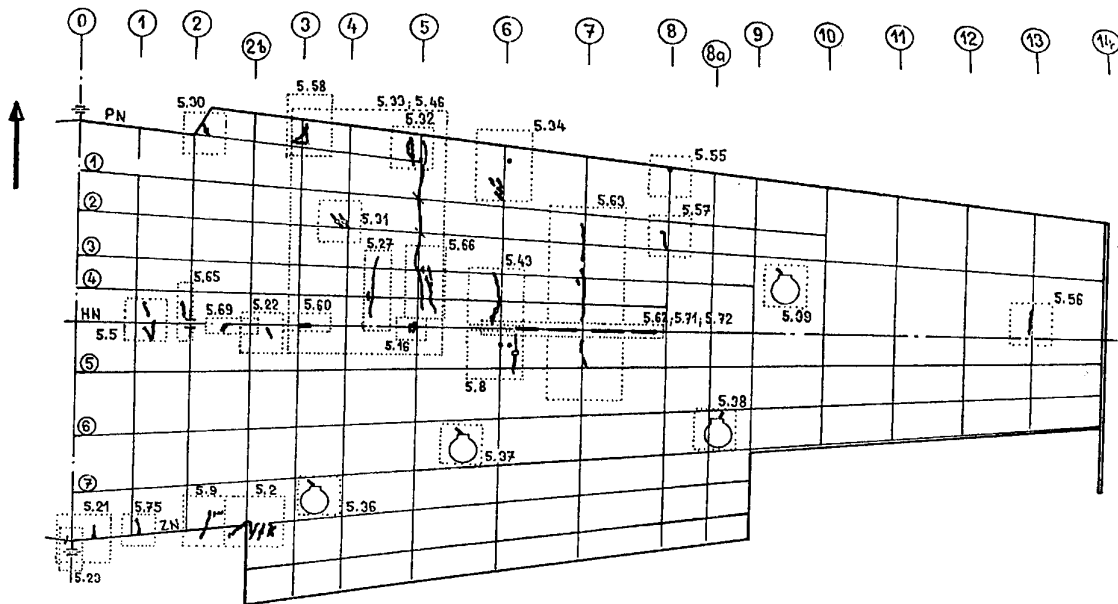


Fig. 5 Sketch of the wing with field of cracks after the test

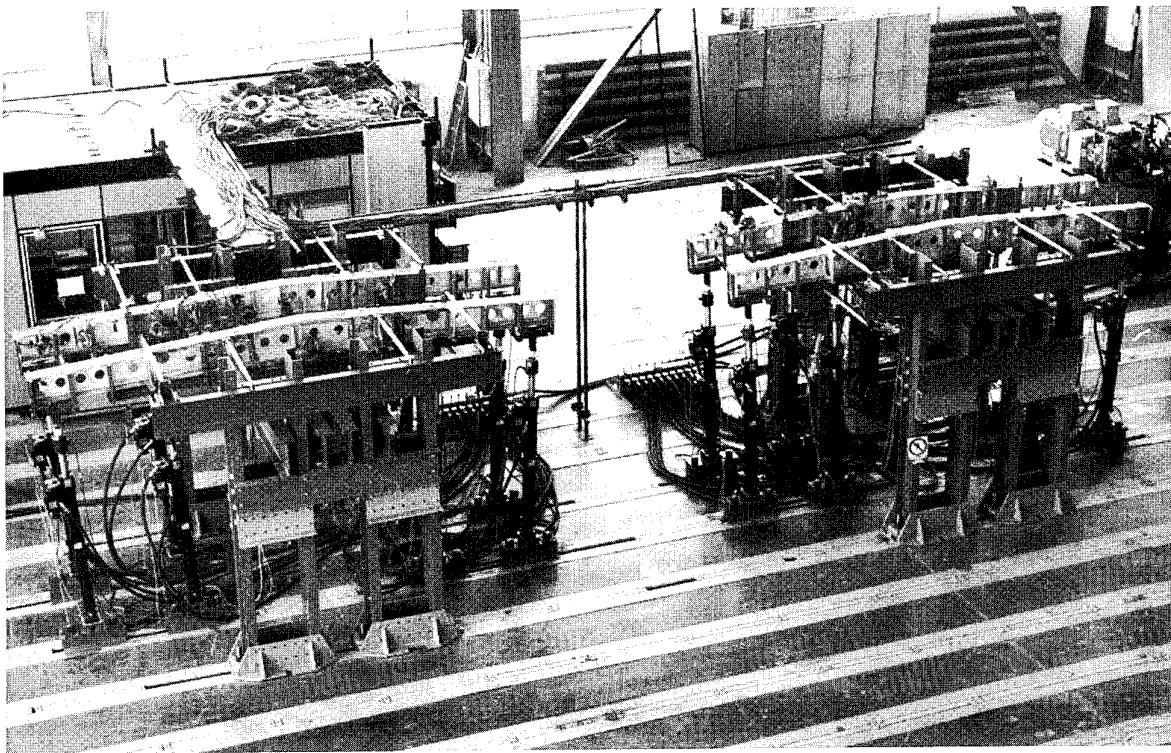


Fig. 6 Wing spar fatigue test arrangement

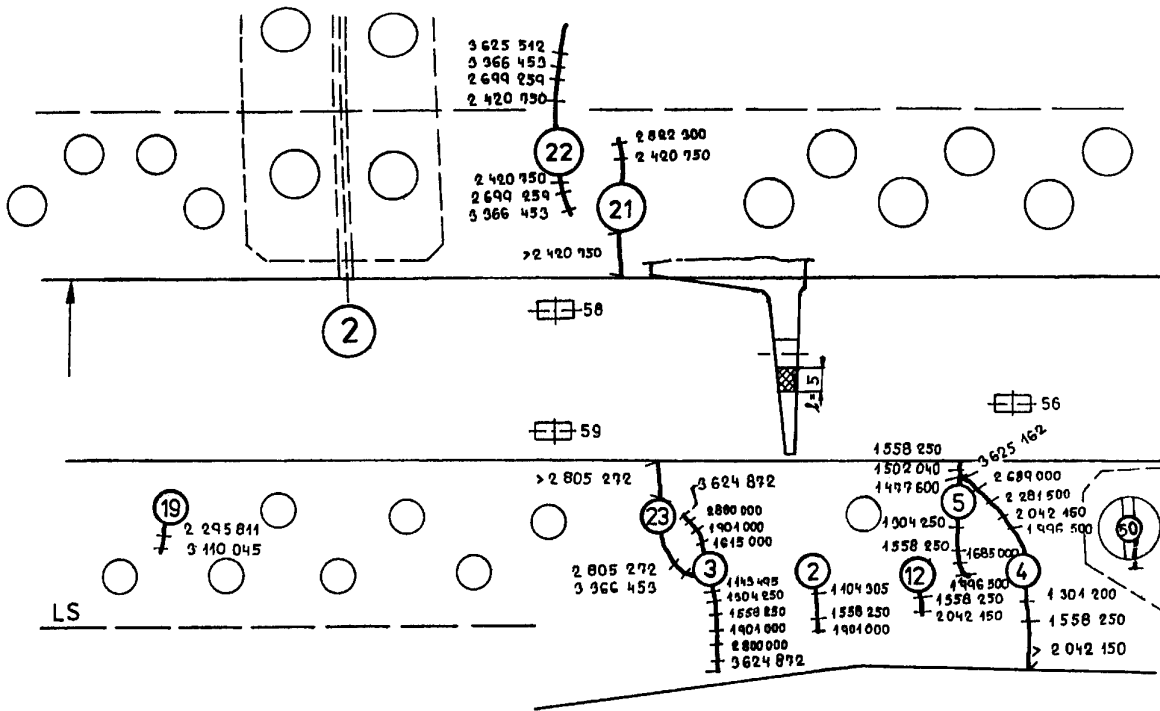


Fig. 7 Sample of the cracked test article

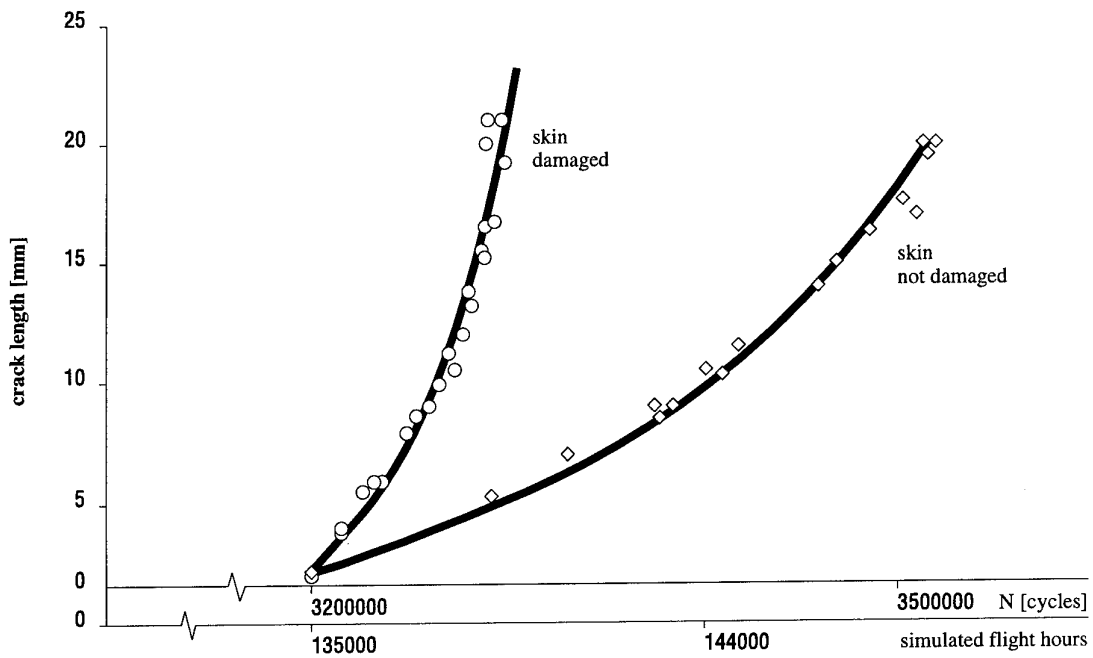


Fig. 8 Influence of the skin damage on crack growth rate at the wing spar

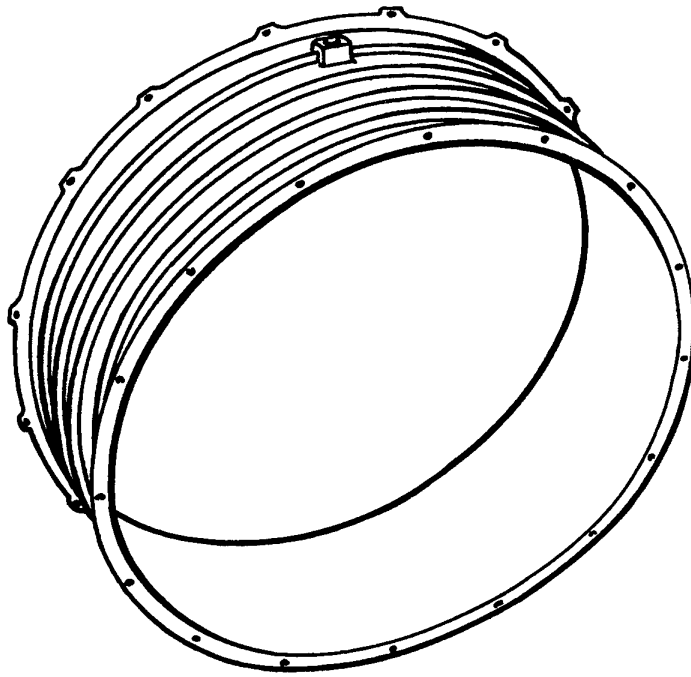


Fig. 9 Air intake ring overall view

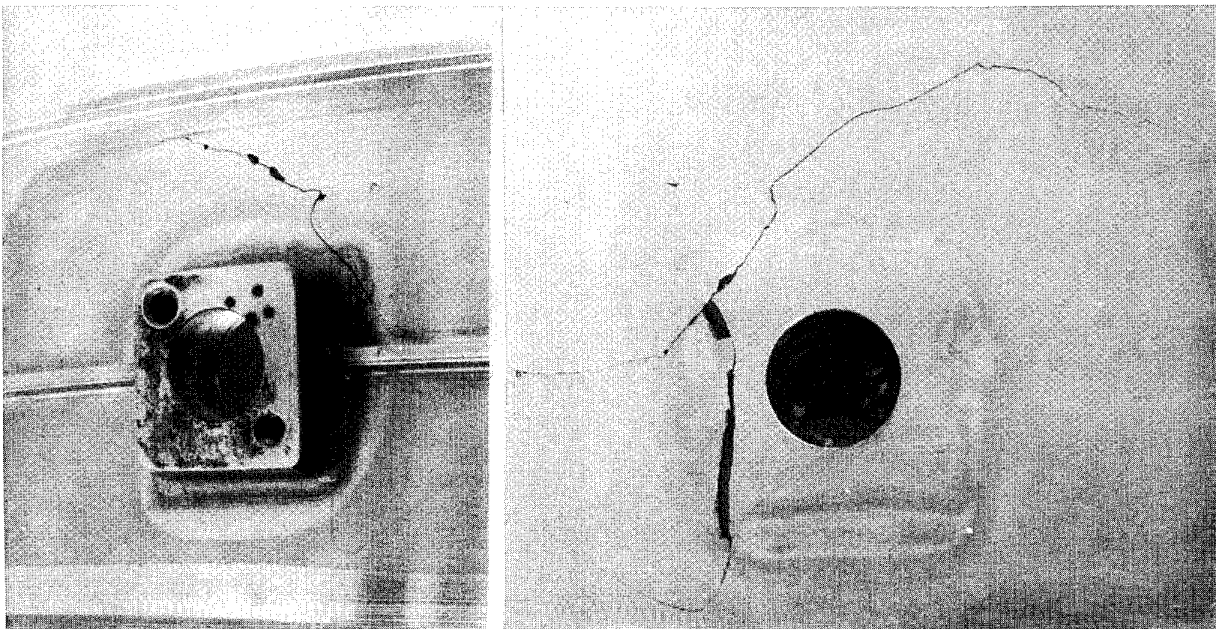


Fig. 10 Crack mesh surrounding the probe pad

ANALYSIS OF AIRCRAFT PANELS WITH WFD, BASED ON THE ELASTIC PLASTIC FINITE ELEMENT ALTERNATING METHOD (EPFEAM) AND T_e^* INTEGRAL

C.R. Pyo, H. Okada and S.N. Atluri

Computational Mechanics Center
Georgia Institute of Technology
A-FRENCH Bldg, Room 225
Atlanta, GA 30332-0356
USA

SUMMARY

Structural integrity evaluation of aging transport aircraft structures is extremely important to insure their economic and safe operation. In an airliner fuselage, pressurization causes stresses in the shell structure. The stiffening elements, such as stringers, frames and tear strips, take a part of the load but the major fraction is taken by the skin, for a typical fuselage structure shown in Fig. 1. A typical situation of Multiple Site Damage (MSD) is the existence of multiple cracks of arbitrary lengths emanating from a row of fastener holes in a bonded, riveted joint in a pressurized fuselage. This problem has been the object of a number of studies in assessing the structural integrity of aging airplanes (Atluri et al. (1991, 1992)) because the residual strength of a

structure with a single crack may significantly be reduced by the existence of adjacent smaller cracks (Broek (1993)). The results of Broek (1993) suggest that the prediction of such degradation of load carrying capacity of the damaged panels be very important. In Pyo et al. (1994), it has been shown that such predictions can be accomplished by analyzing stationary crack problems and employing an appropriate crack tip parameter. However, for a more accurate estimation, of the ultimate load capacity, an analysis of stable crack growth, and link up of cracks is necessary. Studies for stable crack growth problems have been conducted using elastic plastic finite element method (for instance Newmann et al. (1993)).

In this paper, new analytical methods (Elastic Plastic Finite Element Alternating Method (EPFEAM)) for predicting the residual strength of a ductile panel with a row of cracks, and their results are presented. The alternating method is based on an analytical modeling of cracks and on an iterative procedure to satisfy the required boundary conditions for the body under consideration (Nishioka and Atluri (1983), Park, Ogiso and Atluri (1992) and Park and Atluri (1993)), Pyo, Okada and Atluri (1994, 1994)). A finite element solution is required only for the problem without cracks. This greatly reduces the human resource cost in generating the required mesh because a very fine mesh pattern used in usual FEM is not necessary. The EPFEAM that uses the elastic alternating method in conjunction with the initial stress method (Nayak and Zienkiewicz (1972)) as an elastic plastic algorithm, is extended in this paper to analyze stably propagating MSD cracks and their link up. The crack extension is modeled by releasing the cohesive traction ahead of the crack-tip based on an analytical solution. Thus, unlike the more common finite element nodal release technique, the amount of crack growth at any time is independent of the finite element mesh discretization. Among the various fracture criteria to model the crack growth, the T_e^* integral, based on the equivalent domain integral (EDI) (Nikishkov and Atluri (1987)), is employed.

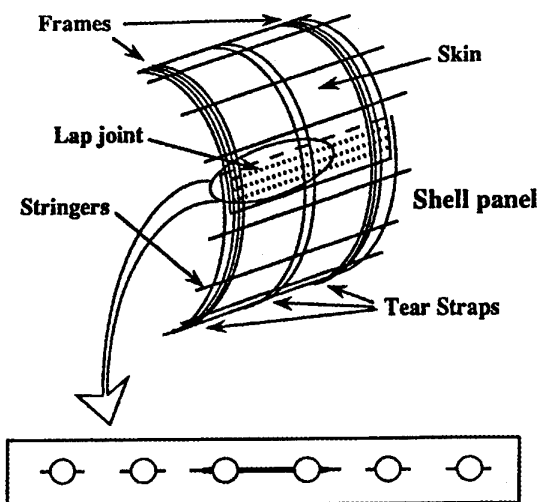


Fig. 1. A typical situation of Multiple Site Damage (MSD)

The procedures of the elastic-plastic finite element alternating method (EP-FEAM) are described in this paper for stationary as well as for stably propagating MSD cracks. Some numerical examples are presented, illustrating the residual strength estimations for a panel with MSD. The analytical results based on the stationary and stable crack propagation analyses are compared. And their differences in their residual strength predictions are also discussed.

ELASTIC PLASTIC FINITE ELEMENT ALTERNATING METHOD (EPFEAM) FOR STATIONARY AND STABLE CRACK PROPAGATION PROBLEMS

The elastic-plastic alternating technique for the MSD cracks has been developed to analyze both stationary, stably propagating MSD cracks and their link up. The T_e^* integral (Aturi (1986)) is employed as the crack propagation criterion. More detailed discussion of the physical significance of the T_e^* integral will be given later along with the analyses of panels with MSD cracks. In the followings, the finite element alternating method for stable crack propagation analysis is mainly discussed. The stationary crack analysis can be seen as a part of the crack propagation algorithm.

In the present stable crack propagation algorithm, the crack is thought to extend an incremental crack length Δa when the T_e^* integral reaches a critical value. After the crack extension, the external load is adjusted so that the T_e^* integral again reaches its pre-assigned critical value. The crack extension is modeled by releasing the cohesive traction ahead of the crack tip. Hence, the analysis is carried out in an incremental fashion, extending the crack tip for a length Δa during each crack propagation step.

The present algorithm consists of two parts. The first one is the elastic-plastic finite element alternating method for stationary crack problem. This is used while the panel is subjected to the external load until the T_e^* integral reaches a critical value, and while the load is being adjusted during subsequent crack-growth so that the T_e^* integral value comes back to its critical value again at any given crack length. The other part is for incremental crack extension, wherein the cohesive tractions ahead of the crack tip over the length of incremental crack growth (i.e., Δa) is released. Thus, the algorithm utilizes two kinds of analytical solutions. One is for a row of cracks of arbitrary lengths that are subjected to arbitrary tractions over their faces. The other solution is for the case the crack face traction is applied at both the ends of the lead crack, over a length Δa , the intended crack-growth increment. This analytical solution is used to release the cohesive traction ahead of the current crack tip. However, the mathematical formulations for both the solutions are essentially the same. The difference lies in only the locations

of crack face tractions (entire crack face or just the edge of the main crack).

The finite element alternating method utilizes two kinds of solutions:

1. An analytical solution to the problem of an infinite sheet with a row of cracks of arbitrary lengths with their crack faces being subjected to arbitrary tractions.
2. Finite element solution of the panel without cracks (called as solution to "uncracked body").

The elastic plastic finite element alternating algorithm uses the elastic finite element alternating technique in conjunction with the initial stress method. An analytical solution for an elastic crack, with arbitrary crack face loading, is used inside an initial stress iterative procedure as an addition to the finite element solution for the uncracked body. Iterative processes of the alternating method and of the initial stress method are performed simultaneously. The details of an elastic analytical solution for collinear multiple cracks in an infinite body, and elastic plastic finite element alternating method, are described below.

The algorithm for initially loading the panel, and for adjusting the load at any point during the subsequent crack-growth, is discussed below as well as illustrated in Figs. 2 and 3.

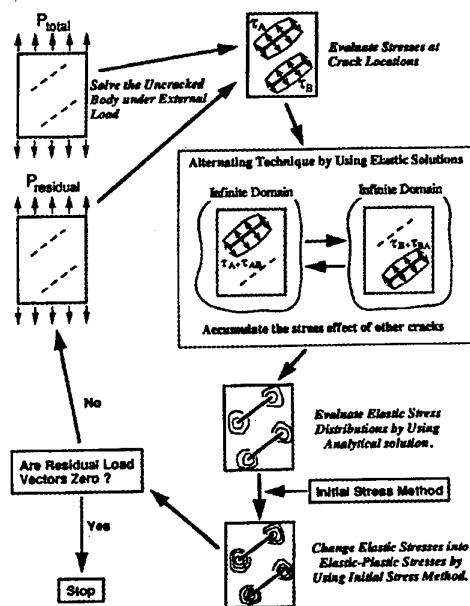


Fig. 2 Algorithm of EPFEAM

1. Initialization ;

$$\{q_o^{(0)}\} = \{0\} : \text{Initialize the}$$

displacements for the FE mesh of the uncracked panel to be zero

$$\{\psi^{(0)}\} = \{P\} : \text{Initialize}$$

the unbalanced nodal forces to be zero

2. Iterating Procedure ;

$$\{\Delta q_o^{(i)}\} = [K_o]^{-1} \{\psi^{(i-1)}\} :$$

Calculate the displacement increments

due to the unbalanced forces for the

uncracked body.

$$\{q_o^{(i)}\} = \{q_o^{(i-1)}\} + \{\Delta q_o^{(i)}\}$$

: Update the displacements for uncracked body.

$$\{\sigma_o^{(i)}\} = [D][B]\{q_o^{(i)}\}$$

: Stresses due to the displacement for the uncracked body, if the material were elastic.

$$\{t_c^{(i)}\} = -[n]\{\sigma_o^{(i)}\}$$

: Crack face cohesive tractions to be reversed.

$$\{t_c^{(i)}\} = -[b^{(i)}]\{U\} : \text{Approximation}$$

$$\{\sigma_c^{(i)}\} = \{\sigma_c([b^{(i)}])\} :$$

Analytical Solution

$$\{\sigma^{(i)}\} = [D^{ep}][D]^{-1}(\{\sigma_o^{(i)}\} + \{\sigma_c^{(i)}\})$$

: Return to the yield surface

$$\{\psi^{(i)}\} = \{P\} - \int_V [B]^T \{\sigma^{(i)}\} dV$$

: Calculate the unbalanced nodal forces

3. Convergence ;

$$\|\Delta q^{(i)}\| < \epsilon \|q\| : \text{Convergence criterion}$$

Until the convergence is achieved, "the Iterating procedure" in Step 2 above is repeated for $i=1,2,\dots$

In this algorithm, as in the case of the elastic alternating technique, the singular stress field is obtained through the analytical solutions for the cracked infinite medium, thus eliminating the need for a very fine mesh discretization around the crack tip.

The algorithm for releasing the cohesive traction during the crack propagation by an amount Δa is described below, and also its concept is illustrated in Fig. 3.

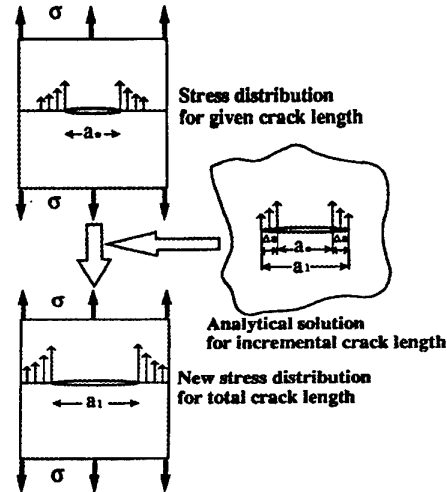


Fig. 3 EPFEM for Crack Propagation Analysis

Algorithm to Release the Cohesive Traction

1. Computation of stresses ahead of the crack tip for the given crack length.

$$\{\sigma_o^{(i)}\} = [D][B]\{q_o^{(i)}\}$$

: Stresses due to the displacement for the uncracked body, if the material were elastic.

$$\{t_c^{(i)}\} = -[n]\{\sigma_o^{(i)}\} : \text{Crack face cohesive tractions to be}$$

reversed.

$$\{t_c^{(i)}\} = -[b^{(i)}]\{U\} : \text{Approximation}$$

$$\{\sigma_c^{(i)}\} = \{\sigma_c([b^{(i)}])\} : \text{Analytical Solution}$$

$$\{\sigma^{(i)}\} = [D^{ep}][D]^{-1}(\{\sigma_o^{(i)}\} + \{\sigma_c^{(i)}\}):$$

Return to the yield surface

$$\text{Convergence and } \varepsilon^* = T_{Cr}^* \longrightarrow \{\sigma_o\} = \{\sigma^{(i)}\}$$

2. Releasing cohesive traction for Δa

$$\{t_c\} = -[n]\{\sigma_o\}: \text{Crack face cohesive tractions for } \Delta a$$

$$\{t_c\} = -[b]\{U\}: \text{Approximation}$$

$$\{\sigma_c\} = \{\sigma_c([b])\}: \text{Analytical Solution}$$

$$\{\sigma\} = [D^{ep}][D]^{-1}(\{\sigma_o\} + \{\sigma_c\}):$$

Return to the yield surface

These procedures can be seen as an iterative algorithm. And it is repeated, until the stress boundary conditions at the edge of the finite body are satisfied. It is equivalent to requiring that the residual traction at the edge of the finite body become zero. The convergence of the FEAM is guaranteed in terms of the Schwartz-Newmann alternating method.

ANALYTICAL SOLUTION FOR COLLINEAR MULTIPLE CRACKS IN A LINEAR INFINITE BODY

Consider the problem when collinear multiple cracks exist, in an infinite isotropic elastic plate along the x axis, and arbitrary normal and shear tractions are applied on the crack surfaces. Each crack is of an arbitrary length. This problem can be solved if the fundamental solution to the problem shown in Fig. 4 is known. In Fig. 4, a normal point force of magnitude P and a shear point force of magnitude Q are applied at a point $x = c$ on the upper surface of the k th crack, and two point forces $-P$, $-Q$ are applied at the point $x = c$ on the lower surface of the same crack. By using this solution as a Green function, the stress fields can be obtained for any arbitrary tractions that exist on the crack faces. In

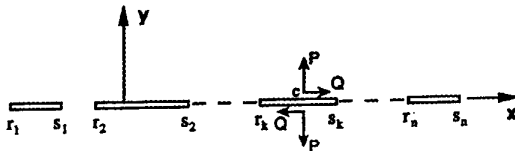


Fig. 4 Fundamental Solution for Co-linear cracks

order to solve this fundamental problem, the results given in Muskhelishvili (1953) are used. Let σ_y^+ , σ_{xy}^+ be stresses

applied on the upper crack surface, and σ_y^- , σ_{xy}^- be stresses applied on the lower surfaces. Then the complex functions for this problem can be obtained as follows:

$$\Phi(z) = \Phi_o(z) + \frac{P_n(z)}{X(z)} - \alpha \quad (1)$$

$$\Omega(z) = \Omega_o(z) + \frac{P_n(z)}{X(z)} + \alpha \quad (2)$$

where

$$\Phi_o(z) = \frac{1}{2\pi i X(z)} \int_L \frac{X^+ p(t)}{t-z} dt + \frac{1}{2\pi i} \int_L \frac{q(t)}{t-z} dt \quad \dots (3)$$

$$\Omega_o(z) = \frac{1}{2\pi i X(z)} \int_L \frac{X^+ p(t)}{t-z} dt - \frac{1}{2\pi i} \int_L \frac{q(t)}{t-z} dt \quad \dots (4)$$

and

$$X(z) = \prod_{k=1}^n \sqrt{z-r_k} \sqrt{z-s_k} \quad (5)$$

$$P_n(z) = c_0 z^n + c_1 z^{n-1} + \dots + c_n \quad (6)$$

$$p(t) = \frac{1}{2} [\sigma_y^+(t) + \sigma_y^-(t)] - \frac{i}{2} [\sigma_{xy}^+(t) + \sigma_{xy}^-(t)] \quad (7)$$

$$q(t) = \frac{1}{2} [\sigma_y^+(t) - \sigma_y^-(t)] - \frac{i}{2} [\sigma_{xy}^+(t) - \sigma_{xy}^-(t)] \quad \dots (8)$$

In Eqs. (3) and (4), the integration path L consists of n segments $L_1, L_2, \dots, L_k, \dots$ and L_n . The segment L_k is from r_k to s_k along the x -axis, r_k and s_k being the end points of k th crack. The complex constants α in Eqs. (1) and (2), and c_0 in Eq. (6) are related to the stresses and rigid body rotation at infinity. If there is no stress and no rigid body rotation at infinity, α and c_0 must be zero. The coefficients in the polynomial of Eq. (6) can be determined from the condition of the single valuedness of displacements as follows:

$$\kappa \int_{\Gamma_i} \Phi(z) dz - \int_{\Gamma_i} \Omega(\bar{z}) d\bar{z} = 0, \quad i = 1, 2, \dots, n \quad (9)$$

Here Γ_i is the contour which surrounds the i th crack in a counterclockwise direction, and $\kappa = 3 - 4\nu$ for plane strain condition and $\kappa = (3 - \nu) / (1 + \nu)$ for plane stress condition, where ν is the Poisson's ratio.

Once the complex stress functions in Eqs. (1) and (2) are determined, the stresses and displacement can be obtained from :

$$\sigma_{xx} + \sigma_{yy} = 2[\Phi(z) + \overline{\Phi(z)}] \quad (10)$$

$$\sigma_{yy} - i\sigma_{xy} = \Phi(z) + \Omega(z) + (z - \bar{z})\overline{\Phi'(z)} \quad (11)$$

$$2\mu(u + iv) = \kappa\phi(z) - \omega(\bar{z}) - (z - \bar{z})\overline{\Phi'(z)} \quad (12)$$

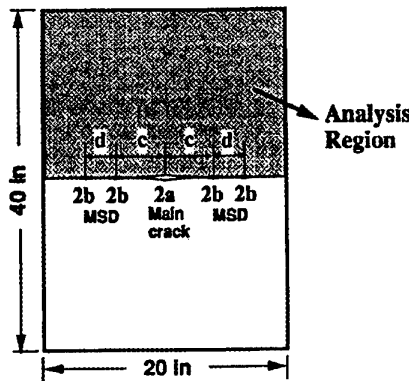
Here $\Phi(z) = \phi'(z)$, $\Omega(z) = \omega'(z)$ and μ is the shear modulus.

By using the solutions of this problem as Green functions, we can obtain the stress and displacement fields for collinear multiple cracks, each of arbitrary length, and each being subject to arbitrary crack surface tractions. The details of this solutions are presented in Park and Atluri (1993).

ELASTIC-PLASTIC ANALYSIS OF FLAT PANELS WITH MSD & DISCUSSION

Material Properties

In order to predict the residual strength of panels, with MSD, made of Aluminum alloy 2024-T3, which has an elastic modulus of 10,470 ksi and Poisson's ratio of 0.3, we use the one dimensional stress-strain relation as approximated by a



Cases	No. of MSD	a	b	c	d
q1	0	3.75	-	-	-
q2	2	3.75	0.25	5.0	-
q3	4	3.75	0.25	5.0	1.5
q4	6	3.75	0.25	5.0	1.5
q5	2	5.25	0.25	6.5	-
q6	2	6.75	0.25	8.0	-

Fig. 5 Configuration of MSD Cracks to be Analyzed

Ramberg-Osgood power law relationship (Pyo, Okada and Atluri (1994)). The constants for the Ramberg-Osgood approximation are: $\alpha=0.2$ and $n=8$. The stress strain relationship is written to be:

$$\frac{\epsilon}{\epsilon_Y} = \alpha \left(\frac{\sigma}{\sigma_Y} \right)^n \quad (13)$$

where σ , ϵ , σ_Y and ϵ_Y are one dimensional uniaxial stress, strain, yield stress and strain at yielding. For the material considered here, σ_Y and ϵ_Y are 33.4 ksi and 0.00314, respectively.

Residual Strength Prediction of Panels with MSD using Stationary Crack Analysis

The EPFEAM is employed in the residual strength prediction for panels with MSD cracks. The configurations of the plates are indicated in Fig. 5. The residual strength of the panels with MSD is defined to be the ultimate hoop stress. EPFEAM is used as an effective and appropriate analytical method. Then an appropriate failure criterion should be employed. The T_e^* (see Atluri (1986)) integral is used in this study and its predictions are discussed in this section.

The T_e^* integral is defined on a small contour around the crack tip, as depicted in Fig. 6. This integral parameter is known to be effective not only for the stationary crack problems but also for fast propagating and stably propagating cracks in a nonlinear solid (see Atluri (1986)). The T_e^*

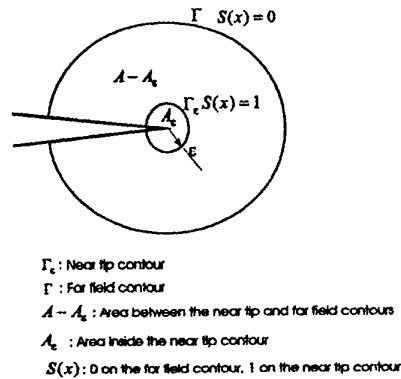


Fig. 6 T_e^* Integral Evaluation on Γ_ϵ Contour

integral in the case of quasi-static problem, can be defined, as:

$$T_e^* = \oint_{\Gamma_\epsilon} \left(Wn_1 - t_i \frac{\partial u_i}{\partial x_1} \right) d\Gamma_\epsilon \quad (14)$$

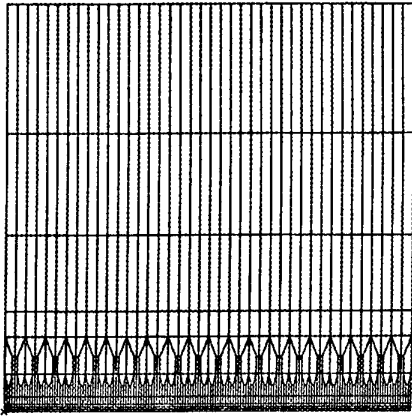


Fig. 7 Finite Element Mesh Used in the Present FEAM Analyses

In the case of propagating crack, the integral contour Γ_ϵ moves along with the crack tip. Then, the T_ϵ^* can be interpreted, for a suitably small value of ϵ , as a scalar parameter that quantifies the severity of the crack-tip fields. Also, the T_ϵ^* integral depends on only the near tip deformation field, so that, in the case of self-similar stable crack propagation, the T_ϵ^* should become a constant value. For the current context of stationary cracks in a panel that is subject to monotonic loading, T_ϵ^* is identical to the J integral (Rice (1968)).

In order to evaluate the T_ϵ^* integral numerically, the contour integral is converted to area integral (equivalent domain integral [see Nikishkov and Atluri (1987)]). This is to make use of the far field quantities to evaluate the near tip contour integral, due to the fact that the quantities near the crack tip may contain a large magnitude of numerical error, which may deteriorate the integral evaluation. The far field quantities are expected to be more accurate than the near tip variables. A function $S(x)$ is introduced in this process. By letting $S(x)$ be 1 on the Γ_ϵ contour and be 0 on a far field contour Γ , the near tip contour integral can be converted to an area integral, as:

$$\begin{aligned}
 T_\epsilon^* &= \oint_{\Gamma_\epsilon} \left(Wn_1 - t_i \frac{\partial u_i}{\partial x_1} \right) d\Gamma_\epsilon \\
 &= \oint_{\Gamma_\epsilon} \left(S(x)Wn_1 - S(x)t_i \frac{\partial u_i}{\partial x_1} \right) d\Gamma_\epsilon \\
 &= - \iint_{A-A_\epsilon} \left\{ \frac{\partial(S(x)W)}{\partial x_1} - \frac{\partial}{\partial x_j} \left(S(x)\sigma_{ij} \frac{\partial u_i}{\partial x_1} \right) \right\} dA
 \end{aligned}
 \tag{15}$$

The failure of the panel is assumed to occur when the T_ϵ^* integral at the tip of main crack reaches its critical value $T_\epsilon^*|_{\text{Critical}}$. $T_\epsilon^*|_{\text{Critical}}$ is set to be 710 lb / in for the radius of the contour $\epsilon \approx 0.125$ in. This value is the saturation value of the T_ϵ^* for the stable crack growth in a single

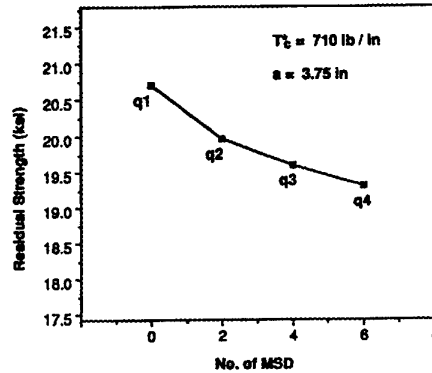


Fig. 8 Reduction of Load Carrying Capacity with Increasing Number of MSD Cracks

cracked panel, presented in the following section¹. The T_ϵ^* integral value should not exceed this saturation value during a large length of crack propagation. Therefore, the ultimate carrying load capacity of a plate can be predicted by employing such $T_\epsilon^*|_{\text{Critical}}$ criterion.

A number of analyses for the plates with MSD cracks have been performed by using only one finite element mesh (depicted in Fig. 7). The interests in terms of the damage

¹In the stable crack propagation analysis, the value of the T_ϵ^* integral is chosen as a function of crack extension such that the EPFEAM results agree with experimental data (Broek(1993)). It has been found that the value of the T_ϵ^* integral increases from the initiation to its saturation (maximum) value.

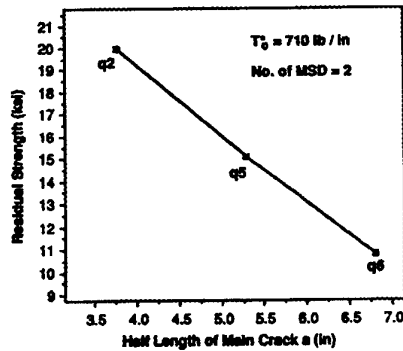


Fig. 9 Reduction of Load Carrying Capacity with Respect to the Length of Main Crack

tolerance design or of assessment of the structural integrity of aging aircraft, lie in the influence of number of MSD cracks ahead of a lead crack on the ultimate load carrying capacity of such damaged panels. Therefore, a number of cases as indicated in Fig. 5 have been analyzed.

The results indicate that the reduction of the residual strength occurs with the number of the MSD cracks, as depicted in Fig. 8. These result have been obtained by analyzing the cases q1, q2, q3 and q4, as indicated in Fig. 5. The reduction of the strength is very significant from 0 to 2-6 MSD cracks. Then, it exhibits a saturation type behavior. To perform such analysis with an ordinary finite element method, the boundary conditions must explicitly be altered for each one of the cases, taking much computer time as well as human-resources. However, in the case of EPFEAM, there is no need to give the boundary conditions explicitly, since only the uncracked panel is analyzed by finite elements. Only a part of input data specifying the position and width of cracks are required to be altered, because of the use of analytic crack solutions. This is one of the advantages of EPFEAM which facilitate a rapid repetitive parametric study on the different configurations of MSD cracks.

In Fig. 9, the influence of the main crack length on the residual strength is shown. It indicates that the reduction of the residual strength is very significant with respect to the size of main crack. This diagram is obtained by analyzing the cases q2, q5 and q6 (as shown in Fig. 8).

Stable Crack Propagation analysis of Panels with Multiple Site Damage (MSD) Using the T_e^* Crack Propagation Criterion

The results of stable crack propagation analyses, based on the above presented EPFEAM with the T_e^* crack propagation criterion, are presented in this section. The cases

analyzed here are shown in Fig. 10. In Broek (1993) these panels are tested for their fracture stresses. There are 6 cases p1-p6 (single crack cases p1-p3, two MSD cracks p4-p5 and four MSD crack case p6). In this section, the validity of the proposed algorithm, based on the EPFEAM with T_e^* criterion, is first confirmed by studying the problem of crack propagation problem in a linear elastic solid. And then the elastic plastic crack propagation analyses are presented.

The same mesh discretization is used for all the analysis presented in this paper. It is one of the significant advantages of the present EPFEAM - only the uncracked panel is modeled by the finite element mesh remains the same, irrespective of the number of cracks in the panel; furthermore, no finite mesh near each crack-tip, as in the traditional finite element analysis, is needed. It is shown in Fig. 7. Mesh size at the crack tip is 0.125 in. The mesh in Fig. 7 is using the EPFEAM of course, much coarser than that required to do similar analyses using CTOA crack propagation criterion² (Newmann et al. (1993)).

Stable crack growth in the Panels with the MSD is analyzed, using the elastic and elastic-plastic finite element alternating method (FEAM). The T_e^* is used as the crack propagation criterion. The T_e^* integral is defined at a small contour around the crack tip, as indicated in Fig. 6. And this small contour moves along with the propagating crack tip. Therefore the integral parameter quantifies the severity of stresses and strains near the crack tip. Thus, for steady crack propagation, this integral parameter is considered to take a constant value.

During stable crack propagation, the T_e^* value changes from its value at the initiation crack-growth to that during the steady state, as the stress and strain distributions around the crack tip change. It is necessary, first, to determine the variation of the T_e^* integral as the crack extends. Therefore, we need three pieces of information on the T_e^* values during the stable crack propagation: the first one is the value at the crack-growth initiation; the second, is its value for steady state; then, we connect these two by some transient behavior. To determine the critical T_e^* integral values, we used the experimental load crack extension ($P-\Delta a$) data for panels with a single crack. The T_e^* integral values [for $\epsilon=0.125$ in] were determined by simulating the $P-\Delta a$ curves computationally, for each of the cases P1-P3, by running the EPFEAM code in its "generation phase". An appropriate set of the T_e^* integral values for the initiation, transition and the steady state have been determined to be: T_e^*

²In Newmann et al. (1993) crack propagation analyses with CTOA criterion was presented. The crack tip mesh size was 0.01 in.

(initiation)=200lb/in; T_g^* (steady-state)= 710lb/in. The P- Δ curve obtained using such T_g^* , and running the EPFEAM code in its "application phase" compares very well with the experimental data, for each of the 3 cases, P1-P3, as shown in Fig. 10. In Fig. 11, three center cracked panels with different initial crack length were analyzed using the EPFEAM. Since the T_g^* integral characterizes the severity of the stress-strain field in the vicinity of the crack tip, the same criterion can be used for the cases with different crack configurations. Thus, the same crack propagation criterion was applied to the panels with MSD cracks.

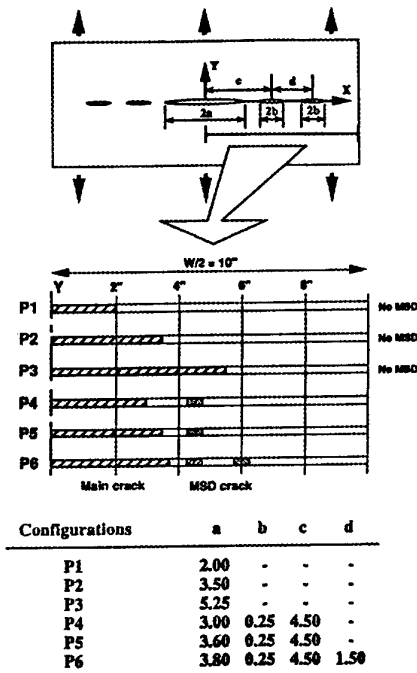


Fig. 10 Configuration of Main and MSD Cracks in a Center Cracked Panel, Analyzed by EPFEAM for Stable Crack Propagation and Compared with Test Data.

First, a panel with two MSD cracks at both the sides of the main crack was analyzed. A stable crack propagation analysis was carried out in its "application phase". The results of EPFEAM were compared with the experimental result (Broek (1993)), as shown in Fig 12. The experiment was carried out under a load control condition. Thus, an unstable fracture occurred when the maximum load was reached. We shall compare the maximum load predicted by the elastic plastic finite element alternating method and the result of the experiment. In this case (p4), the analysis and the experimental study perfectly match with each other. It is mentioned here that, for this particular crack configuration, the maximum load was reached after a small length of crack propagation. Then the load kept dropping as the crack

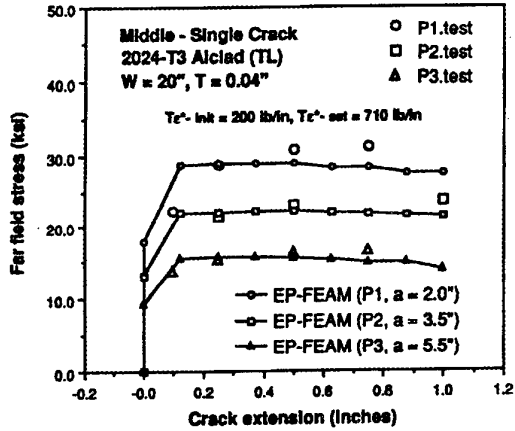


Fig. 11 Generation Phase Analysis for Single Crack Panel Compared with Experimental Data (Very good agreements between the computational predictions and test data are seen for different initial crack sizes)

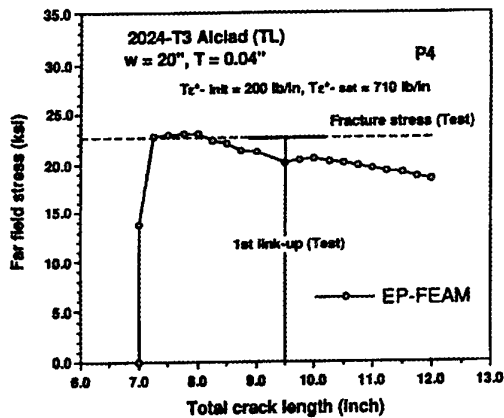


Fig. 12 The Carrying Load-Crack Extension Curve for the Case p4 Predicted by EPFEAM.

extends. Then, the main and MSD cracks link up. After the link up, the load increases slightly. However, in Fig. 12, the link up load and the fracture load in the experiment are indicated to be identical to each other. This is because the link up occurred as a part of the unstable fracture process at the maximum load.

For the case P5 with a lead lager crack, with the same size MSD crack, as in P4, the results are shown in the Fig. 13. Again, the fracture load of the experiment and the maximum load predicted by the elastic plastic finite element alternating method are almost identical to each other. In this case, the

results of EPFEAM indicate that the loads carried by the coupon before and after the link up are almost the same. The load drops at the link up slightly.

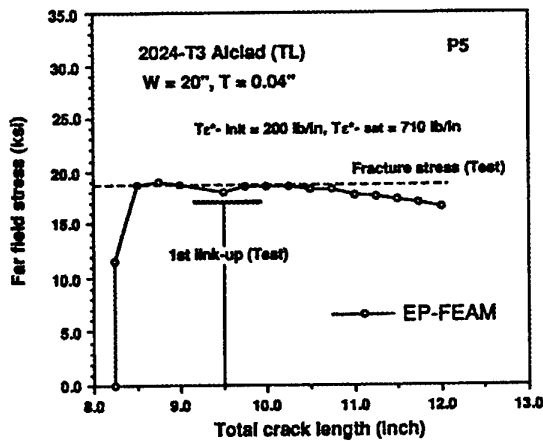


Fig. 13 The Carrying Load-Crack Extension Curve for the Case p5 Predicted by EPFEAM.

For the case of 4 MSD cracks (p6), the results of the elastic plastic finite element alternating method are shown in Fig. 14. The maximum load predicted by the EPFEAM was obtained between the first and second link up. The experimentally observed maximum was also between the first and second link up. Thus, in the experiment, unstable fracture occurred before the second link up, making loads at the fracture and at the second link up identical to each other.

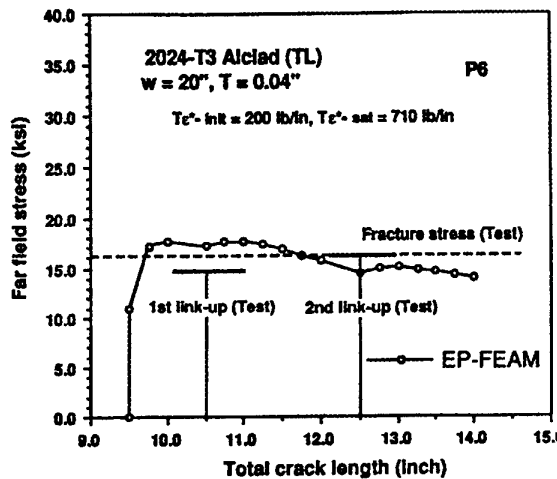


Fig. 14 The Carrying Load-Crack Extension Curve for the Case p6 Predicted by EPFEAM.

The discrepancy between the fracture load predicted by the EPFEAM and the experimental data was within 10 %.

It should be pointed out that the reduction of the fracture load from p1 (smallest single crack case among presented) to p6 (with four MSD cracks) was about 50 % (of that for p1). The magnitude of the reduction of the fracture load was, in fact, predicted with reasonably good precision (within about 10 % of error throughout the cases analyzed). Therefore, the results presented in this paper confirm that the EPFEAM with T_e^* criterion can predict the overall behavior of panels with MSD cracks. Also, the procedures developed in the present research is shown to be effective: 1) to determine the critical T_e^* values by correlating the analysis and experiment in single crack case (or some other available simple cases), and then 2) use the same criterion to treat more complicated cases (such as with MSD cracks).

DISCUSSION & CONCLUSION

Two kinds of methodologies to predict the load carrying capacity of MSD damaged panels have been discussed in this paper. Comparing both the predictions, it seems that the one utilizing only the stationary crack analysis underestimates the strength of such damaged panels. For example, the MSD crack configuration q2 is almost equivalent to p4. Their predictions have been carried out using stationary crack and stably propagating crack analyses, respectively. In the case of q2 the residual strength (hoop stress) is about 20 ksi, whereas in the case of p4, it is about 23 ksi. It can be explained by the wake zone effect, which can relax the severity of the deformation at the crack tip in the case of stably propagating crack. There is a slight increase of carrying load of the plates, during small length of crack propagation. Hence, the residual strength predictions utilizing the stable crack propagation analysis became higher than the other. Furthermore, it is expected to be more accurate than the other also.

However, from an engineering analysis point of view, though EPFEAM is very efficient and cost effective, the stable crack propagation analysis is substantially more expensive than the stationary one. We shall propose an analysis procedure, using both the residual strength prediction methods. First, we shall compare, how much the one using only the stationary crack analysis underestimates the strength compared to the other for a few crack (MSD) configuration. Thus, we can carry out the prediction only using the stationary crack analysis and add the factor of underestimation. Hence, we shall be able to carry out the residual strength analysis for MSD damaged panels, accurately and economically.

A critical issue in application of the T_e^* integral criteria is that how one can measure it for the initiation value and saturation value. And also, it is very important that the T_e^* integral value saturates (becomes a constant value) during the stable crack propagation (steady state). Recently, Okada

et al. (1995) attempted a hybrid experimental/numerical study for measuring the T_e^* integral value during the stable crack propagation, by using a small (1 inch width) 2024T3 SEN specimens. Their results, indeed, indicates that the T_e^* integral saturates after about 0.16 in of crack propagation. Furthermore their results also show that the T_e^* integral values used in this study are very similar to those obtained in Okada et a. (1995) for the similar size of Γ_e contour, as indicated in Table 1 below. Hence, it has been demonstrated that one can obtain the T_e^* integral values, which are necessary to carry out the residual strength predictions, from a fracture test on small samples.

The alternating technique uses a combination of the finite element solution for the uncracked panel, and the analytical

Table 1 T_e^* integral values for similar sizes of Γ_e contour.

	Present Analysis	Okada et a. (1995)
Γ_e contour	0.25 x 0.25 in square	0.24 x 0.24 in square
Initiation	200 lb/in	205 lb/in
Saturation	710 lb/in	680 lb/in

solution for the multiple cracks in an infinite elastic body. The singular nature of the crack solution is embedded in the analytical solution. Thus, a single finite element mesh is used irrespective of the number of cracks. By using these efficient numerical techniques, it allows one easily to conduct parametric analyses for several crack sizes without changing the finite element mesh. The results using the present method agree well with the experimental ones. Thus, the application of elastic plastic finite element alternating method with T_e^* fracture criterion, which is illustrated in this paper, would be a very efficient methodology to study the MSD link-up phenomenon.

Acknowledgment

The support for this work, provided by the FAA under a grant to the Center of Excellence for Computational Modeling of Aircraft Structures at Georgia Institute of Technology, is thankfully acknowledged.

References

- Atluri, S.N. (1986): Energetic approaches and path-independent integrals in fracture mechanics. Computational methods in the mechanics of fracture. Ed. by Atluri, S.N.. Elsevier Science Publisher. B.V.
- Atluri, S.N.; Harris, C.E.; Hoggard, A.; Miller, N.A.; Sampath, S.G. (1992): Durability of metal air frame structures. Technical Publications. Atlanta, USA.

Atluri, S.N.; Sampath, S.G.; Tong, P. (1991): Structural integrity of aging airplanes. Berlin, Heidelberg, New York. Springer.

Broek, D. (1993): The effects of multi-site-damage on the arrest capability of aircraft fuselage structures. FractuREsearch TR 9302.

Murakami, Y. et al. (1987): Stress intensity factors handbook. Pergamon Press, Oxford.

Nayak, G.C.; Zienkiewicz, O.C. (1972): Elasto-plastic stress analysis. a generalization for various constitutive relations including strain softening. Int. J. Mumer. Meth. Engng. 5, 113-135.

Newman, J.C. Jr.; Dawicke, D.S.; Sutton, M.A.; Bigelow, C.A. (1993): A fracture criterion for wide spread cracking in thin sheet aluminum alloys. Int. Committee on Aeronautical Fatigue. 17th Symposium.

Nikishkov, G.P.; Atluri, S.N. (1987): An equivalent domain integral method for computing crack-tip integral parameters in non-elastic thermo-mechanical fracture. Eng. Fract. Mech. 26, 851-867.

Nikishkov, G.P.; Atluri, S.N. (1994): An analytical-numerical alternating method of elastic-plastic analysis of cracks. Comput. Mech. 13, 427-442.

Nishioka, T; Atluri, S.N. (1983): Analytical solution for embedded elliptical cracks, and finite element alternating method for elliptical surface cracks, subjected to arbitrary loadings. Eng. Fract. Mech. 17, 247-268.

Okada, H. Suzuki, Y., Ma, L., Pyo, C. R., Atluri, S. N., Kobayashi, A.S. and Tan, P. (1995): Plane Stress Crack Growth and T_e^* Integral - An Experimental/Numerical Analysis, Submitted ICES'95

Park, J.H.; Atluri, S.N. (1993): Fatigue growth of multiple-cracks near a row of fastener-holes in a fuselage lap-joint. Comput. Mech. 13, 189-203.

Park, J.H.; Ogiso, T.; Atluri, S.N. (1992): Analysis of cracks in aging aircraft structures, with and without composite-patch repairs. Comput. Mech. 10, 169-201.

Pyo, C.R.; Okada, H.; Atluri, S.N. (1994): Elastic plastic finite element alternating method for stationary cracks in multiple site damage (MSD) problems of aircraft panels, Submitted to Computational Mechanics.

Pyo, C.R.; Okada, H.; Atluri, S.N. (1994): Residual Strength Prediction for Aircraft Panels with Multiple Site Damage, using the "EPFEAM" for Stable Crack Growth Analysis, To appear in Comput. Mech.

A CONCEPT FOR THE EVALUATION OF MSD BASED ON PROBABILISTIC ASSUMPTIONS

Peter HORST and Hans-Jürgen SCHMIDT
Daimler-Benz Aerospace Airbus GmbH, Hamburg, Germany
Fatigue and Damage Tolerance Department
Kreetslag 10, 21129 Hamburg

1. SUMMARY

The present paper describes a general approach for the assessment of Multiple Site Damage (MSD), and as a subsequent phenomenon Widespread Fatigue Damage (WFD). A rough outline of the model used is presented. Furthermore, emphasis is put on the fact that a set of parameters will influence MSD as well as WFD, which all show a considerable probabilistic scatter. Some of those parameters are discussed in this paper; especially, the scatter of fatigue data. Manufacturing as well as deteriorating effects are discussed. Finally, an example indicates that the general line of the model works well.

2. INTRODUCTION

There is no doubt that Widespread Fatigue Damage (WFD) as well as MSD largely depend on probabilistic effects. Figure 1 tries to illustrate this fact. WFD may be interpreted as the result of MSD and the residual strength problem. MSD in itself is a result of fatigue (i.e. the initiation of cracks) and subsequent crack growth.

It goes without saying that the design of a structural item will influence both, initiation and crack growth considerably. Even a well designed structural item already exhibits a considerable scatter in the fatigue life. But also further effects like loading, manufacturing and environment will add more probabilistic effects. Therefore, it seems to be obvious that a method for the assessment of MSD has to start with these probabilistic effects.

3. THE MODEL USED

There are different possible approaches to take into account the probabilistic character of the MSD (and hence the WFD) problem. Different fully probabilistic approaches are possible, but they seem to have certain shortcomings. Therefore, in the present paper a mixed model is discussed, i.e. a probabilistic approach is used for the determination of a starting damage scenario; while the subsequent steps (e.g. the damage accumulation, crack growth and residual strength problem) are calculated by a deterministic model.

The overall structure of the model is shown in figure 2, where a indicates the crack length and D indicates the accumulated damage.

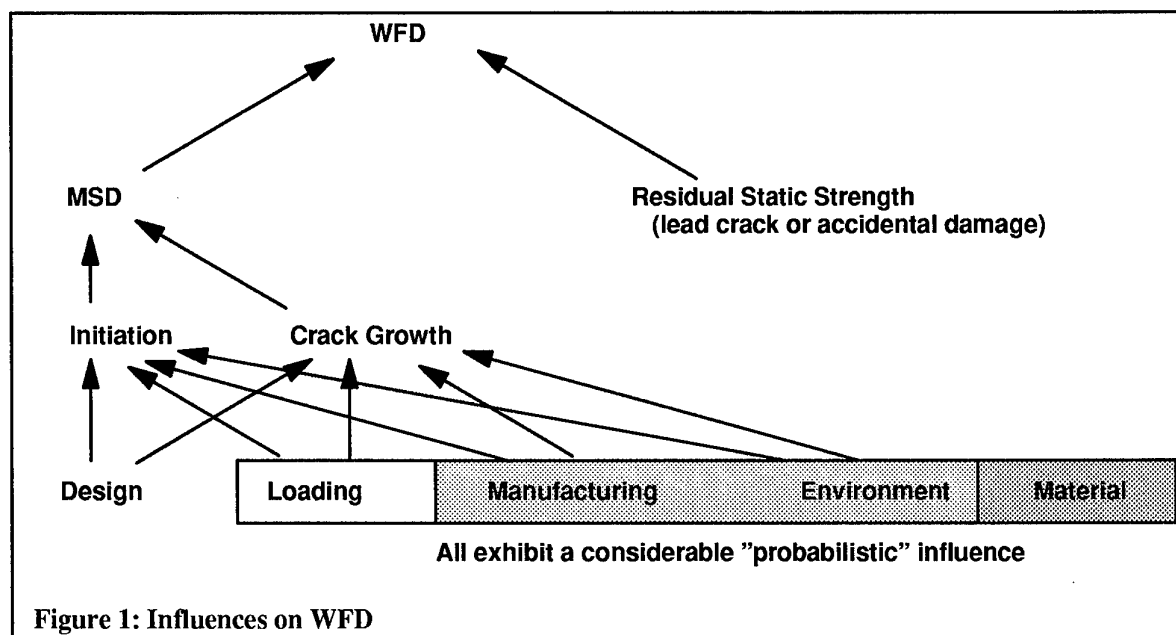


Figure 1: Influences on WFD

```

loop over "n" configurations
  random run for the determination of the initial damage scenario, i.e. definition of damage D(l,0)
  loop over the load cycles "i"
    loop over all objects "l"
      if : object is still in the damage accumulation phase (D(l,i-1) < 1)
        D(l,i) = D(l,i-1) + dD(l,i)
      else if : object is an active crack
        da(l,i) = f(Kl ...) (compound, stress function or fem)
        a(l,i) = a(l,i-1) + da(l,i)
        calculation of plastic zone size
        check link-up criterion
      endif
    check overall residual strength of the structure
  calculation of threshold, interval etc. for a given configuration
calculate statistical values for the problem : mean value, standard deviation etc.

```

Figure 2 : Overall structure of the model

3.1 Calculation of the Damage Scenario

In this model it is assumed that for a given design, manufacturing process and stress level of a joint fatigue test results are known, which reflect the mean value of the fatigue life as well as the scatter of the fatigue life (e.g. in terms of a standard deviation). The fatigue life should be defined up to a relatively small crack size (e.g. 1 mm). It is obvious that, due to different reasons (size effect, detectability etc.) it is not easy to achieve these results, but they are those results which normally are needed for the starting phase of the model.

This model therefore tries to circumvent the problem to calculate the initiation by any local approach. By using such an approach complicated effects which may occur in e.g. in joints (see e.g. in [1]), are automatically included. This means on one hand that theoretical problems are widely excluded from the initiation problem, while on the other hand each new joint has to be tested thoroughly in order to know the special features of the specimen.

If the mean value of the fatigue life and the scatter factor for a single rivet pitch are known, it is possible to use a random process in order to derive a damage scenario for a complete frame-bay or even a complete lap joint. Provided the fatigue life is distributed according to a log-normal distribution, this may be done by means of an ordinary random processor which provides a smooth distribution of random numbers in the interval [0,1] (see e.g. Press et al. [2]), equivalent to

0% – 100%, and by inversion of the log-normal distribution by an approximate method (an analytical inversion is not feasible).

After the damages of all fatigue critical locations have been determined, it is assumed that the fatigue damage at the most damaged location is high enough to start crack growth, while all other locations still have to accumulate more fatigue damage until the crack starts. The fatigue damage rate of each location "l" is calculated by equation (1), meaning that the rate depends on the initial damage

$$dD(l,i) = \frac{N(l)}{N_{\max}} \quad (1)$$

Special attention has to be paid to the interaction of cracks and holes or one-sided cracks with regard to the fatigue problem at the uncracked location. This is either done by using an ellipse – instead of a hole with one crack – in order to calculate the α_k – value or for the interaction by using a compounding method like procedure.

3.2 Crack Propagation Calculation

Generally the crack propagation has been calculated by means of the SIF (stress intensity factor) K_I and the Forman equation (2).

$$\frac{da}{dN} = \frac{c_f \Delta K^{n_f}}{(1 - R) K_{Ic} - \Delta K} \quad (2)$$

The Forman parameters for the aluminum 2024 T3

alloy have been used as follows within this paper :

- $c_f = 2.01 \times 10^{-8}$
- $n_f = 2.70$
- $K_{Ic} = 2256 \text{ MPa} / \text{mm}^{-1/2}$.

This leaves to assess the appropriate SIFs for different crack scenarios, which may or may not include a mutual interaction of the cracks or other objects. The model does not include up to now any special treatment of short cracks, although it starts crack propagation calculation at considerably short crack sizes.

Three different methods of SIF determination are provided in the model:

- the compounding method [3]
- a numerical method based on complex stress functions [4]
- the finite element method.

Since one of the main requirements for the method used within this Monte-Carlo-Simulation-like method is its low computer time consumption, the compounding method is the most promising. All results, which are quoted in this paper are based on this method. Only some facts, e.g. regarding the redistribution of pin-loads after cracking, are based on one of the others.

The basic idea of the compounding method is well known and simple. From a set of known SIFs more complicated ones are determined. Many of these solutions comprise the interaction of one crack with some kind of object, where an object may be a hole, a straight line, an other crack, etc.. The mutual interaction of cracks with a number of objects is now achieved by a certain procedure of summation or product of the influences of all objects. Within this model the general method of Rooke et al. [5] has been adopted, where the SIF is calculated by

$$K_r = K_0 + \sum_{n \neq 0} (K'_n - K_0) + K_e \quad (3)$$

with K_r as the actual SIF including all interactions, K_0 indicating the SIF without interaction with other objects; K'_n is the SIF according to the interaction with one single object "n" and K_e is the most problematic parameter, since it comprises the influence of all objects together. This last term is not very easy to obtain. Based on some assumptions of Rooke et al. this term is not essential for normal rivet row pitches.

Special attention has to be paid to the case of cracks emanating from holes or intersecting other objects. This procedure is very clearly presented in the ESDU data sheet [6]. For pin-loaded fasteners some further assumptions have to be made. The required stress intensity factors for the simple basic configurations mainly have been taken from Rooke and Cartwright

[7], Tada, Paris and Irwin [8] and some single publications. One of the most valuable has been the report on two unequal cracks emanating from a hole by Rooke and Tweed [9].

There are certain shortcomings of the compounding method, e.g. the fact that only a constant remote stress may be treated by this method. But it is shown in the subsequent sections that this is not such an important feature for the given problem.

3.3 Link-Up and Residual Strength

In this model mainly the detection of the link-up of relatively small cracks is essential. This may be treated in different ways. One of the very simple models for this problem seems to be the model proposed by Swift [10]. It actually checks a criterion which is very similar to a "net section yielding" criterion.

The main idea is to use the radius of the plastic zone in front of each crack tip

$$r_p = \frac{K_I^2}{\pi \sigma_y^2} \quad (4)$$

and to apply the contact of both plastic zones as criterion for the link-up of the cracks. This is in line with the argument of Irwin [11] concerning the effective length of the crack. From equation (4) it is obvious that this criterion depends very much on the yield stress σ_y . Within the present model the stress intensity factor K_I has been taken from the compounding method instead of the equations given by Swift in ref. [11].

For the real residual strength problem this model is extremely simple and is therefore easy to be used in the Monte-Carlo Simulation. After all the results of Swift's method are not always too bad, if flat specimens and certain spacings for the rivets are considered. This has been shown by Moukawsher [12]. Actually, the results are even better, if the plastic radius has been derived by means of the compounding method. On the other hand there are some doubts, whether this criterion still holds, if other specimens are used (see e.g. [13] or even exhibit bending).

Anyway, the residual strength model does not have a major influence on the calculated inspection interval, since the number of loading cycles with highly interacting cracks is low for each possible configuration. The real residual strength calculation, which requires the limit load, is only needed in this model, when a complete large panel is assessed. This is not the subject of this paper.

3.4 Performance of the Code

The results of the model have been tested by comparison with experiments, both with and without rivets. Some results for open hole specimens are shown in [4] and [14]. For riveted lap joints test results shown in [15] have been used for comparison, showing quite

reasonable results. This has been performed within the frame of the GARTEUR project SM-AG18: "Assessment of MSD in highly loaded joints".

4. THE CONCEPT

4.1 The Inspection Interval

Different intervals of loading cycles can be defined in the case of MSD and WFD. Figure 3 tries to illustrate these intervals. State "0" is the virgin state of the material, state "1" is the state, where the first crack has been initiated, state "2" is the state where the first crack reached detectable crack size, and state "3" is the final "critical state". The interval between state "3" and "2" is normally referred to as "inspection interval".

The "crack free life" (i.e. the interval between state "1" and "0") is called "threshold" in the following, although this is not exactly the normal understanding.

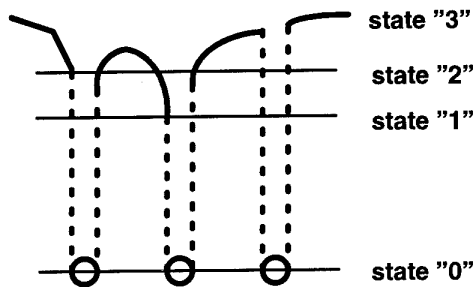


Figure 3: Different states of WFD

The definition of the inspection interval is the same in the present model. But, if the probabilistic aspect of the initiation of the initial damage scenario is taken into account, cracks may initiate at different locations at different times. Therefore, very different configurations may occur, which result in a very different crack propagation behaviour. This means that the inspection interval is not fixed at all, and it even becomes apparent that both of the values, interval and threshold, are linked together. This is mainly discussed in section 5.

What actually does remain is that the results of the Monte-Carlo Simulation may only be treated statistically. This is to say that the inspection interval is also a statistical value. MSD has not to be defined for an interpretation of the results, it is just a part of the possible configurations that may occur. Actually, MSD-like configurations are those which result in a relatively short inspection interval. On the other hand it will follow that the "worst case of equal cracks at all rivet holes" is not only very unlikely to occur; it also is shown that it may only occur after a very long "crack free life".

4.2 Important Features of Multiple Site Damage

4.2.1 Performance

If more than one single crack appears at adjacent rivet holes two major features are responsible for the fact that multiple site damage is a very serious phenomenon [16]:

- in MSD-like scenarios crack sizes tend to be of relatively similar size in a certain region of nearly equal remote stress.
- after reaching a considerable crack size, the cracks start to influence their crack growth mutually.

The first of these facts may only be explained by the fact that for loaded rivet holes the crack growth rate of small cracks is higher than for larger cracks, or for adjacent holes

$$\frac{da_{\text{small}}}{da_{\text{large}}} > 1 \quad (5)$$

This kind of mechanism is also reflected in the MSDS parameter of de Koning [17]. Furthermore, the standard deviation in the initiation of cracks must be small to achieve such a critical state.

If larger cracks additionally are spread over a considerable region, a redistribution of the load transfer at the rivets will also occur, and result in a higher loading of the outer, normally less loaded rivet holes. Some finite element calculations, which have been performed in order to assess the effect of small cracks on the load-transfer redistribution, have shown that this is not a crucial point, as long as the cracks do not exceed a length of some millimeters. Only a small amount of the load-transfer is distributed between the adjacent rivets, both parallel and perpendicular to the rivet row direction.

In longitudinal lap joints (and this is the main subject of the following sections) a nearly quadratic stress distribution is found within one frame-bay. The maximum of this distribution is located in the center of the frame-bay. This stress distribution results in the fact that approximately 8 to 10 rivets are loaded in such a manner that the fatigue life is very similar at these rivets, i.e. MSD is likely to occur at these rivets, if it occurs at all [4]. Therefore, it is sufficient in the first step to look at approximately 9 rivet-spacings in a Monte-Carlo Simulation. Larger models would be necessary, if accidental damages are taken into account. A large effect of the damage scenario of one frame-bay on the other is only essential shortly before the crack scenario is critical in one of the frame-bays. The few load cycles which will occur in this state are not essential for the overall result of the following studies and are therefore neglected in the following calculations.

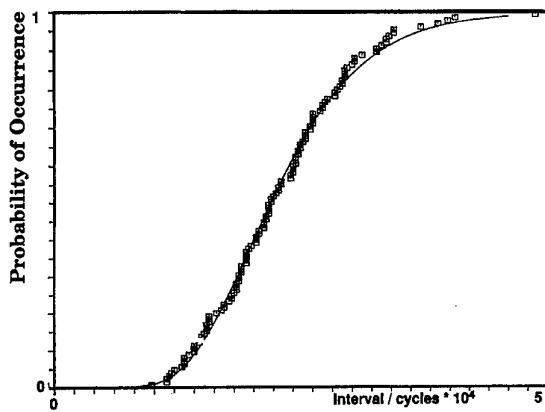


Figure 4: General kind of result of the Model

4.2.2 Results of a Monte-Carlo Simulation

A typical result of a Monte-Carlo Simulation is shown in figure 4. The inspection interval (without safety factor) has been collected for 125 different configurations of a simple two-rivet row lap joint. The results are plotted versus the probability of occurrence. Furthermore, a log-normal distribution has been calculated from these results. Obviously, the log-normal distribution fits the results very well.

The main point that may be derived from this diagram is the fact that the inspection interval is not a constant value at all. The question is, why the results for the interval are so different? The answer is given in figures 5a and 5b. They show the crack propagation in the "worst" and the "best" case, i.e. it is the configuration of the far left and far right result in figure 4.

In figure 5a and 5b the x-position of the rivet-holes in the rivet row as well as the position of the crack tip are plotted on the abscissa. On the ordinate the cycles are plotted. Dashed lines indicate that the rivet-hole remains intact and only damage accumulation takes place, while a solid line indicates that crack propagation has started.

It gets apparent that the "worst case" in figure 5a is a configuration where cracks start at almost all rivets at the same time; this is nearly the classical MSD case. In the "best" case of figure 5b, one single crack starts to grow up to quite a number of cycles before another crack starts to grow; this is almost the classical damage tolerance configuration with one fatigue critical location.

When looking at a Monte-Carlo Simulation the question occurs, how many different damage configurations have to be taken into account. If a real mathematical convergence is needed, millions of different configurations have to be calculated. In this engineering program requirements for the accuracy are surely less high. Figure 5c shows for one example the calculated interval (for three small probabilities of occurrence) as they are calculated for different total numbers of configurations. Obviously, the values vary in the beginning, but already after some hundred configurations the differences are not large anymore, compared to the uncertainties of the calculation model itself. Therefore, 250 different configurations have been used in the following.

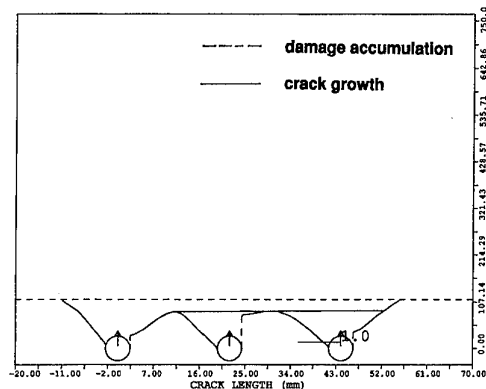


Figure 5a: "Worst Case"

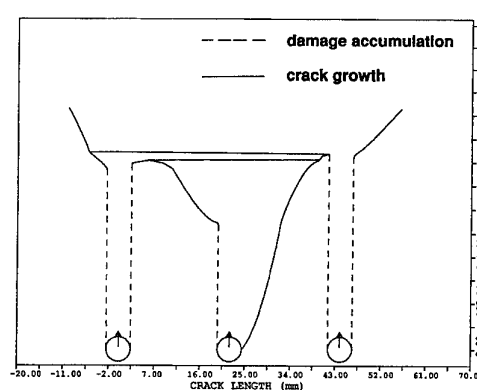


Figure 5b: "Best Case"

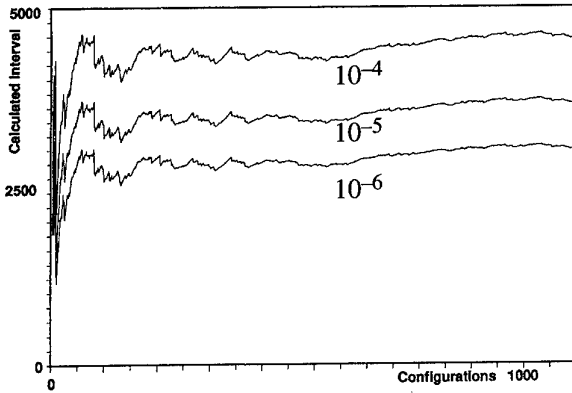


Figure 5c: Convergence of Model

4.3 Significance of Parameters

It may be assumed that different parameters are likely to influence the inspection interval in the case of more than one fatigue critical location. In reference [14] the influence of the following parameters have been tested by means of the Monte-Carlo Simulation described above:

Parameter	Average	Scatter
fatigue life	X	X
detection	X	X
position		X
crack growth		X
friction		X

where detection stands for the probability of detection, position for the position of the rivet in the rivet row, crack growth for a scatter in the crack growth data of the material and friction for the scatter in the load-transfer due to friction between the sheets of the lap joint. While the fatigue life has been assumed to follow a log-normal distribution, all other values have been approximated by a normal-distribution and reasonable scatter factors have been used.

It turns out that only the mean value of the fatigue life, its scatter and the detectable crack length have an important influence on the results of the Monte-Carlo Simulation. This means that only these parameters will be shown in the next sections.

5. NUMERICAL EXAMPLES

The following examples in this section all refer to a joint design as given in the paper [15]. The type of joint is a three rivet row lap joint, pitch 25.4 mm and rivet diameter of 4 mm. Skin thickness is 1.27 mm,

material 2024 T3. Maximum stress level 96 MPa, $R = 0.1$. The general design is shown in figure 6. The basic mean value for the fatigue life has been set to 85,000 cycles, but this may be considered as theoretical, since this value is not supported by tests.

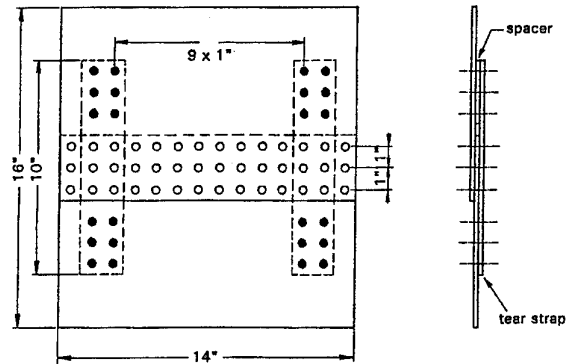


Figure 6: Specimen type (from Vlieger [15])

5.1 General Results

5.1.1 Threshold vs. Interval

This first example has been done in order to show that figures of the type given in figure 4 are not completely representative. In figure 7 the results of 250 different configurations of the above mentioned example have been plotted in a way which allows to see both, inspection interval and threshold (up to detectability). Symbols indicate the result of one single configuration, while the lines engulf areas which include 68.3, 95.4 and 99.7 % of the results. A logarithmic standard deviation of 0.1 has been assumed in this example. In addition, a least square fit line is shown.

It can be seen by this example that the inspection interval and the threshold clearly are linked, i.e. with rising threshold, the inspection interval is decreasing. A decreasing inspection interval signifies that initial damage scenarios occurred, which are relatively near to a "MSD"-scenario.

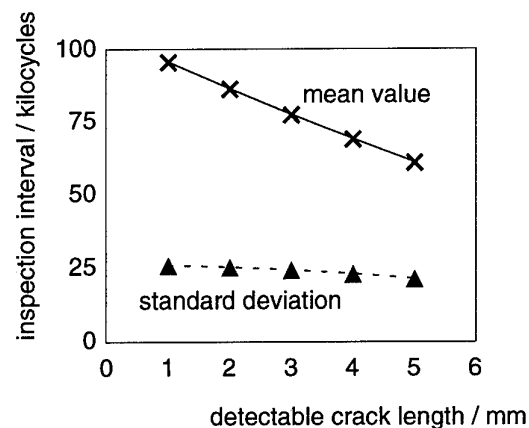


Figure 8: Influence of detectable crack length

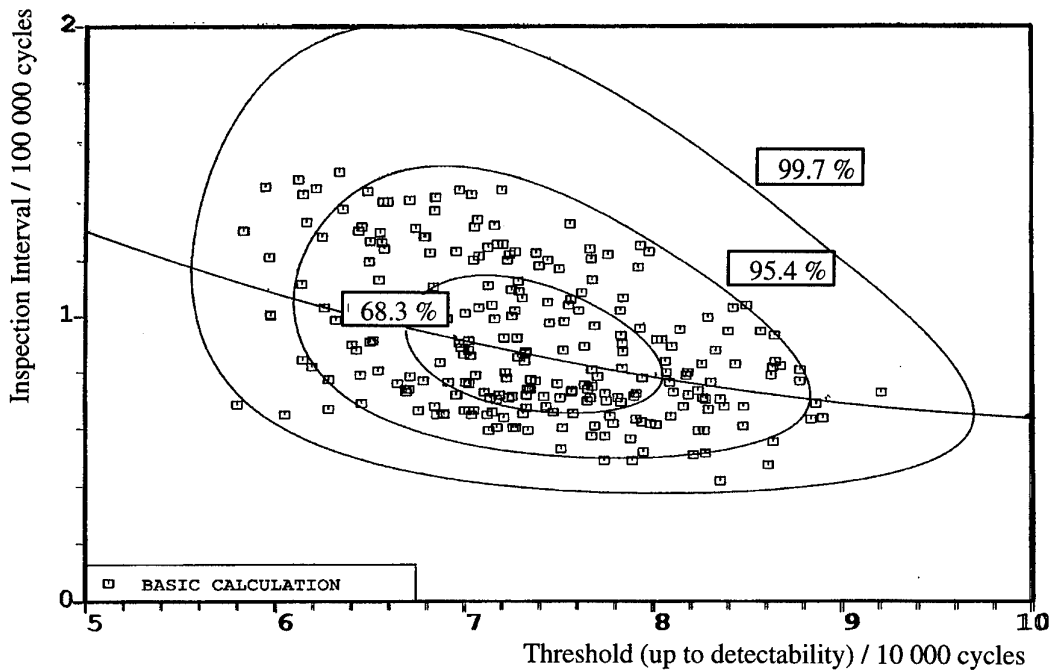


Figure 7: Result of the basic problem, Inspection Interval vs. Threshold up to detectability

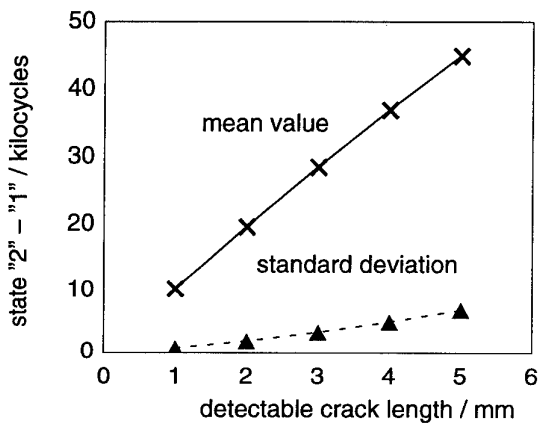


Figure 9: Influence of detectable crack length

5.1.2 Influence of the Detectable Crack Length

The detectable crack length obviously must have a large effect on both the threshold and the interval. Figure 8 illustrates this effect for the case of the inspection interval. Clearly the mean value decreases nearly in a linear way. The standard deviation decreases slightly, but this effect must be interpreted by having in mind that both, mean value and standard deviation are translated from a logarithmic into a normal scale.

A further interesting effect may be found for the influence of the detectable crack length on the crack growth until detection (state "2" – state "1"). Obviously the mean value will increase with increasing detectable crack length. But, the standard deviation is interesting in this case, because this value would be zero, if no interaction of the cracks would occur.

By looking at figure 9, it can be found that the standard

deviation increases significantly with increasing detectable crack length, meaning that also the interaction increases in this interval for increasing detectable crack length. It must be noticed that 5 mm is a common value for the detectable crack length.

5.1.3 Influence of the Standard Deviation of the Fatigue Life

The following figures 10 to 13 show the influence of the standard deviation of the fatigue life on the different intervals, which have been defined in figure 3.

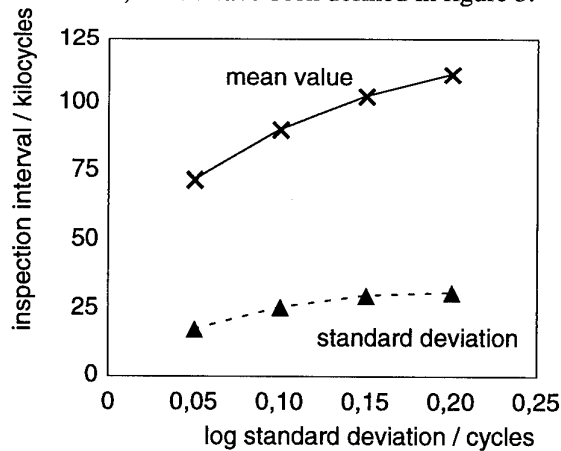


Figure 10: Influence of scatter in fatigue

Figure 10 indicates that the inspection interval is highly influenced by this parameter. Both, the mean value and the standard deviation increase considerably with increasing standard deviation of the fatigue life. The reason for this effect is that with increasing scatter in fatigue life, the probability decreases that cracks initiate at adjacent holes within a short time interval.

Figure 11 shows that the crack growth to detection (state "2" - state "1") is only slightly affected by the scatter in fatigue life. For small scatter factors the interaction of the cracks obviously increases again. Here the comments given in conjunction with figure 9 also hold.

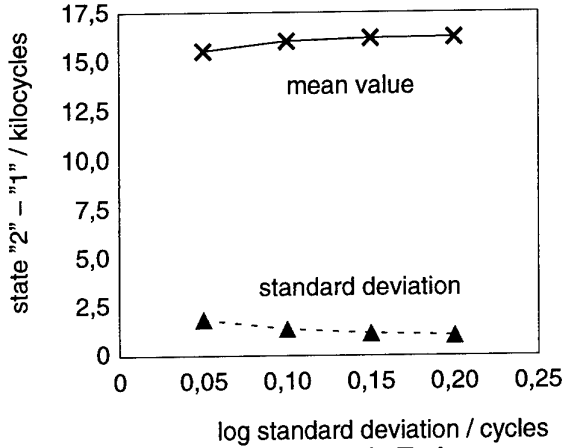


Figure 11: Influence of Scatter in Fatigue

Also the total life is influenced by the scatter of the fatigue life. This is obviously the consequence of the relationship shown in figure 9, which adds to the mean fatigue life. This is illustrated in figure 12.

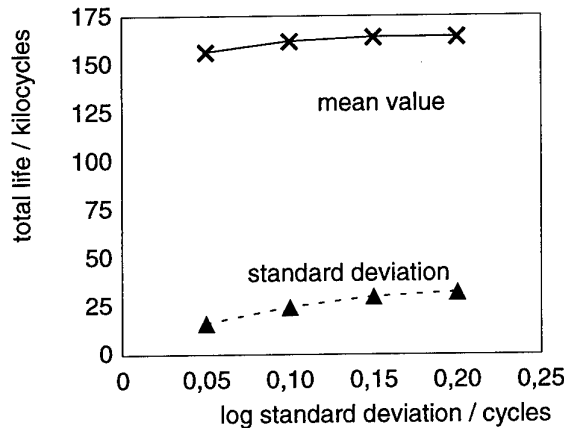


Figure 12: Influence of Scatter in fatigue

Furthermore, the scatter in fatigue life has a large influence on the first crack initiation. This is exactly what is known as the size effect in statistics. Figure 13 indicates that the model also gains this result.

5.2 Influence of Manufacturing

The comments on figure 10 clearly showed that a low scatter in fatigue life results in a higher probability of critical configurations with respect to MSD. Obviously, a good riveting quality will result in such a low scatter value. On the other hand it is clear that the threshold may be misjudged, if only such a small scatter of the fatigue life of an entire population of joints is used.

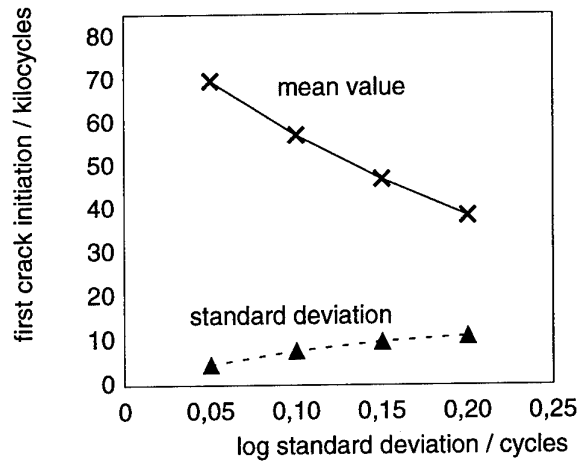


Figure 13: Influence of scatter in fatigue

The squeeze force at riveting may e.g. be one of the parameters which influence the fatigue life of a joint parametrically (see e.g. results of R. Müller, TU Delft [18]). These results indicate that it is very likely that the scatter in one batch of joints, which e.g. has been produced by the same mechanic, may exhibit a very small scatter band. On the other hand someone else may produce another batch with again a small scatter band, but an entirely different mean value in fatigue. If both batches are added they will result in a relatively high overall scatter, which is interesting for the threshold assumption.

This effect has been addressed by using two scatter factors in the Monte-Carlo Simulation, one for the variance in one configuration (called scatter of the fatigue data) and one for the entire process (called standard deviation of the mean value of the fatigue life). The following two figures try to show the effect of this distinction.

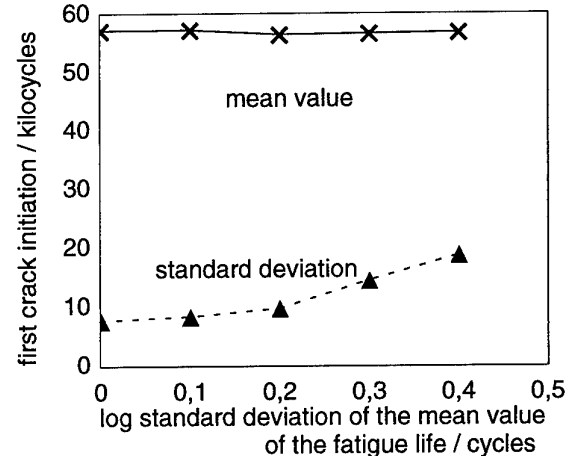


Figure 14: Influence of scatter in mean value

Figure 14 shows the effect of the standard deviation of the mean value in fatigue life on the first crack initiation. While the differences in the mean value of figure 14 can be explained by numerical uncertainties, the standard deviation of the first crack initiation obviously depends on this scatter factor. This will influ-

ence the safety factor for the threshold entirely. Now figure 15 indicates that a scatter in the mean value of the fatigue life does not influence the inspection interval at all. This is relatively logical, because the crack pattern will depend on the scatter within one configuration and not on the overall scatter.

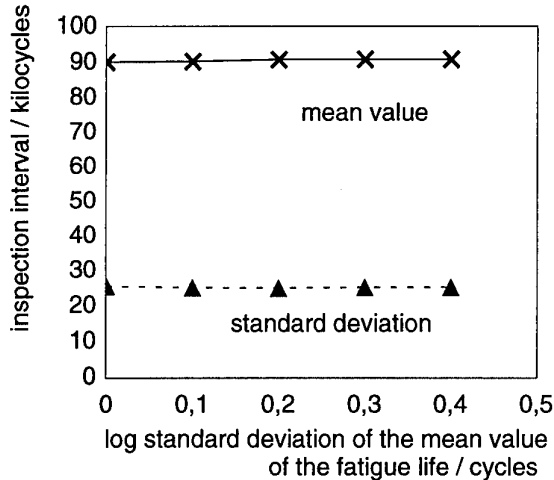


Figure 15: Influence of scatter in mean value

6. DETERIORATING EFFECTS

For well designed joints, MSD will occur so late that it normally would not be interesting for even the extended life of an aircraft. But this may sometimes be changed by deteriorating effects. Deteriorating effects may be caused by environment or by undetected manufacturing. The following example shows the result of an artificially deteriorated joint.

It does not seem to be easy to find test results, which may serve as a representative example for the Monte-Carlo Simulation presented above. Also the following example may not be considered to be perfect, but it provides at least a strong hint that the general approach of this paper is right.

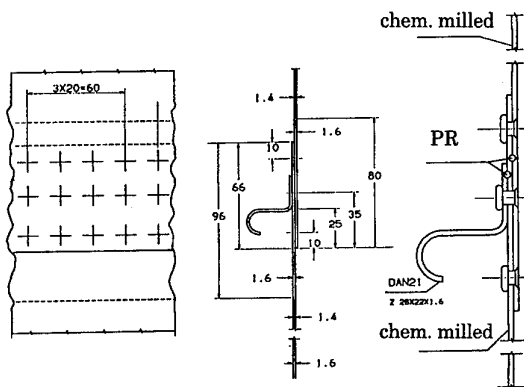


Figure 16: Coupon specimen

The main obstacle for representative full scale tests is the fact that a well designed lap joint is not likely to

exhibit MSD during a reasonable number of flight cycles. Since no company will pay for a full scale test with hundreds of thousands of flight cycles, other measures have to be taken. During a full scale test at Daimler-Benz Aerospace Airbus in Hamburg one lap joint has been manufactured in a way, which was likely to enforce Multiple Site Damage. This was done by means of rivet holes which have been countersunk too deeply.

A deep countersunk rivet hole, which results in a non-protruding rivet head, will show a relatively bad fatigue life behaviour and a reduced scatter of the fatigue life. It is therefore much more likely that MSD will occur in such a lap joint after a relatively short initiation period.

From coupon test specimens of the same lap joint design, the drop in the fatigue life can easily be derived for the appropriate stress level:

- in the case of a normal rivet hole with protruding rivet head:
 - $N_{10\%} = 1,171,039$ cycles
 - $N_{50\%} = 535,268$ cycles
 - $N_{90\%} = 233,653$ cycles
- in the case of a deep countersunk rivet hole with non-protruding rivet head:
 - $N_{10\%} = 132,695$ cycles
 - $N_{50\%} = 114,062$ cycles
 - $N_{90\%} = 94,250$ cycles.

It must be stated that the coupon tests have not been performed in a way which delivered the number of cycles up to a small crack length. Actually, the number of cycles up to a failure of the complete small coupon has been tested. Therefore, the interval between crack initiation and failure of the complete coupon test specimen have also been assessed by means of a Monte-Carlo Simulation. This leads to a decrease of 31,332 cycles for the $N_{50\%}$ value of the deep countersunk specimen.

The general design of the lap joint specimens is shown in figure 16.

The results of the Monte-Carlo Simulation are shown in figure 17. A load-transfer of 37% at the critical rivet row and a detectable crack length of 5 mm have been assumed. The remote stress level (this includes a "coupon" full scale correction term) of 84 MPa were used as remote stress level. Figure 17 shows two distributions: first, the case of the normal protruding head riveting and second the case of the non-protruding head riveting. On the abscissa the "life up to the detectable crack length" is plotted versus the inspection interval. Both values do not include any safety factor. Please note that the results for the calculated interval must be

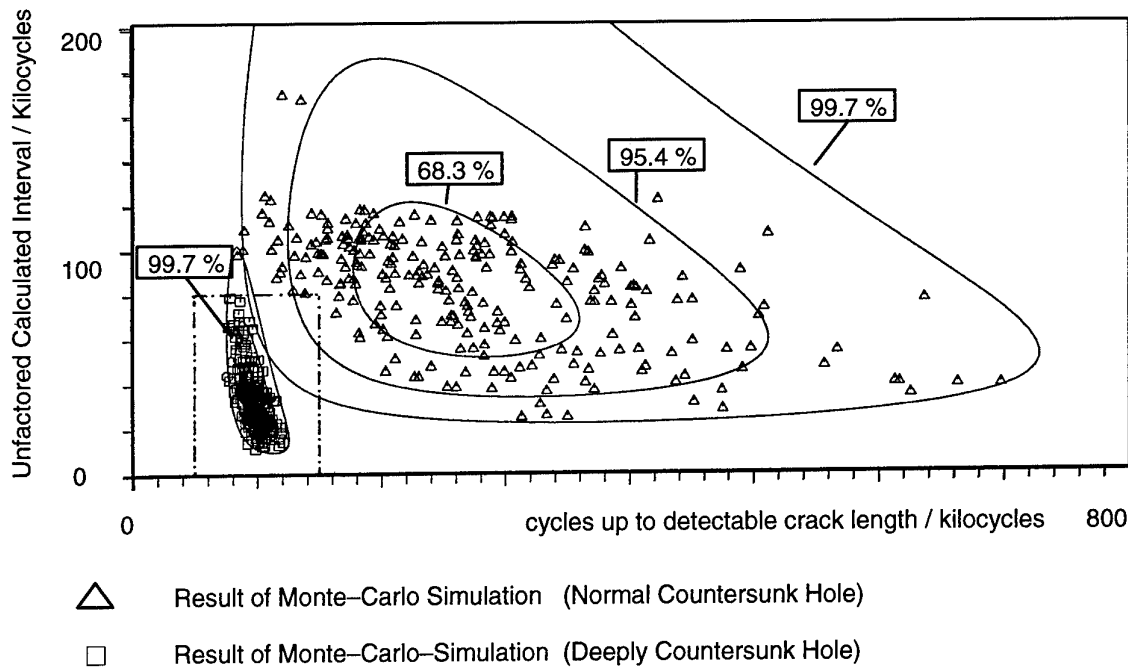


Figure 17 : Comparison of Monte-Carlo-Simulations in the Case of Normal and too Deeply Countersunk Holes

considered as conservative, since the high "coupon-full scale correction term" has also been used for the crack propagation calculation.

A simulation using 250 different damage configurations has been performed in both cases. Symbols indicate the position of the results for each single calculation. Additionally, the distribution of the results has been treated by statistical means, indicating which percentage of points is located within a certain region.

The following points may be derived from figure 17:

- there is an obvious relation between the number of cycles up to detectable crack length and the interval in both cases (see section 4.1).
- the results of both of the types of lap joints are extremely different. While the badly manufactured lap joint exhibits an early initiation of cracks, combined with a high probability of an MSD-like crack scenario (i.e. the inspection interval is small), the properly manufactured lap joint shows a much lower probability that a MSD-like scenario occurs. And if this scenario is likely to occur, it will occur much later in the service life, which is not likely to be reached by the aircraft anyway.

The data given in figure 17 still are completely theoretical. If they are compared with data from the full scale fatigue test mentioned above, the problem occurs that no crack initiation has been found in the

properly manufactured lap joints of the test specimen within 120,000 flight cycles. Therefore, no validation of the Monte-Carlo Simulation of this problem is given, except from the fact that also the Monte-Carlo Simulation provides no damage in this case.

If only the deep countersunk lap joint is considered, this is the region indicated by a dotted line in figure 17, and is plotted in greater detail in figure 18. Additionally to the information of figure 17, results from the above mentioned full scale test are indicated in figure 18. A solid line indicates the region of intervals and fatigue life up to the initiation of a 5 mm crack which has been covered by the test itself, i.e. all points on the upper right-hand side of the solid line were not in the range of the test.

Within the deep countersunk lap joint of the full scale test crack initiation has been found in different frame bays up to different degrees and often with cracks at adjacent rivets. On the other hand, only one of the crack scenarios has nearly reached a critical state after 120,000 flights, while all the others still were not at all critical. The development of the cracks has been monitored by means of eddy current techniques from the beginning. Hence, a good database of initiation up to detectable crack length and interval data exists.

The single finding, where one frame-bay nearly became critical is indicated by a filled dot in figure 18, while for different further frame-bays an arrow indicates the initiation life up to a 5 mm crack and the in-

interval, which was reached at the time when the full scale test has been stopped. The arrow also indicates the region where the real point would have been situated, if the test would not have been stopped at 120,000 flight cycles.

A comparison of the theoretical results as well as the experimental results shows that the one critical scenario was not very probable. But, all measured points from the full scale test indicate that the results of the Monte-Carlo Simulation are very likely to occur. This means that, although the model itself certainly has its shortcomings, it is already able to assess the likelihood of widespread fatigue damage in a considerable way. Furthermore, it supports the thesis that threshold and interval are not fixed values, if more than one fatigue critical location is taken into account.

7. CONCLUSIONS

A probabilistic approach for the assessment of Multiple Site Damage (MSD) has been presented. While, in the case of a single crack the inspection interval is one fixed value, which is related to one fixed threshold value, this is not the case for MSD. Obviously both, the inspection interval and threshold depend on each other and are not fixed anymore.

This thesis is supported by means of a Monte-Carlo Simulation model, which has been tested by comparison with one existing result from a full scale fatigue test. The results are already very good, although the model still is in a preliminary state and needs some refinement.

The main parameters which influencing both the threshold and the interval are : the average crack initiation life, the scatter of the crack initiation life and the detectable crack length. This shows that the design (and the applied stress) as well as the quality of manufacturing, which both influence the fatigue life, are essential for the likelihood of MSD-like scenarios. It therefore is not necessary to anticipate MSD, if both the design and the production of the item are good, and no deteriorating influences such as corrosion occur.

Furthermore, some typical phenomena of MSD are discussed, like e.g. manufacturing and deteriorating effects.

The work on this method will be continued in order to refine and extend the model.

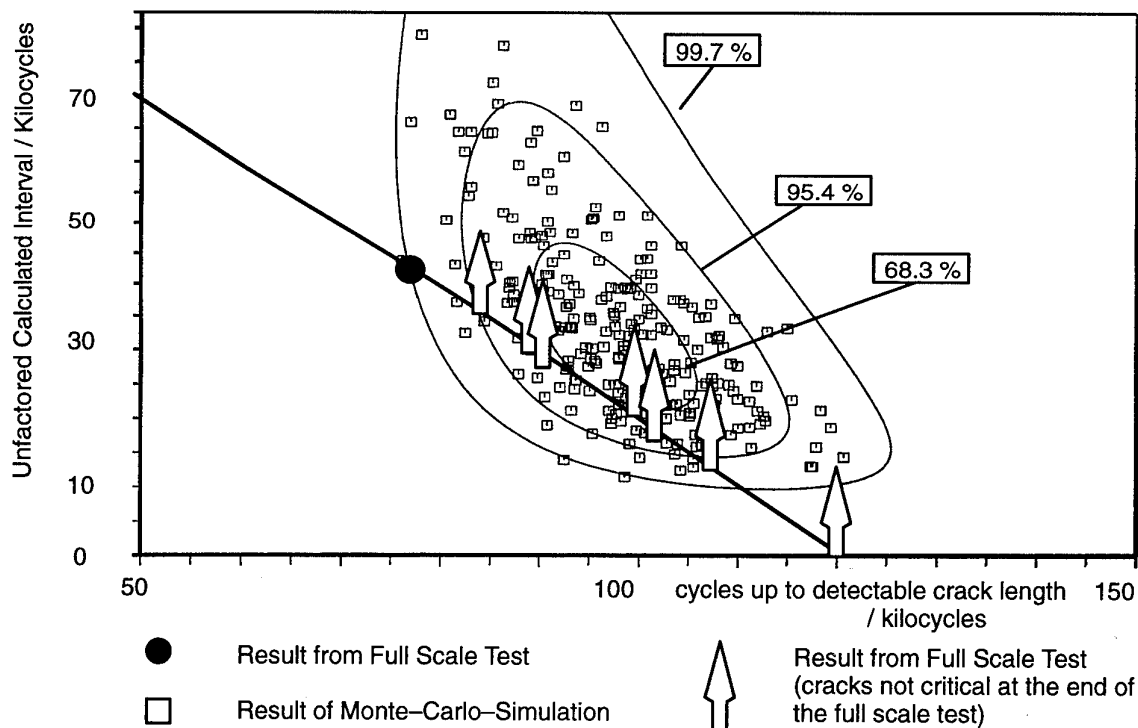


Figure 18 : Comparison of Monte-Carlo-Simulation and Full Scale Test Results of a Lap Joint with Countersunk Rivet Holes too Deep

8. REFERENCES

- [1] Schijve, J., "Multiple-Site-Damage Fatigue of Riveted Joints", in "Durability of Metal Aircraft Structures", eds.: Atluri, Harris, Hoggard, Miller and Sampath, Atlanta, Ga, 1992, pp.2 - 27
- [2] Press, W.H.; Flannery, B.P.; Teukolsky, S.A.; Vetterling, W.T.: "Numerical Recipes - The Art of Scientific Computing", Cambridge University Press, 1988
- [3] Rooke, D.P., "Stress Intensity Factors for Cracks at Fastener Holes in a Row of Fastener Holes", Royal Aircraft Establishment, Techn. Report 81144, 1981
- [4] Horst, P.; Schmidt, H.-J.; Bauch, J.; "Grundlegende Untersuchung zum Einfluß der statistischen Ermüdungsverteilung bei "Multiple Site Damage"", in: "Proceedings of the "Deutscher Luft- und Raumfahrt-Kongress 1992"", Bremen, 29th September to 2nd October 1992
- [5] Rooke, D.P., "Stress Intensity Factors for Cracked Holes in the Presence of Other Boundaries", in: "Fracture Mechanics in Engineering Practice", ed. P. Stanley, London Applied Science Publishers, 1977, pp. 149-163
- [6] "The Compounding Method of Estimating Stress Intensity Factors for Cracks in Complex Configurations Using Solutions from Simple Configurations", ESDU Item Number 78036, 1978
- [7] Rooke, D.P.; Cartwright, D.J., "Compendium of Stress Intensity Factors", HSMO, 1976
- [8] Tada, H.; Paris, P.; Irwin, G., "The Stress Analysis Handbook", Del Research Corp., 1973
- [9] Rooke, D.P.; Tweed, J., "Opening-Mode Stress Intensity Factors for Two Unequal Cracks at a Hole", RAE Technical Report 79105, 1979
- [10] Swift, T., "Damage Tolerance Capacity", in: "Fatigue of Aircraft Materials-Proceedings of the Specialists' Conference, dedicated to the 65th birthday of J. Schijve", eds.: Beukers, A.; de Jong, Th.; Sinke, J.; Vlot, A.; Vogelesang, L.B., Delft University Press, 1992, pp. 351-387
- [11] Irwin, G.R., "Fracture", in: "Handbuch der Physik Vol. VI", ed. Flügge, Springer, 1958, pp. 551-590
- [12] Moukawsher, E.J., "Fatigue and Residual Strength of Panels with Multiple Site Damage", MSc-Thesis, Purdue University, 1993
- [13] deWit, R., Fields, R.J., Mordfin, L., Low, S.R., and Harne, D., "Fracture Behaviour of Large-Scale Thin-Sheet Aluminium Alloy", in: "FAA/NASA Int. Symp. on Advanced Integrity Methods for Airframe Durability and Damage Tolerance", NASA Conference Publ. 3274, 1994, pp. 963 - 983
- [14] Horst, P., Schmidt, H.-J., "On the Significance of Probabilistic Parameters for the Assessment of MSD in the Case of Aging Aircraft", in "Proceedings of the 19th ICAS Congress, 18-23 September, 1994, Anaheim, USA, Vol. 2, pp. 1773 - 1783
- [15] Vlieger, H., "Results of Uniaxial and Biaxial Tests on Riveted Fuselage Lap Joint Specimen", in: "FAA/NASA Int. Symp. on Advanced Integrity Methods for Airframe Durability and Damage Tolerance", NASA Conference Publ. 3274, 1994, pp. 911 - 931
- [16] Schmidt, H.-J.; Horst, P., "Industry Research & Development Needs Regarding Inspection and Maintenance Technologies for Aging Aircraft", in: "Proceedings of the 5th Int. Conf. on Structural Airworthiness of New and Aging Aircraft", Hamburg, Germany, 1993
- [17] de Koning, A.U., "A Parameter Characterizing Structural Sensitivity for Multiple Site Damage (MSD)", NLR CR 92094 L, 1992
- [18] Müller, R. "private communication"

STATISTICAL PROPERTY OF WIDESPREAD FATIGUE DAMAGE

M. Shinozuka and G. Deodatis
 Department of Civil Engineering and Operations Research
 Princeton University
 Engineering Quadrangle
 Princeton, NJ 08544, USA

S.G. Sampath
 Federal Aviation Administration Technical Center, ACD-200
 Atlantic City International Airport
 Atlantic City, NJ 08405, USA

H. Asada
 Airframe Division, National Aerospace Laboratory
 6-13-1 Osawa, Mitaka, Tokyo 181, Japan

SUMMARY

The purpose of the present study is to perform a Bayesian reliability analysis for developing appropriate non-periodic inspection schedules and estimating values of uncertain parameters from data collected during in-service inspections for practical aircraft structural elements. Fuselage structures of an aging aircraft with a number of fatigue-critical elements, having potential to produce widespread damage, are used as a realistic structural model for the analysis. Each element consisting of a skin panel and frames, is subjected to cyclic stress and is designed with the damage tolerance criterion. Probabilistic factors considered in this analysis are fatigue crack initiation and propagation, crack detection capability and failure rates before and after crack initiation. Numerical simulations are performed to demonstrate the efficacy of the Bayesian reliability analysis for the development of inspection schedule and for the estimation of the unknown model parameters.

1 INTRODUCTION

Appropriate inspection schedules play an important role for maintaining and improving the integrity of aircraft structures, particularly the aging aircraft structures. Indeed, rational determination of the inspection schedules, sample size, first inspection time, inspection intervals and so on, represents the key to the effective detection, repair and replacement of the fatigue cracks and resulting failed elements in order to maintain the required reliability of aircraft structure.

Structural reliability analysis is known to be a useful tool for developing appropriate inspection schedules (Refs 1 - 3) because several primary factors such as initial crack length, fatigue crack initiation time, fatigue crack propagation, corrosion, service loads, residual strength and crack detection capability are probabilistic and they need to be treated in the analysis accordingly.

For the reliability analysis to be performed with a high degree of engineering soundness, it is required that probabilistic models used for the analysis should be defined reasonably well. However, the usual paucity of pertinent data makes it difficult for the probability density functions (PDF) of those factors and of their respective parameter values to be determined. It is noted, however, that actual data limited in quantity as well as quality, collected during in-service inspections are the valuable sources of highly useful information that will be utilized not only for the determination of the Bayesian reliability-based inspection schedule but also for the estimation of uncertain parameters in the physical model.

In view of this, the paper concentrates on the development of the Bayesian reliability analysis (Refs 4 - 9) which can estimate appropriate values of uncertain parameters and develop appropriate inspection schedules utilizing small sample data collected during inspections. Monte Carlo simulation techniques are used for the validation of the methodology.

In the present study, a fatigue-critical element is a multiple component of two-bay fail safe structure which consists of three frames, a skin panel, tear straps and shear ties as shown in Figure 1. This element is subjected to cyclic stress from pressure differential and designed in accordance with the damage tolerance principle. The idealization of the element is sketched on the bottom of Figure 1 where the frames are directly attached to the skin by rivets. The center frame and the part of the skin around the rivet are assumed to be susceptible to fatigue crack originating from both sides of the rivet hole and propagating in equal lengths on both sides of the rivet in the longitudinal direction of the fuselage. At some time instant, the crack may appear as shown by dark areas in Figure 1. Two side frames work as crack stoppers. It is further assumed for simplicity that no cracks will originate from the rivet holes located at these two side frames.

There are two types of widespread fatigue damage (WFD); namely, longitudinal multiple site damage (MSD) along rivet lines at skin panel joints and multiple element damage (MED) along rivet lines connecting frames to the skin (Refs 10 - 12). The present analysis addresses only MED in fuselage structure of aging aircraft where a large number of elements exist that can potentially develop multiple element damage.

2 FATIGUE-CRITICAL STRUCTURAL ELEMENT MODEL

2.1 True Element Model

For a fatigue-critical structural element in Figure 1, the material of skin and frames are 2024-T3 and 7075-T6 aluminum alloys, respectively. It is considered that there are several hundreds of these elements in an aging aircraft structure. The failure process consists of crack initiation, propagation and unstable crack growth. Throughout this paper, time is measured in terms of the number of flights.

1) Applied load

Aircraft fuselage structures are subjected to several kinds of loads. In this analysis, however, it is considered that the structural element is only subjected to cyclic constant stress arising from compression and decompression of the cabin for each flight whose range is denoted by Δs due to pressure differential. This stress range depends on a location of the element and Δs is assumed to be a random variable normally distributed.

2) Fatigue crack initiation

After the structural element is subjected to cyclic loading, fatigue cracks initiate simultaneously at both sides of rivet holes in the skin and the center frame. The initial half crack length a_0 is assumed to be the sum of the hole radius r_0 and the initial through crack length a_i as shown in Figure 2. Therefore, the crack propagation period for a corner crack reaching a through crack is included in the time to crack initiation (TTCI). The TTCI t_i is a random variable governed by a two-parameter Weibull distribution:

$$f_0(t_0) = \frac{\alpha}{\beta} \left(\frac{t_0}{\beta}\right)^{\alpha-1} \exp\left\{-\left(\frac{t_0}{\beta}\right)^\alpha\right\} \quad (1)$$

3) Fatigue crack propagation

Fatigue cracks on both sides of the rivet holes of a skin plate a_s and a center frame a_f subjected to cyclic loading propagate under the Paris law with the stress intensity factor range (SIF) modified by the following coefficients β on the basis of manufacturer's experience.

(1) Skin a_s

$$\frac{da_s}{dt} = C_S (\Delta K_S)^{b_S} \quad (2)$$

$$\left. \begin{aligned} \Delta K_S &= \Delta S \sqrt{\pi a_s} \beta_{Frame} \beta_{Bulge} \\ C_S &= 10^{z_S} \end{aligned} \right\} \quad (3)$$

(2) Frame a_f

$$\frac{da_f}{dt} = C_F (\Delta K_F)^{b_F} \quad (4)$$

$$\left. \begin{aligned} \Delta K_F &= \Delta S \sqrt{\pi a_f} \beta_{WF} \beta_{Skin} \\ C_F &= 10^{z_F} \end{aligned} \right\} \quad (5)$$

β_{Frame} and β_{Bulge} are the effects respectively of crack length in the frame and of bulge due to the differential pressure on a skin crack. β_{WF} and β_{Skin} represent respectively the effect of free edge of the frame and the effect of skin crack length on a frame crack. Parameters z_S and z_F are random variables assumed to be normally distributed. Therefore, C_S and C_F are log-normally distributed. Fatigue crack in the frame proceeds first around the rivet hole, and upon propagating through the upper frame a_{F1} , it will propagate into the frame a_{F2} as shown in Figure 1.

The period of skin fatigue crack propagation lies between t_0 and t_f shown in Figures 2 and 3. During that period, the crack propagates from a_0 to a_f . The variables, t_f and a_0 , denote the time and the crack length when the element fails as mentioned below.

4) Element failure criterion

An element can fail either before or after fatigue crack initiation. Before crack initiation, the element is considered to have failed when the stress due to differential pressure exceeds the strength of the element.

On the other hand, after crack initiation, the following two failure modes are considered to exist. A failure due to unstable crack growth occurs when the crack length reaches a certain level a_f which is governed by a failure criterion. This unstable crack is, in general, arrested at both sides of frames because the residual strength increases near the frames. The other failure mode arises when a fatigue crack reaches the 2-bay crack length which is equivalent to a_f . Feddersen's criterion of residual strength is adopted for the condition of unstable crack propagating in this study. This criterion involves yield stress \hat{S}_y and fracture toughness K_{IC} both of which are random variables governed by two-parameter Weibull distributions.

2.2 Element Model for Bayesian Reliability Analysis

External visual inspection is implemented in order to detect skin cracks in the element shown in Figure 1. Therefore, a skin crack propagation a_s is applied to the analysis. As shown in Figures 2 and 3, a_s is visually detectable when it exceeds $a_s^* = r_h + a_{min}$. The variables r_h and a_{min} denote the rivet head radius and the minimum detectable crack length due to visual inspection respectively. The detectable crack

propagation period lies between t_0^* and t_f . Consequently, the TTCI of this model t_0^* is much longer than that for the true model t_0 .

1) Fatigue crack initiation

For simplicity, the TTCI of the model for the Bayesian reliability analysis is assumed to be a random variable with density function following a two-parameter Weibull distribution:

$$f_0^*(t_0|\beta^*) = \frac{\alpha}{\beta^*} \left(\frac{t_0}{\beta^*}\right)^{\alpha-1} \exp\left\{-\left(\frac{t_0}{\beta^*}\right)^\alpha\right\} \quad (6)$$

Uncertainty is introduced in the TTCI through the scale parameter β^* which is considered to be a random variable.

2) Fatigue crack propagation

The period of skin fatigue crack propagation is defined between t_0^* and t_f when the element fails. In other words, during that period, the crack propagates from a_0^* to a_f . The following Paris equation is used to present a skin fatigue crack propagation in this analysis:

$$\frac{da_s}{dt} = C (a_s)^{b/2} \quad (7)$$

$$C = 10^z$$

where C or z are functions of cyclic stress and stress intensity factor with modification coefficients. Integrating Eq. (7) from a_0^* to the current crack length a_s at time t , the following expression is obtained:

$$a_s(t-t_0^*) = \{-b'10^z(t-t_0^*)-a_0^*\}^{-1/b'} \quad (8)$$

$$b' = (b-2)/2$$

$$a_0^* = r_h + a_{min}$$

Uncertainty in fatigue crack propagation is introduced by a random variable z . It should be noted that when the crack length reaches a_f , the structural element fails.

3) Inspection

All structural elements are inspected by external visual inspection at the time of each inspection. If a skin crack is detected in an element, the crack length is assumed to be measured accurately. It is assumed that element failure can be detected always if it exists during the inspection process. Therefore, the probability of detecting the element failure is equal to unity.

4) Probability of crack detection for visual inspection

Information on the probabilities of crack detection (POD) is necessary in the present analysis.

(1) Probability of detection for a crack

The probability that a crack will be detected, $D(a_s^*|d)$, by visual inspection depends on the crack size in excess of the radius r_h of the rivet head (see Figure 2) and is assumed to be given by a three-parameter Weibull function as shown below:

$$D(a_s^*|d) = 1 - \exp\left\{-\left(\frac{a_s^* - a_{min}}{d - a_{min}}\right)^\epsilon\right\} \quad (9)$$

Then, the probability that the crack will not be detected is given by:

$$\bar{D}(a_s^*|d) = 1 - D(a_s^*|d) \quad (10)$$

where $a_s^* = a_s - r_h$ and a_{min} denote the inspectable and the minimum detectable crack length respectively (see Figure 2).

(2) Probability of detection for cracks at a rivet

Both sides of the rivet head are inspected for cracks. Therefore, the probability $D_i(a_s^*l_d)$ that at least the crack on the one side is detected is given by:

$$D_i(a_s^*l_d) = 1 - \overline{D}_i(a_s^*l_d) \quad (11)$$

where $\overline{D}_i(a_s^*l_d)$ is

$$\overline{D}_i(a_s^*l_d) = [\overline{D}_i(a_s^*l_d)]^2 \quad (12)$$

An assumption has been made here that the crack in the skin is always symmetric with respect to the central rivet axis.

5) Repair or replacement

If an element is found not to be intact in the skin, the following actions are taken:

- 1] If a crack is detected in the skin of the element, it is repaired and the element regains its initial strength.
- 2] If the element is found to have failed, it is replaced by a new one.
- 3] If the skin crack or failure in the element is detected, internal inspection is performed for a center frame. If the frame is found to have a crack or to have failed, the frame is also repaired or replaced and regains its initial strength.

Hence, after the repair or replacement, the element is back to its initial state.

6) Failure rate and element reliability

Based on the element failure criterion, following two failure rates are defined.

(1) Before crack initiation

The failure rate at time instant t before crack initiation is a very small constant and given by:

$$h(t) = \exp(r) = h_0 \quad (13)$$

The same failure rate is used in approximation in the present Bayesian reliability model with the time instant t for fatigue crack initiation even if a fatigue crack is propagating between t_0 and t_0^* .

The reliability of an element before crack initiation during the service period from time instant T_i up to time instant t ($> T_i$) is given by:

$$U(t-T_i) = \exp\left\{-\int_{T_i}^t h(\tau)d\tau\right\} = \exp\{-(t-T_i)\exp(r)\} \quad (14)$$

in which T_i is the time of service initiation for the element under consideration.

(2) After crack initiation

A two-parameter Weibull function is adopted for the failure rate after crack initiation at time instant t :

$$h(t) = \frac{\alpha_f}{\beta_f} \left(\frac{t}{\beta_f}\right)^{\alpha_f-1} + \exp(r) \quad (15)$$

The reliability of an element after crack initiation during the service period from the time of crack initiation t_0^* up to time instant t is given by:

$$\begin{aligned} V(t-t_0^*) &= \exp\left\{-\int_{t_0^*}^t h(\tau)d\tau\right\} \\ &= \exp\left\{-\frac{1}{\beta_f^{\alpha_f}}(t^{\alpha_f}-t_0^{*\alpha_f}) - (t-t_0^*)\exp(r)\right\} \quad (16) \end{aligned}$$

7) Uncertain parameters

Following two parameters have to be estimated from inspection data such as the number of cracks, crack sizes and whether or not failures were observed. Other parameters are assumed to be known.

- 1] Scale parameter β^* in Eq.(6)
- 2] Crack propagation parameter z in Eq.(8)

3 FORMULATION OF BAYESIAN RELIABILITY ANALYSIS**3.1 Possible Events at Time of Inspection**

At the time of the j -th inspection, performed at time T_j on a certain element, one of the following three events may occur (knowing that this element was repaired or replaced during the l -th inspection performed at time T_l with $l < j$):

- 1] $\{A; j, l\}$ = event that the element is found to have failed at the time of the j -th inspection T_j , or equivalently event that failure of the element occurred during the time interval $[T_{j-1}, T_j]$. This event consists of the following two mutually exclusive events:
 - E_{1j} = event that the element failed before crack initiation, sometime during the time interval between the two consecutive inspections at T_{j-1} and T_j .
 - E_{2j} = event that the element failed after crack initiation, sometime during the time interval between the two consecutive inspections at T_{j-1} and T_j .
- 2] $\{B_1(a); j, l\}$ = event that the element is found not to have failed at the time of the j -th inspection T_j but a crack of length between a_j and a_j+da_j is detected in the element. Event $\{B_1(a); j, l\}$ is alternatively denoted by E_{3j} .
- 3] $\{B_2; j, l\}$ = event that the element is found not to have failed at the time of the j -th inspection T_j and no crack is detected in the element. This event consists of the following two mutually exclusive events:
 - E_{4j} = event that the element did not fail in the time interval $[T_{j-1}, T_j]$ and no crack exists in the element at the time of inspection T_j .
 - E_{5j} = event that the element did not fail in the time interval $[T_{j-1}, T_j]$ but a crack exists in the element which is not detected at the time of inspection T_j .

In the following, the probabilities of these five events will be evaluated for a particular element in terms of the probability density and distribution functions $f_0^*(t|\beta^*)$ and $F_0^*(t|\beta^*)$ of the TTCL reliability functions $U(t)$ and $V(t)$ and probability of crack detection $D_i(a|d)$.

Event E_{1j}

Event E_{1j} consists of two mutually exclusive events, E_{1j}^a and E_{1j}^b , defined as follows:

- 1] E_{1j}^a = event that the element fails before crack initiation sometime during the time interval $[T_{j-1}, T_j]$, under the condition that no crack would have initiated in the element before T_j if failure did not occur sometime during the time interval $[T_{j-1}, T_j]$. The probability P_{1j}^a of event E_{1j}^a is given by:

$$P_{1j}^a = \{1 - F_0(T_j - T_j/b)\} \{U(T_{j-1} - T_i) - U(T_j - T_i)\} \quad (17)$$

- 2] E_{1j}^b = event that the element fails before crack initiation sometime during the time interval $[T_{j-1}, t]$, under the condition that a crack would have initiated at time instant t ($T_{j-1} < t < T_j$) if failure did not occur sometime during the time interval $[T_{j-1}, t]$. The probability P_{1j}^b of event E_{1j}^b is given by:

$$P_{1,j}^b = \int_{T_{j-1}}^{T_j} f_0(t-T_j/b) \{U(T_{j-1}-T_j) - U(t-T_j)\} dt \quad (18)$$

Finally, the probability $P_{1,j}$ of event $E_{1,j}$ is given by:

$$P_{1,j} = P_{1,j}^a + P_{1,j}^b \quad (19)$$

Event $E_{2,j}$

Event $E_{2,j}$ consists of two mutually exclusive events, $E_{2,j}^a$ and $E_{2,j}^b$, defined as follows:

- 1] $E_{2,j}^a$ = event that a crack initiated at some time instant t in the time interval $[T_i, T_{i+1}]$ ($i=1, \dots, j-2$), the crack was not detected during all subsequent inspections (from inspection at time T_{i+1} up to inspection at time T_{j-1} inclusive) and the element failed sometime during the time interval $[T_{j-1}, T_j]$. The probability $P_{2,j}^a$ of event $E_{2,j}^a$ is given by:

$$P_{2,j}^a = \sum_{i=1}^{j-2} \left\{ \int_{T_i}^{T_{i+1}} f_0^*(t-T_j/\beta^*) \cdot U(t-T_j) \cdot [V(T_{j-1}-t) - V(T_j-t)] \cdot \left[\prod_{k=i+1}^{j-1} \{1 - D_i(a(T_k-t)z)\} \right] dt \right\} \quad (20)$$

- 2] $E_{2,j}^b$ = event that a crack initiates at some time instant t in the time interval $[T_{j-1}, T_j]$ and the element fails sometime during the time interval $[t, T_j]$. The probability $P_{2,j}^b$ of event $E_{2,j}^b$ is given by:

$$P_{2,j}^b = \int_{T_{j-1}}^{T_j} f_0^*(t-T_j/\beta^*) \cdot U(t-T_j) \cdot [1 - V(T_j-t)] dt \quad (21)$$

Finally, the probability $P_{2,j}$ of event $E_{2,j}$ is given by:

$$P_{2,j} = P_{2,j}^a + P_{2,j}^b \quad (22)$$

Event $E_{3,j}$

Event $E_{3,j}$ is defined as follows:

- $E_{3,j}$ = event that the element is found not to have failed at the time of the j -th inspection and a crack of length between a_j and a_j+da_j is detected in the element.

Since a crack of length between a_j and a_j+da_j is found at the time of the j -th inspection, the time instant t_0^* of initiation of this crack can be computed from Eq.(8) as follows:

$$a_j = a_s(T_j - t_0^*z) = [-b \cdot 10^z (T_j - t_0^*) + a_0^{*b}]^{-1/b} \quad (23)$$

$$t_0^* = T_j + \frac{1}{b \cdot 10^z} (a_j^b - a_0^b) \quad (24)$$

Then, the probability $p_{3,j}da_j$ of event $E_{3,j}$ is given by:

$$p_{3,j}da_j = f_0^*(t_0^*-T_j/\beta^*) dt_0^* U(t_0^*-T_j) \cdot V(T_j-t_0^*) \cdot \left[\prod_{k=i+1}^{j-1} \{1 - \delta \cdot D_i(a_s(T_k-t_0^*z))\} \right] \cdot D_i(a_s j/z) \quad (25)$$

On the right-hand-side of Eq.(25), t_0^* is to be replaced by the expression shown in Eq.(24) and dt_0^* is calculated with the aid of Eq.(24) as:

$$dt_0^* = \frac{d^*t_0}{da_s j} \cdot da_s j = \frac{da_s j}{10^z a_s^{b/2}} \quad (26)$$

In this way, the right-hand-side of Eq.(24) is expressed completely as a function of a_j . In Eq.(25), δ is given by:

$$\delta = \begin{cases} 1 & \text{for } T_k \geq t_0^* \\ 0 & \text{for } T_k < t_0^* \end{cases} \quad (27)$$

Event $E_{4,j}$

Event $E_{4,j}$ is defined as follows:

- $E_{4,j}$ = event that the element did not fail in the time interval $[T_{j-1}, T_j]$ and no crack exists in the element at the time of inspection T_j . The probability $P_{4,j}$ of event $E_{4,j}$ is given by:

$$P_{4,j} = \{1 - F_0^*(T_j - T_j/\beta^*)\} \cdot U(T_j - T_j) \quad (28)$$

Event $E_{5,j}$

Event $E_{5,j}$ is defined as follows:

- $E_{5,j}$ = event that the element did not fail in the time interval $[T_{j-1}, T_j]$ but a crack exists in the element which is not detected at the time of inspection T_j . The probability $P_{5,j}$ of event $E_{5,j}$ is given by:

$$P_{5,j} = \sum_{i=1}^{j-1} \left\{ \int_{T_i}^{T_{i+1}} f_0^*(t-T_j/\beta^*) \cdot U(t-T_j) \cdot V(T_j-t) \cdot \left[\prod_{k=i+1}^j \{1 - D_i(a_s(T_k-t)z)\} \right] dt \right\} \quad (29)$$

Event A , B_1 and B_2

Finally, the probabilities of events $\{A: j, l\}$, $\{B_1(a): j, l\}$ and $\{B_2: j, l\}$ are easily obtained as

$$P\{A: j, l\} = P_{1,j} + P_{2,j} \quad (30)$$

$$P\{B_1(a_s j): j, l\} = p_{3,j} da_s j \quad (31)$$

$$P\{B_2: j, l\} = P_{4,j} + P_{5,j} \quad (32)$$

From here on, $P_m\{A: j, l\}$, $P_m\{B_1(a): j, l\}$ and $P_m\{B_2: j, l\}$ are written for $P\{A: j, l\}$, $P\{B_1(a): j, l\}$ and $P\{B_2: j, l\}$, respectively, in order to indicate that these probabilities are for the element number m .

3.2 Reliability of an Element After the Latest Inspection T_j

The reliability of two types of elements at time instant t^* after the j -th inspection (but before the $(j+1)$ -th inspection, i.e. $T_j < t^* < T_{j+1}$) is calculated in the following:

1) Elements repaired or replaced at the j -th inspection

Elements are repaired or replaced at the j -th inspection in the case of events $\{A: j, l\}$ or $\{B_1(a): j, l\}$, respectively. Writing $R(t^*; \text{Repair})$ instead of $R(t^*; \text{Repair or Replacement})$ for brevity, the reliability $R(t^*; \text{Repair})$ of an element of this type is computed as the sum of the following two probabilities:

- 1] Probability that the element will survive during the time interval $[T_j, t^*]$ and no crack will initiate before t^* ,
- 2] Probability that a crack will initiate in the element sometime during the time interval $[T_j, t^*]$, but the element will survive during the same time interval.

The reliability $R(t^*; \text{Repair})$ is then calculated as:

$$R(t^*; \text{Repair}) = \{1 - F_0^*(t^* - T_j | \beta^*)\} \cdot U(t^* - T_j) + \int_{T_j}^{t^*} f_0^*(t - T_j | \beta^*) \cdot U(t - T_j) \cdot V(t^* - t) dt \quad (33)$$

2) Elements not Repaired at the j-th Inspection

An element is neither repaired nor replaced at the j-th inspection in the case of event $\{B_2; j, l\}$. The reliability $R(t^*; \text{No Repair})$ of an element of this type is computed as the sum of the following three probabilities (denoted by Q) divided by the probability of event $\{B_2; j, l\}$ (which is given by $P_{A_j} + P_{B_j}$):

- 1] Probability that the element will survive during the time interval $[T_j, t^*]$ and no crack will initiate before t^* ,
- 2] Probability that a crack will initiate during the time interval $[T_j, t^*]$, but the element will survive during the time interval $[T_j, t^*]$,
- 3] Probability that a crack initiated at some time instant t during the time interval $[T_i, T_{i+1}]$ ($i = 1, \dots, j-1$) and this crack was not detected during all subsequent inspections (from inspection at time T_{i+1} up to inspection at time T_j inclusive) and the element will survive during time interval $[T_j, t^*]$.

Therefore, $R(t^*; \text{No Repair})$ is calculated as:

$$R(t^*; \text{No Repair}) = \frac{Q}{P\{B_2; j, l\}} \quad (34)$$

The expression for Q appearing in Eq.(34) is given by:

$$Q = \{1 - F_0^*(t^* - T_j | \beta^*)\} \cdot U(t^* - T_j) + \int_{T_j}^{t^*} f_0^*(t - T_j | \beta^*) \cdot U(t - T_j) \cdot V(t^* - t) dt + \sum_{i=1}^{j-1} \int_{T_i}^{T_{i+1}} f_0^*(t - T_i | \beta^*) \cdot U(t - T_i) \cdot V(t^* - t) \cdot \left[\prod_{k=i+1}^j \{1 - D_k(a_k - t|z)\} \right] dt \quad (35)$$

It should be noted that $R(t^*; \text{No Repair})$ indicates the probability that the element survives during the time interval $[T_j, t^*]$ (event A) under the condition that the element has not been repaired or replaced at the j-th inspection (event B). Then, Eq.(34) follows immediately from:

$$P\{A \cap B\} = P\{A|B\} \cdot P\{B\} \quad (36)$$

considering that $P\{A \cap B\} = Q$, $P\{A|B\} = R(t^*; \text{No Repair})$ and $P\{B\} = P\{B_2; j, l\}$.

3.3 Bayesian Analysis

1) Uncertain parameters and their prior joint density function

Initially, it is assumed that β^* and z are jointly and uniformly distributed according to the following prior joint density function:

$$f^0(\beta^*, z) = \frac{1}{(\beta_{\max}^* - \beta_{\min}^*)(z_{\max} - z_{\min})} \quad (37)$$

where:

$$\beta_{\min}^* \leq \beta^* \leq \beta_{\max}^*; \quad z_{\min} \leq z \leq z_{\max} \quad (38)$$

2) Likelihood function resulting from j-th inspection

The likelihood function LF_j for the entire structure as a result of the j-th inspection is calculated as:

$$LF_j = \prod_{m=1}^M LF_j^{(m)} \quad (39)$$

where $LF_j^{(m)}$ is the likelihood function for element m resulting from the j-th inspection and M is the total number of elements in the structure.

For a specified element m, consider that replacement due to failure or repair due to a detected crack occurred at inspections $T_{i_1}, T_{i_2}, \dots, T_{i_r}$, where r indicates the number of times the element has been repaired or replaced before the j-th inspection. Consequently,

$$i_1 < i_2 < \dots < i_r < j \quad (40)$$

It is pointed out that i_1, i_2, \dots, i_r are all known at the time of the j-th inspection since the entire inspection history of each element is considered to be known. It is noted that i_1, i_2, \dots, i_r as well as r take values unique to each element. Then, the likelihood function for element m resulting from the j-th inspection is given by:

$$LF_j^{(m)} = P_m\{X: j, i_r\} \cdot \prod_{k=1}^r P_m\{Y: i_k, i_{k-1}\} \quad (41)$$

In Eq.(41), X stands for either A or $B_1(a_k)$ or B_2 depending on the result of the j-th inspection for element m. Specifically, if at the time of the j-th inspection, element m is found to have failed, then X stands for A. If it is found to have a crack of length between a_k and $a_k + da_k$, then X stands for $B_1(a_k)$. If it is found intact, then X stands for B_2 . Also, in Eq.(41), Y represents either A or $B_1(a_k)$ depending on the result of the i_k -th inspection for element m. Specifically, if at the time of the i_k -th inspection, element m is found to have failed, then Y stands for A and if element m is found to have a crack of length between a_{k-1} and $a_{k-1} + da_{k-1}$, then Y stands for $B_1(a_{k-1})$. Finally, for the case where element m is found intact at all inspections prior to the j-th, the product appearing in Eq.(41) is set equal to unity and Eq.(41) takes the form:

$$LF_j^{(m)} = P_m\{X: j, i_0\} \quad (42)$$

where i_0 denotes the time of initiation of service for the structure. At this juncture it is very important to note that the likelihood function LF_j defined in Eq.(39) is conditional to give values of β^* and z , since $LF_j^{(m)}$ defined in Eqs.(41) and (42) is obviously conditional to given values β^* and z .

3) Posterior joint density function of uncertain parameters

The posterior joint density function of the two uncertain parameters β^* and z immediately after the j-th inspection, is given by:

$$f^1(\beta^*, z) = \frac{LF_j \cdot f^0}{\int_{\beta_{\min}^*}^{\beta_{\max}^*} \int_{z_{\min}}^{z_{\max}} (\text{Numerator}) d\beta^* dz} \quad (43)$$

4) Reliability of entire structure at time instant t^* after the latest inspection T_j

The reliability of the entire structure consisting of M elements at time instant t^* after the latest inspection T_j is denoted by $\bar{R}_M(t^*)$ and calculated as:

$$\bar{R}_M(t^*) = \int_{\beta_{\min}^*}^{\beta_{\max}^*} \int_{z_{\min}}^{z_{\max}} R_M(t^* | \beta^*, z) \cdot f^1(\beta^*, z) d\beta^* dz \quad (44)$$

where:

$$R_M(t^*|\beta^*, z) = \left[\prod_{m=1}^{M_1} R_m(t^*; \text{Repair}) \right] \cdot \left[\prod_{m=1}^{M_2} R_m(t^*; \text{No Repair}) \right] \quad (45)$$

where M_1 = number of elements either repaired or replaced at the j -th inspection, M_2 = number of elements found intact at the j -th inspection and $M_1 + M_2 = M$. In Eq.(45), $R_m(t^*; \text{Repair})$ and $R_m(t^*; \text{No Repair})$ are identical with the reliabilities $R(t^*; \text{Repair})$ and $R(t^*; \text{No Repair})$ defined in Eqs.(33) and (34), respectively. The subscript m is used to indicate that these reliabilities are associated with element m . Note that $R_M(t^*|\beta^*, z)$ defined in Eq.(45) is conditional to given values of β^* and z , since $R_m(t^*; \text{Repair})$ and $R_m(t^*; \text{No Repair})$ are obviously conditional to given values of β^* and z .

3.4 Calculation of Time T_{j+1} for Next Inspection

Assuming that the entire structure must maintain its reliability above a prespecified design level throughout its service life, the time T_{j+1} for the next inspection after the latest one performed at T_j is calculated using:

$$\bar{R}_M(t^*) \geq R_{\text{design}} \quad (46)$$

where R_{design} denotes the prespecified design level of reliability for the entire structure. The time T_{j+1} of the $(j+1)$ -th inspection is then estimated as the maximum value of t^* that satisfies Eq.(46) as follows:

$$T_{j+1} = t^* = \bar{R}_M^{-1}(R_{\text{design}}) \quad (47)$$

It is pointed out that following the procedure to calculate the time T_{j+1} for the next inspection described above, ensures that the reliability of the entire structure remains above the prespecified design level R_{design} throughout the service life of the structure.

4 NUMERICAL EXAMPLE

It is considered that all the values of a true structural element model listed in Table 1 are approximately corresponding to these that are applicable to an actual fuselage structural design.

As for the Bayesian reliability analysis which can evaluate an appropriate non-periodic inspection schedules, two essential uncertain parameters are considered: β^* and z . They are set to be jointly and uniformly distributed according to the following initial prior joint density function in the form previously shown by Eq.(37). The minimum and maximum values of these parameters, and their ranges and increments are given by the engineering judgement as follows:

$$\beta^*_{\min} = 17,000 \text{ flights}; \quad \beta^*_{\max} = 66,000 \text{ flights}; \\ \beta^* = \beta^*_{\max} - \beta^*_{\min} = 47,000 \text{ flights}; \quad \Delta\beta^* = 3,500 \text{ flights}$$

$$z_{\min} = -4.1; \quad z_{\max} = -2.7; \quad \bar{z} = z_{\max} - z_{\min} = 1.4; \quad \Delta z = 0.1$$

Therefore, in the following example, both of these ranges are divided into 14 intervals for numerical analysis.

The aircraft is assumed to have 100 to 200 fatigue-critical elements, namely, critical rivet holes. The service life is 50,000 flights and the minimum reliability level for the entire structure throughout its service life is set equal to $R_{\text{design}} = 0.8$. This indicates that the reliabilities of one element for both 100 and 200 fatigue-critical elements are 0.998 and 0.999, respectively under the assumption of

independence. The value of parameter r in the failure rates for before and after crack propagations is assumed to be $r = -18$ which is derived from the failure rate of 10-8/flight hour and the design life of 60,000 flight hours. Therefore, the reliability of an element is equal to be $U(t=60,000 \text{ hours}) = 0.999$. The standard deviation σ_z of z for the parameters of fatigue crack propagations of skin and frame in Eqs.(2) to (5) is set at 0.154. The speeds of fatigue crack propagation between twice and half the mean crack propagation speeds of skin and frame in Figure 4 account for 95% of all fatigue cracks.

The values of the parameters, ϵ and a_{\min} in the POD of Eq.(9) are given as $\epsilon = 1.4$ and $a_{\min} = 0.04$ inches based on the field data of fatigue cracks visually detected (Ref 13). A parametric study on the parameter d in the POD is performed for $d = (1.2, 1.4, 1.6, 1.8)$ inches shown in Figure 5, in order to investigate its effect on crack detection capability.

Values of other parameters are determined on the basis of engineering judgement, analyses, test results, service experience and so on.

The results of one simulation for each combination of $M = (100, 200)$ and $d = (1.2, 1.4, 1.6, 1.8)$ inches are depicted in Tables 2 and 3. These results include the non-periodic inspection schedule, number of failed elements, number and length of detected cracks. The corresponding structural reliability for the entire structure as a function of time is displayed in Figures 6 and 7.

In the case that the number of critical elements increases, the number of inspections during service life for each parameter d in the POD increases in order to maintain the same target reliability R_{design} , and the numbers of failed elements and detected cracks also increase. The first inspection times T_1 for $M = (100, 200)$ and $d = (1.2, 1.4, 1.6, 1.8)$ inches are implemented after approximately 30,000 flights due to the ranges of the parameter values, β^* and z , introduced by the engineering judgement in this analysis. It is reasonable that the first inspection has been implemented when much time has passed since an aircraft was put into service.

When the value of the parameter d in the POD gets larger (i.e., the crack detection becomes less efficient), the number of inspections increases, and the inspection intervals become shorter to keep the minimum level of reliability R_{design} for the entire structure. When the number of critical elements and the value of the parameter d become large, several elements would have failed before they were detected by external visual inspection. Consequently, higher POD is required for the case that the number of critical elements becomes large.

The posterior joint density functions of the uncertain parameters, β^* and z , after the third inspection are plotted in Figures 8 and 9 for $M = (100, 200)$ and $d = (1.2, 1.4, 1.6, 1.8)$ inches, respectively. The concentration of posterior joint density at the modal values for $M = 100$ is sharper than that for $M = 200$, because the number of cracks found at the third inspection for $M = 200$ is smaller than that for $M = 100$. Exception is the case when $d = 1.2$ inches.

5 CONCLUSIONS

The multiple element damage in fuselage structures of an aircraft is analyzed and the usefulness of the Bayesian reliability analysis has been demonstrated. The results of the numerical examples verify that this analysis can indeed generate appropriate non-periodic inspection schedules while estimating uncertain parameters even if a large number of crack data are not collected during inspections. The present study considered only one aircraft available for inspection. If a fleet of aircraft can be inspected as in the actual case, a large number of cracks and possibly failures will be found, making the Bayesian analysis even more practical.

6 REFERENCES

1. Yang, J.-N. and Trapp, W.J., "Reliability Analysis of Aircraft Structures under Random Loading and Periodic Inspection", AIAA J., 12, 12, December 1974, pp.1623-1630.
2. Shinozuka, M., "Development of Reliability-Based Aircraft Safety Criteria: An Impact Analysis", AFFDL-TR-76-31, Vol.1, April 1976.
3. Paliou, C. and Shinozuka, M., "Reliability and Durability of Marine Structures", J. Structural Engineering, ASCE, 113, 6, June 1987, pp.1297-1314.
4. Shinozuka, M., Itagaki, H. and Asada, H., "Reliability Assessment of Structures with Latent Cracks", in "Fracture Tolerance Evaluation", US-Japan Cooperative Seminar, December 1981, pp.237-247.
5. Asada, H., Itagaki, H. and Ito, S., "Effect of Sampling Inspections on Aircraft Structural Reliability", in "ICOSSAR '85, the 4th International Conference on Structural Safety and Reliability", IASSAR Publication, Vol.1, May 1985, pp.I.87-I.96.
6. Itagaki, H. and Yamamoto, N., "Bayesian Analysis of Inspection on Ship Structural Members", in "ICOSSAR '85, the 4th International Conference on Structural Safety and Reliability", IASSAR Publication, Vol.3, May 1985, pp.III.533-III542.
7. Fujimoto, Y., Itagaki, H., Ito, S., Asada, H. and Shinozuka, M., "Bayesian Reliability Analysis of Structures with Multiple Components", in "ICOSSAR '89, the 5th International Conference on Structural Safety and Reliability, ASCE Publication, Vol.3, August 1989, pp.III533-III542.
8. Deodatis, G., Fujimoto, Y., Ito, S., Spencer, J. and Itagaki, H., "Non-Periodic Inspection by Bayesian Method I", Probabilistic Engineering Mechanics J., 7, 4, 1992, pp.191-204.
9. Ito, S., Deodatis, G., Fujimoto, Y., Asada, H. and Shinozuka, M., "Non-Periodic Inspection by Bayesian Method II: Structures with Elements Subjected to Different Stress Levels", Probabilistic Engineering Mechanics J., 7, 4, 1992, pp.205-215.
10. Federal Aviation Administration, Advisory Circular, "Damage-Tolerance and Fatigue Evaluation of Structure", AC No.25.571-1B(Draft), July 1993.
11. Swift, T., "Widespread Fatigue Damage Monitoring - Issues and Concerns", in "FAA/NASA International Symposium on Advanced Structural Integrity Methods for Airframe Durability and Damage Tolerance", NASA Conference Publication 3274 Part 1, May 1994, pp.829-870.
12. Goranson, U.G., "Damage Tolerance - Facts and Fiction", in "The 17th Symposium of the International Committee on Aeronautical Fatigue (ICAF)", Vol.1, June 1993, pp.3-105.
13. Endoh, S., Tomita, H., Asada, H. and Sotozaki, T., "Practical Evaluation of Crack Detection Capability for Visual Inspection in Japan", in "The 17th Symposium of the International Committee on Aeronautical Fatigue (ICAF)", Vol.1, June 1993, pp.259-280.

Table 1 Values of Parameters in Numerical Example

Item	Values for true model	Bayesian analysis	
		Model value	Range for estimation
-Service life (flights)		50,000	
-Minimum level of reliability	R_{design}	0.8	
-Total number of critical elements	M	100, 200	
-Parameters of TTCI in Eq.(1)			
2-parameter Weibull	α	4	4
	β (flights)	40,000	
	β^* (flights)	Unknown	17,000 to 66,000
-Rivet head radius r_h (in)		0.18	0.18
-Initial half crack length for true model a_0 (in)		0.1	
-Initial half crack length for Bayesian analysis a_0^* (in)			0.22
-Minimum detectable crack length	a_{min} (in)		0.04
-Effective width (in)	W_S	40	
	Frame W_{F1}	14	
	W_{F2}	2	
-Maximum allowable crack length $a_{max}=W/2$ (in)			20
	Skin $a_{S,max}$	20	
	Frame $a_{F1,max}$	7	
	$a_{F2,max}$	1	
		2024-T3 (Skin:S)	7075-T6 (Frame:F)
-Yield stress S_y (ksi)			
2-parameter Weibull	α_{S_y}	19	19
	β_{S_y} (ksi)	49	70
-Fracture toughness K_{Ic} (ksi \sqrt{in})			
2-parameter Weibull	$\alpha_{K_{Ic}}$	12	12
	$\beta_{K_{Ic}}$ (ksi \sqrt{in})	140	65
-Fatigue crack propagation in Eqs.(2) to (5)			
Normal	b	3.8	3.4
	μ_z	-9.5	-9.0
	σ_z	0.154	0.154
in Eqs.(7) & (8)	b		4.0
	z		Unknown
-Cyclic stress range in Eqs.(2) to (5)			
Normal	Δs (ksi)		
	$\mu_{\Delta s}$ (ksi)	18	
	$\sigma_{\Delta s}$ (ksi)	0.9	
-Parameters of POD in Eq.(9)	ϵ		1.4
	d (in)	1.2, 1.4, 1.6, 1.8	
-Parameters of failure rate in Eq.(15)	r		-18
	α_f		5.5
	β_f (flights)		37,000

Note: 1 ksi=6.895 MPa, 1 in=2.54 cm, 1 ksi \sqrt{in} =1.099 MPa \sqrt{m}

Table 2 Inspection Results and Schedule
(Uncertain Parameters : β^* and z)

1) M=100 and d=1.2 inches

Inspection No.	Inspection time : T (flights)	Number of failed elements	Number of detected cracks	Detected crack length (inches)
1	30,460	0	0	
2	38,300	0	0	
3	42,580	0	7	0.43, 2.42, 3.39 1.04, 0.58, 7.45 0.29
4	47,430	0	1	0.26

2) M=100 and d=1.4 inches

Inspection No.	Inspection time : T (flights)	Number of failed elements	Number of detected cracks	Detected crack length (inches)
1	30,460	0	0	
2	38,010	0	0	
3	42,230	0	7	0.41, 1.83, 2.21 0.85, 0.53, 3.15 0.31
4	45,480	0	1	0.27
5	48,850	0	1	1.45

3) M=100 and d=1.6 inches

Inspection No.	Inspection time : T (flights)	Number of failed elements	Number of detected cracks	Detected crack length (inches)
1	30,460	0	0	
2	37,770	0	0	
3	41,930	0	7	0.40, 1.50, 1.70 0.74, 0.50, 2.08 0.30
4	44,230	0	1	0.37
5	46,730	0	0	
6	49,720	0	1	0.63

4) M=100 and d=1.8 inches

Inspection No.	Inspection time : T (flights)	Number of failed elements	Number of detected cracks	Detected crack length (inches)
1	30,460	0	0	
2	37,570	0	0	
3	41,680	0	5	0.38, 1.30, 0.47 1.60, 0.29
4	43,670	1*	1	2.78
5	45,630	0	1	0.30
6	47,600	0	0	
7	49,870	0	2	0.58, 3.80

* Failure after crack initiation

Table 3 Inspection Results and Schedule
(Uncertain Parameters : β^* and z)

1) M=200 and d=1.2 inches

Inspection No.	Inspection time : T (flights)	Number of failed elements	Number of detected cracks	Detected crack length (inches)
1	27,590	0	1	0.88
2	37,070	0	2	0.27, 0.82
3	41,960	0	7	0.40, 1.53, 1.74 0.75, 0.50, 3.51 1.02
4	45,260	0	0	
5	49,240	1*	4	1.94, 1.05, 0.59 1.09

* Failure after crack initiation

2) M=200 and d=1.4 inches

Inspection No.	Inspection time : T (flights)	Number of failed elements	Number of detected cracks	Detected crack length (inches)
1	27,590	0	0	
2	34,900	1*	1	0.52
3	37,500	0	2	0.25, 0.43
4	39,140	0	1	0.32
5	40,640	0	4	0.81, 0.85, 0.79 0.63
6	42,600	0	0	
7	44,840	1*	1	0.93
8	46,650	0	2	0.38, 0.34
9	48,190	0	1	0.76
10	49,910	0	4	4.02, 0.65, 1.38 0.84

* Failure after crack initiation

3) M=200 and d=1.6 inches

Inspection No.	Inspection time : T (flights)	Number of failed elements	Number of detected cracks	Detected crack length (inches)
1	27,590	0	0	
2	34,670	1*	1	0.50
3	36,930	0	1	0.37
4	38,820	0	1	0.51
5	40,680	0	2	0.80, 1.08
6	43,150	0	2	1.56, 2.06
7	46,400	1*	1	2.37
8	48,910	0	6	2.01, 0.52, 0.39 1.51, 0.94, 0.67

* Failure after crack initiation

4) M=200 and d=1.8 inches

Inspection No.	Inspection time : T (flights)	Number of failed elements	Number of detected cracks	Detected crack length (inches)
1	25,790	0	0	
2	34,480	1*	1	0.49
3	36,480	0	1	0.35
4	38,110	0	0	0.79, 0.32
5	40,030	0	3	0.69, 0.82, 0.53
6	41,850	0	0	
7	43,890	1*	1	4.03
8	46,080	1*	2	0.31, 1.83
9	47,720	0	2	0.37, 0.68
10	49,230	0	3	2.39, 1.92, 0.38

* Failure after crack initiation

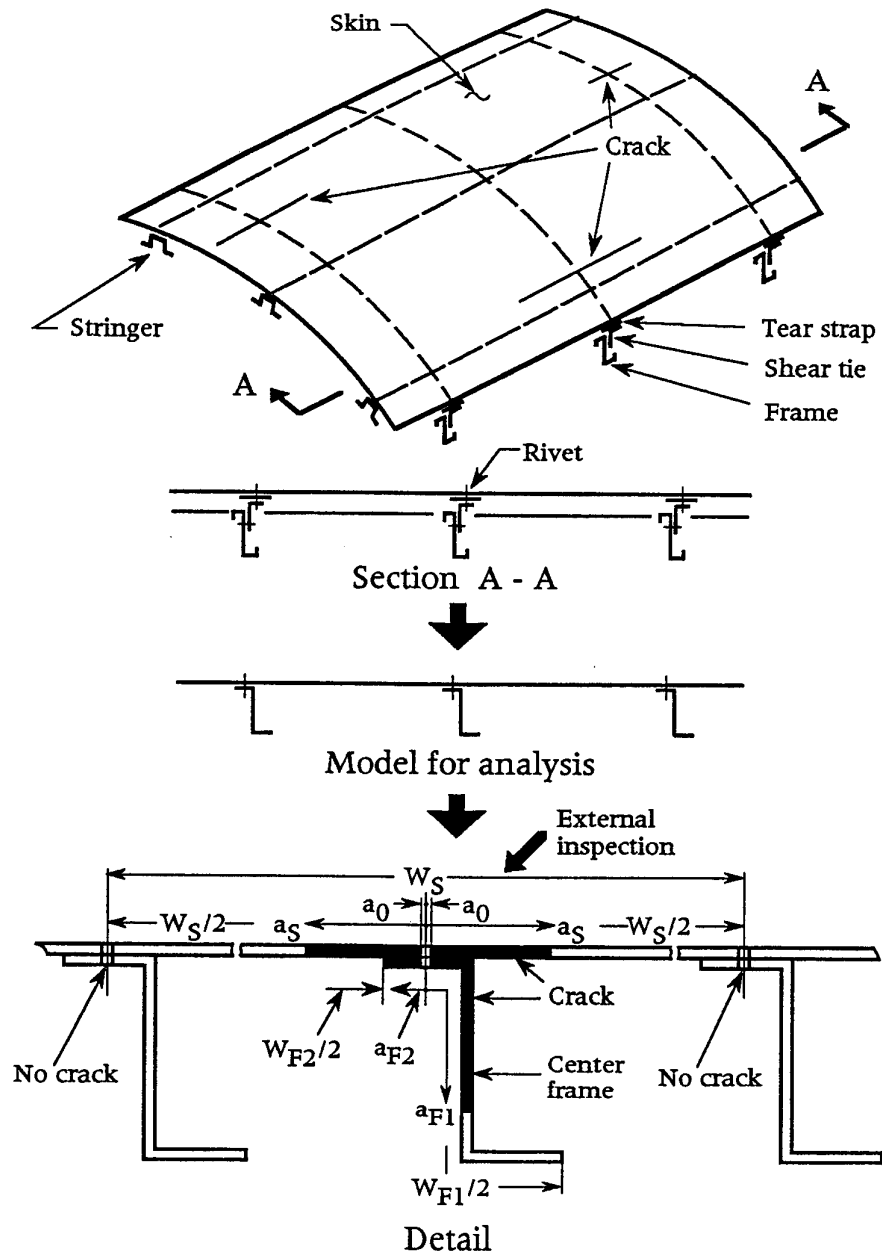


Figure 1 Fuselage Structural Model

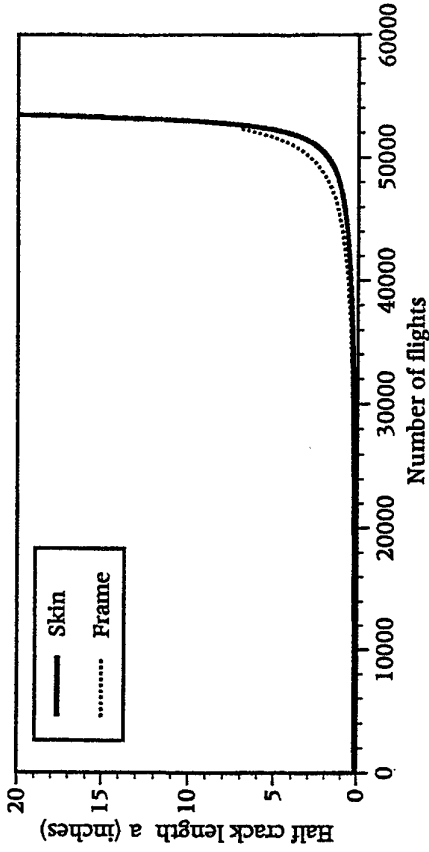


Figure 4 Mean Fatigue Crack Propagations for Frame and Skin

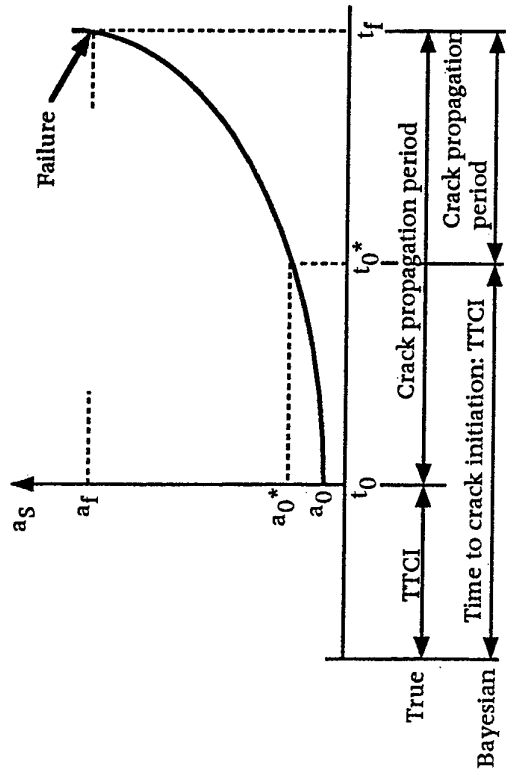


Figure 3 Fatigue Crack Initiation and Propagation for True Model and Bayesian Analysis Model

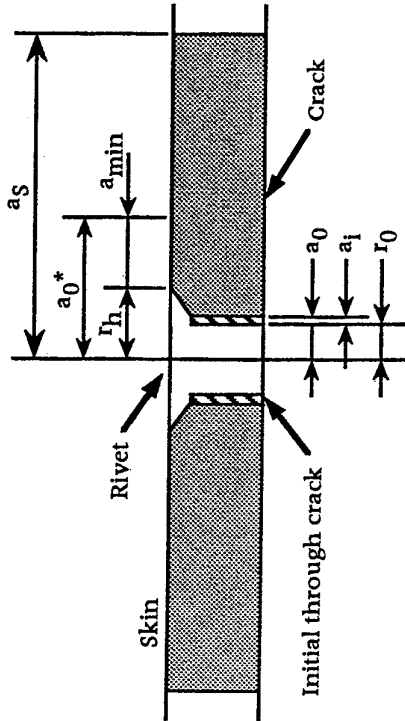


Figure 2 Definition of Rivet and Crack

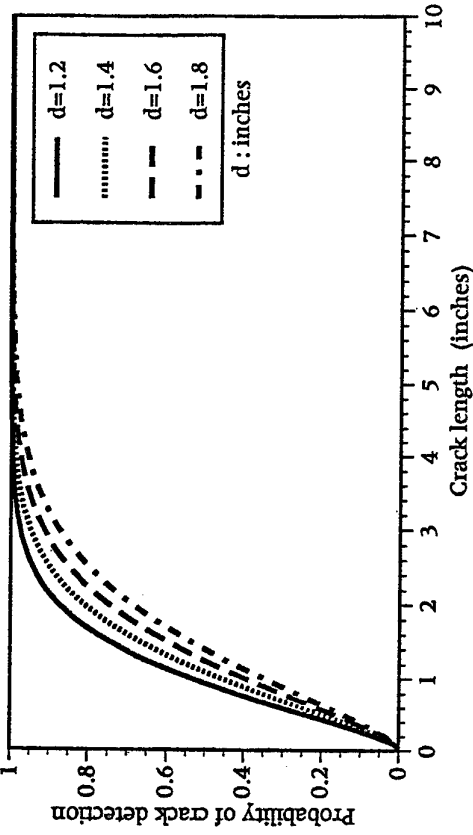


Figure 5 Probability of Crack Detection for Visual Inspection

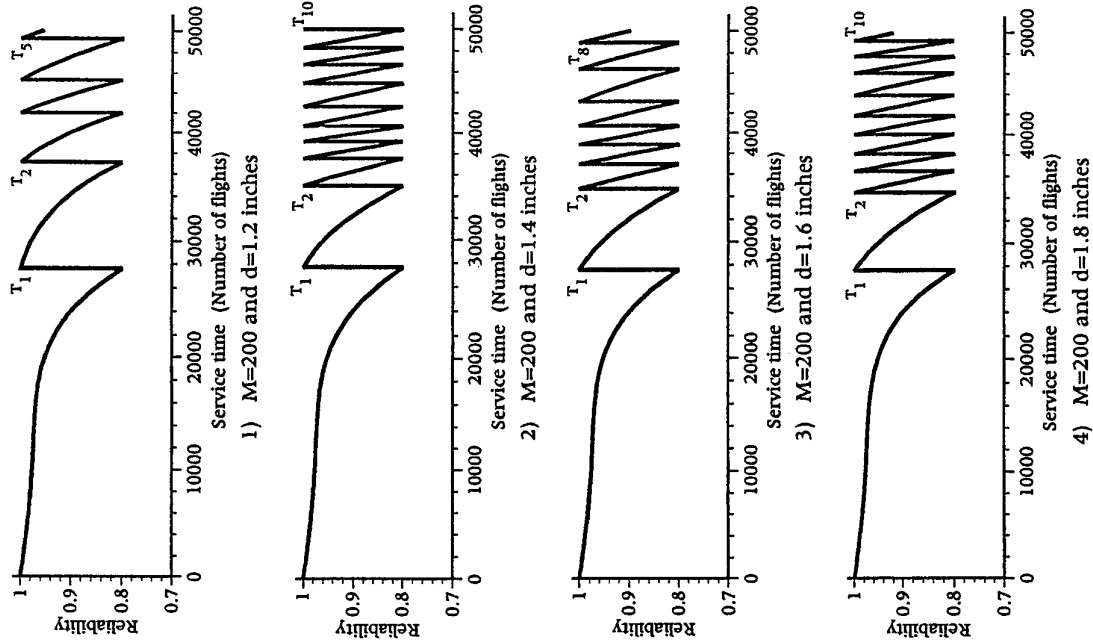


Figure 6 Inspection Schedule and Structural Reliability (Uncertain Parameters : β^* and z)

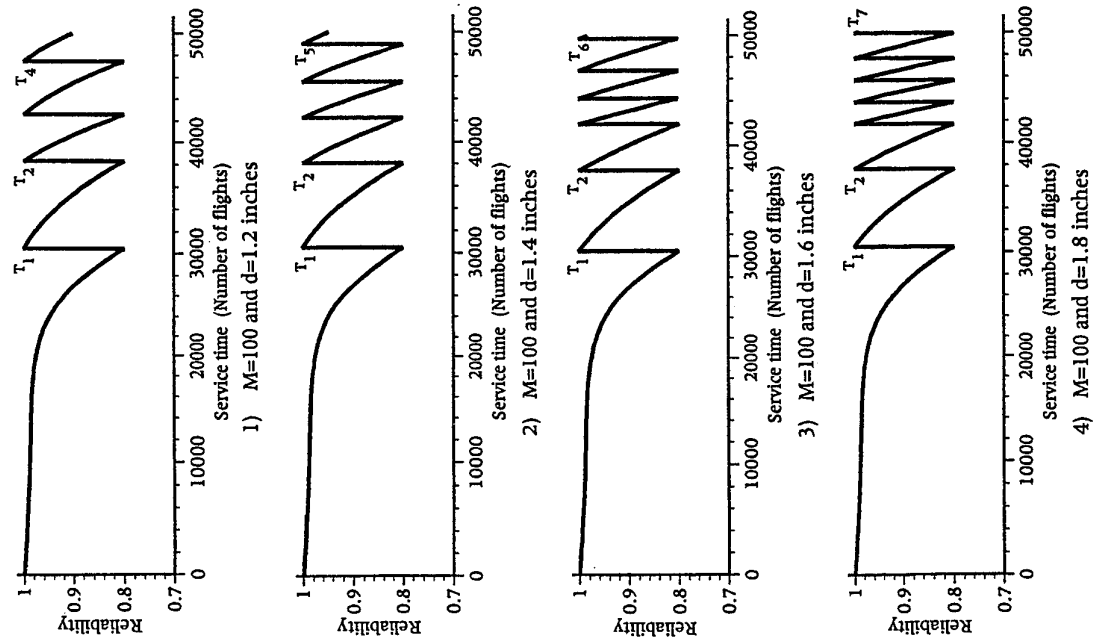
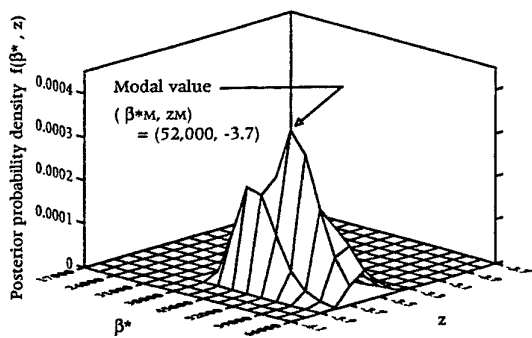
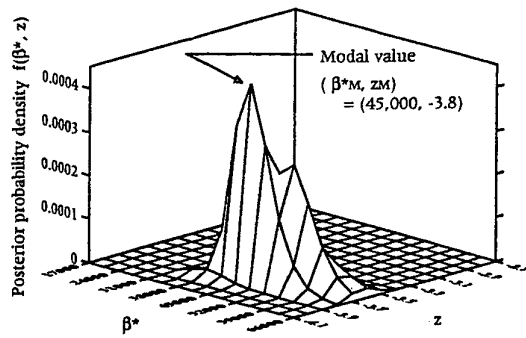


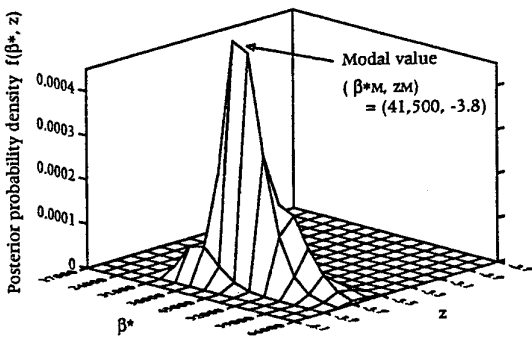
Figure 7 Inspection Schedule and Structural Reliability (Uncertain Parameters : β^* and z)



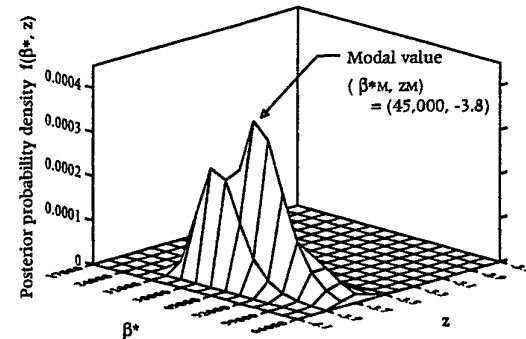
1) M=100 and d=1.2 inches



2) M=100 and d=1.4 inches

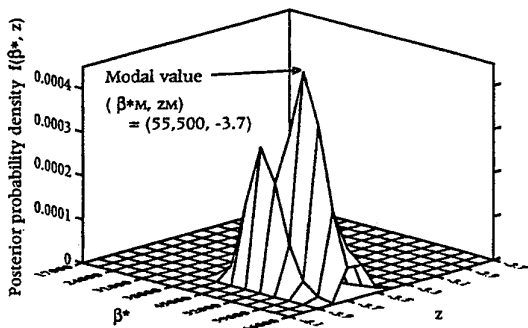


3) M=100 and d=1.6 inches

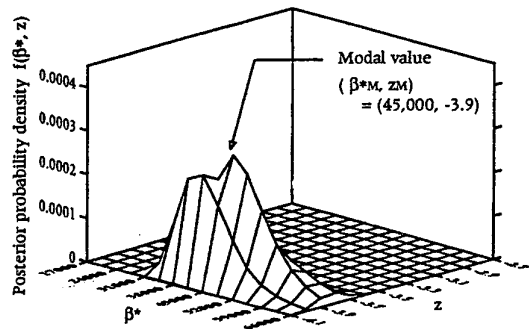


4) M=100 and d=1.8 inches

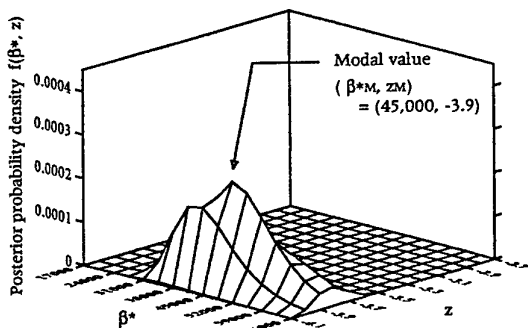
Figure 8 Posterior Joint Probability Density Functions at 3rd Inspection (Uncertain Parameters : β^* and z)



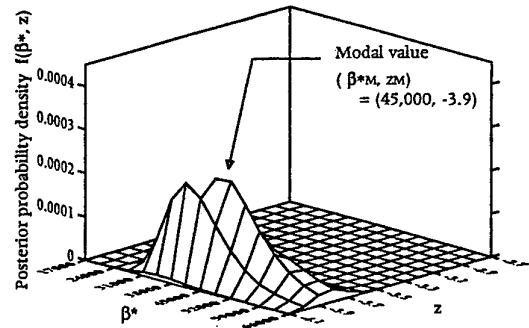
1) M=200 and d=1.2 inches



2) M=200 and d=1.4 inches



3) M=200 and d=1.6 inches



4) M=200 and d=1.8 inches

Figure 9 Posterior Joint Probability Density Functions at 3rd Inspection (Uncertain Parameters : β^* and z)

RISK ANALYSIS IN THE PRESENCE OF CORROSION DAMAGE

A.P. Berens
University of Dayton Research Institute
300 College Park
Dayton, OH 45469-0120 USA

J.G. Burns
Structural Integrity Branch
Wright Laboratory
Wright-Patterson Air Force Base, OH 45433 USA

1. SUMMARY

To quantify the potential damaging effects of corrosion in an aging fleet of aircraft, a structural risk analysis computer code was used to calculate the probabilities of fracture under statically defined corrosion scenarios. The analysis was performed using results from a damage tolerance evaluation of a critical location on an observation class, ground support aircraft. A realistic equivalent initial flaw size distribution was assumed for the start of the analysis. Corrosion conditions, defined in terms of five and ten percent thickness loss, were imposed for two subsequent periods in the life of the aircraft. The effects of detecting and repairing or not detecting the corrosion were modeled. For the scenarios and conditions assumed in this analytical sensitivity study, undetected corrosion effects led to order of magnitude increases in risk. These results indicate that corrosion damage could well impact safety in the aging aircraft fleets.

2. INTRODUCTION

The United States Air Force (USAF) has traditionally treated corrosion in aircraft structure as a durability issue. While the primary objective has been to prevent the initiation of corrosion through the proper choice of materials and coatings, corrosion does occur as evidenced by the high cost of corrosion related maintenance [1]. Although the scheduling of corrosion maintenance can be impacted by its frequency of occurrence for a particular fleet, no schedule adjustments are currently made for the structural safety inspections as determined by damage tolerance analyses [2]. However, as the aging fleets are used beyond their design lives, concern has arisen as to the potential joint effects of

corrosion and widespread fatigue damage on the structural integrity of critical details, i.e., on structural safety.

To evaluate the potential joint effects of fatigue damage and corrosion on safety, an analytical framework for modelling these effects must first be established. While fatigue damage can be modelled by fracture mechanics, to date there are no generally accepted metrics for quantifying the extent of corrosion damage or predicting its development. The damage resulting from environmental attack can take many forms and can lead to enhanced crack growth rates (corrosion fatigue), thickness loss (increased stresses), intergranular and stress corrosion cracking (stress risers), pitting (stress risers), and dimensional changes which increase the state of stress in the structure. Since these types of corrosion damages correlate with fracture mechanics concepts, analyses based on fracture mechanics are considered to provide at least first order approximations of the effects of corrosion damage [3].

In particular, evidence is building (at least for 2024 series aluminum and, possibly, for 7075 series aluminum), that corrosion effects can be approximated in a fracture mechanics based analysis in terms of thickness reductions, corrosion equivalent crack sizes, and accelerated crack growth [4,5]. Thickness loss affects both the stresses experienced by the structure and the stress intensity factor at the stress riser being analyzed but the crack growth rates can be obtained from laboratory specimens. The corrosion equivalent crack sizes are stress concentrations that are correlated with

intergranular and stress corrosion cracking and the largest corrosion pits that may be present in the structure. Accelerated crack growth results from corrosion fatigue has typically been accounted for by using conservative crack growth data from corrosive environments.

Initial sensitivity studies of corrosion effects on structural safety have been performed using deterministic analyses [6]. This paper is directed at the analysis of the corrosion effect of thickness loss on structural integrity as quantified in terms of the single flight fracture probability of a critical structural detail in an observation class, ground support aircraft. There are no current models for predicting thickness loss as a function of time (calendar months or flight hours). Thus, corrosion scenarios were defined by statically imposing five percent thickness reductions at two points in the life of an airframe. The fracture risks as a function of flight hours from the resulting corrosion scenarios are compared to the baseline fracture risks of no thickness loss throughout the usage intervals.

3. PROF COMPUTER PROGRAM

The stochastic structural analysis of the corrosion scenarios was performed using the Probability Of Fracture (PROF) computer code [7,8]. This code was specifically written to interface with the data that is available as a result of the USAF Aircraft Structural Integrity Program (ASIP). Figure 1 is a schematic of the program which illustrates the types of data required to perform an analysis and the probability of fracture (POF) output that is calculated as a function of flight hours. Under ASIP, crack life predictions (**a** versus **T**) are available for every known critical location. This implies the availability of: a) the flight by flight stress spectrum (from which the distribution of maximum stress per flight can be obtained); b) stress intensity factors as a function of crack size (**a** versus **K/s**), and, c) fracture toughness, K_{cr} , (from which a distribution can be inferred). The initiating crack size distribution can be obtained tear down inspections or, as in this study, from equivalent initial flaw sizes. Probability of detection as a function of crack size, $POD(a)$, is a characterization of the capability of the non-destructive inspection system used during the safety inspections.

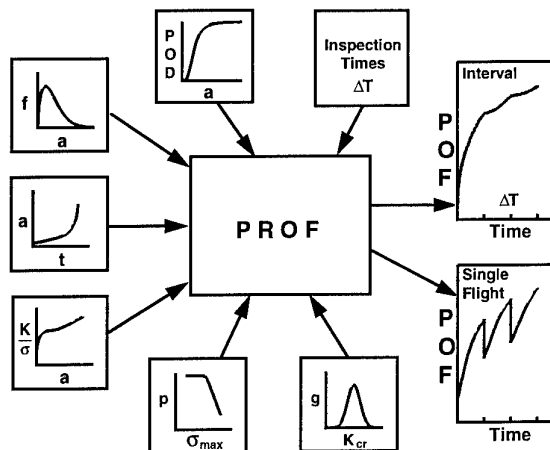


Figure 1. Probability Of Fracture (PROF) Schematic.

PROF uses the deterministic **a** versus **T** curve to project the percentiles of the crack size distribution as a function of flight hours, Figure 2. At a given number of flight hours, the singleflight probability of fracture is calculated from the distributions of crack size, maximum stress per flight and fracture toughness; i.e., single flight probability of fracture is the probability that the maximum stress intensity factor (combination of the distributions of max stress per flight and crack sizes) during the flight exceeds the critical stress intensity factor.

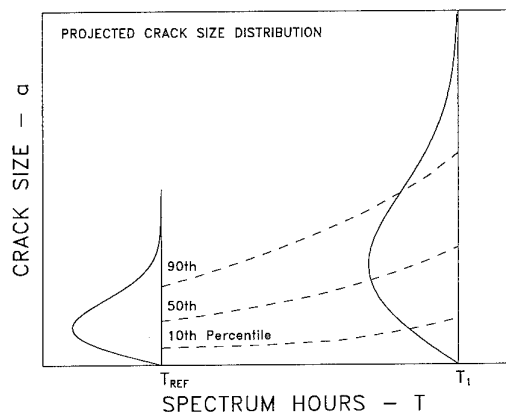


Figure 2. Crack Size Distribution as a Function of Flight Hours

At a maintenance cycle, the distribution of crack sizes changes in accordance with the $POD(a)$ function and the equivalent repair crack size distribution, Figure 3. PROF produces both the pre- and post-inspection crack size distributions. The availability of these distributions allows

changing the analysis conditions at inspection the times which are set by the analyst.

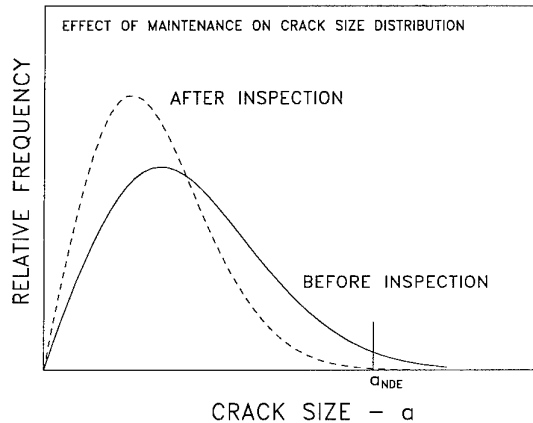


Figure 3. Change in Crack Size Distribution at an Inspection.

The a versus T , a versus K/s , and crack size distributions are input to PROF in tabular form. Fracture toughness is modelled by a normal distribution. Maximum stress per flight is modelled by the Gumbel extreme value distribution. The $POD(a)$ function is modelled by a cumulative lognormal distribution with parameters m and s . Fifty percent of the cracks of size $\exp(m)$ would be detected. The parameter, s , determines the flatness of the $POD(a)$ function with smaller values of s implying steeper $POD(a)$ functions.

Sensitivity studies have been performed on the application of PROF in representative problems [7]. These studies have indicated that, although the absolute magnitudes of the fracture probabilities are strongly dependent on the input, relative magnitudes tend to remain consistent when factors are varied one at a time. Because of the indefinite nature of some of the input data, particularly the crack size information, absolute magnitudes of the fracture probabilities are highly suspect. However, it is believed that relative differences resulting from consistent variations in the better defined input factors are meaningful. In particular, the changes introduced through the thickness reductions that will be associated with degrees of corrosion can be expected to produce meaningful relative differences.

4. DETAILS OF THE REPRESENTATIVE STRUCTURE

The structural detail selected for this sensitivity analysis was a critical location on the wing lower front spar vertical flange of an observation class, ground support aircraft, Figure 4. The detail was manufactured from 2024-T3511 aluminum. All of the data from the damage tolerance analyses of 20 locations were available for the aircraft. This particular location was selected because it was in a region of concern with respect to corrosion and it ranked fourth in severity among the twenty.

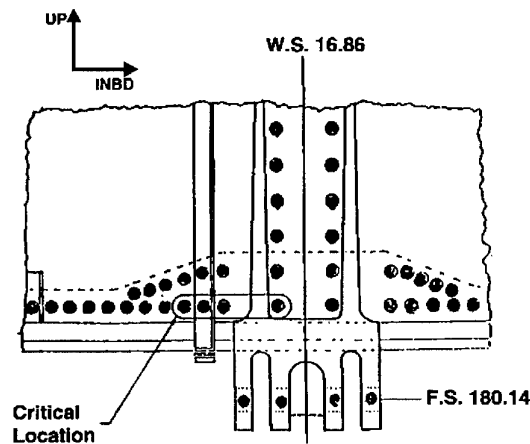


Figure 4. Critical Location at Wing Lower Front Spar Vertical Flange.

Figure 5 presents a versus T curves for the baseline condition (labeled 100%) and the crack growth life curves for the thickness of the detail reduced to 95 and 90 percent. The USAF method for determining inspection intervals for this location is also indicated in Figure 5. The first

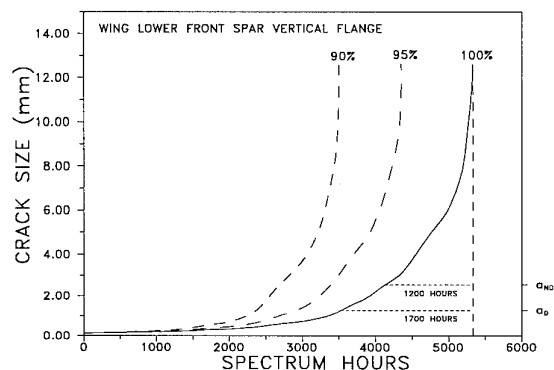


Figure 5. Crack Growth Life Curves for Critical Location at Wing Lower Front Spar Vertical Flange.

inspection of this location would be performed at 850 flight hours (half the flight time required for a 1.25 mm crack to grow to failure under the expected usage spectrum). Because the reliably detected crack size was stated as 2.54 mm for this location, the second and subsequent inspections would be performed at 600 hours (half the flight time required for a 2.54 mm crack to grow to failure. For later reference, note that the 95 percent and 90 percent crack growth life curves would require inspection intervals of 485 and 400 hours, respectively, for the second and subsequent inspections.

The flight-by-flight spectrum used to generate the crack growth life curves was obtained from exceedance curves representative of aircraft usage. The Gumbel fit of the maximum stress per flight distribution was obtained using the method outlined in [7]. This distribution was applied only to the analyses using the baseline data. When analyses were performed using decreased thicknesses, the parameters of the Gumbel distribution were scaled as follows. If \mathbf{X} has a Gumbel distribution and $\mathbf{Y} = \mathbf{cX}$,

$$P\{\mathbf{X} \leq \mathbf{x}\} = \exp\{-\exp[-\mathbf{x}-\mathbf{A}]/\mathbf{B}\}$$

and

$$\begin{aligned} P\{\mathbf{Y} \leq \mathbf{y}\} &= P\{\mathbf{cX} \leq \mathbf{y}\} = P\{\mathbf{X} \leq \mathbf{y}/\mathbf{c}\} \\ &= \exp\{-\exp[-\mathbf{y}-\mathbf{cA}]/\mathbf{cB}\} \end{aligned}$$

The distribution of maximum stress per flight from the scaled stress is also Gumbel with the original parameters multiplied by the scaling factor.

The reset crack length after an inspection for the critical location was set at $a_{\text{NDE}} = 2.54$ mm. This quality of inspection could be achieved by an eddy current system. A common characterization of a_{NDE} is that, given a population of cracks of size a_{NDE} , 90 percent of the cracks will be detected using the inspection system. Experience in the characterization of semi-automated or automated eddy current systems has indicated that a value of s of about 0.5 is reasonable. Therefore, assuming that $\text{POD}(1.27) = 0.5$ and $\text{POD}(2.54) = 0.9$ lead to $m = \ln(1.27)$ and $s = 0.54$. These are the values that were used in all of the PROF runs.

Since there were no available data from which to infer a crack size distribution to initiate the stochastic analyses, it was assumed that the structure had an initial quality equivalent to that which was determined for the A-7D aircraft [9]. This initial quality can be characterized in terms of a Weibull distribution of equivalent crack sizes with a scale parameter of 0.03 mm and a shape parameter of 0.77. Crack growth for very small crack sizes was modelled by back exponential extrapolation from fracture mechanics based crack growth which began at 0.13 mm. Note that very small cracks have no influence on the probability of fracture.

There are also no data to characterize the quality of the sites in which cracks have been detected and repaired. Therefore, based on engineering judgement, it was assumed that the quality of repaired cracks can be characterized by an exponential distribution of equivalent crack sizes with the parameter, \mathbf{b} , determined such that the probability of an equivalent repair crack exceeding 1.27 mm was 0.001 ($\mathbf{b} = 0.18\text{mm}$).

Using the baseline conditions, as defined above, the PROF calculated single flight probabilities of fracture are shown in Figure 6. PROF does not output probability of fracture (POF) values less

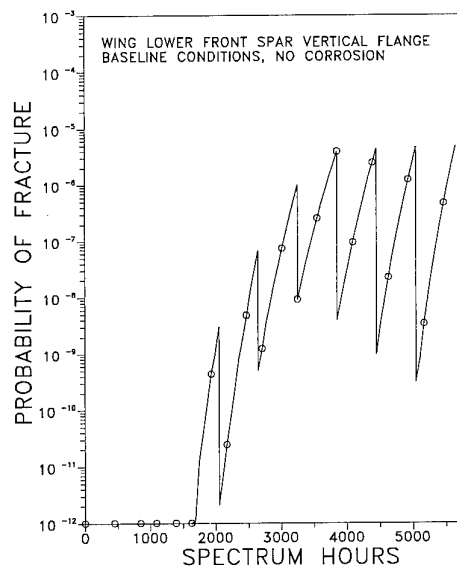


Figure 6. Fracture Risks for Baseline Conditions.

than $1e(-12)$. The sharp drops in POF at 600 hour increments are due to the reduction in the crack size distributions at the maintenance cycles. After about 3850 hours, the cycles of fracture risks tend to stabilize. The absolute magnitudes of these baseline fractures probabilities should not be precisely interpreted.

5. CORROSION SCENARIOS

For the purposes of this first order analysis of the effects of corrosion on the probability of fracture, corrosion scenarios were defined by the introduction of thickness reductions at two fixed numbers of flight hours. Since this aircraft was being operated an average of 27 hours per month in a corrosive environment, an effective five percent thickness reduction at the 2050 hour inspection (76 months) would not be unreasonable. A second five percent reduction (for a total of 10 percent) would not be unreasonable after another 1800 hours (67 months). Six scenarios were defined from these two corrosion events for comparison with the baseline single flight fracture probabilities of Figure 6. (Note: 5% corrosion should be interpreted as corrosion damage that produces an effective thickness reduction of 5%.) The six scenarios are as follows:

Case 1) 5% corrosion at 2050 hours - undetected.

Case 2) 5% corrosion at 2050 hours - detected.

Case 3) Case 1 plus 5% more corrosion at 3850 hours undetected.

Case 4) Case 1 plus 5% more corrosion at 3850 hours detected.

Case 5) Case 2 plus 5% more corrosion at 3850 hours undetected.

Case 6) Case 2 plus 5% more corrosion at 3850 hours detected.

When the corrosion is detected, it is repaired by returning the detail to the as manufactured quality but reduced in thickness to the corrosion level. Thus, the structure with repaired corrosion damage is essentially a new structure but with increased operating stresses.

Although not included in this paper, an upper bound can be calculated for the continuously increasing corrosion damage by also running the analysis for the reduced thickness conditions for previous usage intervals. For example, using the five percent reduced thickness stress spectrum for the initial conditions would be an upper bound for the corrosion damage that could be evolving between 0 and 2050 hours. Such bounds can almost be inferred from the fracture probabilities presented for the above six cases.

6. RESULTS

6.1 Case 1

Figure 7 compares the fracture probabilities for the scenario in which five percent corrosion is introduced and not detected at 2050 hours. As the large equivalent initial cracks mature into real cracks, the ratio of the fracture probabilities range between one and two orders of magnitude and the gap between the two is increasing. The reduced thickness structure has not reached the equilibrium that is typical of PROF risk analyses. This case may not be realistic as corrosion damage was assumed to be present but not increase over the period of 13 years represented in the 3600 flight hours.

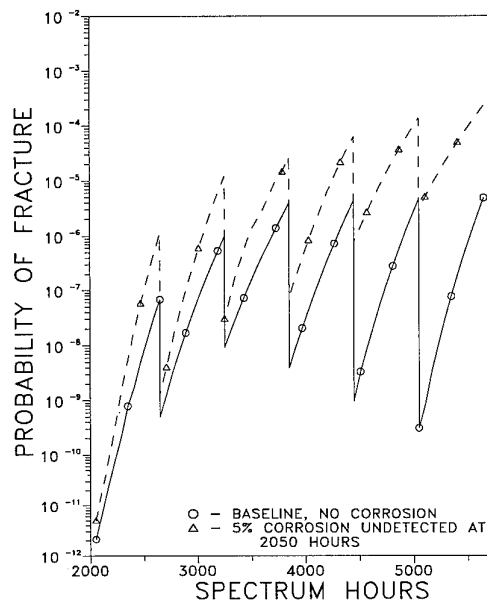


Figure 7. Fracture Risks for Baseline Conditions and 5% Corrosion Undetected at 2050 Hours.

Because the crack growth life curve for the five percent reduced thickness structure led to inspection intervals of 485 hours (Figure 5), the risk analysis was performed with this reduced inspection interval. These results are shown in Figure 8. With the reduced inspection intervals,

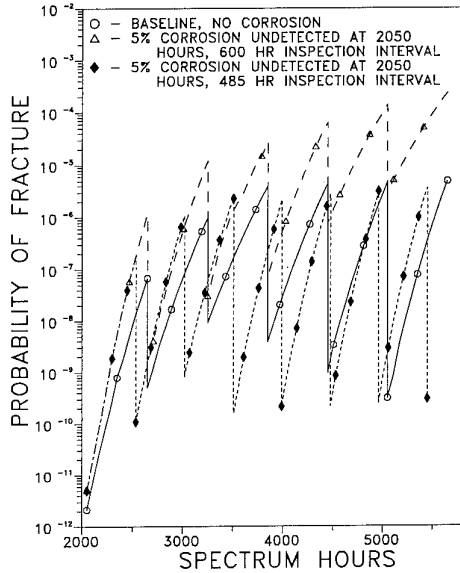


Figure 8. Fracture Risks for Baseline Conditions and 5% Corrosion Undetected at 2050 Hours - 2 Inspection Intervals.

the fracture probabilities are essentially equivalent to those of the baseline (uncorroded) structure. That is, the analysis indicates that shortening the intervals between inspections would provide equivalent safety. However, since corrosion was not detected at this location, some other criterion would be needed to trigger the reduced inspection intervals.

6.2 Case 2

In Case 2, it is assumed that the corrosion is detected and repaired returning the structure to an essentially pristine, albeit thinner, condition. Initially, the fracture probabilities are orders of magnitude smaller for the repaired structure, but, because of the higher stress levels in the repaired structure, the failure risks eventually exceed those of the baseline, uncorroded structure, Figure 9.

6.3 Case 3

When the second round of corrosion thinning is introduced at 3850 hours (1800 hours after the first) and is not detected, the probability of fracture increases by at least another factor of five

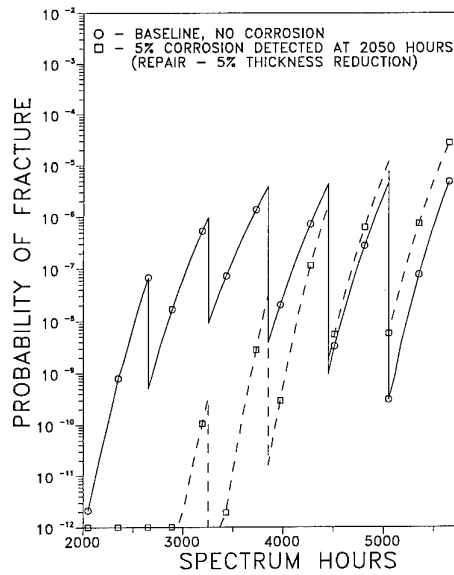


Figure 9. Fracture Risks for Baseline Conditions and 5% Corrosion Detected at 2050 Hours.

in the next 1800 hours, Figure 10. Under this severe scenario, the risk to the corroded structure at the end of the analysis is about 500 times greater than that of the uncorroded, baseline structure. Using the 400 hour inspection

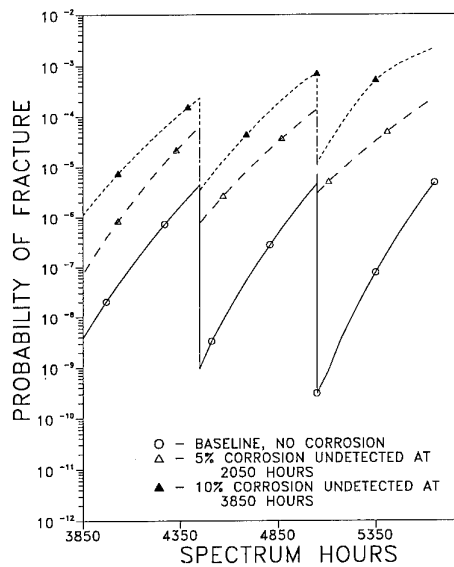


Figure 10. Fracture Risks for Baseline Conditions, 5% Corrosion Undetected at 2050 Hours, and 5% More Corrosion Undetected at 3850 Hours.

intervals, as calculated from the crack growth life curve for the 90 percent structure, again greatly reduces the risks of fracture but not to the same extent as was apparent in the analysis of the five percent corrosion, Figure 11.

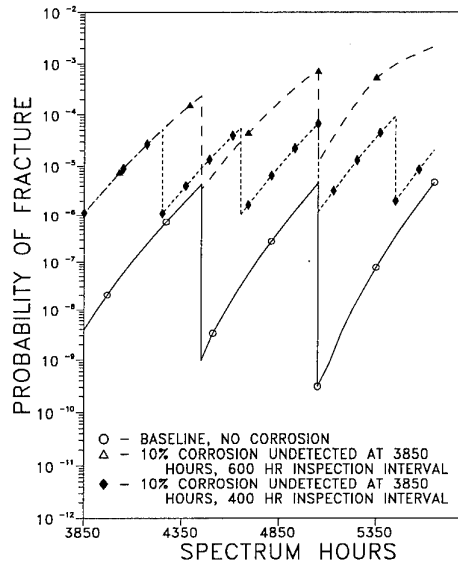


Figure 11. Fracture Risks for Baseline Conditions, 5% Corrosion Undetected at 2050 Hours, and 5% More Corrosion Undetected at 3850 Hours - 2 Inspection Intervals.

6.4 Case 4

If the ten percent corrosion damage is detected for the first time at 3850 hours, the structure was again assumed to be returned to its pristine state. Now, however, the stress levels are ten percent greater, the equivalent initial cracks grow faster, and the corresponding fracture probabilities become equivalent to those of the baseline structure, Figure 12. Had the analysis continued beyond 5650 hours, the risks associated with the ten percent thinned structure would have exceeded those of the baseline. It might be noted that a ten percent thickness reduction is typically permitted in the repair of corrosion and at this level the differences in fracture probabilities might become unacceptable in aging aircraft fleets.

6.5 Case 5

Figure 13 presents the fracture probabilities for the scenario in which the five percent corrosion at 2050 hours is detected and repaired but the five

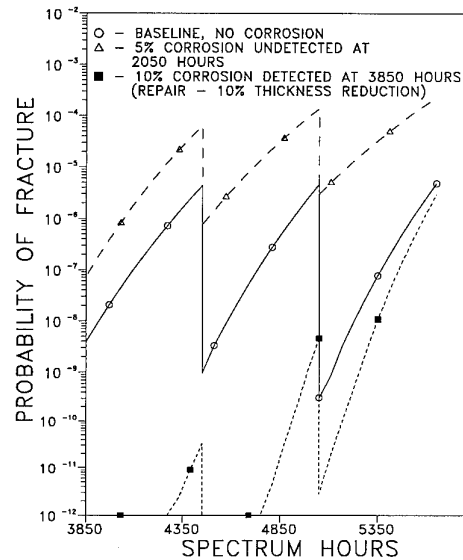


Figure 12. Fracture Risks for Baseline Conditions, 5% Corrosion Undetected at 2050 Hours, and 10% Corrosion Detected at 3850 Hours.

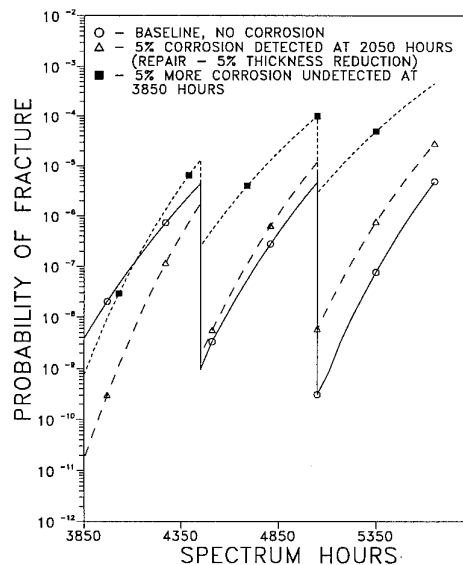


Figure 13. Fracture Risks for Baseline Conditions, 5% Corrosion Detected at 2050 Hours, and 5% More Corrosion Undetected at 3850 Hours.

percent additional corrosion reduction at 3850 hours is not detected. These results are entirely consistent with those that have been observed earlier. The structure was renewed at 2050 hours and the fracture probability at 3850 hours is still less than that of the baseline. However, due to the increased stress levels, the risks associated with the thinned material rapidly surpass those of the baseline structure.

6.6 Case 6

The final case considered is that for which both episodes of corrosion thickness reductions were detected and repaired, Figure 14. The risks for this scenario are the smallest over the range of the analysis but would be expected to exceed those of the baseline over an extended analysis period.

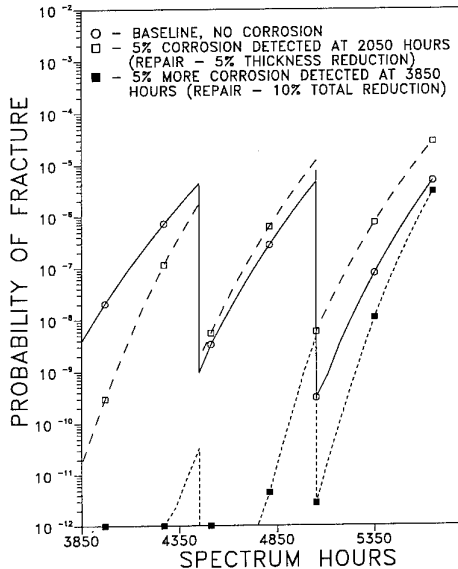


Figure 14. Fracture Risks for Baseline Conditions, 5% Corrosion Undetected at 2050 Hours, and 5% Corrosion Detected at 3850 Hours.

7. SUMMARY

The interaction between the thinning effects of corrosion and fatigue cracking on the structural integrity of representative airframe structure were evaluated in terms of single flight probabilities of fracture as a function of flight hours. The first order methodology assumed that the effect of corrosion damage on fatigue crack growth could be modelled by reduced structural thickness. Six simple corrosion damage scenarios were defined by introducing five percent increments of corrosion thickness loss at two times in the aircraft's history. Time histories of the probability of fracture were calculated using the PROF risk analysis computer code. The fracture risks from the corrosion scenarios were compared to those from a baseline condition which was the driver for the planning of the safety inspections for the critical location.

In all but two of the corrosion scenarios, the fracture risks associated with the reduced structural thickness exceeded those of the

baseline condition by at least an order of magnitude. In the remaining two scenarios, the structure had been "renewed" at the second corrosion insertion and was operating at stress levels that were ten percent greater than the baseline. Although the fracture probabilities were less than those of the baseline at the end of the analysis, it was apparent that these scenarios would soon produce high risks in comparison with the baseline condition.

The results of this preliminary study indicate that, when the inspection intervals are set by damage tolerance analysis of cracks in pristine structure, the effects of corrosion may be a safety issue as well as a durability issue. It was also noted that shortening inspection intervals could significantly lower the fracture risks.

8. LIST OF REFERENCES

1. "Corrosion Summary," Department of the Air Force, WR-ALCRP 400-1, WR-ALC/CNC, Robins Air Force Base GA, 31098-5990, USA, March 1991.
2. Tiffany, C.F., "Some Thoughts on Corrosion Research and Current USAF/Boeing Activities," presented at Corrosion Workshop, WL/FIBE, Wright-Patterson Air Force Base, OH 45433, USA, July 1994.
3. Bucci, R.J., H.J. Konish, M.Kulak, and D.W.Hoepfner, "An Engineering Protocol for Evaluating Implications of Metallic Corrosion of Airframe Damage, Life and Risk Assessment," FAA/NASA International Symposium on Advanced Structural Integrity Methods for Airframe Durability and Damage Tolerance," Hampton, VA, USA, May 1994.
4. Koch, G.H. and E. Hagerdorn, "The Effect of Corrosion on Fatigue Cracking of Aluminum Alloys," presented at Corrosion Workshop, WL/FIBE, Wright-Patterson Air Force Base, OH 45433, USA, July 1994.

5. Scheuring, J. and A.F. Grandt, Jr., "An Evaluation of Fatigue Properties of Aging Aircraft Materials," presented at 1994 USAF Structural Integrity Program Conference, San Antonio, TX, USA, December 1994.
6. Doerfler, M.t., A.F. Grandt, Jr., R.J. Bucci, and M. Kulak, "A Fracture Mechanics Based Approach for Quantifying Corrosion Damage," presented at Tri-Service Conference on Corrosion, Orlando, FL, USA, June 1994.
7. Berens, A.P., P.W. Hovey and D.A. Skinn, "Risk Analysis for Aging Aircraft Fleets, Volume 1 - Analysis," WL-TR-91-3066, Wright Laboratory, Air Force Systems Command, Wright-Patterson Air Force Base, OH 45433-6553, USA, October 1991.
8. Burns, J.G., W.P. Johnson, and A.P. Berens, "Aging Aircraft Structural Damage Analysis," Fatigue Management, AGARD Conference Proceedings 506, May 1991.
9. Rudd, J.L. and T.D. Gray, "Quantification of Fastener-Hole Quality," Journal of Aircraft, Vol. 15, No. 3, March 1978.

RISK ASSESSMENT OF AN AGING MILITARY TRAINER AIRCRAFT

John W. Lincoln
 ASC/ENF BLDG 125
 2335 Seventh Street STE6
 Wright-Patterson Air Force Base, Ohio 45433-7809
 USA

1. SUMMARY

The paper examines the adequacy of the U.S. Air Force damage tolerance inspection criterion for protecting the safety of the flight of an aging military trainer aircraft. This is done through a risk assessment on the basis of cracks found in teardown inspections of retired wings. The crack population is combined with stress probabilities representing service experience to determine single flight probability of failure and the single aircraft probability of failure after a given time. These quantities are then used as a basis for judging the required inspection interval. For the case studied, the 0.9 probability of detection inspection criterion in the Air Force damage tolerance requirements may be unconservative.

2. INTRODUCTION

Several methods have been used by aircraft structural engineers to preclude the catastrophic consequences of fatigue cracking. One method that has been widely used and is still being used in the United States and in Europe is the reliability method. In this method, the structure is tested with simulated operational loads for multiple lifetimes to obtain the desired confidence that the service aircraft would not fail. In the late sixties and early seventies, the mathematical basis for the reliability method was established. Another approach that has been used with considerable success is the damage tolerance method. In this method the analyst assumes that the structure has a remotely occurring (rogue) defect at the time of manufacture and then selects the material and determines the stress to achieve the desired inspection program. In the early seventies the U.S. Air Force (USAF) elected to stop using the reliability method as a primary means and ensuring safety and started using the damage tolerance method. The authors of the USAF damage tolerance requirements chose to make the method deterministic rather than probabilistic. That is, the initial flaw (or crack) is a specific number, and the critical crack length is based on a specific load. Also, the inspection capability is based on one point of the probability of detection function. That is, all cracks longer than the one corresponding to this one point of the probability of detection function are assumed to be found when the aircraft is inspected. Experience with the method through numerous damage tolerance assessments has demonstrated the wisdom of the choice of the deterministic approach. There was, however, a question in the minds of the authors about the portion of

the damage tolerance requirements that defined the recurring inspection interval. The point selected from the inspection probability of detection (POD) functions was the point associated with a ninety percent probability of detection. The selection of ninety percent probability of detection as an acceptable reliability for inspections was somewhat arbitrary. Part of the motivation for this selection was that this probability could be relatively easily established through a laboratory program. However, the question is: "Is ninety percent probability of detection adequate to protect safety?"

It is the purpose of this paper to examine this question for a particular weapon system. The method used to address this question is yet another method that may be used to protect the safety of aircraft. It is referred to as the risk assessment method. The method is probabilistic in that it uses both the crack size and stress probability distributions and the complete inspection POD function to determine the single flight and the single aircraft probability of failure at a given time. On the basis of these quantities, one can permit flight based on what is conceived as an acceptable risk.

The opportunity to address this question arose when a service flight loads survey on an Air Force trainer showed that in the late seventies there was a mission change. This change made the load environment considerably more severe than that used in a damage tolerance assessment of this trainer in the mid-seventies time period. The consequence of this increased usage severity was determined by an update of the damage tolerance assessment. This new assessment, which as in the previous assessment used the ninety percent POD for inspections, showed that the inspection frequency should be increased by approximately a factor of three. This would, of course, significantly increase the inspection costs and associated aircraft downtime. To determine if this increased inspection burden was essential to maintain the safety of these aircraft, a risk assessment was performed.

3. RISK ASSESSMENT METHODOLOGY

The details of the risk assessment method and a computer program listing are given in Reference 2. The essential features of the method as applied to the trainer aircraft of interest are described as follows. There are several input data items that are required. One of these is a description of populations of cracks that are

representative of the critical locations in the structure. This is usually the most difficult to obtain of all of the input data and, consequently, is the chief inhibitor to more widespread use of risk assessments. Fortunately, for this trainer, there was a data base from which an estimate of crack population could be made. Over the past several years, destructive teardown inspections have been made on retired trainer wings to provide insight into the possibility of a cracking problem. In all, 19 wings have been torn down and detailed inspections made to quantify the extent of cracking. These examinations revealed that in the critical locations (approximately 100 fasteners or drain holes per wing), roughly 25% of the holes had cracks. The upper bound of these cracks was approximately 2.5 millimeters. The crack findings detailed in Table 1 for the wing layout shown in Figure 1. These data were judged to be an adequate raw data base to define the crack population.

Obviously, not all of the wings were torn down at the same number of equivalent hours of trainer usage. Therefore, first step in the process was to get the crack lengths referenced to the same number of flight hours. To minimize the changes in the observed individual aircraft crack lengths, the average of the 19 aircraft equivalent number of trainer hours was used. This average was calculated to be 10,200 hours. The crack lengths at 10,200 hours for a given aircraft of the 19 were then derived by a fracture analysis that provided the basis for calculating the length the crack would be or would have been at 10,200 hours. These calculated crack lengths, a , were then used to generate a sample cumulative probability distribution P , such as shown in Reference 3. The next step in the process was to derive an analytical expression for the cumulative probability. This is needed to facilitate needed computations and to extrapolate the cumulative probability distribution to approximately 10^{-6} . The log normal and the Weibull probability distributions were used to try to fit the sample cumulative probability. The Weibull distribution proved to be significantly superior to the log normal distribution, but as can be seen from Figure 2, there is a different Weibull slope (shape parameter) for small cracks than for large cracks. The large cracks are the only ones that significantly contribute to the risk, so consequently the small crack portion may be ignored. This two mode characteristic is not without precedent. Data taken from a teardown inspection of the C-5A wing also displayed this same feature. Figure 3 shows the derived Weibull distributions for the three critical locations on the lower wing skin.

Another data item required for this analysis is the probability of exceeding a given stress at a critical location in a single flight. The data base from which this is derived is the stress exceedance function, which is the number of times a given stress is exceeded. The exceedance function is often used as an input for a durability or damage tolerance analysis and therefore is

usually available. The cumulative probability for stress is derived from the exceedance function as follows. First, the exceedance function ordinate is transformed to exceedances per flight by multiplying the number of exceedances per hour by the number of hours per flight. Second, the exceedances per flight greater than one are made equal to one. Finally, if it is assumed that there is no more than one counted exceedance per flight, then the resulting function defines the fraction of the flights for which a given stress is exceeded. This function is, therefore, the cumulative probability of exceeding a given stress in a single flight. The cumulative probability for stress was numerically extrapolated to approximately 10^{-6} . This extrapolation was based on the shape of the tail of exceedance function for this type of aircraft. Variations in these extrapolations, that were judged to be reasonable, were studied, and it was determined that the actions derived from this risk assessment would not be significantly changed. However, it must be pointed out that for any given aircraft there could be a "rogue" defect, or it may be subjected to a "rogue" stress that would not be derivable from the probability functions. The risk of these events is not quantifiable, but on the basis of previous service experience, it appears to be small. The exceedance functions are shown in Figure 4, and the resulting cumulative probabilities for stress are shown in Figure 5.

The remaining input data items are the critical crack size versus stress shown in Figure 6, the crack length versus flight hours as shown in Figure 7, and the inspection probability of detection function shown in Figure 8. The shape of the probability of detection function for the ultrasonic inspection of the trainer aircraft was taken from Reference 1. The probability of detection from Reference 1 was shifted so that the 0.90 probability of detection flaw size (2.54 mm) used in the trainer damage tolerance analysis was a point of the risk assessment probability of detection function. This provided a consistent basis from which the results of the damage tolerance assessment could be compared with the risk assessment. It is noted that the probability of detection function is used quite differently in the risk assessment than in the damage tolerance assessment. For the risk assessment, the entire function is usually used since the probability of detecting the cracks in the crack length exceedance function is needed. In the damage tolerance assessment, as indicated earlier, only one point of the probability of detection function is used.

Since the crack size at a location in the structure at a given time does not depend on the stress that may occur at this location after this time, the joint probability density function for crack size and stress is the product of the crack length and stress probability density functions. The crack size probability density function is immediately available since the Weibull parameters were derived for the crack length cumulative probability. The stress probability density function is somewhat more

difficult to obtain since the cumulative probability for stress was available only in numerical form. A differentiation was, therefore, required to derive the desired result. The joint probability density function (P_j) for wing station 0.0 for crack length a and stress s is shown in Figure 9. For stresses less than those encountered once per flight, this function is zero. This is a consequence of the cumulative probability function for stress having zero slope up to the once per flight stress. For stresses that have greater than once per flight occurrence, the joint probability density function is greater than zero. It should be noted that since the crack length density function decays rapidly toward zero as the crack length increases. The joint density function also decays rapidly in the crack length direction. The joint density function, of course, properly represents the relative importance of the stress and crack size. This joint probability distribution is time dependent since the crack length is time dependent. The surface formed by a vertical projection of the critical crack length versus stress line divides the volume under the joint probability density function into two volumes (see Figure 10). The volume under the shaded surface is the single flight probability of failure, P_f , as shown in Reference 2, is calculated from

$$P_f = \iint_R P_j dA$$

where R is the region "outside" the critical crack size versus stress line in the stress-crack length plane. This is the single flight probability of failure for one point in this location in the structure. At this location there is more than one fastener hole subjected to the same stress field. However, there will generally be a different crack size in each of these holes. Therefore, the probability of failure at a given hole does not depend on the probability of failure of another hole at this location. Thus, the single flight probability of failure of all N points (e.g., fastener holes) at this location is one minus the single flight probability of no failure for one point to the N th power. The single flight probability of failure may be easily used to compute the probability of failure after a given number of flights for a single aircraft or a group of aircraft. One may also compute an estimate of the expected number of losses for a group of aircraft.

3.1 Risk Interpretation

At this time, the USAF is primarily oriented towards the use of the deterministic damage approach for ensuring safety of their aircraft. The risk assessment methodology, however, can be useful for analyzing aircraft components nearing the end of their useful lives. It provides the manager with decision making information not available by other means. The single flight probability of failure provides the manager with an instantaneous view of the risk at some point in time of the aircraft's life. This quantity may, however, be

difficult to interpret. One basis for interpretation of this quantity is to relate it to the risk we accept in our every day living. For example, the risk of a major accident that we accept in driving an automobile to work and back home is of the order of 10^{-6} . Another basis that a manager could use for interpretation is the precedents that have been set for aircraft. For most military systems, a single flight probability of failure of 10^{-7} or less is considered adequate to ensure safety for long-term operations. For single flight probability of failure greater than 10^{-7} , consideration should be given to limiting the exposure by modification or replacement. If this quantity is 10^{-5} or greater for an extended period of time, the failure rate should be considered unacceptable. The probability of failure after a given number of flight hours or the expected number of aircraft losses are quantities that are generally more meaningful to the decision maker. These quantities are also useful for judging the influence of changes in an inspection program. The nature of the analysis itself relieves the manager from at least part of the interpretation problem. The reason for this is found in the crack growth function. As the cracks become longer (which increases the risk), the crack growth rate grows larger, accelerating the risk. The consequence of this is, in the absence of inspections, the single flight probability of failure will change from acceptable to definitely unacceptable in a relatively few flight hours. This feature is depicted in some of the results discussed below.

3.2 Discussion of Results

In the mid-seventies, a damage tolerance assessment was performed for the trainer discussed above in Air Training Command usage. This study concluded that the wing center section should be inspected at intervals of 1350 flight hours. This was based on an inspection capability of 2.54 mm (corner crack) and an inspection at one half of the safety limit (the time required to grow a 2.54 mm crack to a 5.5 mm critical size crack). In the late seventies, a usage change took place that made the loading environment more severe. A damage tolerance reassessment was made for this new usage, and it was found that, under the same ground rules, the recurring inspection interval should be changed to 430 hours. It is noted that 430 hours are one half of the calculated 860 hours safety limit. The safety limit is the point in time at which the aircraft would have to be inspected or restricted until the inspection was accomplished.

To provide a preliminary evaluation of the necessity of performing inspections at an increased rate, a risk assessment for the new usage, but old inspection schedule, was performed. The results of this calculation are shown in Figure 11. It was assumed (arbitrarily) that an inspection had been performed at 9,600 flight hours. The next inspection would have been scheduled for 10,950 hours. It is seen from Figure 11 that the single flight probability of failure has risen significantly long

before the next inspection would be due. On the basis of the accumulation of these single flight failure probabilities, the probability of failure for a single aircraft was found to have increased to 0.4 before the next inspection was due. This was obviously too high for safe operations.

Next, the risk was calculated for a recurring inspection interval of 400 hours (slightly less than the damage tolerance assessment derived 430 hours). The associated single flight probability of failure for this case is shown in Figure 12. The 400 hour interval shows a significant improvement over the 1350 hour interval. The single flight probability of failure may be used to compute the probability of failure of a single aircraft after a given number of flights. This calculation is accomplished by subtracting from one the product of the probability of no failure of the given number of single flights. However, when these single flight probabilities are converted to the probability of failure for a single aircraft (see Figure 3), it was found that long-term operation would result in a greater than desired chance for loss of an aircraft.

When the inspection interval was reduced to 300 hours from 400 hours, the probability of failure for a single aircraft was reduced by approximately a factor of five. This is shown in Figure 13. The resultant chance of loss of an aircraft was small enough to be accepted. Further reduction of the inspection interval to 200 hours reduced the single aircraft probability of failure to approximately 5×10^{-5} . This reduced the risk, but the reduction was not judged to be required to protect the safety of these aircraft.

4. CONCLUSIONS

Before a conclusion is made on the adequacy of the inspection criteria used in the damage tolerance assessment of this trainer aircraft, it must be remembered that some of these wings were in the latter stage of their life. They have operated safely for many years with the inspection program derived from the damage tolerance assessment. The risk assessment results show that this successful operational experience should have been expected. The risk assessment also shows that inspections are extremely influential in reducing the probability of failure. This may be seen from a comparison of Figs. 11 and 12. The problem with this trainer is that a significant population of cracks has grown and is becoming close to critical length in the high time aircraft. Therefore, the probability has increased that a crack could be missed by the inspection process and become critical. It turned out for this trainer that the 0.9 probability of detection, which was used in the damage tolerance assessment for the new usage, provided an inspection interval of 430 hours. This inspection interval if used on high time aircraft may not adequately protect safety. This conclusion is derived from the risk analysis results shown in Figure 11. For this trainer, if the damage tolerance assessment had used

a detectable flaw size corresponding to 0.94 probability of detection, then a safe interval would have been provided. In other words, the probability of detection for the damage tolerance assessment required only a relatively small change. It is not known at this time if the results found in this study can be generalized. Therefore, for aircraft that have cracks derived from fatigue (i.e., aging), the structural engineer should use all methods available to him to define inspections and/or modifications that will ensure that safety of flight is protected. The materials and stresses for new aircraft should be selected such that the risk of failure throughout the aircraft's life is low without inspections. This goal is believed to be met through the guidance in AFGS-87221A for the U.S. Air Force damage tolerance requirements.

5. REFERENCES

1. Lewis, W.G., Dodd, B.D., Sproat, W.H., and Hamilton, J.M., "Reliability of Nondestructive Inspections-Final Report," SA-ALC/MME 76-6-38-1, Dec. 1978.
2. Lincoln, J.W., "Method for Computation of Structural Failure Probability for an Aircraft," ASD-TR-80-5035, July 1980.
3. Gumbel, E.J., "Statistical Theory of Extreme Values and Some Practical Applications," National Bureau of Standards Applied Mathematics Series 33, Feb. 1954.

CRITICAL LOCATION	NO. OF WINGS	HOLES PER WING	TOTAL HOLES	TOTAL CRACKS	PERCENT CRACKED
W.S. 0.0 FASTENER	19	49	931	211	22.7
W.S. 0.0 DRAIN	19	1	19	4	21.1
W.S. 26.6 FASTENER	19	6	114	57	50.0
W.S. 26.6 DRAIN	19	2	38	23	60.5
W.S. 40.0 FASTENER	19	44	836	247	29.6

Table 1 Summary of findings from wing teardown inspections

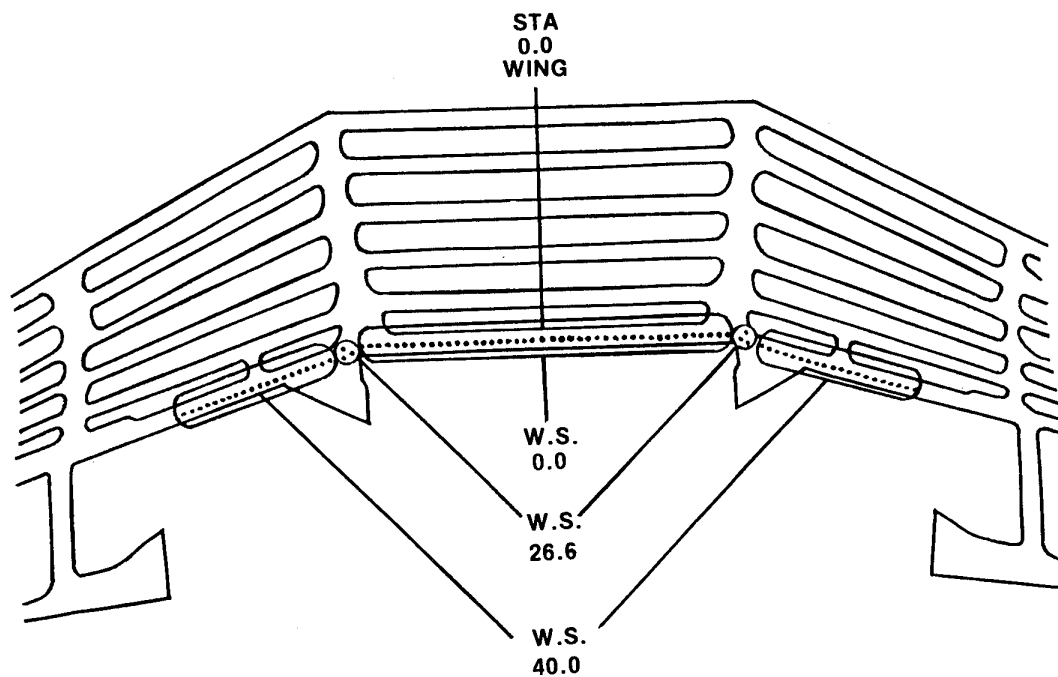


Figure 1 Critical areas in the wing skin

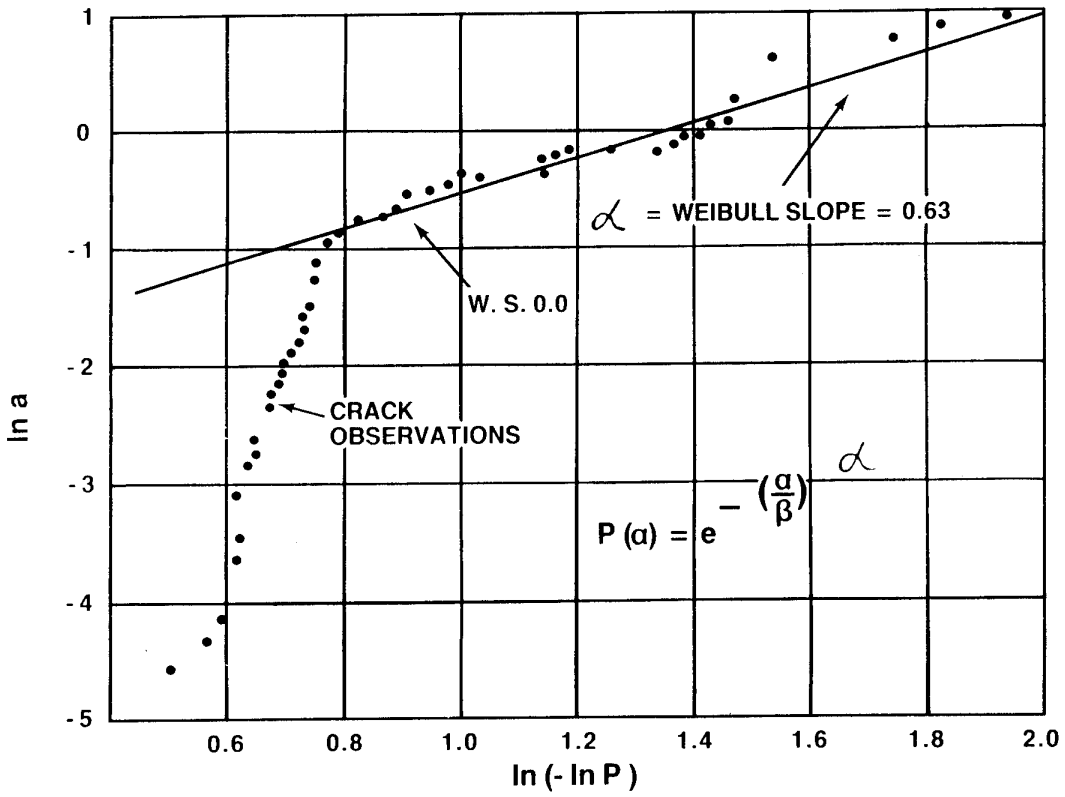


Figure 2 Weibull fit to observed cracks

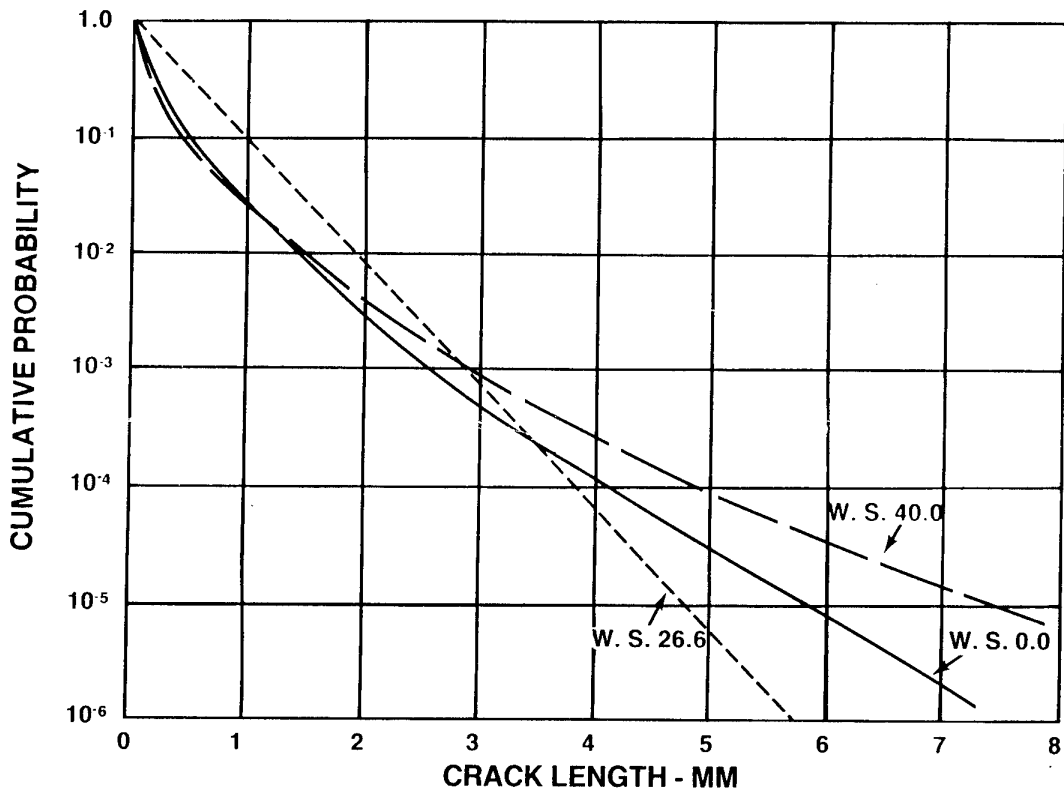


Figure 3 Derived cumulative probability of exceeding a given length

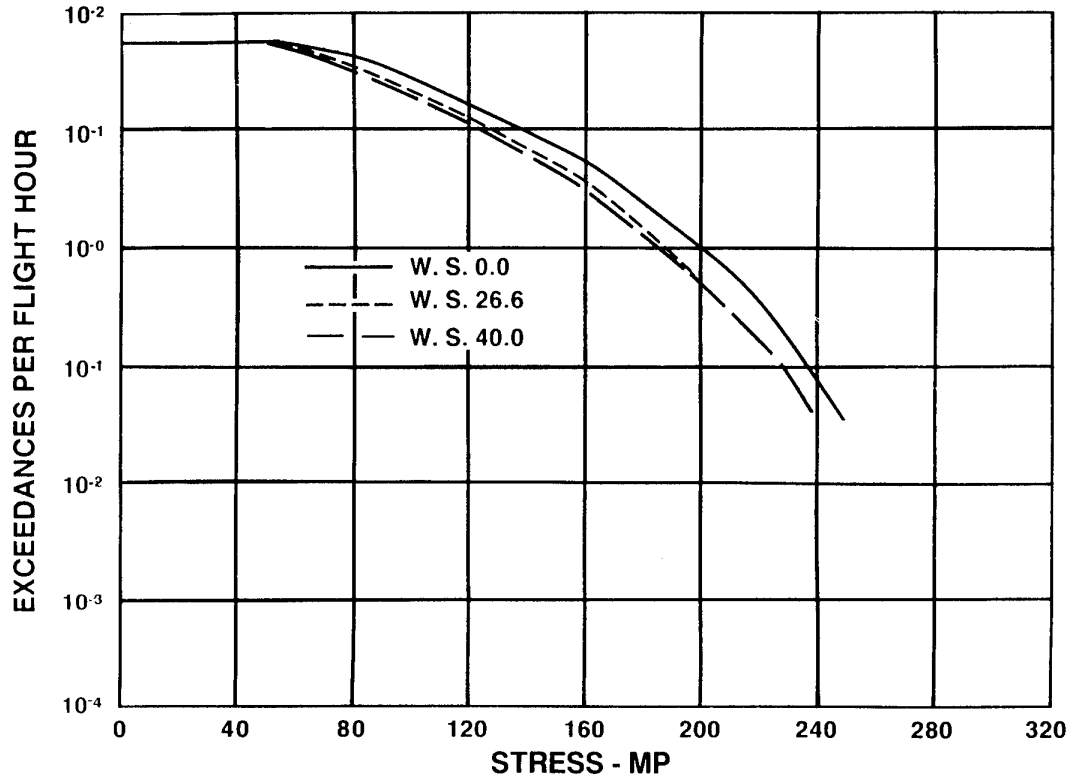


Figure 4 Wing stress exceedance function

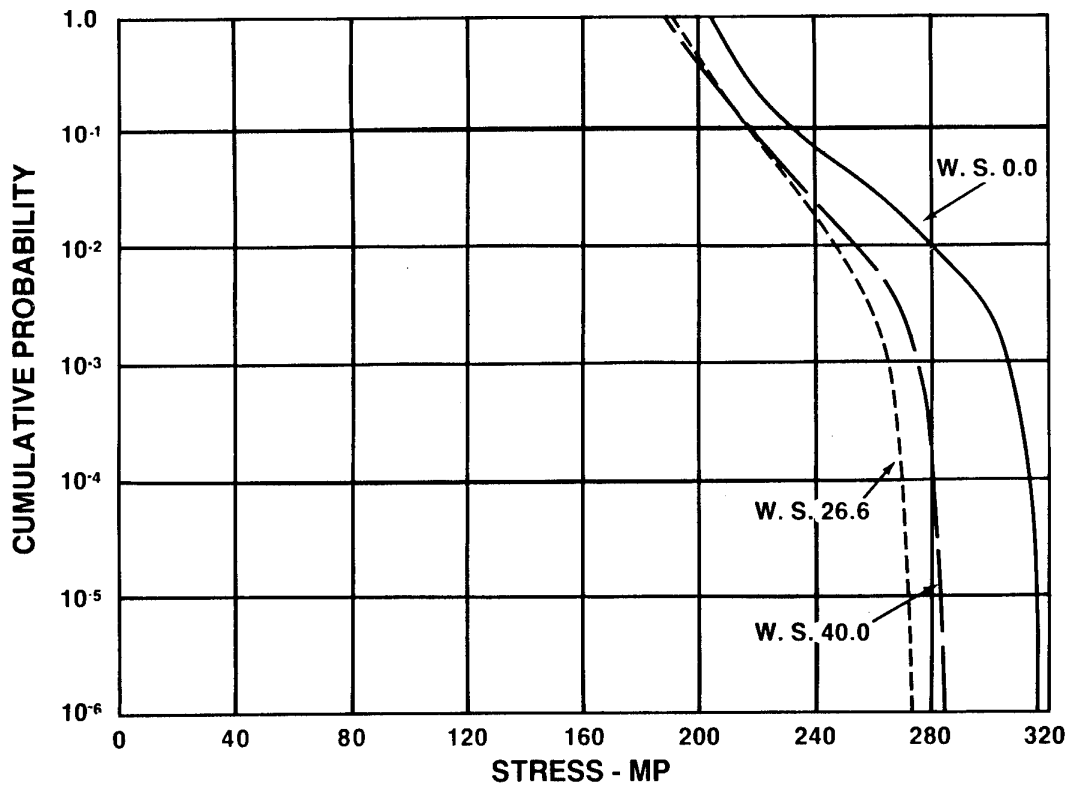


Figure 5 Wing stress probability function

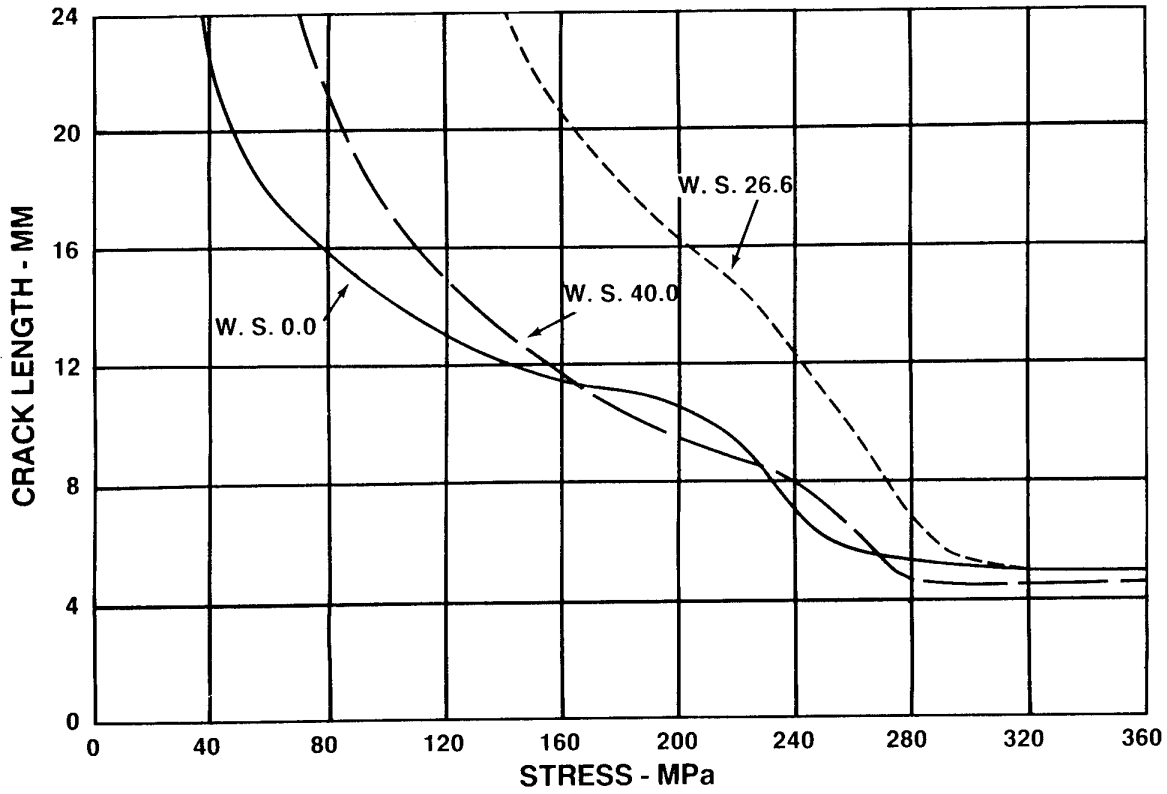


Figure 6 Critical crack length in wing structure

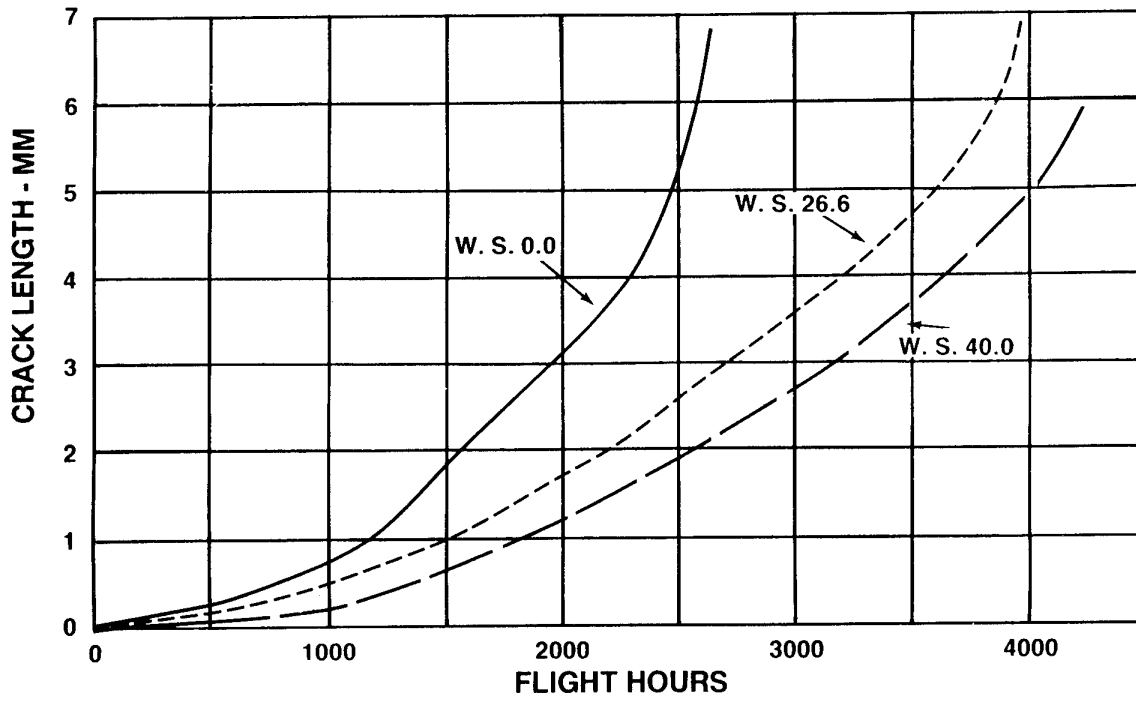


Figure 7 Crack growth at critical locations

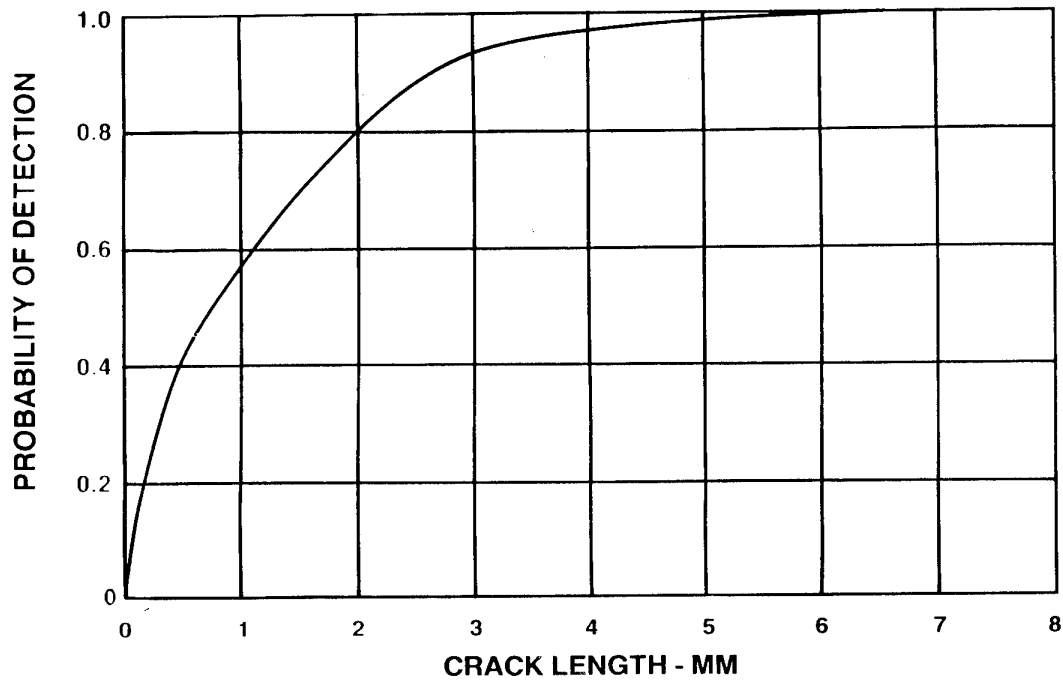


Figure 8 Wing Inspection reliability

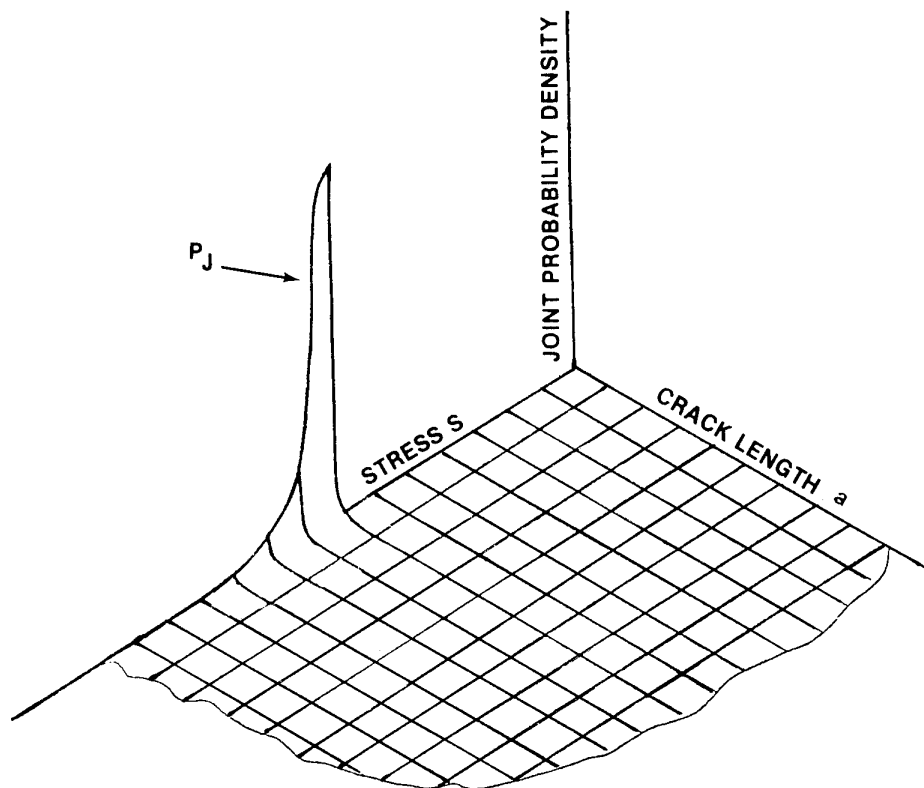


Figure 9 Joint probability of crack length and stress

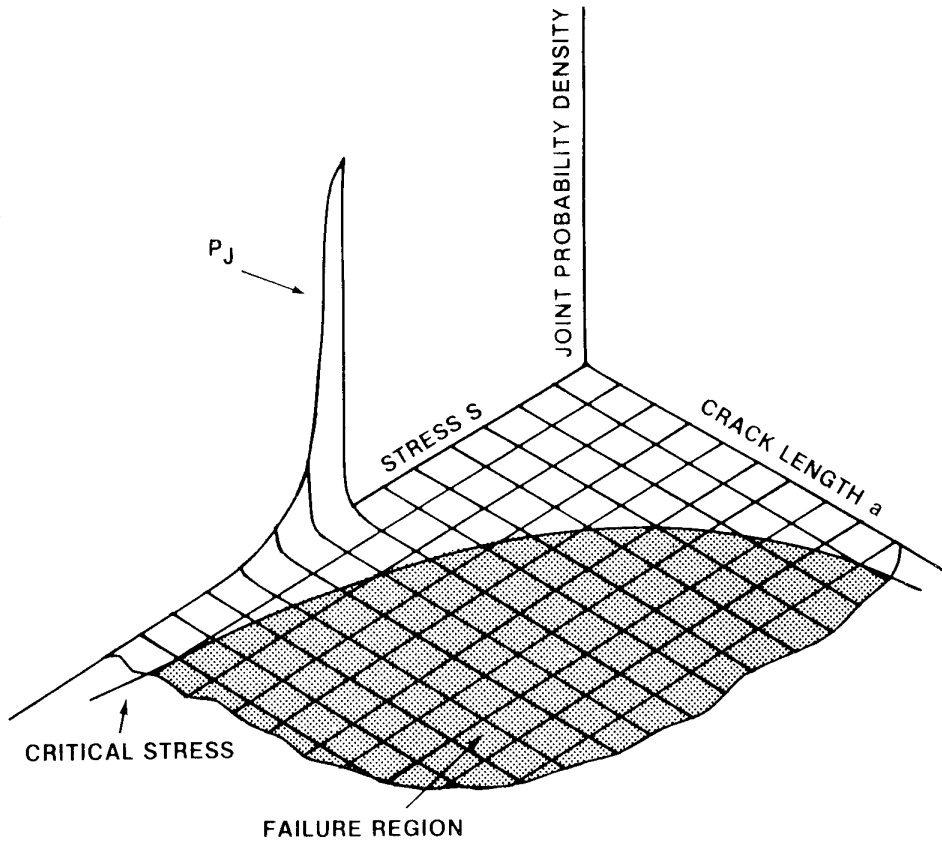


Figure 10 Basis for computing failure probability

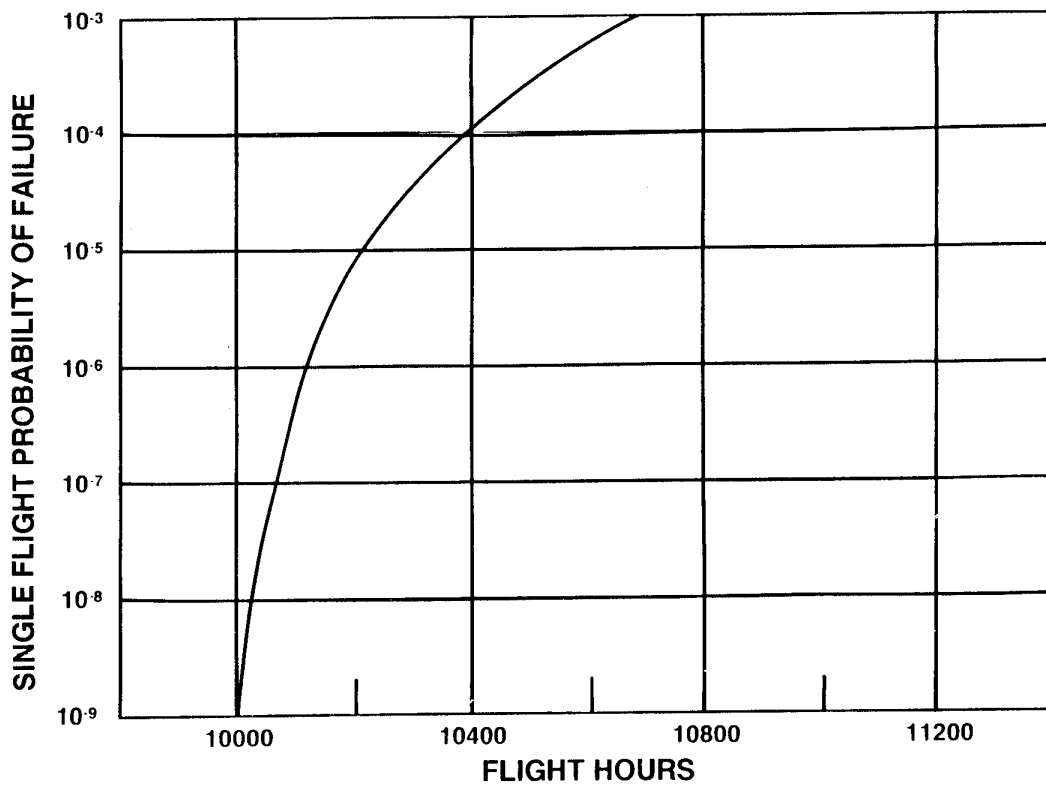


Figure 11 Single Flight probability of failure for original inspection program

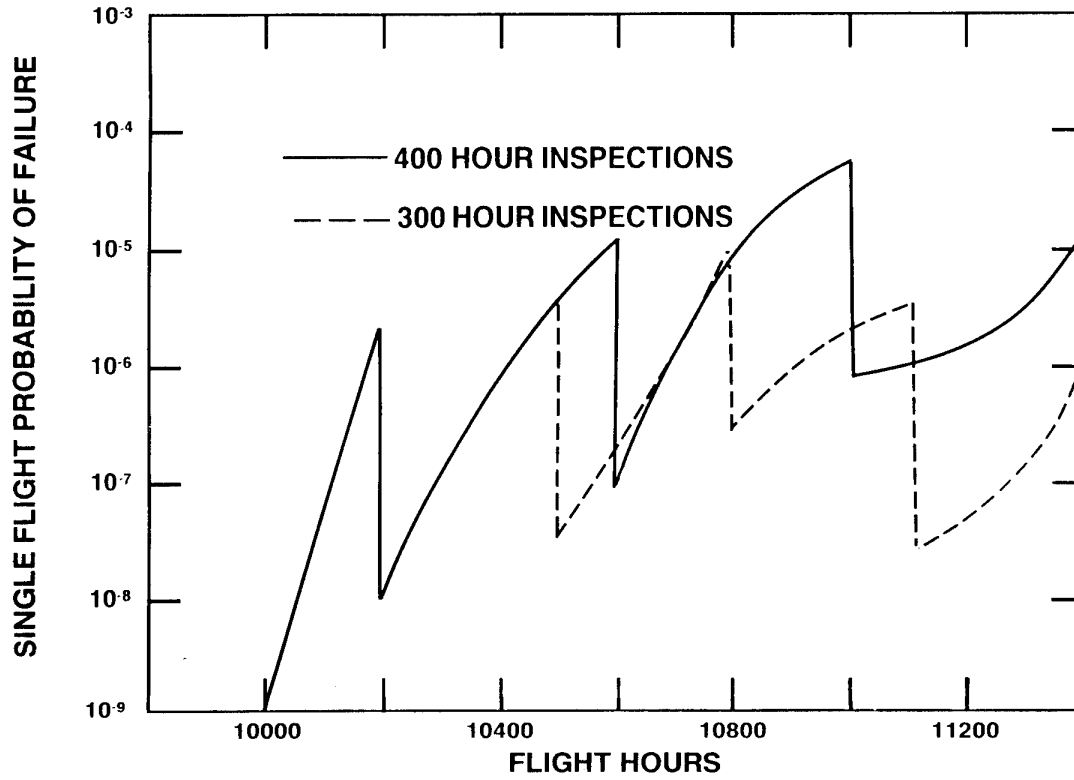


Figure 12 Impact of inspections on single flight failure probability

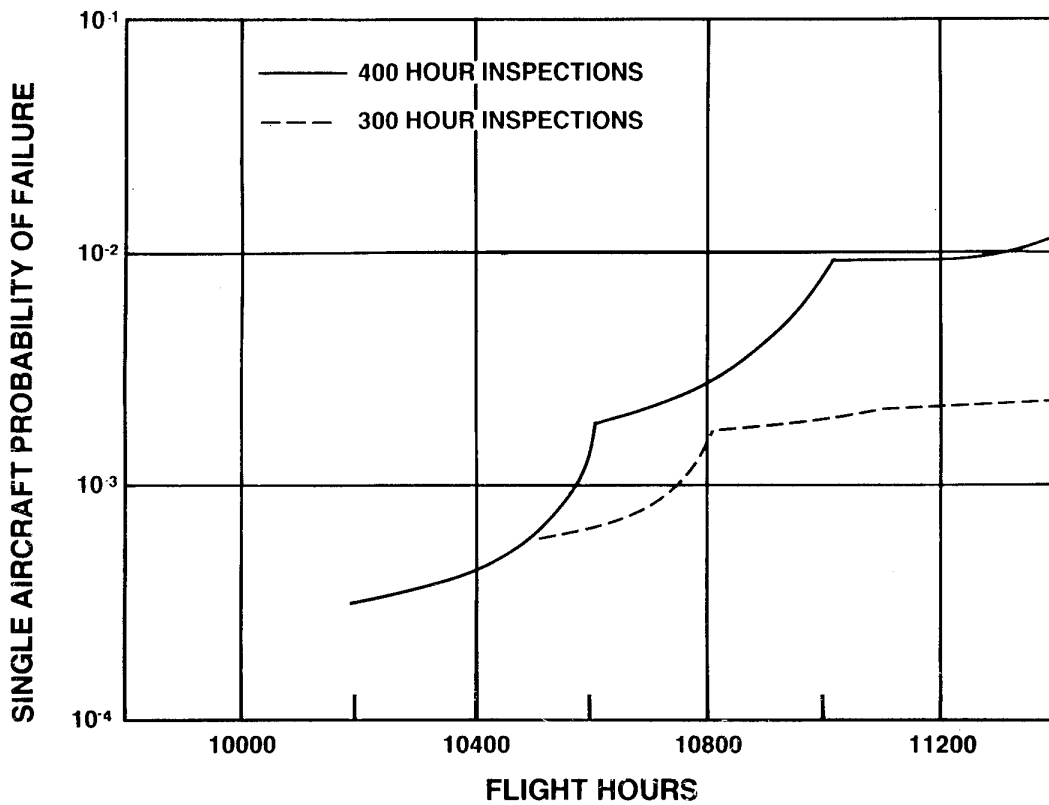


Figure 13 Impact of inspections of failure probability

DESTRUCTIVE TEARDOWN OF A C-141 LOWER INNER WING SURFACE

J.B. Cochran, R.P. Bell, G.M. Weitz, R.E. Alford
 Lockheed Aeronautical System Company
 Dept. 73-25, Zone 0160
 86 South Cobb Drive
 Marietta, Georgia 30063-0160
 USA

SUMMARY

As part of a structural assessment of the C-141 aircraft for life extension feasibility, the United States Air Force Scientific Advisory Board (SAB) directed a teardown inspection on a high time C-141 inner wing lower surface. The teardown inspection was performed at Lockheed Aeronautical System Company (LASC), Marietta Ga., in 1993. This paper will address the following:

- ◆ Why was the teardown required?
- ◆ The condition of the aircraft before the teardown
- ◆ Teardown procedure
- ◆ How the results of the teardown were used.

The teardown program was performed over six months. Eight thousand, seven hundred and sixty-two holes on the right wing were inspected by automatic bolt hole eddy current (ABHEC). One hundred and fifty-three flaws were detected initially, with the final number of two hundred and eighty-nine confirmed flaws. The results of the teardown were used by the Air Force to carry out an inspection/repair program that maintained a safe operational environment for the C-141B aircraft.

1 INTRODUCTION

The C-141 wing is constructed of 7075-T6511 extruded panels on the upper and lower surfaces, connected by truss type ribs. The inner wing surfaces consist of six to eleven wing panels, spliced together using taper-lok fasteners. The inner wing lower surface is shown on Figure 1.

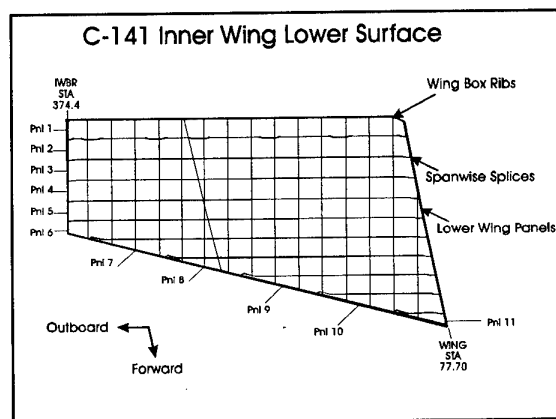


Figure 1

Each panel consists of a skin plus four or five integrally stiffened risers. These risers contain weep holes and riser rib clip attachment holes. The weep holes allow the fuel to flow between the risers. Riser rib clips are used to attach the wing box ribs to the upper and lower panels. Figure 2 shows a typical inner wing lower panel.

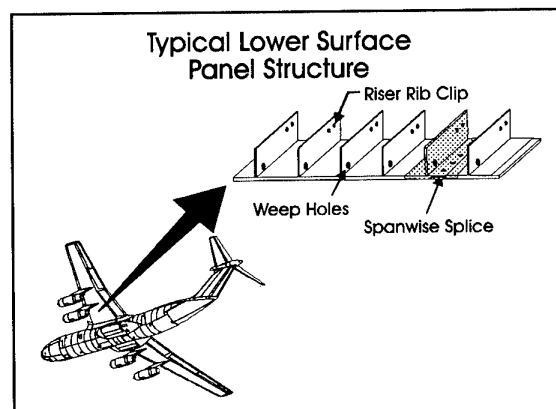


Figure 2

2 WHY THE TEARDOWN WAS REQUIRED

LASC performed durability and damage tolerance analysis (DADTA) in the late 1970's that predicted the surface of the wing would last 45,000 damage hours, as long as recommended modifications were performed. This prediction was based on crack growth analysis of the lower surface spanwise splices. Although most of the modifications were performed, the weep hole ream and cold work modification recommended in 1983, was never accomplished. Due to too numerous weep hole cracks found in service, it became necessary to determine the extent of weep hole cracking and its effect on the structural integrity of the wing. In January 1993 a Scientific Advisory Board (SAB) directed a teardown inspection be performed on a C-141 inner wing lower surface, to answer the following questions:

- ◆ Can the lower surface spanwise splices achieve 45,000 damage hours ?
- ◆ What is the extent of the weep hole damage ?
- ◆ Are there riser rib clip attach hole cracks ?

The results were to be used to evaluate the fail safety of the wing lower surface, since cracks from riser rib clip attach holes and spanwise splice holes combined with weep hole cracks could cause catastrophic failure of the wing lower surface.

3 CONDITION OF THE AIRCRAFT BEFORE THE TEARDOWN

Aircraft 66-0186 was at LASC for WS 405 maintenance during 1992 and 1993. Inspections had been completed and repair work was in progress, when a stop work order was issued on February 2, 1993. At that time cracks had been found in 99 weep holes on the inner wings: 48 on the right wing (shown as dots on Figure 3) and 51 on the left wing. Several WS 405 repairs were in work as shown on Figure 4 as triangles. Repairs to the lower surface consisted of five beam caps, three wing panels and three inner/outer splice fitting repairs. Although the aircraft had experienced only 23,824 flight hours, due to severe usage the calculated damage hours on the lower wing surface were greater. The inner/outer wing transition area had 45,000 damage hours, while the general area had 39,000 damage hours. During this time similar weep hole damage was being found in the force.

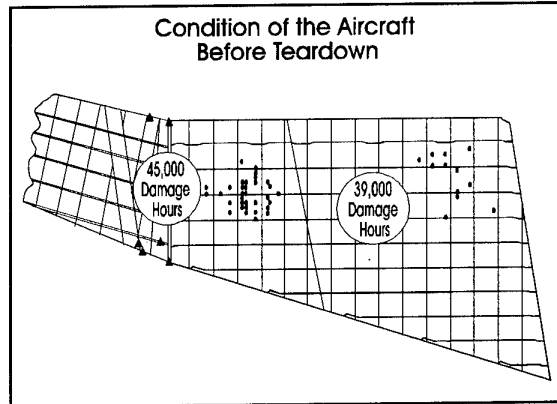


Figure 3

4 THE TEARDOWN PROCEDURE

Because of the similar damage being found on other C-141 aircraft, there was an urgent need for the SAB to obtain this teardown information to determine force management action. It was possible, by tremendous team work between engineering and the experiment shops to accomplish the whole process including the report in six months. The sequencing and the time frame are shown in Figure 4. Preparations began in March, with inspections starting at the end of April. The results of the non-destructive inspection (NDI) were constantly being updated as the inspection progressed. WR-ALC and members of the SAB were briefed periodically as new information was discovered. The most time consuming portion was the enhanced visual inspection, using 10 power microscopes, performed by the metallurgical laboratory. The report was completed September 2, 1993.

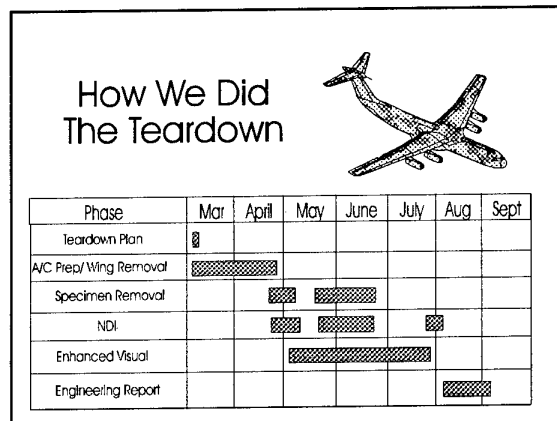


Figure 4

The process began by unbolting the left and right wings at the center to inner wing joint. The right inner wing upper and lower panels were then unbolted at the inner to outer wing joint and a saw cut was made at the front and rear beams inboard of the joint. The right inner wing was then moved to

the teardown inspection location. The right outer wing and the entire left wing were sent to storage. The right wing lower surface was positioned with the lower surface up, so that spanwise splice holes could be numbered and sections marked for cutting. Four foot sections were then cut out, fasteners were carefully removed in each section and the holes cleaned. ABHEC inspection was performed on every hole, and then the disassembled sections were sent to the metallurgical laboratory. The teardown sequence is graphically shown below.

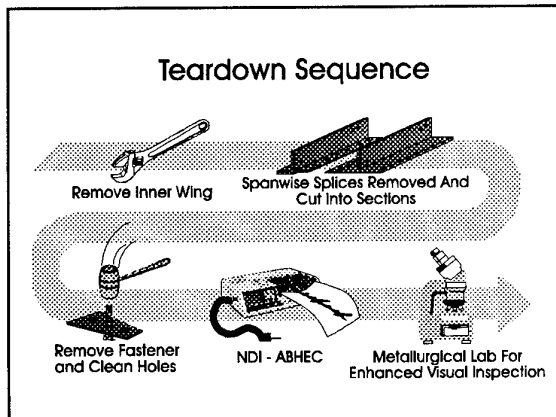


Figure 5

The C-141 wing panels contain five integrally stiffened risers. The main emphasis of the teardown inspection was on the spanwise splice and riser holes. Each splice section contains two panels forming the lap joint with an integral riser. The shaded area in Figure 6 shows this area that received the NDI and enhanced visual inspection.

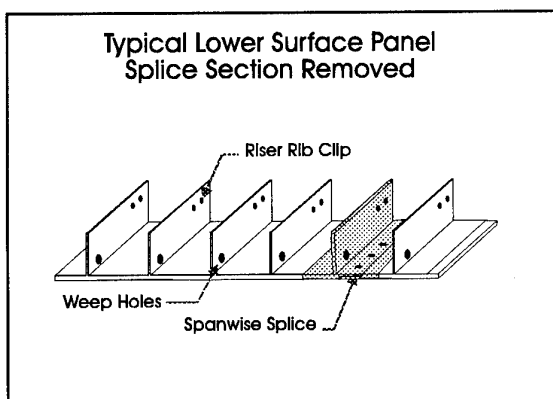


Figure 6

Seven spanwise splices were marked and divided into eight sections each. These sections started at every other wing box rib. Hole numbers and orientation were scribed on the panels before any parts were cut. This was necessary so that when the parts were stripped and etched they could still be identified. The seven splices and the rear beam were then cut

from the right wing lower surface. Figure 7 shows the splices and the sections.

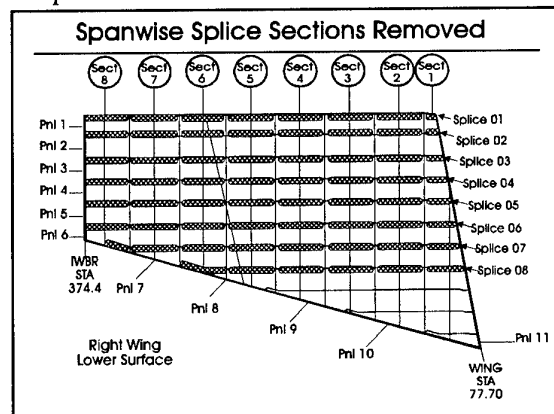


Figure 7

Once an entire splice was removed, it was cut into eight sections. The remaining panel sections were later removed for weep hole and riser rib clip attachment hole NDI. NDI started as soon as fasteners were removed and holes cleaned in each four foot section. When a crack indication was found, the hole was marked and a photograph of the section taken. All open holes in the sections were inspected.

The C-141 spanwise splices are held together by taper-lok fasteners. Taper-loks are interference fit fasteners and must be removed by knocking out with a mallet. Special care must be taken so that the hole is not damaged when the fastener is removed. If a hole is damaged, then flaw data can be lost. A tool is screwed on to the threaded end of the fastener, which prevents the end from being deformed, so that it can pass through the hole without scoring the wall. After the fasteners were removed, the holes were then cleaned with solvent using a non-abrasive brush.

As shown on Figure 8, a thorough inspection of the right wing lower surface was performed. Automatic bolt hole eddy current (ABHEC) was performed on all holes in the following areas:

- ◆ Seven spanwise splices (splice 02 trough 08)
3714 holes
- ◆ Holes common to the rear beam (splice 01)
2051 holes
- ◆ Riser weep holes
735 holes
- ◆ Riser rib clip attachment holes
898 holes
- ◆ Riser bulkhead attachment holes
200 holes

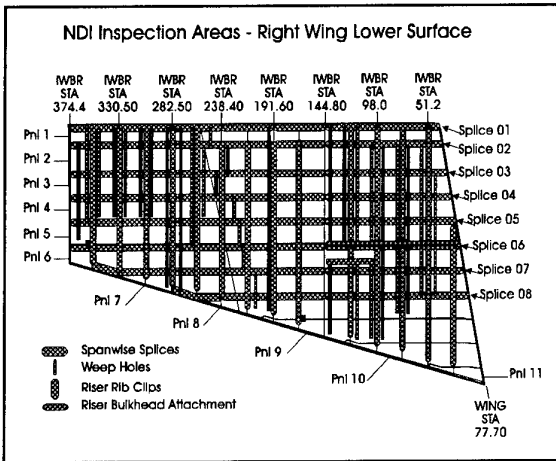


Figure 8

After the NDI on a splice was completed, all crack indications were cut out. The remaining splice and the crack indications were then sent to the metallurgical lab. If the indications were confirmed as cracks by two metallurgists, the fracture surface was broken open and crack codes and lengths were recorded. The remaining parts received a visual inspection, were logged in and checked for identification. Then they were sent to be stripped of paint and acid etched. The etching removes the anodize layer and enhances the cracks for microscopic inspection. The cracks found by NDI were not sent to be acid etched, because the etching could disturb the fracture surface of the larger cracks. The etching was used to enhance the small cracks for microscopic inspection. Figure 9 shows the sequence of the enhanced visual inspection.

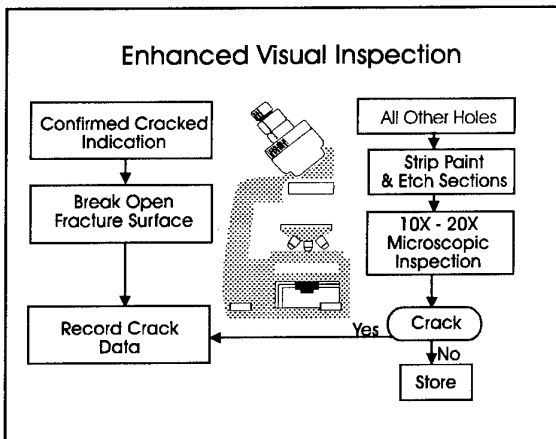


Figure 9

Once the section was etched, every hole was inspected using a 10 to 20 power microscope. Both surfaces of the part around the hole, as well as the hole wall were inspected. Mirrors mounted on dowels at 45 degrees, were used to aid in the inspection of the hole walls. While viewing the hole through the microscope, dowels of the appropriate

diameter were inserted in the holes and rotated to inspect the entire hole wall. When a suspected crack was found a second metallurgist would confirm or deny it's existence. All conditions observed including crack length, crack type and any other pertinent data were recorded in a log book. Cracks as small as .005 inches were found during the microscopic examination. The smallest crack found by ABHEC was .03 inches, but most of the cracks found by ABHEC were .05 inches or greater.

5 HOW THE RESULTS WERE USED

The progression from raw data to corrective force action is shown in Figure 10. Once the data was gathered and organized, the analysis began. Based on these analyses, conclusions were drawn, action items were identified and a corrective action program was defined.

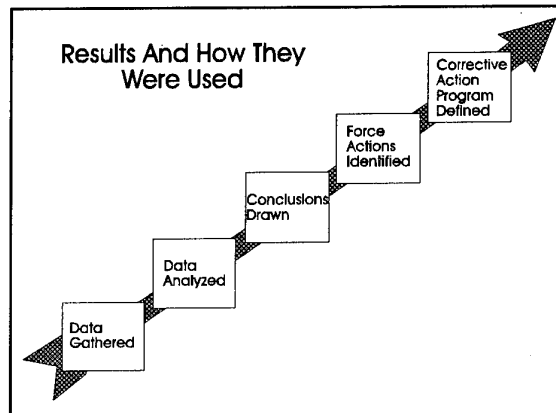


Figure 10

There was a tremendous amount of data gathered from the approximately eight thousand holes inspected. In order for this data to be organized in a usable manner, it was entered into computer files as it was gathered. The data could then be sorted into different types of cracks (weep hole, spanwise splice holes, rib clip attachment holes, etc.). Summaries of each type of crack were compiled. From this list the crack locations were plotted by computer on a plan view of the wing. Computer generated plots were made of each crack type for any condition selected. Finally, histograms of the number of cracks versus crack lengths were made for each type of crack to pictorially present this data.

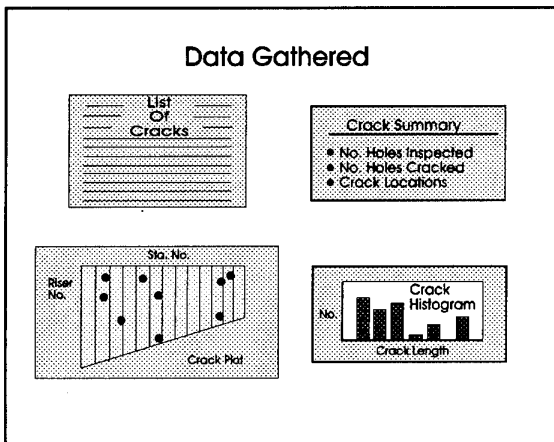


Figure 11

Three areas of interest were analyzed:

- ◆ Weep holes
- ◆ Spanwise splice holes
- ◆ Riser rib clip attachment holes

Using the compiled crack data, statistical crack distributions and crack growth analysis were performed on the three crack types as shown in Figure 12. This information was then used to perform standard risk calculations. This produced probability of failure versus accumulated damage hours for the three crack types.

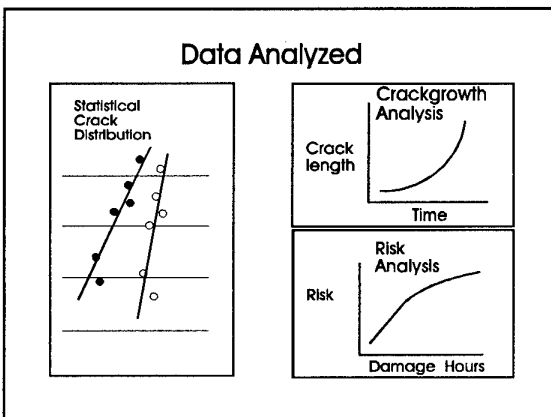


Figure 12

6 CONCLUSION

All objectives of the teardown were met and no surprises were discovered. The service life limit was identified. As anticipated, there were multi-site and multi-element damage observed in the weep holes. Teardown aircraft 66-0186 was correlated with the

force and the statistical and risk analysis was used for projecting damage in the rest of the force.

High damage aircraft were removed from service due to the high probability of failure because of weep hole cracks. Remaining aircraft were inspected from the exterior of the wing within a period of ninety days. WR-ALC developed a new NDI procedure for inspecting the weep holes inside the wing tanks. This was necessary to find the small cracks that degrade the fail safe capability of the structure. This procedure required modified equipment and production of a new tool.

LASC and WR-ALC engineering defined three repair methods for weep hole cracks.

- ◆ Small cracks:
Holes were reamed until the crack was removed and the hole cold worked to retard any further crack initiation.
- ◆ Large isolated cracks:
Composite patches were installed.
- ◆ Large multiple cracks in the same wing panel:
Entire panel was replaced.

These repairs were accomplished within a year at three different repair facilities.

This teardown provided valuable information that was used to make critical safety of flight decisions for the C-141B force. This plan was a superb joint effort by LASC and United States Air Force engineers for managing the force. Inquiries of specific details and subsequent force management initiatives are obtainable from Warner Robins C-141 engineering branch (LJLE).

MULTIPLE SITE FATIGUE DAMAGES OF AIRCRAFT STRUCTURES

G.I.Nestérenko

Central Aero-Hydrodynamic Institute

(TsAGI)

Zhukovsky, 140160,

Moscow region, Russia

ABSTRACT

A methodology for ensuring the damage tolerance of aircraft structures with multiple site fatigue damages is reported. Examples of such damage in wings and fuselages in the course of fatigue strength certification tests and in service are shown. Residual strength criteria for such structures are provided.

INTRODUCTION

Currently, efforts of aviation specialists are directed to ensuring safe operation of aging airplanes (i.e., the airplanes flown for a long time). One of major problems in such airplanes is from multiple site damage in various structures.

In 1972 AN-10A passenger airplane has been lost due to multiple site fatigue damages of a wing lower surface. In 1988 passenger Boeing 737-200 has lost a pressurized body sheet because of multiple site fatigue cracks in a longitudinal skin overlap. In connection with these events aviation specialists of both the USSR and the USA have conducted research aimed at ensuring safe operation of structures that have multiple site fatigue damages.

The problem of multiple site fatigue damage to airplane structures has been widely discussed at international conferences in the last decade. Standards, manuals and circulars are being complemented with requirements to substantiate safety of airplane structures with multiple site fatigue damages. Below, a solution of multiple site fatigue damage problem in Russian aircraft structures is provided.

METHODOLOGY FOR ENSURING DAMAGE TOLERANCE

The "multiple source fatigue damage" term is intended to mean a set of fatigue cracks or fractures in a single structural component or in several components in one particular cross section of the structure. The used in Russia term "multiple source fatigue damage" is similar to a widely used term "widespread fatigue damage" (WFD) including "multiple site damage" (MSD) and "multiple element damage" (MED). Further the term "multiple site fatigue damage" is used in this paper.

The problem of multiple site fatigue damage in aircraft structures was dealt with in the USSR by aircraft designers, fatigue experts and scientists since the catastrophe with the Antonov AN-10A turboprop in 1972 [1]. During flight the wing lower panels have failed due to multiple site fatigue damage in stringers and a skin. In the fracture zone the stiffeners had interface adapters, whereas the skin was a single sheet. The multiple cracks have formed in both the stiffeners and the skin at the ends of the adapters. The damage

had been a multiple site fatigue one due to structural features of the wing center section. A uniform distribution of increased local stresses in stiffeners and skin at the ends of the adapters has been a major cause of almost simultaneous initiation of several cracks. These cracks were growing at nearly equal rates. The service life of AN-10A airplanes had been established in accordance with the safe-life principle. For the wing area wherein the fatigue failure occurred, no in-service flaw-detection measures had been prescribed because this area had not been found to be critical when fatigue testing the AN-10A airframe. In these tests the wing loading programme was insufficiently close to in-service loading. After the catastrophe the same areas in other copies of AN-10A were inspected - many of them had multiple site fatigue damages in stringers and skin.

To evaluate the airplane load at which the wing had been broken, a special programme of AN-10A wing residual strength determination has been developed and implemented. This programme included experimental study of skin sheet residual strength, residual strength and crack growth rate for full-size stiffened panels of the wing, residual strength of two copies of AN-10A that were flown for a long time and had multiple site fatigue damages in the wing zone under study.

The test data generated include residual strength of sheets made out of alloys D16T (similar to 2024 - T3 alloy) and B95 T1 (similar to 7075-T6 alloy) and having transverse rows of fastener holes; each sheet was damaged with a large lead crack and a number of short cracks at the holes [2]. Features of fatigue crack growth and static fracture of stiffened structures with multiple site damages have been outlined [3]. Main points of a method for predicting the residual strength of build-up structures with multiple site damages have been formulated; residual strength of AN-10A wing has been predicted [4].

Thereafter both the multiple site fatigue crack growth rate and the residual strength of structures with multiple site damages were estimated experimentally for full-size airplane structures tested for fatigue and damage tolerance in laboratory conditions. Note that the Russian principle "ekspluatatsionnaya zhivuchest" ("operational survivability") incorporates simultaneously the fail-safe principle and the damage tolerance principle. However, for short, this more comprehensive principle will hereafter be denoted with the term "damage tolerance." Methods for ensuring safety of an airframe with multiple site fatigue damage are based on testing of full-size structures; it has been a main method because there exist many different patterns of multiple site fatigue damage depending on design features. Without having accomplished the appropriate experiments on a full-size structure we cannot in most

cases predict analytically a specific mode of multiple site fatigue damage of the given structure.

It is assumed that a cross section of a structure comprises some 10 elements with identical fatigue life and a multiple site fatigue damage is really in a structure if at least two elements show cracks. Probabilistic analysis indicates that these assumptions dictate the required amount of equivalent "flight hours" of the full-size structure in lab conditions to be three airplane service life goals in order for us to reveal the likelihood of in-service multiple site fatigue damage [5]. The tests were conducted in the USSR of full-size structures of almost all types of airplanes for fatigue and damage tolerance. The high-time structures of these types have also been tested for fatigue and damage tolerance. These structures were tested for at least three design service lives. At the last stage of evaluations the structures were tested for strength under a design limit load ($P_{lim} = 0.67P_{ult}$). In some cases the structures failed under this load due to multiple site fatigue damage. After the tests the structures were torn down and inspected to detect small cracks, including the multiple site ones. Crack surfaces were fractographed and the crack evolution curves were plotted for crack lengths of over 0.3 mm - 0.5 mm.

These experiments have been a basis for determining growth rates and critical lengths of multiple site cracks; inspection and repair intervals were established for the structural zones prone to multiple site fatigue damage. Recommendations on ensuring the damage tolerance were developed.

A survey of fatigue damage of structures showed that a high reliability of a structure is ensured when designers fulfil simultaneously the damage tolerance requirements [5] for the cases of multiple site cracks in a single component (a stiffened panel) and multiple site cracks in several components of one particular cross section of the structure. On the basis of this principle the designers are advised to ensure at the design stage the required residual strength of a wing in the following cases simultaneously (see [5]):

- a complete failure of one of the stiffened panels, no cracks in the other panels;
- one two-bay skin crack with centre stiffener broken simultaneously in each of several panels of a particular cross section of the wing.

To ensure the residual strength of the structure with a two-bay skin crack and a broken centre stiffener, the following opportunity is taken into account: after a long service the short cracks can originate in the skin from fastener holes for the intact side stiffeners at both sides of the broken centre stiffener. This was accounted for by the evaluation of residual strength of the structure having the above mentioned standardized damage after testing the structure for three planned service lives and the propagation of the two-bay crack ends through the fastener holes for side stiffeners [6].

As the critical multiple site fatigue cracks in longitudinal joints in pressurized fuselage skin sheets are known to be very short and hardly detectable in service, therefore the

recommendations are given to design these joints in compliance with the safe-life principle [6].

RESIDUAL STRENGTH

Ensuring the residual strength in structures with multiple site fatigue damages is one of primary concerns in the field of multiple site fatigue damage in airframes. For the USSR airplanes this concern was dealt with on the basis of survey and summation of test data on residual strength of various types of airframes with multiple site fatigue cracks (Figs. 1 - 10). Figures 1 - 10 represent structures of airplane wings and bodies, types and locations of multiple site fatigue damages in primary elements, structural alloys, relative values of net stresses σ_{fract} , and stress intensity factors K_{fract} at which the structures have failed.

Surfaces of fatigue cracks are painted black in these figures. The values of $\sigma_{fract net}$ and K_{fract} have been referred, respectively, to the yield strength $\sigma_{0.2}(F_{ty})$ and to the fracture toughness $K_c^y(K_c^{app})$ (in the case of plane stress state) or to a plane-strain fracture toughness K_{Ic} .

The breaking net stresses $\sigma_{fract net}$ were calculated taking into account the component cross-section reduction due to cracks and fastener holes. A crack longitudinal section areas were calculated on the basis of initial crack length a_0 . The length of the structure cross-section where the net area and $\sigma_{fract net}$ were computed was determined in the following way. The initial length equal to a span of the multiple site fatigue damage zone was assumed. The cross section design length was assumed to be extended (in comparison with the initial length) to the left, by two lengths of a leftmost crack, and to the right, by two lengths of a rightmost crack.

The stress intensity factor K was computed by conventional techniques. The stress intensity factor value $K = K_{fract}$ was computed for a crack with maximum size, accounting for interaction of this crack with neighboring ones.

The experimental data analysis in Figs. 1 - 10 showed that residual strength of a structure with multiple site fatigue damage is influenced by a great number of various factors: structural design features, component bending stress, material plasticity, arrangement of the multiple site cracks, stable growth of cracks under single static loading, holes.

A special-purpose experiment for evaluation of residual strength of sheets with a single centre through crack showed that if both ends of the crack are at the holes then a residual strength capability of the sheet with holes turns out to be higher than that of the sheet without holes at the crack ends. This increase in residual strength is as great as 5 - 10% for plates of about 5-mm thick made of D16T alloy (similar to 2024-T3), 30 - 35% for plates of about 10-mm thick made of D16T, 40 - 45% for plates of about 5-mm thick of B95 T1 alloy (similar to 7075-T6).

It follows from Figs 1 - 10 that the values of the stress intensity factors K_{fract} at which the structure failed were

equal to K_{Ic} and $(0.4 - 1.0)K_c^y$; the breaking net stresses $\sigma_{fract\ net}$ were $(0.3 - 0.9) \sigma_{0.2}$.

After the multiple site fatigue damages in the structure have been detected during the fatigue tests (Figs 1 - 10), the airplanes were operated further. Damage tolerance of structural zones with multiple site fatigue damages was analyzed to establish inspection intervals and deadlines for reworking these zones. When estimating damage tolerance, the allowable crack lengths were specified conservatively.

CONCLUSION

Test data survey demonstrated great variety of types of multiple site fatigue damage in airframes.

No versatile criterion of residual strength of a structure with multiple site damages have yet been proposed. Residual strength of structures with such damages is affected by structural design features, holes, component bending stresses, material plasticity, arrangement of multiple site cracks, stable growth of cracks under single static loading. Structures with multiple site damages fail when stress intensity factors K_{fract} are within a range from K_{Ic} to K_c^y and when net stresses $\sigma_{fract\ net}$ are $(0.3 - 0.9) \sigma_{0.2}$.

The most reliable method for studying damage tolerance of structures with multiple site damages is the experimental evaluation of damage tolerance of structures in tests for fatigue and damage tolerance.

The structural fracture capabilities in the presence of multiple site fatigue damage which have been represented above and in references [7 - 12], are anticipated to contribute to solving the problem of multiple site damage in aircraft structures both at the design stage and in service.

REFERENCES

1. G.I. Nesterenko. Discussion on Aging Aircraft. - The 8th International Conference on Fracture (ICF-8), Kiev, Ukraine, June 8-12, 1993. Published at TsAGI. 60 pp.
2. I.S. Yablonsky, S.I. Ol'kin, A.V. Yegorshev, G.G. Zaveryukha. Strength of Sheet with Transverse Row of Holes Damaged by Fatigue Cracks. - In: Residual Strength of Wing Structures. - Trudy TsAGI, issue 1607, Moscow, 1974, p.11-15.
3. A.V. Yegorshev, G.I. Nesterenko. Some Features of Fatigue Fracture of Structures and their Components. - In: Residual Strength of Wing Structures. - Trudy TsAGI, issue 1607, Moscow, 1974, p.3-6.
4. G.I. Nesterenko. On the Multicomponent Structure Residual Strength Calculation. - In: Residual Strength of Wing Structures. - Trudy TsAGI, issue 1607, Moscow, 1974, p.23-31.
5. G.I. Nesterenko. Damage Tolerance of Aircraft Structures. - In: Strength, Reliability and Life of Aircraft Structures. - Proceedings of Kiev Institute of Civil Aviation Engineers, issue 2, Kiev, 1976, p.60-70.
6. G.I. Nesterenko. Requirements to Ensuring Damage Tolerance of Passenger and Transport Aircraft Airframes at the Stage of Design. - In: Collection of Reports at the Conference "System Approach to Aircraft Structure Service Life Requirements." - TsAGI, 1984, book 1, p.199-207.
7. T. Swift. The Influence of Slow Growth and Net Section Yielding on the Residual Strength of Stiffened Structure. - Federal Aviation Administration. Presented at the 13th Symposium of International Committee on Aeronautical Fatigue, Pisa, Italy, May 22 - 24, 1985, pp. 2.10/7 - 2.10/46.
8. U.G. Goranson. Damage Tolerance: Facts and Fiction. Boeing Commercial Airplane Group, USA. - Presented at the 17th Symposium of International Committee on Aeronautical Fatigue, Stockholm, Sweden, June 9, 1993, 53 pp.
9. A.W. Hoggard. Maintaining the Safety of an Aging Fleet of Aircraft. Proceedings of the 16th Symposium of the International Committee on Aeronautical Fatigue, May 22-24, 1991, Tokyo, Japan, p.113-136.
10. P. Tong, S.G. Sampath and D. Broek. Aging Aircraft. Detection of Multiple Site Damage, and the Risk of Failure. Proceedings of the 16th Symposium of the International Committee on Aeronautical Fatigue, May 22-24, 1991, Tokyo, Japan, p.237-254.
11. H.P. Lehrke and A. Schopf. Analysis of Multiple Crack Propagation in Stiffened sheet. Proceedings of the 16th Symposium of the International Committee on Aeronautical Fatigue, May 22-24, 1991, Tokyo, Japan, p.255-276.
12. M. Nakata, T. Nishimura and K. Naba. Damage Tolerance Assessment on the Multi-Site Cracks for the YS-11 Aircraft. Proceedings of the 16th Symposium of the International Committee on Aeronautical Fatigue, May 22-24, 1991, Tokyo, Japan, p.355

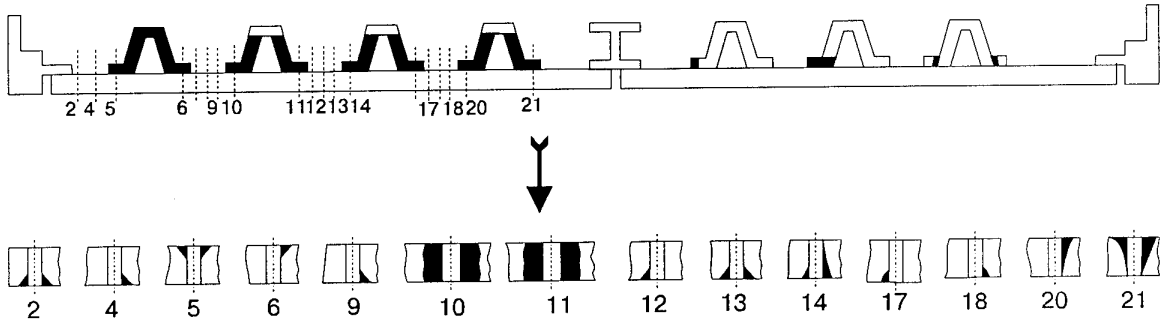


Figure 1. Damages of skin and stiffeners in stiffener interface zone on wing lower surface:

Д16Т alloy; $\sigma_{\text{fract net}} = 0.8\sigma_{0.2}$; $K_{\text{fract}} = 0.5K_c^y$

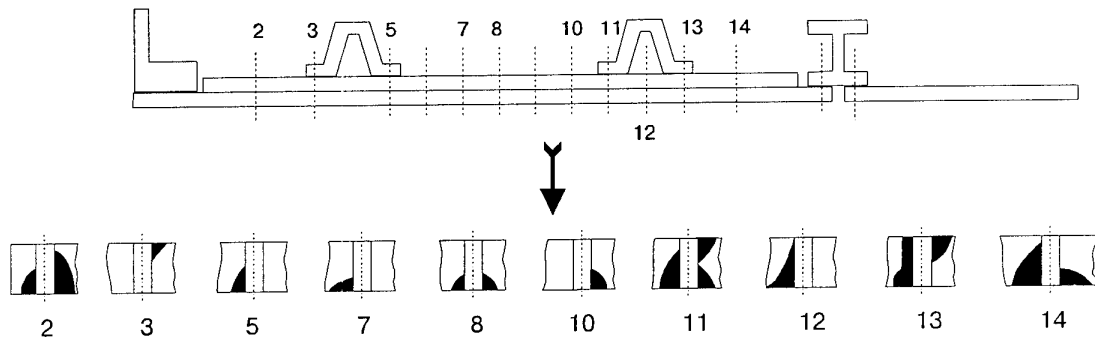


Figure 2. Damages in strip coupling the skin sheets on wing lower surface:

В95Т1 alloy; $\sigma_{\text{fract net}} = 0.4\sigma_{0.2}$; $K_{\text{fract}} = K_{\text{lc}} = 0.4K_c^y$

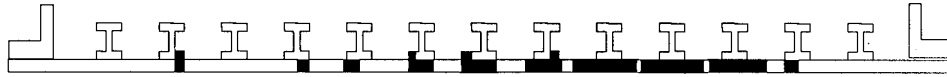


Figure 3. Damages of skin and stiffeners at the doubler edge on wing lower surface:

$$\text{Д16Т alloy; } \sigma_{\text{fract net}} = 0.9\sigma_{0.2}; \quad K_{\text{fract}} = 0.5K_c^y$$

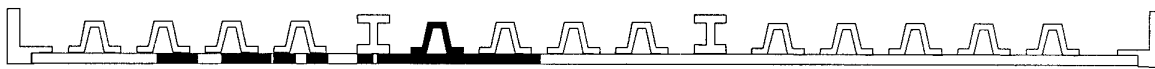


Figure 4. Damages of skin at the doubler edge on wing lower surface:

$$\text{B95Т1 alloy; } \sigma_{\text{fract net}} = 0.45\sigma_{0.2}; \quad K_{\text{fract}} = K_c^y$$



Figure 5. Damages of skin and stiffeners on wing lower surface near fuel holes in the

$$\text{stringers: Д16Т alloy; } \sigma_{\text{fract net}} = 0.7\sigma_{0.2}; \quad K_{\text{fract}} = K_c^y$$

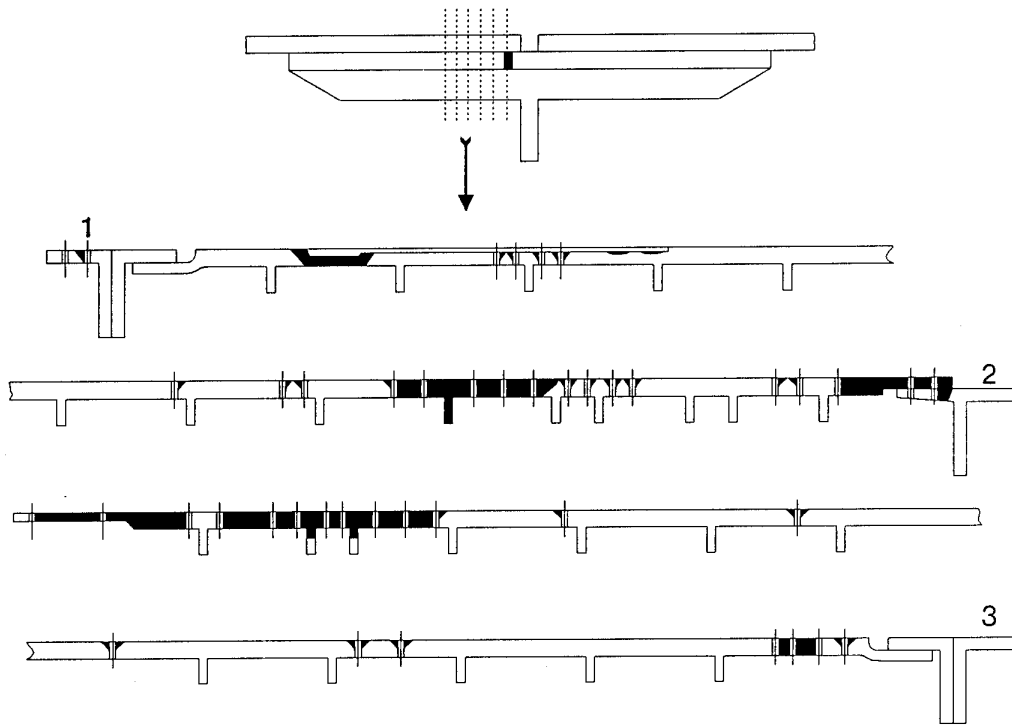


Figure 6. Damages to spars and panel interface component on wing upper surface:

$$\text{Д16Т alloy; } \sigma_{\text{fract net}} = 0.3\sigma_{0.2}; \quad K_{\text{fract}} = 0.5K_c^y$$

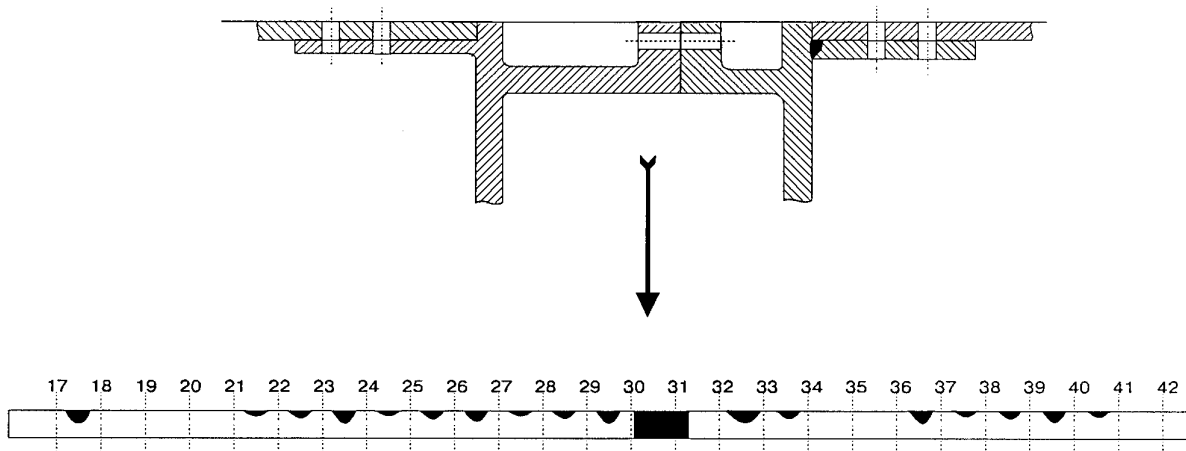


Figure 7. Damages of panel interface component on wing upper surface:
 Д16Т alloy; $\sigma_{\text{fract net}} = 0.7\sigma_{0.2}$; $K_{\text{fract}} = 0.75K_c^y$

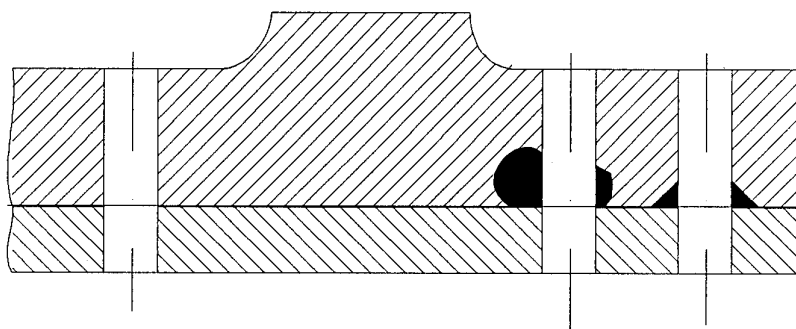


Figure 8. Damages in wing hinge assembly:
 В93Т1 alloy; $\sigma_{\text{fract net}} = 0.4\sigma_{0.2}$; $K_{\text{fract}} = K_{Ic}$

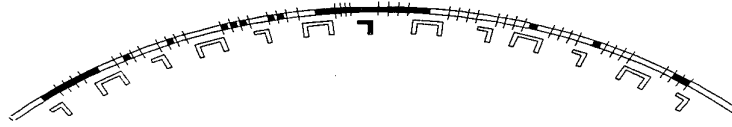


Figure 9. Damages of stringer and doubler on circumferential joint of skin around pressurized fuselage: Д16Т alloy; $\sigma_{\text{fract net}} = 0.75\sigma_{0.2}$; $K_{\text{fract}} = K_c^y$

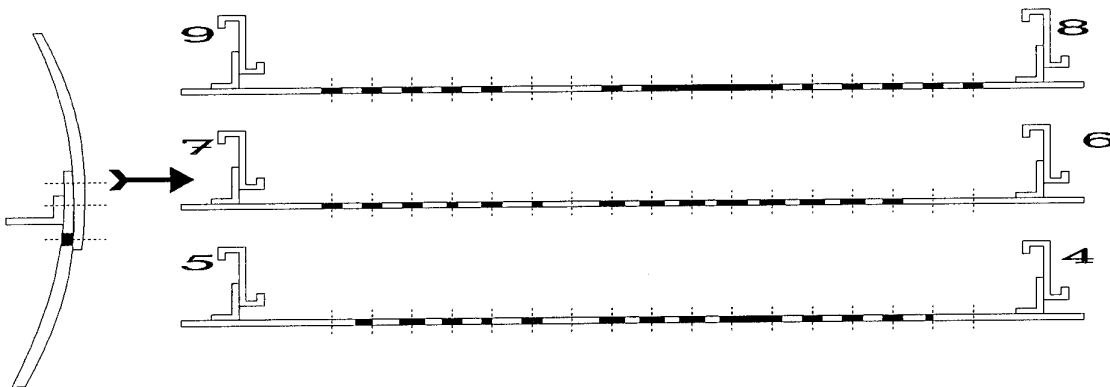


Figure 10. Damages of pressurized fuselage skin near longitudinal skin joint: Д16Т alloy; $\sigma_{\text{fract net}} = 0.7\sigma_{0.2}$; $K_{\text{fract}} = 0.5K_c^y$

Avoiding WFD - a guide to the fatigue design regulations for British military aircraft

Eur Ing Dr. Arthur Cardrick FIMechE

Principal Consultant

Structures Department
Defence Research Agency
Farnborough, Hants GU14 6TD
UNITED KINGDOM

SUMMARY

The loss some years ago of a large section of the cabin roof from an ageing Boeing 737 thrust the spectre of Widespread Fatigue Damage (WFD) into the public domain and gave new impetus to regulations for preventing fatigue life from being undermined by corrosion or repairs. This paper begins with some examples of major fatigue tests in which classical WFD failures have occurred and goes on to consider how the Fatigue Regulations for British Military Aircraft combat the threat presented by WFD as well as the wider threats presented by corrosion, repairs and increases in the severity of service loading. The paper closes by illustrating how the antithesis of WFD - damage concentrated in just one location - might be used to improve the safety and durability of future designs.

1 INTRODUCTION

On the afternoon of 28 April 1988 a Boeing 737 of Aloha Airlines took off and climbed steadily in good weather conditions. The aircraft had already made eight similar flights that day and there was no particular concern that it had accumulated the second highest number of flight cycles (landings) in the world-wide 737 fleet. When, however, the aircraft reached its cruising altitude of 24,000 feet, the calm was shattered by the separation of a large section of the cabin roof. The spectre of Widespread Fatigue Damage¹ (WFD) had entered the public domain².

The Aloha incident also gave new impetus to regulations designed to prevent the fatigue life established for certification from being undermined by corrosion or repairs³. *Corrosion and ill-controlled repairs* can undermine any fatigue certification philosophy, but WFD becomes significant only when

the safe life of a structure is exceeded and safety becomes dependent upon the effectiveness of regular inspections.

For military aircraft, in particular, another generic threat must be considered. The *severity of service loading is often increased* by changes in operational requirements. Such was the case during 1957 when the US Air Force Strategic Air Command (SAC) began using a high-altitude bomber, the B-47, for low-altitude missions⁴. At the time there were about 2,000 of these aircraft in service and they provided the backbone of SAC. To the relatively severe gust environment was added a demanding pull-up manoeuvre. Less than a year after the change was introduced, aircraft began to break-up due to fatigue damage. At the height of the crisis five aircraft were lost in as many weeks. This lesson has been well-learned by the military airworthiness authorities.

This paper is entitled 'Avoiding WFD' and I shall begin with some examples of major fatigue tests in which classical WFD failures have occurred. However, it would be inappropriate for me to discuss how we combat WFD without also considering those other parts of the Fatigue Regulations for British Military Aircraft⁵ which are designed to combat the wider threats presented by corrosion, repairs and increases in the severity of service loading.

The paper closes by looking ahead to consider how the safety and durability of components might be improved by designing them so that damage is concentrated in just one location - the antithesis of WFD. This approach, termed the 'Perceptible Distress' concept is expected to be particularly advantageous for helicopter dynamic components.

2 EXAMPLES OF WFD REVEALED BY MAJOR FATIGUE TESTS

2.1 Transport Aircraft Pressure Cabins⁶

Type B - crack of about 4.5 m appeared along lap joints after about 40,000 pressurization cycles - no sign of damage in visual inspection 400 cycles previously - about 75% of rivet holes contained fatigue cracks.

Type B/C - crack of about 1.5 m appeared along lap joints after about 70,000 pressurization cycles - no sign of damage in visual inspection 2,000 cycles previously - about 75% of rivet holes contained fatigue cracks.

Type T - crack of about 3.25 m appeared along lap joints after about 100,000 pressurization cycles - no sign of damage in visual inspection 500 cycles previously - about 75% of rivet holes contained fatigue cracks.

Type HD - crack of about 2 m appeared along lap joints after about 100,000 pressurization cycles - no sign of damage in visual inspection 4,000 cycles previously - about 75% of rivet holes contained fatigue cracks.

2.2 Transport Aircraft - Other Features⁶

Type H - Wing Planks - crack of about 0.3 m severing four planks and causing complete rupture of top surface after about 10,000 flight cycles (landings) - no sign of damage in visual inspection about 60 cycles previously - three of the four planks contained fatigue cracks.

Type A - Flap Track - crack of about 0.3 m caused failure of multi-element beam after about 40,000 flight cycles (landings) - no sign of damage in visual inspection about 2,000 cycles previously - cracking in bottom plate, reinforcing 'fail-safe' strap, boom and web.

2.3 Combat Aircraft⁷

Type H - Attachment flanges of rib forming fuel-tank wall - extensive cracking of adjacent chordwise holes revealed by tear-down inspection after *exhaustive testing*.

Type T - Lower Wing Skin - extensive cracking of adjacent chordwise holes revealed by tear-down inspection after *exhaustive testing*.

3 THE FATIGUE DESIGN REGULATIONS FOR BRITISH MILITARY AIRCRAFT

Most of the aircraft designed to the British Regulations have been combat-types which are necessarily compact and inaccessible for fatigue-related inspections (Figure 1). In these circumstances the safe-life philosophy has served us well. Such structures tend not to have the *combination* of uniform stresses, similar adjacent features and relatively-high stress levels that are usually associated with WFD. Although some failures have been found to occur by this mode in exhaustive tests, they have presented no special problems since regular fatigue-related inspections are not required for safe-life designs.

The service life of a military aircraft type is now often determined by the fatigue life of the airframe. By amortising the first-cost of the fleet over the life of the airframe it is apparent that each 1% of fatigue life can be worth in excess of £10 million. In consequence, a new impetus has been given to identifying avenues for extending the fatigue lives of existing fleets, influencing the fatigue policies adopted for collaborative projects and exposing shortcomings in fatigue aspects of designs competing for off-the-shelf purchases.

The main features of the Fatigue Regulations for British Military Aeroplanes (Def Stan 00-970, Chapter 201) are summarised in Figures 2 to 21.

4 THE ANTITHESIS OF WFD - THE CONCEPT OF 'PERCEPTIBLE DISTRESS'

If a component were shown to have just *one fatigue-critical feature* under all loading conditions and if the *health* of this feature were monitored using the damage-tolerance approach, then the component could safely remain in service until the monitored feature showed signs of distress - avoiding the need to monitor service loads and interpret them using a cumulative damage algorithm. Since the damage-tolerance philosophy would need to be applied to only one feature of the component, it would be

realistic to provide special instrumentation to avoid the need for regular inspections and overcome any difficulties associated with compactness and inaccessibility.

In principle, the 'Perceptible Distress' concept would be applied by first sizing *each* fatigue-critical feature of a component to achieve the required service life using the normal safe-life factors to account for scatter in fatigue performance. Thus, for airframes, the service life would typically be about 30% of the life that would be expected to be obtained on test with a much lower figure for helicopter dynamic components (Figure 22).

The next step would be to select just *one* feature of the component, such as a lug, in which detectable crack propagation would be well established before the strength of the feature was appreciably reduced. This feature would then be re-sized so that the safe-life factors were largely removed (Figure 23). The life of the component would then be governed by the *reliability* of the monitored feature.

Two fundamental conditions would need to be satisfied:

- a) the typical life of the monitored feature would always need to be sufficient to provide satisfactory reliability and
- b) the minimum factor between the typical life of the monitored feature and that of the unmonitored features would need to be established for a representative range of service loading severities (Figures 24 and 25).

If the *typical* life of the monitored feature was shown to be lower than the *safe* life of the unmonitored features, the component could remain in service until the monitored feature showed signs of distress or, to satisfy reliability considerations, to a service life at which about 1 in 20 components would be expected to show signs of distress.

If the typical life of the monitored feature could not be shown to exceed the safe life of the unmonitored features, but was nevertheless sufficient to ensure that the chance of an unmonitored feature failing first was no higher than say 1 in 20, then the component would need to be withdrawn from service before the probability of failure in the *monitored* feature exceeded

1 in 50. The life associated with this probability would need to allow for scatter in fatigue performance and contain a suitable allowance for uncertainties in service loading. In this way the probability of failure in an unmonitored feature would be confined to 1 in 1000.

It is emphasised that reliable instrumentation is as important to the success of this concept as the ingenuity and resourcefulness of the designer.

5 CONCLUDING REMARKS

The loss some years ago of a large section of the cabin roof from an ageing Boeing 737 thrust the spectre of Widespread Fatigue Damage (WFD) into the public domain and gave new impetus to regulations for preventing fatigue life from being undermined by corrosion or repairs.

Examples have been given of major fatigue tests in which classical WFD failures have occurred and it has been explained how the Fatigue Regulations for British Military Aircraft combat the threat presented by WFD as well as the wider threats presented by corrosion, repairs and increases in the severity of service loading.

Looking to the future, it has been explained how the safety and durability of components might be improved by concentrating damage into just *one* location - the antithesis of WFD - and *proving* this to be the case for a representative range of service loading severities. Ideally, the feature at this location would exhibit perceptible distress which could be monitored directly.

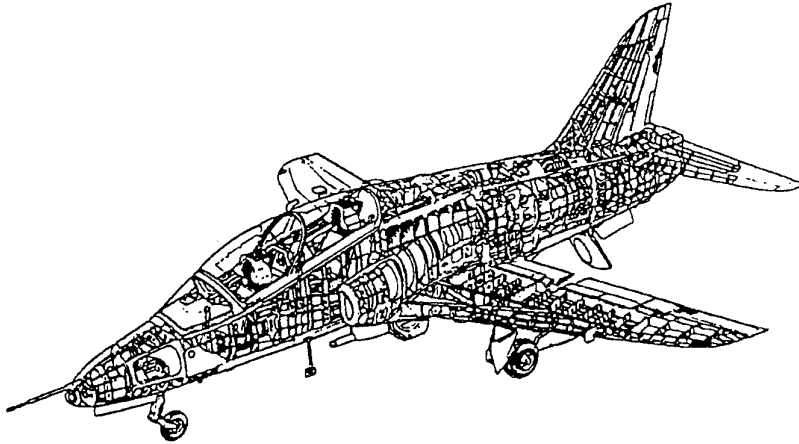
6 REFERENCES

- 1 R. D. J. Maxwell *Fail-Safe Philosophy*. proc. ICAF International Symposium on Fail-Safe Structures, London, July 1973
- 2 *Aircraft Accident Report - Aloha Airlines, Flight 243, Boeing 737-200, N73711, near Maui, Hawaii, April 28, 1988*. National Transportation Safety Board Report NTSB/AAR-89/03, June 1989
- 3 T. Swift *Repairs to damage-tolerant aircraft*. proc. FAA/NASA International Symposium on Structural Integrity of Aging Airplanes, Atlanta, Georgia, March 1990

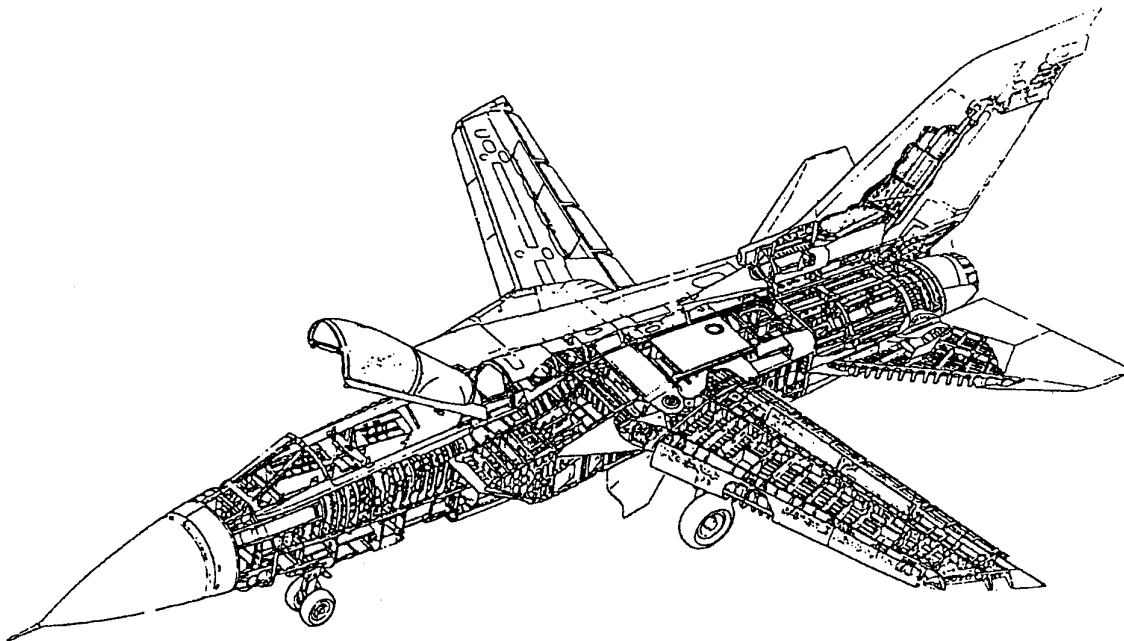
- 4 G. R. Negaard *The history of the Aircraft Structural Integrity Programme*. C. D. Johnson Aerospace Structures Information and Analysis Center, Air Force Flight Dynamics Laboratory, Wright-Patterson Air Force Base, Ohio, June 1980
- 5 *Design and Airworthiness Requirements for Service Aircraft*. Ministry of Defence, London
- 6 Unclassified extracts from the Royal Aircraft Establishment submission to the eighteenth meeting of the Technical Committee of the Airworthiness Requirements Board, June 1977 (not for public release)
- 7 Unclassified extracts from recent Fatigue Audits of British military aircraft (not for public release)

© British Crown Copyright 1995 / DRA

Published with the permission of the Controller of Her Britannic Majesty's Stationery Office



Hawk T Mk1



Tornado ADV



Figure 1 Examples of structures to which Safe-Life regulations apply.

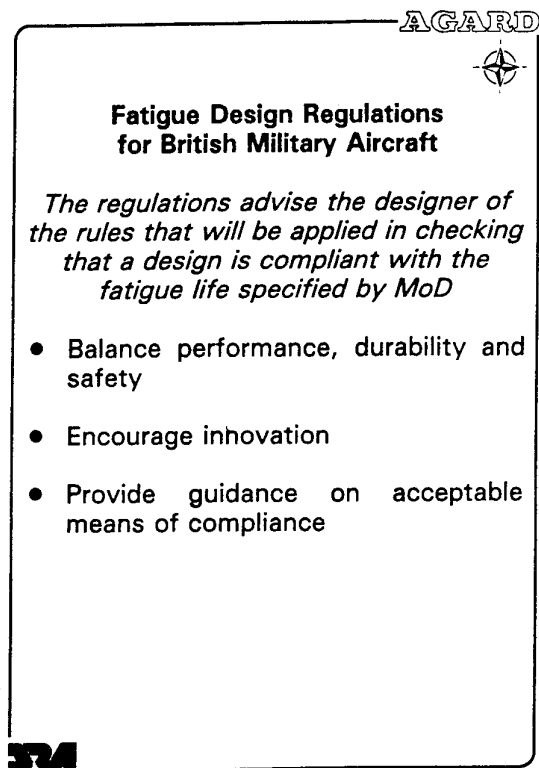


Figure 2

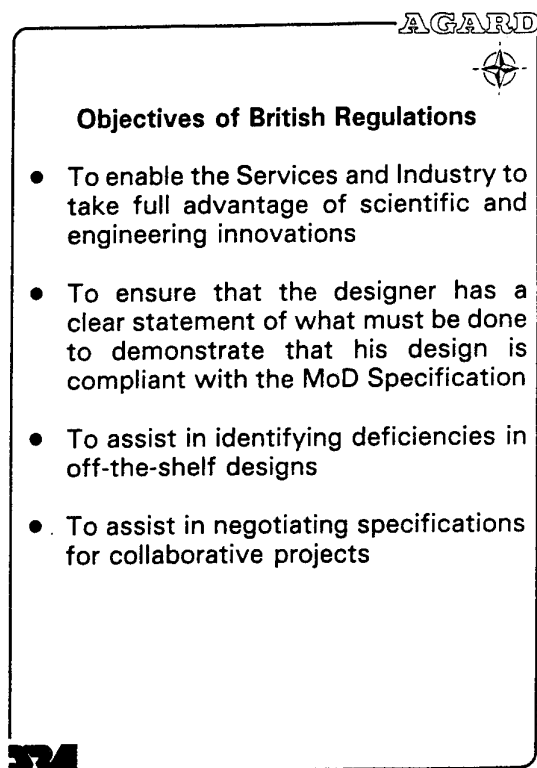


Figure 3

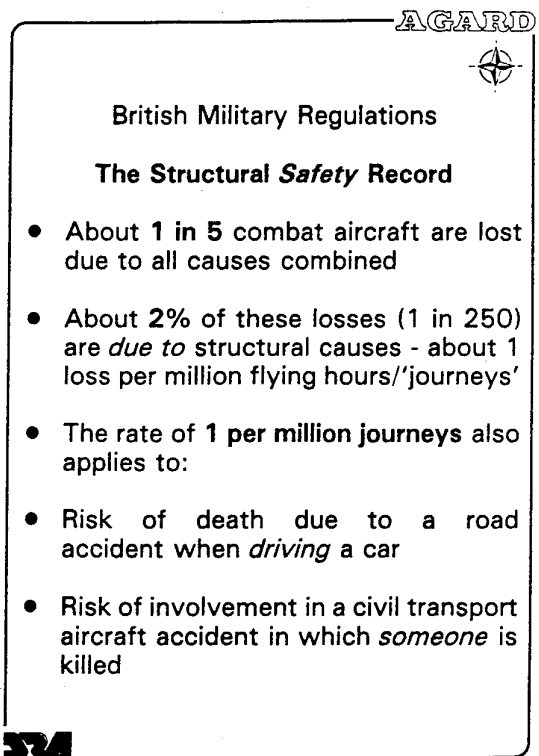


Figure 4

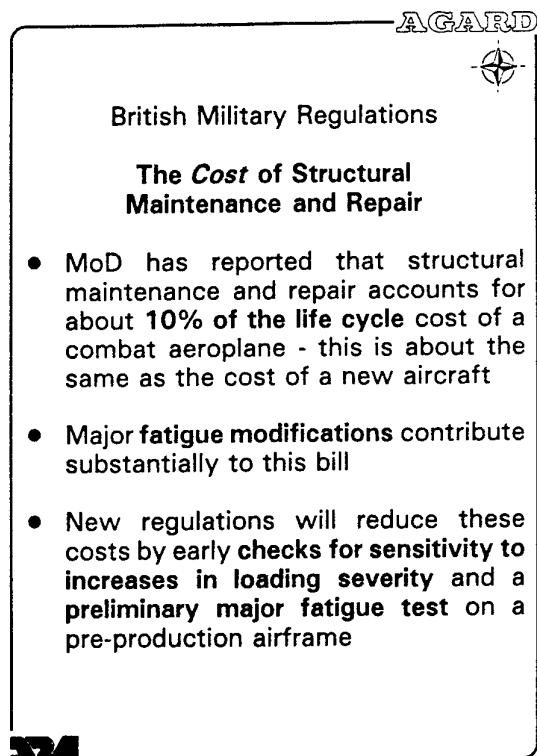


Figure 5

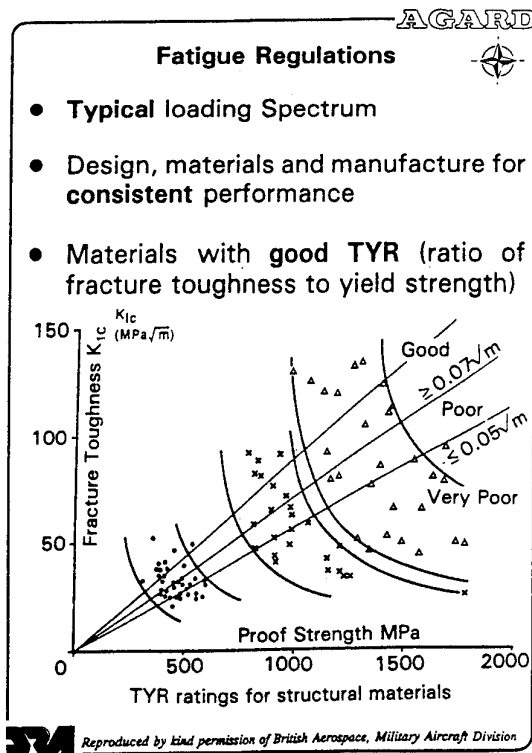


Figure 6

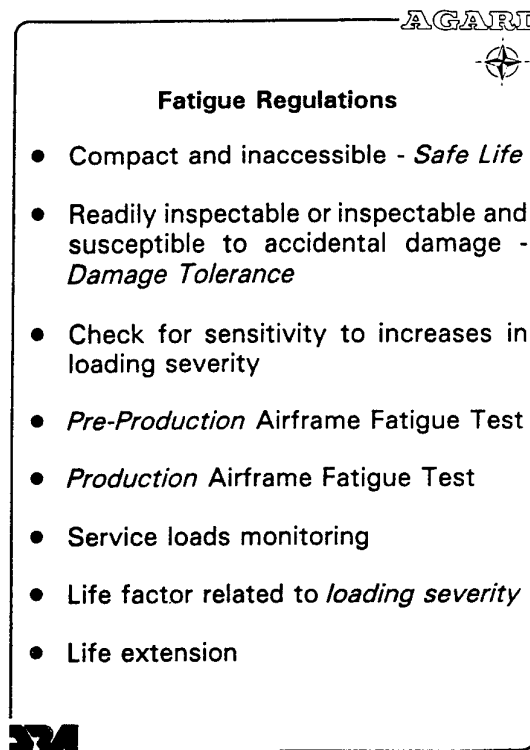


Figure 7

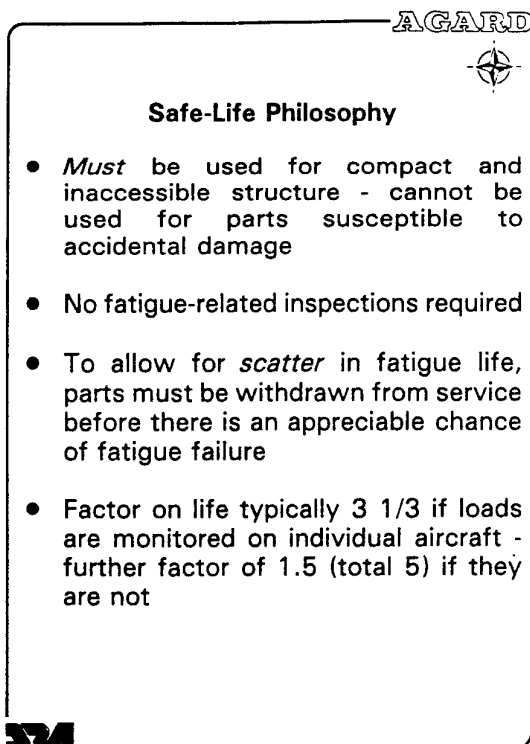


Figure 8

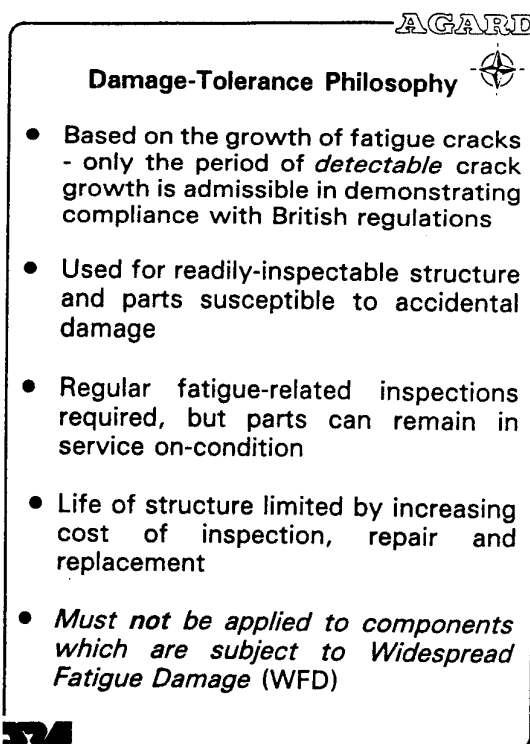


Figure 9

AGARD



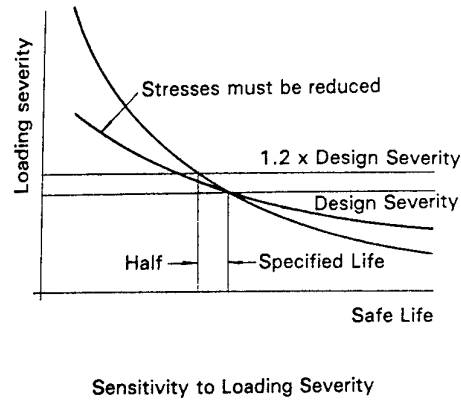
Sensitivity to Loading Severity

- The loading spectrum used for design is a best estimate of the typical usage
- In the longer term, changes in role and increases in mass can increase the severity of the loading spectrum by a stress factor of 1.2 or more
- To ensure that the life of the structure is not limited by parts with an *exceptionally high* sensitivity to loading severity, all safe-life parts must have a life of at least half the specified life when their stresses are increased by a factor of 1.2; a corresponding check is applied to damage-tolerance parts.

SM

Figure 10

AGARD



SM

Figure 11

AGARD



Pre-Production Airframe Fatigue Test

- Structural maintenance and repair has been estimated to account for about 10% of life cycle costs
- This means that the cost per aircraft is about the same as the cost of the aircraft itself
- The cost of a major fatigue test is also said to be much the same as the cost of one production aircraft
- The Pre-Production Major Fatigue Test should reduce maintenance and repair costs by at least 20% and so for a fleet of 250 aircraft the return on investment should be at least 50:1

SM

Figure 12

AGARD



Production Airframe Fatigue Test

- Applies to airframes of safe-life design and any major safe-life assemblies of damage-tolerance designs
- Confirms the effectiveness of any modifications arising from the Pre-Production Airframe Fatigue Test
- Confirms that changes arising from production considerations have not adversely affected fatigue life
- The Production Major Fatigue Test is also the main vehicle for extending fatigue life and therefore represents an even greater return on investment than the Pre-Production Test

SM

Figure 13

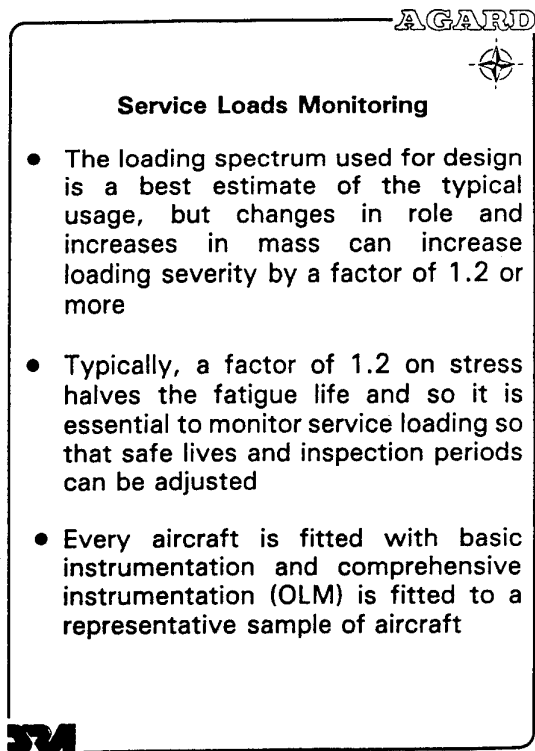


Figure 14

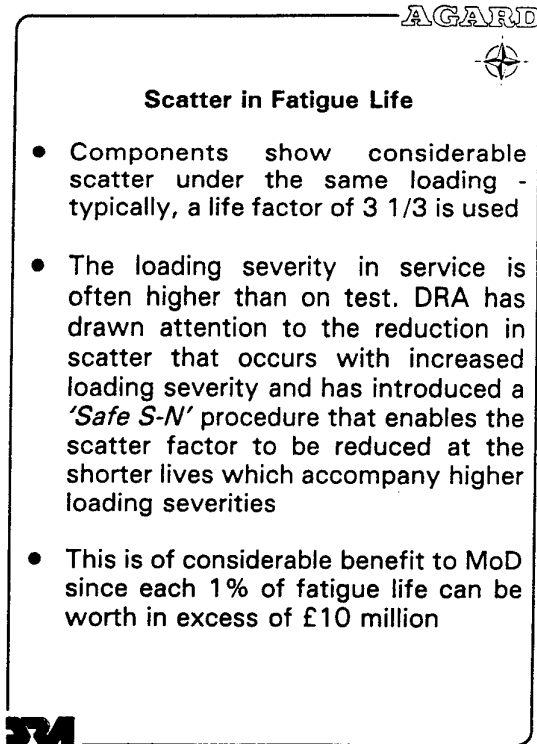


Figure 15

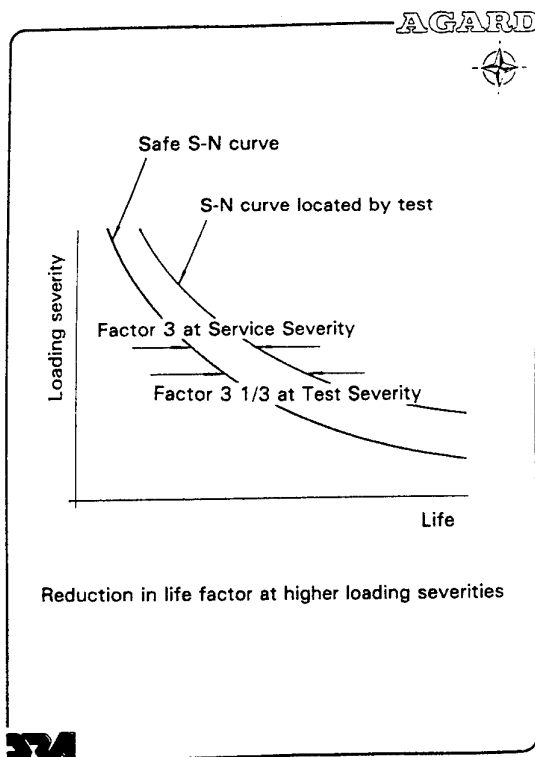


Figure 16

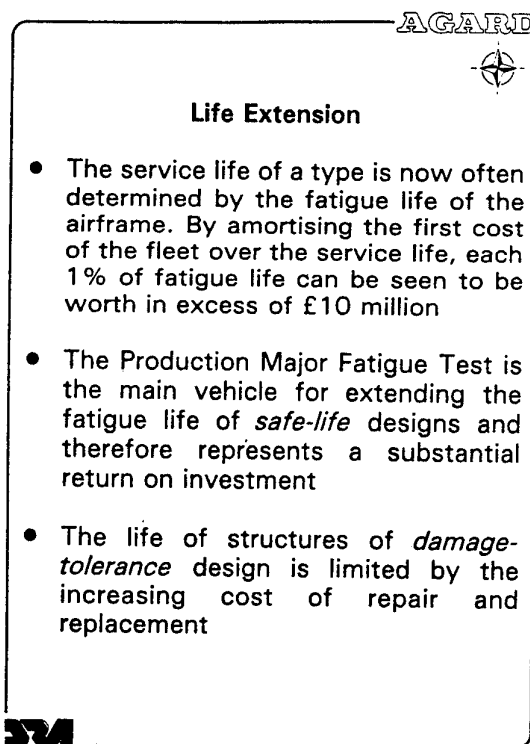



Figure 17

AGARD




Safe-Life and Damage-Tolerance Design

- Corrosion of fatigue-sensitive parts *must* be prevented
- Loads *must* be monitored to enable safe-lives/inspection frequencies to be adjusted using a damage algorithm - unless *health* is monitored *continuously*
- Repairs *must* be controlled
- Details of *all repairs* *must* be recorded so that any interactions can be identified
- Guidance on the scope of *minor repairs* of a routine nature (accidental damage, etc) *must* be underpinned by a generic fatigue substantiation
- *Other repairs* *must* be underpinned by a special fatigue substantiation

SM

Figure 18

AGARD



Widespread Fatigue Damage (WFD) in the context of Safe-Life Design


- Regular *fatigue-related inspections* *not required*
- *Exhaustive* tests done to identify (map) *all* fatigue-sensitive features
- Components *withdrawn from service* *before there is an appreciable risk of failure* - service life typically *about 1/3 test life* when probability of failure is about 1 in 1000
- Failure mode *unimportant*, and so **WFD is not a threat**

Essential to prevent corrosion, monitor loads/health and control repairs

SM

Figure 19

AGARD



Widespread Fatigue Damage (WFD) and Damage-Tolerance Design


- Regular *fatigue-related inspections*
- *Limited* tests of crack propagation rates at *selected* features - *other fatigue-sensitive features* *not mapped* by an exhaustive test
- When the service life reaches 1/2 test life (to serious cracking) the probability of *serious cracking* rises to about 1 in 20
- Components which are subject to WFD *must* be substantiated using the **safe life** philosophy - probability of failure limited to about 1 in 1000

Essential to prevent corrosion, monitor loads/health and control repairs

SM

Figure 20

AGARD



Widespread Fatigue Damage (WFD) as a threat to damage-tolerance compliance

For a damage-tolerance compliance to be undermined by WFD there must be an unfavourable combination of circumstances

- There *must* be a uniform stress field
- There *must* be a series of similar adjacent features to initiate cracking
- The stress levels *must* be high enough for 'unzipping' to occur before cracking becomes perceptible
- The service life *must* be in excess of the safe life

Essential to prevent corrosion, monitor loads/health and control repairs

SM

Figure 21

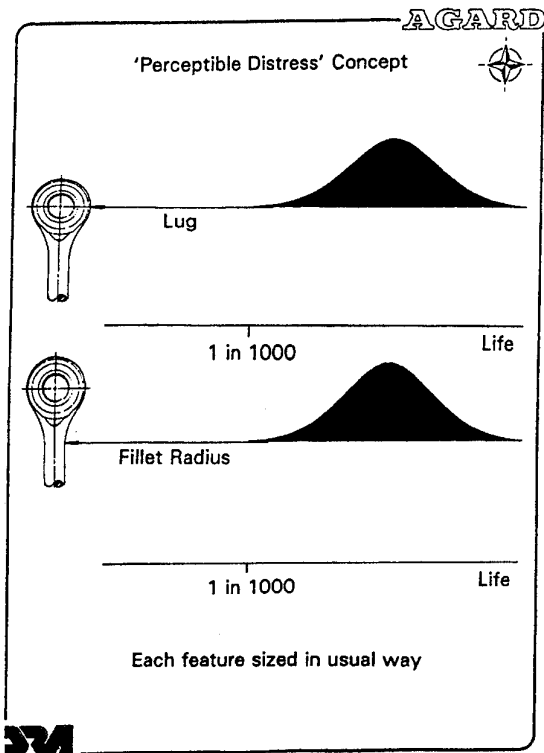


Figure 22

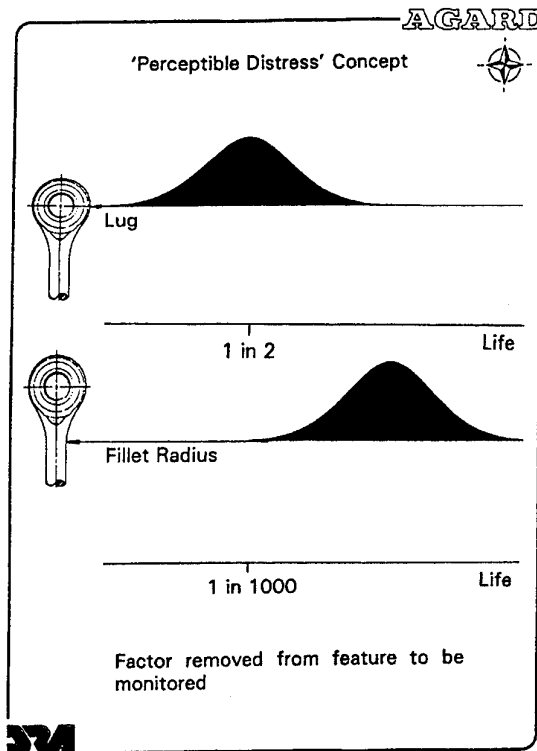


Figure 23

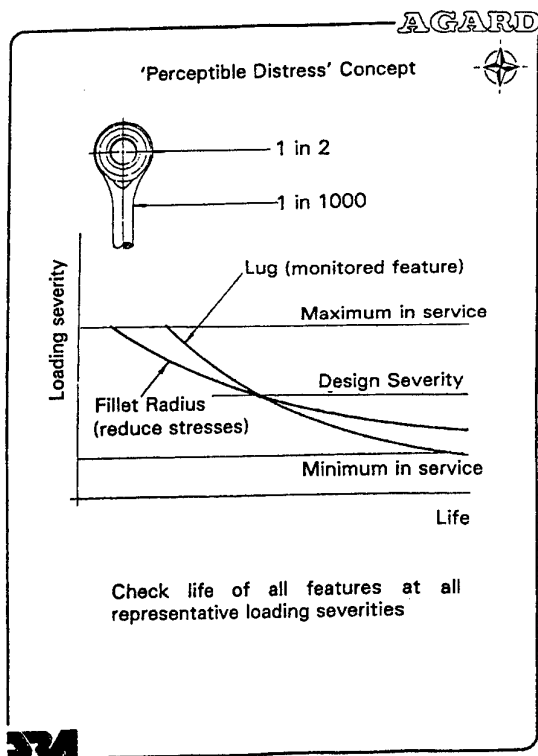


Figure 24

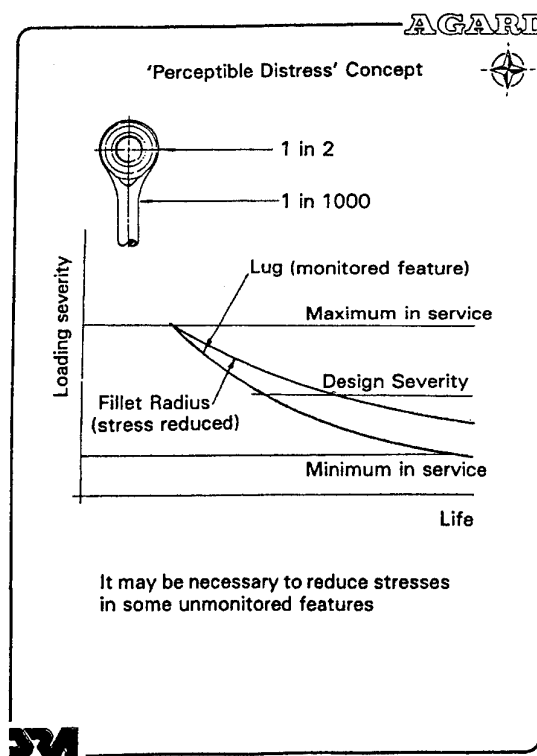


Figure 25

LIVING WITH WIDE SPREAD FATIGUE DAMAGE

R. Jones¹, E. S. Wilson² and S. Hammond¹

¹ Department of Mechanical Engineering, Monash University, Clayton, Victoria 3168, Australia.

² Aircraft Structural Integrity, HQ Logistics Command, Royal Australian Air Force, 350 St. Kilda Road, Melbourne, Victoria, 3004, Australia.

SUMMARY

The purpose of this paper is to address Australian experiences in the field of wide spread fatigue damage (WSFD). The examples presented in this paper deal with WSFD in Mirage, Macchi, F111C and F/A-18 aircraft, and were specifically chosen so as to highlight future assessment and certification requirements.

1. INTRODUCTION

In the twelve years since Mann [1] produced his overview paper on Australian directions in aircraft fatigue there have a number of very significant structural changes both within the RAAF, academia and in the industry at large. The high acquisition costs associated with the purchase of modern military aircraft, coupled with existing economic and market forces, has also resulted in utilization of aircraft beyond their original design life. This trend, in operating existing aircraft approaching or beyond their intended design life, is often reflected in an increasing number of structurally significant defects and increases the possibility of a reduction, or loss, of structural integrity. To meet this challenge, of assessing and managing the operational performance of ageing aircraft, it is essential that a valid certification methodology, coupled with simple (to use) and yet accurate tools for the assessment of structural integrity be developed. To this end the present paper, which concentrates on the phenomenon of WSFD, describes a range of cracking problems associated with Mirage, Macchi, F111C and F/A-18 aircraft, together with the recent Royal Australian Air Force (RAAF) approach to aircraft structural integrity management [2]. From these specific case studies it is shown that there is a basic similarity in many of these problems and that a method of rapidly assessing the structural integrity of components containing complex three dimensional cracks, including interacting cracks, under realistic loading would be very beneficial.

A brief discussion is also presented on the recent RAAF policy on repairs [2], which requires that

“(1) damage tolerant principles are applied for the design of repairs, and modifications, with particular care taken of the potential interaction of multiple repairs;

(2) inspection intervals are established to ensure their continued integrity, and

(3) assessment is made of their impact on the structural integrity management of the aircraft.”

2. CRACKING IN RAAF MIRAGE IIIO AIRCRAFT

2.1 Full Scale Fatigue Test

During full scale fatigue testing of Mirage IIIO fighter aircraft wings at the Swiss Federal Aircraft Factory (F+W) fatigue cracks were discovered at the innermost bolt holes along the rear flanges of the main spars, with failure associated with cracking at bolt hole number 5. The test was then continued with a starboard RAAF Mirage IIIO wing (2190 hours service) and a port Swiss Mirage IIIS wing (510 hours service). After a relatively short test life cracks were then found at the inner most bolt holes. Cracking was also found in a number of other locations including Frame 26. Cracking was also experienced in the lower (tension) wing skin both at the fairing hole (nearest the main spar) and at the fuel decant hole in the lower wing skin, see [1,3] for more details.

2.1.1 Wing Cracking:

Following this test crack indications were confirmed at identical locations, both in the spar and in the lower wing skin, in wings of the RAAF Mirage IIIO fleet. At

bolt hole number one the existence of two single leg anchor nut (SLAN) rivet holes meant that the cracking developed at the SLAN holes as well as at the main bolt holes. We were thus faced with the problem of distributed and interacting (three dimensional) flaws.

This phenomenon prompted the development of a life enhancement scheme for the main spar using interference fit steel bushes [1]. This essentially stopped cracking at the main bolt-holes and made the SLAN hole the next critical item, see [1]. There were also instances when poor manufacturing processes meant that the SLAN rivet holes were not correctly aligned, i.e. straight. This resulted in a significantly greater level of crack interaction. A potential remedy for this problem was subsequently produced. This involved the bonding of close fit rivets into the SLAN holes, see [3].

To overcome the skin cracking in the (nearby) lower wing skin two boron epoxy repairs were developed, one for drain hole cracks and one for fairing hole cracks. These were implemented throughout the RAAF fleet and were present, with no evidence of failure, until retirement of the fleet. Because of the fatigue criticality of the spar the repair design was driven by the need not to compromise the original (uncracked) stress distribution, see [3] for details.

2.1.2 *Frame 26:*

The F+W fatigue test undertaken in Switzerland also resulted in a major failure, together with a number of nearby cracks, in the fuselage Frame 26. The major crack occurred at hole 18 on the left side of Frame 26A and extended across the entire flange and well into the web. Other cracks occurred in the region between holes 1 and 23 and included; a 9 mm crack in the inner strap plate and small (less than 3mm long) cracks in holes 4, 7, 8, 18, 20 and 22. Prior to the major crack being detected significant cracking had also occurred in the outer strap plate in the bottom of the frame. At the time of the failure this region contained cracks with lengths of 40 mm, 31mm, 20mm, 18mm, and 12mm.

Following the F+W fatigue test the RAAF undertook an inspection program and found "limited" cracking in fleet aircraft. The only cracks reported were at holes in the inner flange in the vicinity of station 800. In general the crack lengths (down the bore of the holes) did not exceed 3mm and were significantly beneath the critical crack sizes.

3. CRACKING IN RAAF MACCHI MB326H AIRCRAFT

3.1 Macchi Recovery Program

The Macchi MB326H is an excellent example of the importance of understanding and managing WSFD. In this case AerMacchi conducted a series of fatigue tests on the MB 326 structure in order to meet the requirements of the Italian Air Force Specifications and AvP 970. Failure occurred in the

- i) centre section lower spar
- ii) Wing Assembly Fitting (WAF) and main lower spar cap.

However, whilst fatigue tests on the fin revealed cracking at the main fin attachment no major failures occurred.

In the late 1970's fatigue cracking was discovered, in RAAF service aircraft, in the 04A centre section and this led to a change in the management philosophy for this component. In the early 1980's a Life-of-Type Extension Program (LOTEX) was carried out by the Commonwealth Aircraft Corporation (CAC) and Hawker de Havilland (HDHV) to extend the operational life of the MB326H. In June 1985 HDHV was tasked to complete a DADTA, using modern fracture mechanics principles, to define the economic life and to formulate a Force Structural Maintenance Plan.

In November 1990 Macchi aircraft A7-076 suffered a port wing failure whilst in an estimated 6g manoeuvre. It was subsequently found that failure was caused by fatigue cracking originating from the "D17" rivet hole in the lower spar cap. As a result of this event a Macchi Recovery Program was initiated to determine the structural condition of the fleet and to reassess the fatigue lives and management philosophies of the main structural components. As recommended in DEF STAN 00-970 a tear down inspection program was established. In this program ten post LOTEX wings, two fuselages, two fins and five horizontal tail planes were destructively inspected, see [4] for details.

3.1.1 *Wing Structure*

Six of the wings showed significant cracking indications. Of the, approximately, 1000 holes which were examined 100 revealed fatigue cracks, including major cracking in the D series rivet holes.

3.1.2 Fuselage Structure

Mild to severe corrosion was found in the screw holes of the upper and lower spars and fatigue cracking was also found in the lower spar bolt holes.

3.1.3 Empennage Structure

Mild to severe stress corrosion cracking in the upper and lower spar caps of the horizontal tail planes.

3.2 Wing Spar Cracks

This program revealed the fatigue critical locations in the centre section lower spar boom to be bolt holes 3-6 and 17-20. The flaws were highly three dimensional in nature and, from the failure investigation of aircraft A7-076, the failure process had involved a number of interacting cracks. In this case cracking had progressed from a Web attachment Fastener hole through the flange as well as from the nearby Wing Attachment Fastener (rivet) Hole, see Figure 1. Fractographic evidence also indicated multiple crack origins at the root of the rivet hole, see Figure 1. To assist in establishing the critical crack size a detailed 3-D finite element analysis of this cracking was performed. This established that once the main crack had grown past the flange the stress intensity factor was essentially equal to its fracture toughness.

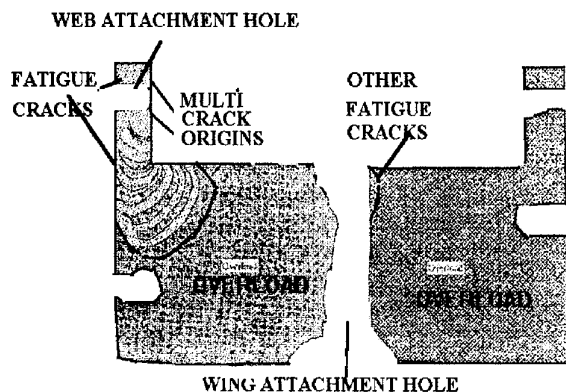


Figure 1. Cross section view of failure surfaces in the Macchi spar.

As result of the MRP the purchase of new wings is being pursued. A more detailed description of this program, its underlying philosophy and the Macchi

Aircraft Structural Integrity Management Plan (ASIMP) is given in [4]

4. CRACKING IN RAAF F111C AIRCRAFT

F-111C aircraft in service with the Royal Australian Air Force (RAAF) have been found to experience cracking in a number of locations; viz:

4.1.1 Wing Pivot Fitting (WPF)

Cracks have been found in Stiffener Runout Number 2 (SRO #2) and in Mouse Hole number 13 (MH#13). Cracking in SRO #2 has, in some instances led to failure, during Cold Proof Load Testing (CPLT) in the USA [5,6]. Interestingly the concept of performing CPLT, at -40° C, was first introduced to ensure continued structural integrity of the USAF F111 fleet, see [5]. The current load cycle applied during CPLT, which is referred to as SIP III, involves loading to -2.4g, 7.33g -3.0g, 7.33g. Stiffener Runout No. 2 (SRO #2), on the upper surface of the WPF, is the most critical location. Here the local bending field results in compressive yielding under high positive g loads. The negative g loads then produce very high tensile strains. It is these tensile strain that were responsible for failure in CPLT.

As outlined in [7] the wing consists of a 2024-T856 aluminium wing skin fastened to the D6ac steel WPF with stainless steel fasteners. The problem area, in which cracking is occurring, is in the runout region on the top surface of the WPF.

To overcome this problem it was necessary to: 1) Determine critical crack sizes and inspection intervals, both for unmodified and modified aircraft. 2) Change the geometry of the local region, thereby reducing the K_I ; and 3) Provide an alternate load path so as to partially by pass the critical region. To achieve the first two requirements a series of detailed finite element analyses were performed and the results used in conjunction with fractographic observations and fatigue meter histories. To meet the third objective a boron epoxy doubler (reinforcement) was developed [7].

To meet the requirements for continued airworthiness it was necessary to determine the associated inspection intervals. To this end it was necessary to obtain the residual stress, after CPLT, and the stress "per g" both with and without doubler and with various grind out configurations. To obtain this information required a

detailed elastic-plastic analysis since during CPLT SRO #2 undergoes gross plastic yielding. This analysis program was supported by series of full scale structural testing. (In this test program the strains in the vicinity of SRO#2 were found to be in excess 18,000 $\mu\epsilon$.)

Classical techniques for modelling this cyclic (plastic) behaviour had inherent difficulties in representing the response to large cyclic inelastic strain excursions. Indeed, the use of classical analysis techniques resulted in a predicted inspection interval, for the modified structure, of under 500 hours. This contrasts with the service experience which has shown that with both the doubler and change in the runout geometry there has been little further cracking. Indeed, for modified aircraft there has been no further cracking since 1985, see [9] for more details.

To overcome this shortcoming the use of a "unified constitutive" model, see [8, 9], was used. With this approach the stress per g and the residual stress thus calculated were consistent with fleet experience and resulted in an extension of the inspection interval from under 500 hours to more than 1400 hours.

4.1.2 *Cracking in Mouse Hole 13*

Cracking has also been detected in fuel flow hole (FFH) number 13, i.e. FFH #13 (also known as mousehole MH#13) in the upper stiffeners of the WPF. As in the stiffener runout this region experiences large compressive strains, with values in excess of 20,000 $\mu\epsilon$ being measured during proof load tests. The large negative g loads (strains) then produce very high tensile strains and it was believed that it was these tensile strain that are responsible for the cracking at MH#13.

To maintain the structural integrity of the aircraft these cracks are routinely removed, i.e. blended out. To determine the "optimum blendout" shape a series of finite element studies were performed. However, despite modification of the shape of MH#13 evidence of crack growth continues, albeit at a reduced rate. Fortunately all of the cracks found to date emanate in "lower" region between the MH#13 and the lower titanium shear web. The other side of the MH is essentially flush with the upper plate of the WPF. Consequently, cracking near the MH plate intersection, i.e. in the upper region of MH#13, would a) be difficult to inspect, and b) removal any such crack(s) could mean intrusion into the upper plate thereby significantly impinging on the damage tolerance of the aircraft. In this context it has also been

found that the blending out of MH#13 can slightly increase the stresses in the upper region. An evaluation into various innovative ways to increase the damage tolerance of this region is currently under way.

4.2 **Cracking in The Wing Carry Through Box Sealant Injection Hole**

The wing carry through box (WCTB) of F111C aircraft contains several small threaded holes in its upper plate for injecting liquid sealant, referred to as sealant injection holes (SIH). These lie between the upper plate and the shear web flanges which make up the WCTB, see [10]. Minor cracking was found in two RAAF F-111C aircraft WCTB during inspections prior to the second CPLT program. To date cracking has been confined to locations near the end of the WCTB, which is thought to be the location of the maximum bending and shear stresses. The SIH's are sometimes found to contain a number of (interacting) cracks and for F-111A aircraft a crack was found which was greater than the nominal critical crack size for this location.

The recovery process involves reaming out the cracks in stages to enable a profile of the crack to be established. In some cases inspection of the holes has resulted in damage requiring re-work [10]. Unfortunately, cold working of the hole and/or filling it with a plug is not possible due to the small size of the SIH.

5. **CRACKING IN RAAF F/A-18 TEST ARTICLE**

The various fatigue test(s) undertaken by McDonnell Douglas in support of the F/A-18 have indicated a large number of potential hot spots, including the FS488 aft bulkhead flange, mold line and wing attachment lug. To further assess the fatigue performance of the FS488 aft bulkhead a full scale fatigue test was performed in Australia on a stand alone FS488 bulkhead. The test was performed to primarily address the region of the wing attachment lug. In this test failure resulted from a fatigue crack approximately 6 mm deep. However, post-failure inspection of the test article revealed the presence of several hundreds of cracks within the critical region, see [11]. A fractographic evaluation of the specimen revealed that this population of cracks exhibited similar crack growth rates and that the cracks remained very small throughout the life of the component. Furthermore, the markings on the critical

crack could essentially be traced back to the beginning of the test, see [11] for more details.

In this test it was found, see [11], that existing NDI techniques could not be relied upon to find the critical crack. This conclusion highlights the need to develop both advanced NDI techniques as well as new analysis tools for the assessment of structural integrity, particularly when the critical component contains large numbers of interacting three dimensional flaws.

6. IMPLICATIONS FOR DESIGN AND ANALYSIS METHODOLOGIES

In previous sections we have seen that the trend in operating existing aircraft approaching or beyond their intended design life is often reflected in an increasing number of structurally significant defects. Indeed, the long service life of "ageing" aircraft increases the possibility of a reduction, or loss, of structural integrity due to fatigue. The particular problems discussed in this paper have been chosen to highlight importance of understanding and managing ageing structures and to highlight the need for simple (to use) and yet accurate damage assessment tools. From these case studies it is apparent that

1) A method of rapidly analysing cracks, including interacting cracks, in complex geometries and under realistic loading conditions, together with a capability to account for complex crack interaction is required.

The cracking in the Macchi spar, the F/A-18 488 aft bulk head and Mirage III wing skin are good illustrations of this.

2) A method is required for the rapid design and certification of composite repairs to primary structure.

This must allow for load dwells as well as for creep-fatigue interaction. The boron epoxy doubler on the F111C WPF is an apt illustration of this requirement.

6.1 Developments in the Analysis of 3-D Cracks

As outlined above one of the major operational requirements is for simple and accurate techniques for the rapid assessment of structural integrity. Consequently, the challenge is to develop analytical tools, which are simple to use, and which will allow the accurate and rapid assessment of complex

(structural) damage states. To achieve this goal the finite element alternating method [12,13] has been applied and is under development both in Australia and in the United States. One advantage of this method is that the cracks need not be modelled explicitly.

The alternating finite element technique makes extensive use of the analytical solution for a 3-D elliptical flaw subject to arbitrary crack face loading. In this context one of the first relevant solutions was obtained by Green and Sneddon [14] who solved the problem of a penny shaped crack, subject to uniform tension at infinity. Kassir and Sih [15] solved the problem of uniform shear loading along the crack face and obtained an exact solution in terms of two harmonic potential functions. This work was subsequently generalised by Vijayakumar and Atluri [13] who considered arbitrary normal as well as shear loading. These authors derived expressions for stress-intensity factors near the flaw border, as well as for stresses in the far-field, for these generalised loadings. The key to implementing this solution in the finite element alternating technique was the development, by Nishioka and Atluri [12], of a general procedure for evaluating the necessary elliptic integrals. To date this technique has been successfully applied to solve a range of three dimensional problems; viz. thick plates [12], pressure vessels [16], aircraft attachment lugs [17] and was recently extended by Hammond, Jones, Williams and Atluri [18] to include arbitrary interacting cracks.

One major advantage of this technique is that by combining the finite element method with the analytical solution we enable accurate results to be obtained using only a relatively coarse mesh. Furthermore, since cracks are not modelled explicitly this means that the crack configuration can be changed without complex re-meshing and as the crack geometry changes it also removes the need for tedious re-meshing. Consequently, for problems associated with WSFD and MSD the finite element alternating method provides a very efficient and cost effective method of analysis.

6.2 Semi-Elliptical Surface Flaws in a Semi-Infinite Body

6.2.1 A Single Flaw

To illustrate this approach let us first consider a single semi-elliptical surface flaw, with a surface crack length of $2a_1$ and a depth of a_2 , in an (semi) infinite body. For numerical purposes, in accordance with

common practice, the body was regarded as being infinite if its edges are further than five times the semi-major crack length away from the crack centre.

To model this situation using the finite element alternating technique only one quadrant was modelled, using a 6x6x6 mesh, because of the two planes of symmetry inherent in this problem. For the purposes of this analysis, the material properties were chosen as $E=70 \times 10^9 \text{ Nm}^{-2}$ and $\nu=0.33$, i.e aluminium and a remote tensile stress of 1000 MPa was assumed. In the first set of cases considered we have $a_1=18\text{mm}$, the width $b=200\text{mm}$ and the crack aspect ratios (a_2/a_1) was varied.

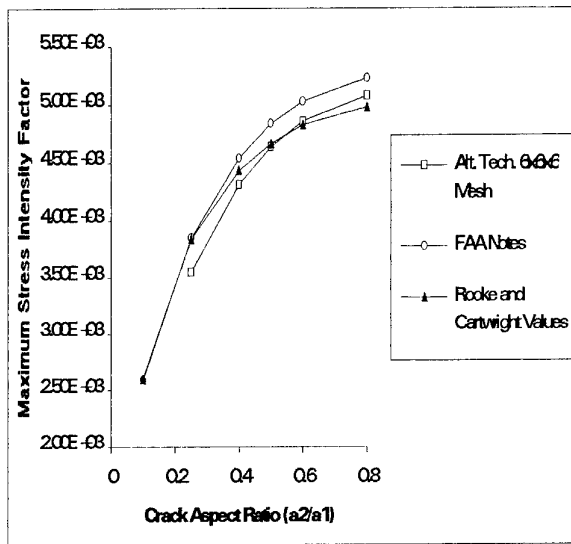


Figure 2. Comparison of the maximum stress intensity factor versus crack aspect ratio (a_2/a_1) for a semi-elliptical surface flaw in a semi-infinite body with [19,20]. (In all cases $a_1=18\text{mm}$ and $b=200\text{mm}$)

In this instance the maximum stress intensity factor occurs at the point on the crack face which is deepest into the solid. To illustrate the accuracy of this technique the values obtained for the maximum stress intensity factor, for different crack aspect ratios, were compared with two different sets of published values, [19,20]. The results of this analysis can be seen in Figure 2. The mean difference between the finite element alternating technique values and those of Rooke and Cartwright [19] is 3.8%, whilst between the finite element alternating technique and those published by the FAA [20] is 4.6%. Given the

uncertainties quoted (approximately 5%) in the published values these differences were deemed to be well within acceptable limits. Furthermore, the values obtained also tend to lie between those given in [19] and those given in [20]

6.2.2 Two Identical Surface Flaws

Having established the validity of the model for one crack, the problem was subsequently extended to include two interacting coplanar semi-elliptical surface cracks in a semi-infinite body, see Figure 3. In the following cases the crack aspect ratio (a_2/a_1) was fixed at 0.8 and d , the distance between the centres of the two cracks, was held constant at 100 mm. The crack separation ratio ($\lambda=2a_1/d$) was then allowed to vary, and values of the mode I stress intensity factor were calculated at 5° increments along the crack front.

The results of this analysis can be seen in Figure 4. This graph indicates that for two interacting cracks, the point of maximum stress intensity factor is no longer the point which lies deepest into the solid. This behaviour is in fact only seen when the cracks are relatively far apart ($\lambda < 0.3$) and are essentially acting independently of each other. As the crack spacing decreases, the position of the point with the largest K_I gradually shifts away from C ($\theta=90^\circ$), the point furthest into the solid, towards point A ($\theta=0^\circ$). Physically this means that as crack spacing decreases interaction effects become more pronounced and the cracks begin to grow preferentially towards each other rather than progressing further into the bulk of the solid.

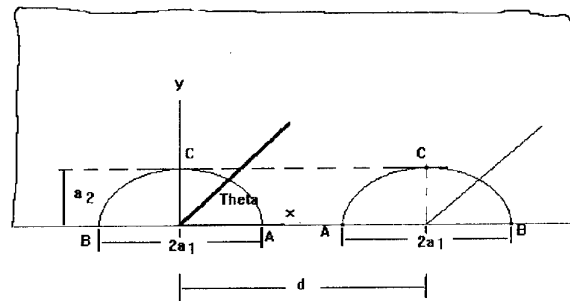


Figure 3. Two identical interacting surface flaws

To investigate the effect of crack aspect ratio on the stress intensity factor, and on the magnification factors, attention was then focused on the point of the crack which was deepest into the solid. In all cases the distance between the crack centres was fixed at 100 mm. Two different crack separation ratios were considered; viz. $\lambda=0.5$ and $\lambda=0.8$. As d was fixed at 100 mm the first case implies that $a_1 = 25$ mm whilst the second implies $a_1 = 40$ mm. The values of a_2 were then allowed to vary. The relationship between stress intensity factor at C ($\theta=90^\circ$) and crack aspect ratio is illustrated in Figure 5. It must be remembered that the position of the maximum stress intensity factor is different for these two curves. Figure 5 shows that as the cracks get larger (ie. as a_2 increases) the stress intensity factor at C° also increases. It thus appears, that at the point where the cracks protrude deepest into the solid, the crack separation is a more crucial factor than the crack shape.

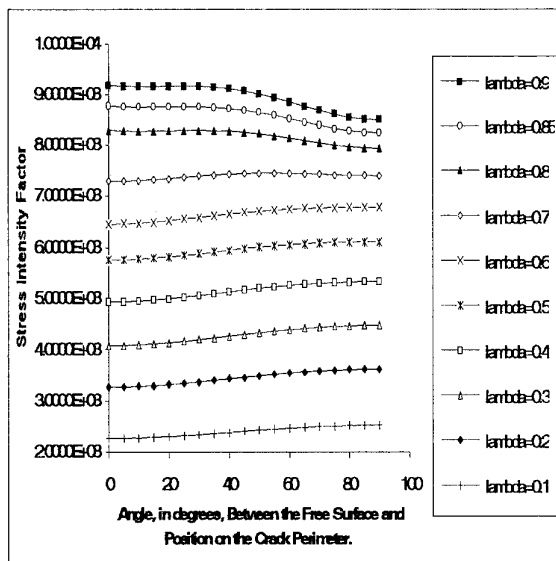


Figure 4. Variation in maximum stress intensity factor with elliptic angle, $0 < \theta < 90$, for one of a pair of semi-elliptical surface flaws in a semi-infinite body. (In each case $a_2/a_1 = 0.8$, with (λ) lambda = 0.1, 0.2, 0.3, 0.4, 0.5, 0.6, 0.7, 0.8, 0.85 to 0.9)

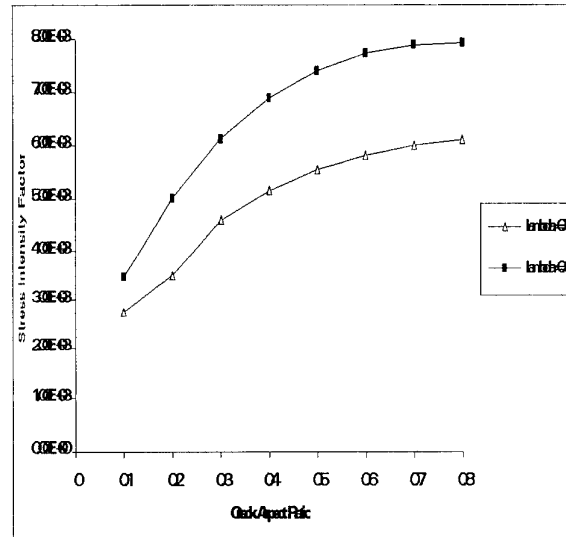


Figure 5. Variation in maximum stress intensity factor with crack aspect ratio for one of a pair of identical semi-elliptical surface flaws in a semi-infinite body. (In all cases $d = 100$ mm, Δ - lambda = 0.5, \square - lambda = 0.8)

7. RAAF STRUCTURAL INTEGRITY PROGRAM

In the recent restructuring of the RAAF (AirLogistics) the ASI Section (ASI-LSA) of the Directorate of Technical Airworthiness (DTA-LSA) is responsible for the carriage of ASI management. Central to this policy is the objective of ASI management: "... to enable operations to be conducted within an acceptable level of risk of structural failure and to preserve the asset to its planned life-of-type". The resultant RAAF aircraft structural integrity management plan is clarified in the recent RAAF Technical Airworthiness Management Manual [2] which

- a. Describes the RAAF Aircraft Structural Integrity Program
- b. Defines the standards and procedural guidance necessary to achieve, maintain and assure structural integrity of RAAF and Army aircraft
- c. Establishes a standard with which individual ASIP's, which are specific to a particular aircraft fleet, shall conform; and
- d. Specify an acceptable method of compliance with the ASIP requirements."

To achieve these objectives [2] requires that the following outcomes must be achieved; viz:

- “constraint of the risk of failure of an aircraft to an acceptable level
- achievement of the planned rates of availability
- avoidance of the un-forecast cost of re-furbishment
- achievement of the planned life-of-type”

Furthermore, when discussing repairs it is required [2] that

“(1) damage tolerant principles are applied for the design of repairs, and modifications, with particular care taken of the potential interaction of multiple repairs;

(2) inspection intervals are established to ensure their continued integrity; and

(3) assessment is made of their impact on the structural integrity management of the aircraft. When a damage tolerant assessment is unable to be completed within the time scale required for the return of the aircraft to operational status the procedures described in Annex F are to be implemented”

7.1 Composite Repairs For Primary Structure

The Australian experience [2, 3, 7, 9] has shown that composite repairs are often particularly useful for maintaining continued airworthiness. However, when considering the certification of composite repairs to primary structure two important points need to be addressed, viz:

- 1) The development of an appropriate certification standard/methodology;
- 2) The development of accurate and rapid design tools.

The first point was the topic of two recent reports [21,22] which detailed a potential certification process, based on existing FAA guidelines, together with a history of previous failures. Interestingly, this study revealed the importance of accounting for interlaminar failure (in the doubler/repair) in the design process, see [22].

The advent of damage-tolerant design has (to some extent) complicated the approval procedures both for

mechanical and for adhesively bonded repairs. In some cases the repairs may be airworthy when completed, but it may not be possible to complete the damage-tolerance evaluation for long term airworthiness before returning the aircraft to service. These practicalities have resulted in an FAA Advisory Circular, AC No: 25.1529-1, whereby an interim repair approval process is allowed. Initially, the repair is required to be structurally sound relative to static strength. However, final approval of the repair is only given when long term (ie. continuing) airworthiness has been evaluated, see [21].

A modified form of the FAA approach has subsequently been recommended in [21, 22]. However, it was also recommended that composite repairs should not be attempted to damaged structures where the residual strength has been reduced beneath 1.2 times limit load, see [21, 22] for more details.

In this context it has been shown [22] that the failure loads of composite joints/repairs are often load history dependent. This is clearly shown in Figure 6, which presents the measured displacements (at the load point) and failure loads for a symmetric graphite epoxy lap joint tested at various loading rates. In this work the loading rates were 0.01, 0.1, 10 and 200 kN/s.

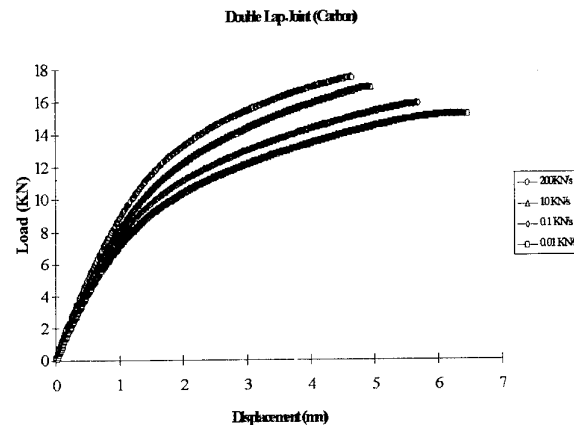


Figure 6. Experimental load displacement curves for a symmetric graphite epoxy lap joint with loading rates varying of 0.01, 0.1, 10, and 200 kN/s.

To account for this observed load history dependence the (“Hart-Smith”) design formulae [24] used in the PABST [25] program are being extended and a “constitutive equation based” approach to the design of bonded joints and, by analogy, composite repairs is under development [23]. One specific objective of this work, besides obtaining a more accurate representation

of the stress-strain state in the joint/repair, is to address the, commonly observed, problem of interlaminar failure in the composite repair (doubler) itself, see [22], a failure mechanism that is not addressed in [24].

To assess the susceptibility of joints/repairs to interlaminar failure requires a knowledge of the associated fracture toughnesses. Here recent work at Monash has revealed that the measured values of G_{IC} are strongly load history dependent. Consequently, one of the major thrusts of the research program is to develop valid analytical and experimental tools and the associated materials data base capable of accounting for this observed load history dependence.

7.2 Summary

The RAAF views Aircraft Structural Integrity management as a critical activity in the Life-of-Type management of the fleet and the Defence Science and Technology Organisation is a key element in the overall ASI management program. However, the need for indigenous expertise in this field is high and wherever possible the RAAF is trying to provide greater Australian Industry involvement. Consequently, Design Support and Technology Support Networks are now being established to facilitate access to local expertise.

8. CONCLUSION

Since Mann [1] produced his over view paper on Australian directions in aircraft fatigue there have been a number of very significant changes both within the RAAF, Universities and in the Australian Aerospace industry. The problem of aging aircraft has also become even more acute and visible, both nationally and internationally. It is in this environment that the RAAF has produced its recent manual [2] on the management of structural integrity and this approach is reflected in the Macchi MB326H Aircraft Structural Integrity Management Plan [4].

The problems discussed in this paper have been chosen to illustrate particular aspects of this phenomenon as well as to highlight perceived future needs, both in the fields of certification and in damage assessment. Furthermore, given the importance of maintaining continued airworthiness and the diversity of potential problem areas it is believed that collaboration, both inter and intra nationally is essential if significant

progress is to be achieved.

9. References

1. Mann J. Y., "Aircraft fatigue-with particular emphasis on Australian operations and research", Defence Science and Technology Organisation, Aeronautical Research Laboratory, Structures Tech. Memo 361, 1983.
2. Technical Airworthiness Management Manual, Defence Instruction (Air Force) AAP 7001.053, November 1994.
3. R. Jones, "Chapter 4, Crack patching: Design aspects", Bonded repair of aircraft structure, edited by A. A. Baker and R. Jones, Martinus Nijhoff, 1988.
4. Young G. D., Macchi MB326H Aircraft Structural Integrity Management Plan, Issue 1, RAAF Logistics Systems Agency, Logistics Command, Melbourne, Australia, December 1994.
5. Buntin, W.D., "Concept and conduct of proof test of F-111 production aircraft", Paper presented to R. Aero. Society, 27 October 1971, London, England.
6. Bland, L., "Final engineering report: A8-112 wing pivot fitting failure investigation, (Manufacturing processes)", FZM-12-5130A, General Dynamics, Fort Worth, USA, June 1982.
7. Molent L., Callinan R. J. and Jones R., "Design of an all boron epoxy doubler for the F-111C wing pivot fitting: Structural aspects", Journal of Composite Structures, 11, 1, pp. 57-83, 1989.
8. Kuruppu M. D., Williams J. F., Bridgford N., Jones R. and Stouffer D. C., "Constitutive Modelling of the elastic-plastic behaviour of 7050-T7451 Aluminium Alloy", J. of Strain Analysis, 27, 2, 85-92, 1992.
9. Jones R., Molent L., Paul J., Saunders T., Chiu W. K. (1994), "Development of a composite repair and the associated inspection intervals for the F111C stiffener runout region", FAA/NASA International

- Symposium on Advanced Structural Integrity Methods for Airframes Durability and Damage Tolerance, NASA Conference Publication 3274, Part 1, pp 339-351, 1994.
10. Molent L., "Stress analysis of F-111A sealant injection holes", Defence Science and Technology Organisation, Aeronautical Research Laboratory, Aircraft Structures Tech. Memo 502, 1989.
 11. Barter S. and Clark G., Fatigue and fracture control in components from modern military aircraft, Proceedings International Aerospace Congress 1991, Melbourne, Australia, 12-16th May, 1991, Vol 1, pp35-43, 1991.
 12. Nishioka, T. and Atluri, S.N., "Analytical Solution for Embedded Elliptical Cracks, and Finite Element Alternating Method for Elliptical Surface Cracks, Subject to Arbitrary Loadings", Eng. Fracture Mech., Vol. 17, No. 3, 1983, pp. 247-268.
 13. Vijayakumar K. and Atluri S. N., "An embedded Elliptical Crack, in an Infinite Solid, Subject to Arbitrary Crack-Face Traction". Journal of Applied Mechanics. Vol. 48 March 1981.
 14. Green, A.E. and Sneddon, I.N., "The Distribution of Stress in the Neighbourhood of a Flat Elliptical Crack in an Elastic Solid", Proc. of the Cambridge Phil. Soc., Vol. 46, 1950, pp. 159-163.
 15. Kassir, M.K. and Sih, G.C., "Three-Dimensional Stress Distribution Around a Crack Under Arbitrary Loading", J. Appl. Mech., Vol. 33, 1966, pp. 601-611.
 16. Nishioka, T. and Atluri, S.N., "Analysis of Surface Flaws in Pressure Vessels by a New 3-Dimensional Alternating Method", J. Pressure Vessel Tech., Vol. 104, No. 4, 1982, pp. 299-307.
 17. Nishioka, T. and Atluri, S.N., "An Alternating Method for Analysis of Surface Flawed Aircraft Structural Components", AIAA J., Vol. 21, No. 5, 1983, pp. 749-757.
 18. Hammond S., Jones R., Williams J. F. and Atluri S. N., Developments in the assessment of flaw criticality", Proceedings 6th Australian Aeronautical Conference, pp 173-177, 20-23 March, 1995, published by The Institution of Engineers Australia, National Conference Proceedings NCP 95/1, ISBN (Book) 0 85825 624 X, March 1995.
 19. Rooke, D.P. and Cartwright, D.J., "Compendium of Stress Intensity Factors", Her Majesty's Stationery Office, London, 1976.
 20. Swift, T. "Damage Tolerance Technology, A Course In Stress Analysis Oriented Fracture Mechanics", Federal Aviation Administration.
 21. Jones R. and Smith, "Continued Airworthiness Of Composite Repairs To Primary Structures For Military Aircraft", Proceedings 6th Australian Aeronautical Conference, pp 311-316, 20-23 March, 1995, published by The Institution of Engineers Australia, NCP 95/1, ISBN (Book) 0 85825 624 X, also in Journal of Composite Structures (in press).
 22. Jones R. , Chiu W. K. and Smith, R., "Airworthiness Of Composite Repairs: Failure Mechanisms", Engineering Failure Analysis, (in press)
 23. Jones R. , Tripit B., Chiu W. K. and Tomas J., "Lap joint theory revisited", Journal of Polymers and Polymer Composites, 1995, vol 3, pp 1-9.
 24. Hart-Smith L. J., Adhesively bonded double lap joints, NASA Langley Research Center Report NASA CR-112235, January 1973.
 25. Thrall E. W., Primary adhesively bonded structure technology (PABST): Design handbook for adhesive bonding, USAF Technical Report, AFFDL-TR-79-3119, 1979.

DAMAGE TOLERANCE TO WFD (*) ON COMBAT AIRCRAFT AN APPLICATION TO A METALLIC WING LOWER PANEL

R.J. Cazes and F. Goerung
Dassault Aviation
DGT/DEC
78, Quai Marcel Dassault
92214 Saint-Cloud
FRANCE

Synopsis

Maintaining the structural integrity of aircraft in prolonged service requires consideration to be given to inspections for detecting possible multiple damage.

This paper presents an assessment of the structural behaviour of a (metallic) underwing panel of which several bays between stiffeners may be corroded both on their surface and within their thickness.

The analysis of tolerance to damage highlights the importance of statistical feedback from inspections for establishing hypotheses of structural damage with which to predict behaviour, and highlights the particular attention to be paid to structures in a saline or corrosive environment.

Introduction

The concept of "Resistance to damage" implies that structures which are able to tolerate the presence of cracked elements by ensuring cracks are slowly propagated and to tolerate the presence of broken elements by providing load path redundancy [1]. On this basis, the strength of the remaining undamaged structure must be sufficient to ensure safety in flight during a specified operating period.

The structural analysis is carried out in several stages (Fig. 1)

- selection of critical points of the structure
- establishment of initial damage hypotheses
- calculation of residual strengths
- establishment of a structural maintenance programme

Within this context, the implementation of structural inspections, with prior identification of the detection thresholds applying to the recommended NDT methods, allows each critical area, which should be accessed for inspection (...and repair), to be attributed a time in operation which can be extended at intervals.

(*) *"Widespread Fatigue Damage"*

Widespread structural damage

The simultaneous occurrence and/or the interaction of damage (coalescence and/or rapid extension before detection) is liable to compromise, providing the required factors of safety, the residual resistance to the maximum loads in flight.

The types of damage most frequently cited [2] are (Fig. 2) :

- "multi-site" damage (MSD) which can mainly occur on neighbouring elements (lines of attachment holes, for example) or as a result of a fabrication surface damage (long, continuous scratch, for example). Their coalescence can lead to a sudden loss of residual strength.
- "multi-element" damage (MED) which can occur on periodically spaced strengthening elements. Damage of this type generally causes a reduction of load path redundancy.

Under these conditions, an aggravating factor (corrosion for example) is likely to lead to the development of "widespread" damage in those areas which combine :

- repetitive structural elements (for example regularly spaced, identical frames or stiffeners),
- approximately comparable loads or stress levels on all of these elements.

The subject of this paper has been derived from a case of corrosion noted in operation on the MERCURE aircraft. (*)

- (*) The MERCURE twin-engine commercial jet, with a capacity of approximately 150 passengers, was designed by Dassault Aviation at the beginning of the 1970s. Approximately ten of the planes were put into service on internal French routes with the (successfully achieved) objective of completing 40,000 flights (objective proven on the basis of 120,000 simulated flights in the fatigue testing cell). The final (gradual) withdrawal of those aircraft still in service is planned for mid 1995.

Corrosion damage on the MERCURE

The damage which concerns us here was discovered after approximately fifteen years of operational service. They concern the lower skin (fully machined stiffened panel made from 2024 T351) of the centre section and the external wings, and have various causes :

- for the centre section : external corrosion due to the presence of water condensation over the lower surface of the skin (Fig 3),
- for the wings : internal corrosion due to bacteriological action in the bottom of the fuel tank (Fig 4).

This corrosion has, in both cases, caused material damage over several, frequently neighbouring panel bays, which has led to variable reductions in thickness over their surface and sometimes reaching several mm in depth.

- Mechanism of deterioration : bacterial corrosion

Various families - microscopic organisms (fungus, bacteria) present in the particles and the impurities in suspension in the air or the fuel can contaminate the aircraft's structural tanks. Under certain conditions of temperature and humidity, these micro-organisms will proliferate and form more or less viscous and putrid clusters or filaments. These colonies concentrate themselves on the walls of the tanks, in the lower parts where undrained liquid remains and where these clusters find the water necessary for their growth. Some of these micro-organisms use oxygen, others don't. Finally, these colonies can come away from the walls of the tanks and affect the operation of the fuel gauges and (or) block the filters, all the more so if they amalgamate with various foreign bodies.

These micro-organisms indirectly destroy the enamel and the seals. In fact they reduce the sulphates which can be present in this area. This oxydoreduction creates sulfuretted compounds which, when mixed with the free water which accumulates in the retention points or with the water in emulsion in the fuel, produce sulphuric acid.

This has two consequences :

- there is a risk that the leak tightness of the structure will no longer be assured,
- the corrosive action of the products of the micro-organism's metabolism gradually strips the internal surface of the tanks.

Thus, the paint work, then the anodised chrome are gradually destroyed, leaving the aluminium alloy of the underwing panel exposed to corrosion.

Study on a combat aircraft wing panel

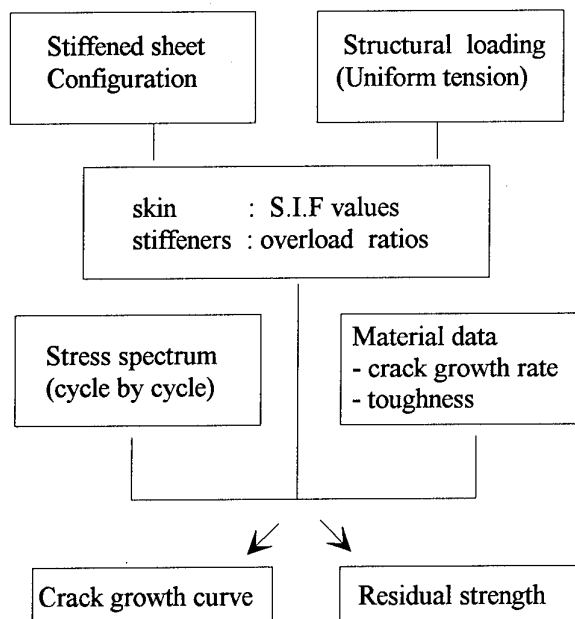
On a combat aircraft, the lower wing is one of the elements most subject to fatigue stresses and generally the one containing the points which are most critical to the sizing of the elements.

The optimisation of stresses with respect to operating lifetime objectives ("free crack life" and "crack propagation life"), by ensuring that the values obtained remain as close as possible to allowable stress values, leads to the generation of more or less uniform stresses over large areas of the skin (Fig 5). These areas, with their repetitive layout and iso-stress conditions, provide conditions that are favourable to the development of multiple damage.

The studied example here relates to the development of assumed cracks on an wing lower skin with machined stiffeners, where corrosion has been modelled by reducing the thickness of the skin or that of the stiffeners.

The influence on the crack growth rates and residual strengths is evaluated for various crack scenarios and two types of alloy (2214 T651 and 7010 T7451).

The procedure adopted for the study of cracks (Fig. 6), in accordance with the principles of fracture mechanics, is recalled below :



Panel damage modelling

The calculations were carried out for a model representing a flat panel symmetrically consisting of 6 contiguous bays with 25 mm high regularly spaced machined stiffeners (pitch $2b \approx 80$ mm), subjected to a tensile force (see Fig 7). Considering loads at the end of the panel relates an uniformly imposed displacement on the original (non corroded) panel definition. The resulting loading distribution is applied unchanged on other (cracked) panel configurations.

Corrosion damage was represented by a thinner strip over the full width of a :

- skin : - 20 % or - 40 % of the nominal thickness (original $t = 3$ mm)
- stiffeners : - 50 % of the nominal thickness (original = 2.8 mm) over half the height.

The configurations used for the calculation of crack growth rate and residual strength are respectively (Fig.8) :

- A : cracking of skin within a central bay between two stiffeners (all stiffeners partially corroded or not corroded at all)
- B : cracking of skin about a completely broken stiffener (other stiffeners partially corroded or not corroded)

The results are presented in parametric form as a function of reduction in material thickness (Δt) due to corrosion.

Stress Intensity Factor (SIF)

The SIFs at the tips of the cracks are obtained from energy equilibrium which gives the following relationship :

$$K(a) = \sqrt{E \frac{\Delta W}{\Delta S}}$$

where :

- a = the crack half length
- K = SIF in mode I
- E = Young's Modulus of the material
- ΔW = energy expended by external forces for a crack extension of Δa
- ΔS = surface cracked during extension ($\Delta S = t \times \Delta a$)

The SIF values have been calculated for the previously defined load distribution. The results are further presented in Tables 1 and 2 in chapter "Results of calculations".

It should be noted that the technical literature ([4] and [5]) allows the SIFs to be calculated for stiffened panels

and in particular used for the basic case (Fig. 8-A) of this study from the stiffening ratio :

$$\mu = \frac{A_{st}}{A_{st} + 2bt}$$

where :

- A_{st} = standard section of stiffener
- $2b$ = bay pitch between stiffeners
- t = thickness of skin

The value of the ratio μ for the different cases modelled varies between 0.2 and 0.3.

Stiffener overload

The overload on the stiffeners adjacent to the cracked section, is represented by the relationship :

$$L(a) = (F_{max}/A_{st}) / (F_{remote}/A_{st_{nominal}})$$

where :

- F_{max} = overall load on the stiffener in the damaged section
- F_{remote} = imposed load applied at the ends of the stiffener
- A_{st} = section of stiffener in the presence of "corrosion"
- $A_{st_{nominal}}$ = undamaged stiffener standard section

The results are further presented in the tables 1 and 2.

Residual strength

For this example of study, the critical crack lengths are those associated with $1.2 \times$ Limit Load (g-load factor $n = 1.2 \times 9$). The associated panel loading stress is considered proportional to the load factor ($\sigma/g \sim 22$ Mpa in nominal thicknesses).

The determination of the critical lengths is obtained from the comparison of 2 criteria (*) :

- the obtention of an SIF value (K_{max}) at the tip of the crack which is equal to the toughness (K_c), for in-plane stresses of the material in 3 mm thickness :

$$K_{max} = K_c$$

- the obtention of the failure load (F_{ult}) the most heavily loaded stiffener (ultimate stress σ_{ult} , without giving any consideration to stress gradients)

$$F_{max} = \sigma_{ult} \times A_{st}$$

- (*) there have been no consideration of yielding in the remaining skin.

The characteristics of the two materials considered for this study are :

sens TL	(2214 T651)	(7010 T74)
σ ultimate (σ ult)	~ 450 MPa	~ 500 MPa
Toughness (Kc)	~ 100 MPa \sqrt{m}	~ 130 MPa \sqrt{m}

The critical values $[K/K_0]_c$ (*) and $[L]_c$ are established in table 3 to allow the determination of the lengths for the required residual strength.

- (*) K_0 = SIF for infinite non stiffened panel
- K = SIF for studied stiffened panel
- L = stiffener overload ratio

Results of calculations on panel (SIF and L)

Notation : a = crack half-length
 2b = regular spacing of stiffeners
 $K_0 = K_0 = \sigma \sqrt{\pi a}$

- Calculation A : Crack in the middle of a bay between 2 unbroken stiffeners

TABLE 1

		a/2b	0.1	0.2	0.3	0.4	0.45	0.50
K/K ₀	$\Delta t = 0\%$	1.00	0.99	0.99	0.98	0.95	0.77	
	$\Delta t = 20\%$	1.21	1.19	1.18	1.15	1.10	0.88	
	$\Delta t = 40\%$	1.55	1.51	1.48	1.42	1.35	1.04	
	MCD *	1.26	1.25	1.23	1.21	1.18	1.05	
L	$\Delta t = 0\%$	1.09	1.11	1.15	1.22	1.31	1.60	
	$\Delta t = 20\%$	1.16	1.18	1.23	1.30	1.38	1.71	
	$\Delta t = 40\%$	1.27	1.30	1.35	1.43	1.56	1.86	
	MCD *	1.33	1.36	1.41	1.48	1.59	1.87	

- Calculation B : Cracks to either side of a severed stiffener

TABLE 2

		a/2b	0.2	0.4	0.6	0.8	0.9	1.00
K/K ₀	$\Delta t = 0\%$	1.17	1.07	1.02	0.99	0.96	0.74	
	$\Delta t = 20\%$	1.34	1.23	1.18	1.13	1.09	0.82	
	$\Delta t = 40\%$	1.82	1.55	1.44	1.36	1.29	0.93	
	MCD *	1.41	1.27	1.21	1.16	1.13	0.96	
L	$\Delta t = 0\%$	1.11	1.22	1.31	1.42	1.58	2.09	
	$\Delta t = 20\%$	1.28	1.32	1.38	1.50	1.62	2.15	
	$\Delta t = 40\%$	1.38	1.42	1.51	1.63	1.77	2.32	
	MCD *	1.50	1.54	1.61	1.74	1.88	2.38	

- * MCD = Multiple Corrosion Damage
- $\Delta t = -20\%$ within the bottom of the panel
- and -50% over half the stiffeners height

- Residual strength for 1.2 x Limit Load

TABLE 3

	a/2b	0.2	0.4	0.6	0.8	0.9	1.00
$[K/K_0]_c$	2214 T651	1.80	1.25	1.03	0.89	0.84	0.80
	7010 T7451	2.35	1.63	1.34	1.16	1.09	1.03
$[L]_c$	2214 T651	1.80	1.80	1.80	1.80	1.80	1.80
	7010 T7451	2.00	2.00	2.00	2.00	2.00	2.00

The results are presented in graphic form in figure 9.

Fatigue load spectrum

The loading used for lifetimes evaluation was determined from statistical information obtained in service from aircraft in the French Air Force. The load factor spectra ($n_{max} = 9$) was broken down into randomly distributed, discrete repetitive blocks of 200 flights (6 different flight profiles) (Fig. 10).

Crack propagation life evaluation

The rates of propagation were established by experimenting on plate test samples (notched sheets). Loads were applied to these test samples in accordance with the flight spectrum described above. The results obtained are average growth rates per flight $da/flight = f(K_{max})$, where K_{max} is the SIF value associated with $n = 9$ in accordance with the crack length.

The crack growth rates have been established [5] for both of the aluminium alloys (2214 T651 and 7010 T74) in a number of different environments (laboratory, wet air and salt wet air) (Fig. 11).

The experimental $da/flight$ curves which, moreover are useful for validating the predictive models, were linearised (Fig. 12) and used in the time of propagation calculations presented here.

Panel critical cracking lengths and life times

The tables 4 and 5 have been established by integrating the $da/flight = f(K_{max})$ laws for cracking in the presence of corrosion (depth Δt equal to 20% and 40% of nominal thickness) in previous different ambient environments. The growth rates of the assumed cracks were established by considering these values of Δt to remain constant during cracking (propagation of a crack in the centre of a bay from an initial length of $2 a_1 = 6.35$ mm).

Life times for 2214 T651

Skin crack at the centre of a bay between 2 unbroken stiffeners

TABLE 4

	air labo (Reference)	wet air
$\Delta t = 0\%$ (Reference)	1	x 0.8
$\Delta t = -20\%$	x 0.62	x 0.47
$\Delta t = -40\%$	x 0.41	x 0.30
MCD *	x 0.51	x 0.38

- * MCD = - 20% within the bottom of the panel and
- 50% over half the stiffeners height

Life times for 7010 T7451

Skin crack at the centre of a bay between 2 unbroken stiffeners

TABLE 5

	air labo (Reference)	wet air
$\Delta t = 0\%$ (Reference)	1	x 0.61
$\Delta t = -20\%$	x 0.65	x 0.38
$\Delta t = -40\%$	x 0.42	x 0.23
MCD *	x 0.53	x 0.30

- * MCD = - 20% within the bottom of the panel and
- 50% over half the stiffeners height

Critical lengths for 1.2 x Limit Load

Skin cracking either side of a broken stiffener

reminder of notation :

a = crack half length

2b = bay pitch between stiffeners

TABLE 6

		2214 T651	7010 T74
$\Delta t = 0\%$	(nominal)	2 x (a/2b = 0.60)	2 x (a/2b = 1)
MCD *	corroded	2 x (a/2b = 0.35)	2 x (a/2b = 0.70)

- * MCD = - 20% within the bottom of the panel and
- 50% over half the stiffeners height

All of these results are presented in diagrammatic form in figure 13.

Conclusion

This study of resistance to damage on the wing skin of a combat aircraft shows that the assumption of widespread degradation affecting material thickness gives predicted crack growth rate and residual strength values that are very severe (Fig. 13).

The repetitive nature of the constituent elements (evenly spaced stiffeners) and the uniform stress levels which exist mean that any (multiple) damage which may eventually be present has a particularly penalising effect. To be able to fully predict the behaviour on aircraft requires basic hypotheses to be established that reflect reality as far as possible.

Within this context, possible corrosion located in a petrol storage area adds the particularly serious prospect of internal, non perforating damage, progressively reducing the thickness of the skin over a large area, or over the height of the stiffeners, and not easily detected from without (Fig. 14). A notable reduction in the possibilities for detecting damage before reduction of residual strengths occurs, in particular for materials having high crack propagation rates in wet environments, leads us to recommend :

- the early implementation of preventive actions to ensure the durability of the surface protections (see example in Appendix).
- the selection (theoretical studies and feedback from inspections), of those areas of the structure which are prone to these sorts of damage in order to implement the (economic?) actions necessary for the required level of safety.

REFERENCES

- Ref. [1] Military Specification Airplane - Damage Tolerance Requirements MIL-A-83.444 (USAF), 1974
- Ref. [2] Goranson U.G. - "Damage Tolerance - Facts and Fiction" - 14th Plantema Memorial Lecture (ICAF), Stockholm, 1993.
- Ref. [3] Poe C.C. - "Stress Intensity Factors with a cracked sheet with Riveted and Uniformly Spaced Stringers" - NASA Technical Report R-358 Langley Research Centre, May, 1971.
- Ref. [4] Nicholls, Jefferson, Martin - "Integral Structures Practical Applications of Fracture Mechanics" - AGARD Conference Proceeding N° 257, 1980.
- Ref. [5] Goerung F. - "Influence de l'environnement sur la vitesse de propagation des fissures de fatigue (2214 T651 et 7010 T7451)" - CNAM Thesis, 1993.

ACKNOWLEDGEMENTS

The authors wish to thank their colleagues Mr. GOURLAOUEN for his advice and comments, Mrs. BOYER for the Finite Element modelling and Mrs CREVEFOSSE for the text issue.

In the event of alteration of the coatings or of structural corrosion, factory repairs will be required to be carried out before decontaminating treatment can proceed (cleaning and finishing of the corroded areas and repair of seals).

APPENDIX

Treatment of bacteriological contamination

There are four main factors which allow micro-organisms to proliferate in fuel tanks :

- a temperature of between 25 and 35°C
- the presence of free water or water in emulsion in the fuel
- the presence of oxygen (for aerobic organisms)
- a period of time of between 0 days (germs already present in the fuel at the time of filling) and 1 month (maximum germination period).

- Preventive measures

Being unable to take any action concerning the first 3 factors, preventive maintenance will aim firstly to limit, as far as possible, the accumulation and the stagnation of water in the tanks by means of regular draining, and secondly to periodically destroy the existing organisms by means of a fungicidal or bactericidal additive which will significantly reduce their growth. With this in mind, Dassault-Aviation has recommended the injection of 135 ppm of a BIOBOR decontaminating additive, or similar, in the fuel stream, at best using a venturi device during the filling of the fuel tenders.

The decontaminant comes in a liquid based on boron compounds which are soluble in Kerosene. In addition to a fungicidal action, it has been noted that this product has a cleaning effect which may cause various impurities to be removed from the bottom of the tanks. Operations are carried out before and after treatment to reduce the risk of the filters becoming blocked in flight.

- Curative measures

The application of a treatment to cure biological contamination is required in the case that contaminants are shown to be present in the fuel either through testing or following the occurrence of operating anomalies on the motor pump, the transfer valves or the gaugers.

Comment : the actions to be carried out prior to eventual treatment of the contamination are

- a more detailed analysis of the fuel
- inspections of the tanks and the fuel circuits to assess the extent of structural deterioration

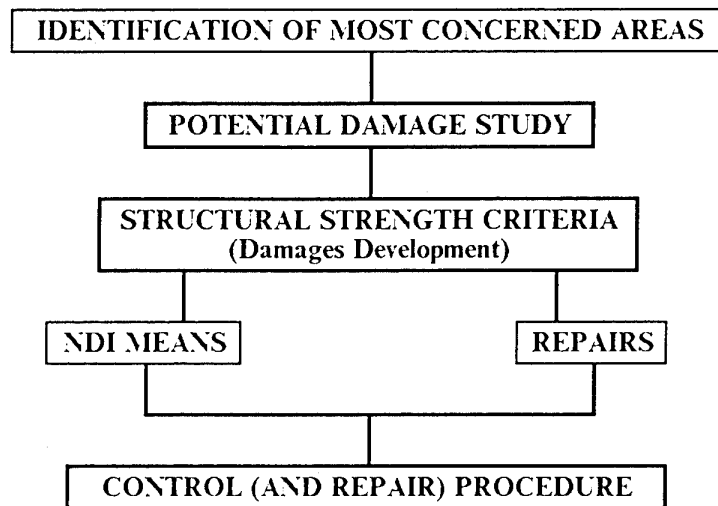
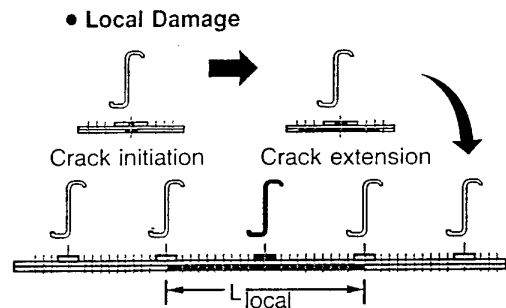
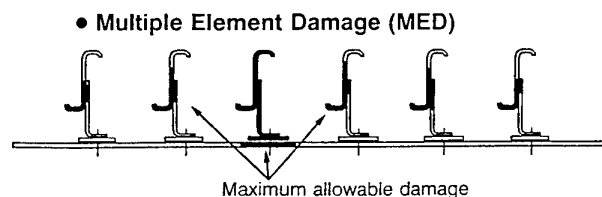
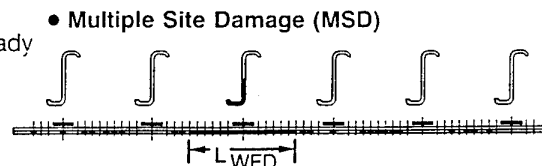


Fig. 1 - Chartflow of In-Service Inspection Criteria



- Maximum allowable damage shown
- Damage connection up to this size is tolerated
- No significant damage beyond this region
- All MSD or MED within this area is local and already accounted for in damage tolerance analysis



- Widespread similar details
- Similar stresses
- Structural interaction with reduced allowable damage

"Damage Tolerance : Facts and Fiction"
Goranson U.G. - 14th Plantema Lecture
ICAF, Stockholm, 1993

Fig. 2 - Prone Features for Widespread Fatigue Damage

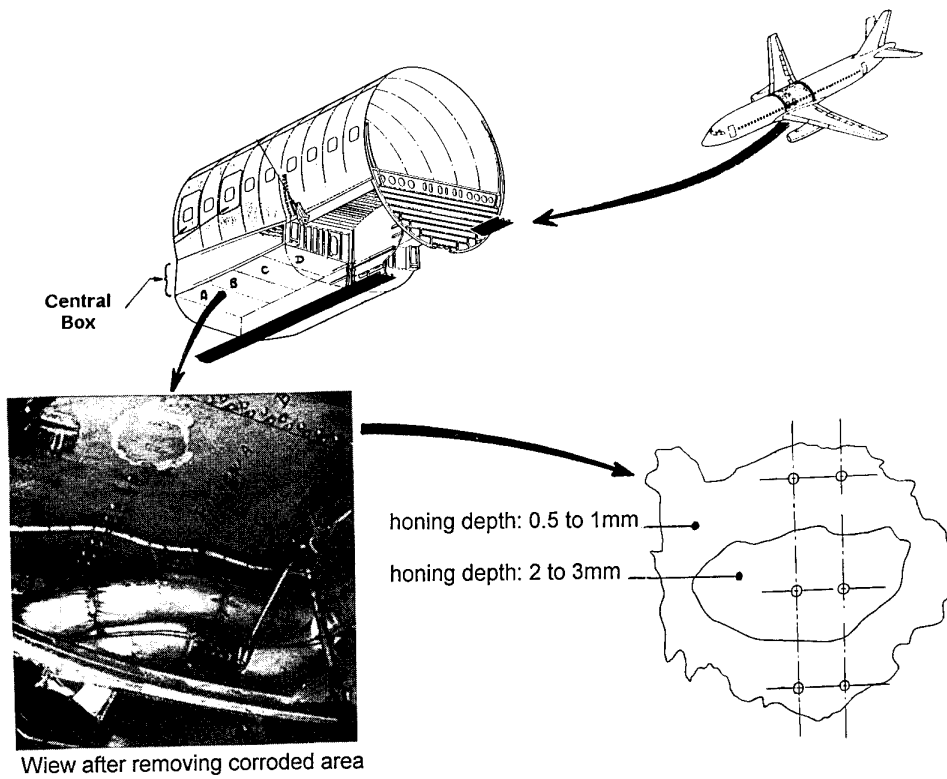


Fig. 3 - MERCURE Aircraft : External Corrosion on Central Structural Box

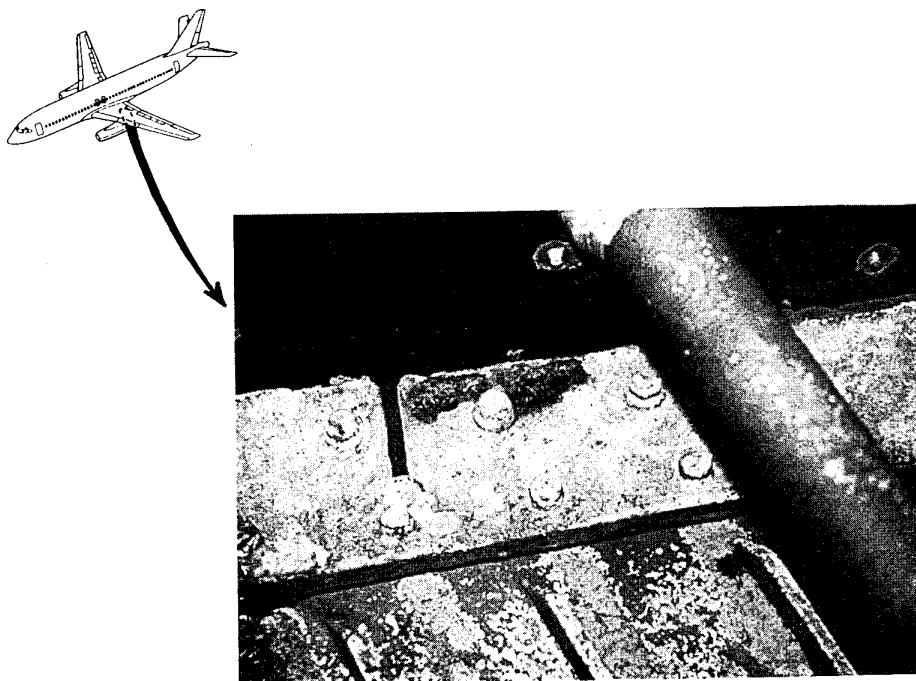


Fig. 4 - MERCURE Aircraft : Internal Corrosion on Wing Lower Panel

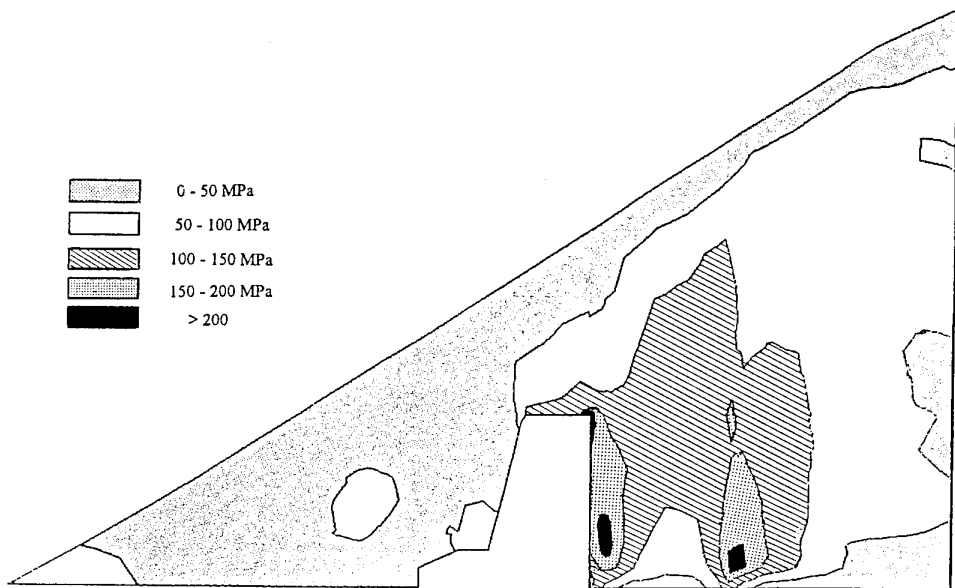


Fig. 5 - MIRAGE 2000 - Wing Lower Panel : Stress Distribution (Limit Load)

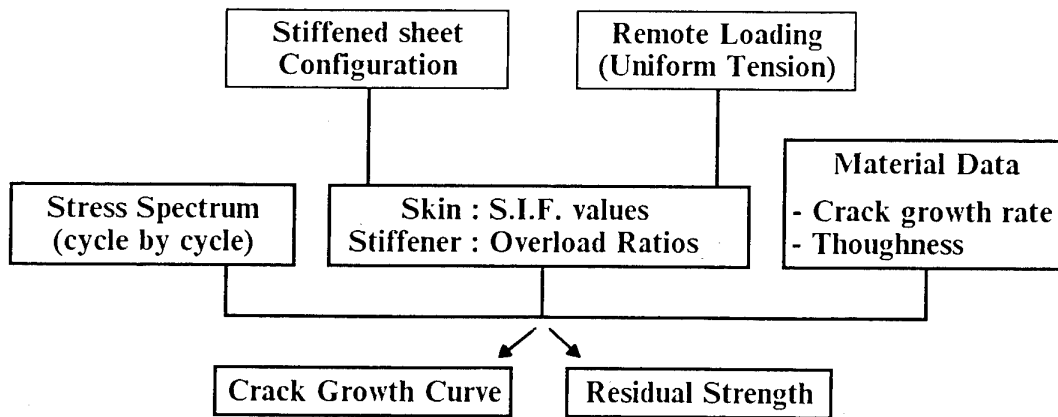


Fig. 6 - Principle of Crack Behaviour Study

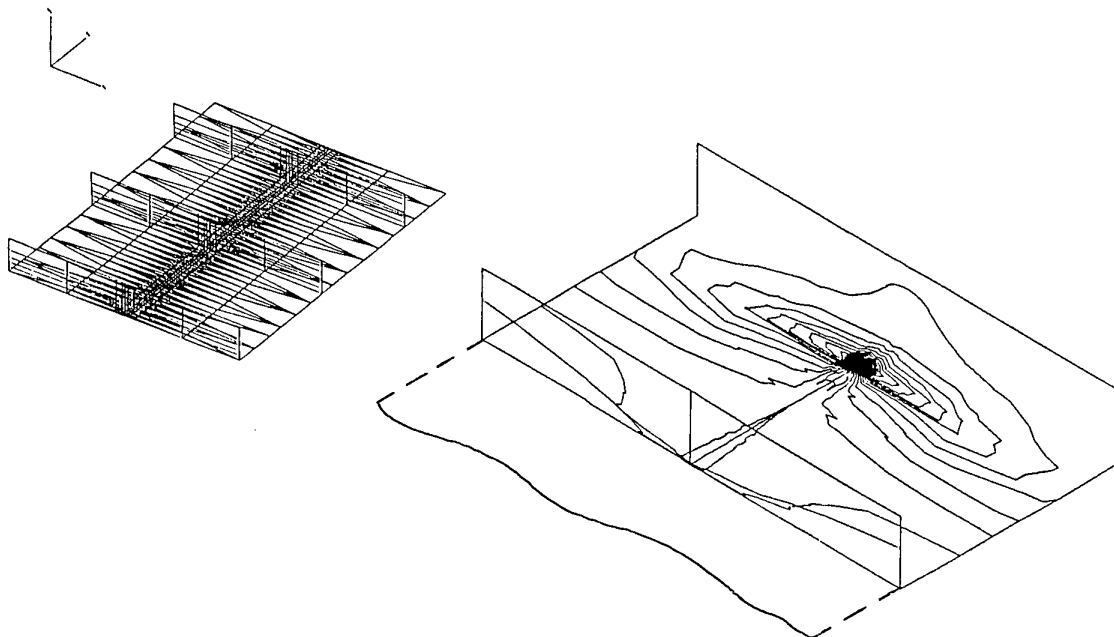


Fig. 7 - Wing Lower Surface : Crack about a Broken Stiffener

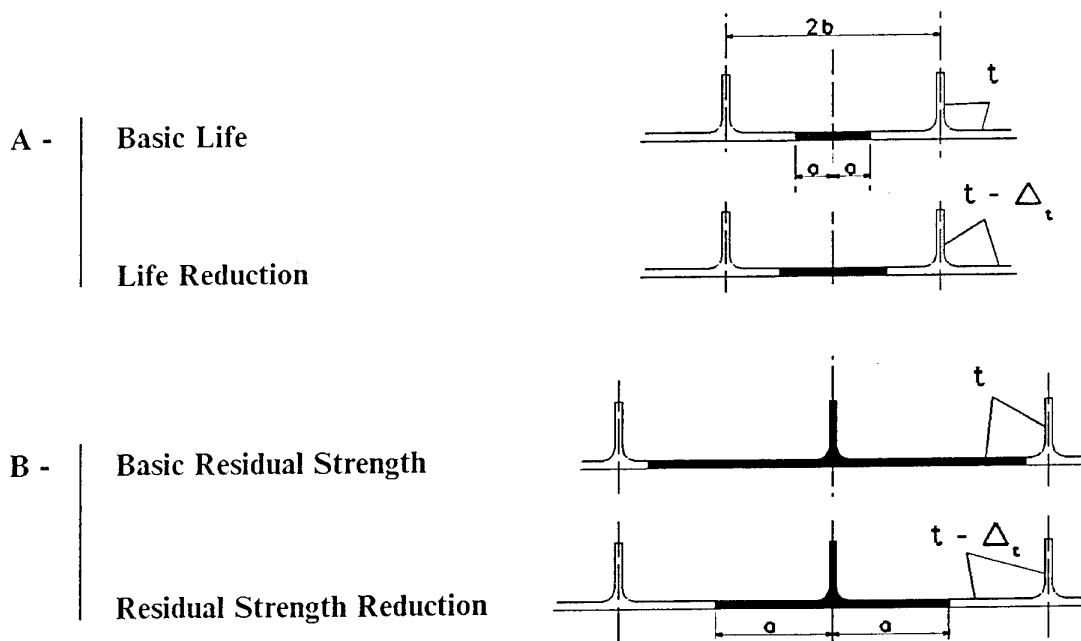
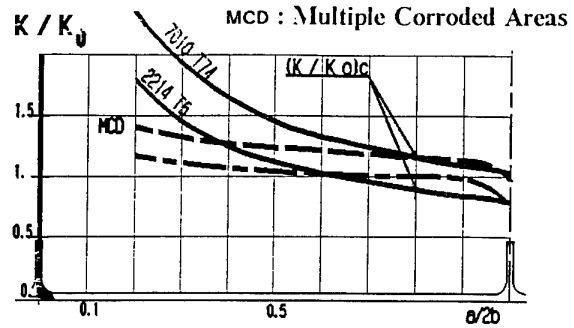
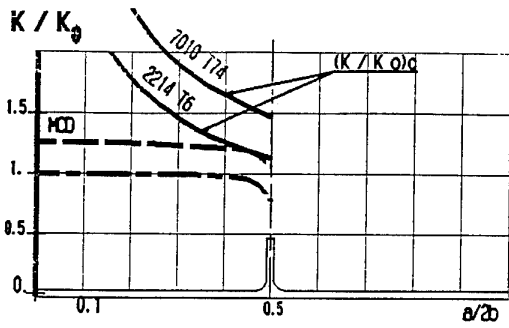


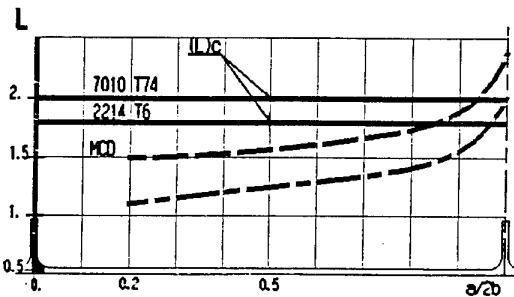
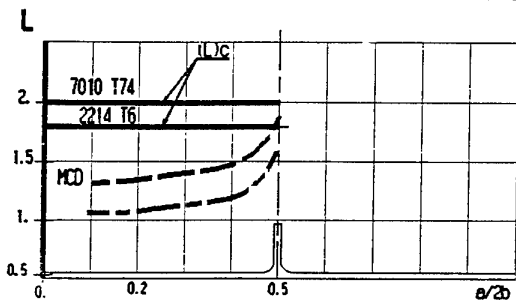
Fig. 8 - Wing Lower Surface : Studied Damage (Integrally Stiffened Panel)

Stress Intensity Factor

$$K_0 = \sigma \sqrt{\pi a}$$



Stiffeners Overload Ratios



A - Crack between Stiffeners

B - Crack about a Broken Stiffener

Fig. 9 - Cracks with/without Multiple Corroded Areas

DEFINITION DES VOLS.

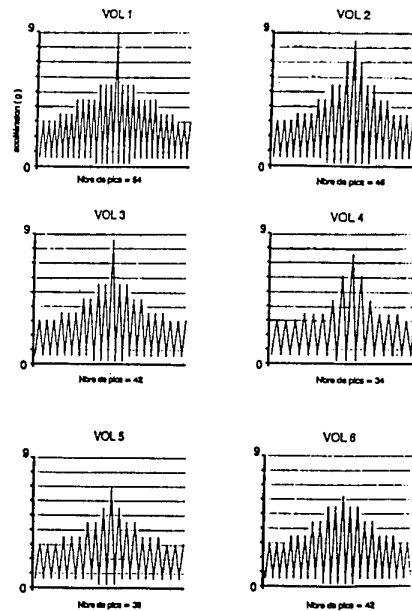
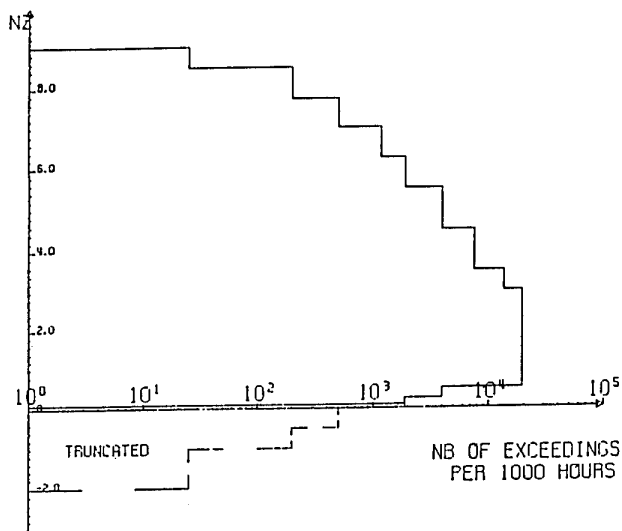


Fig.10 - Loading Spectrum for Crack Study (Maneuver Exceedances Spectrum)

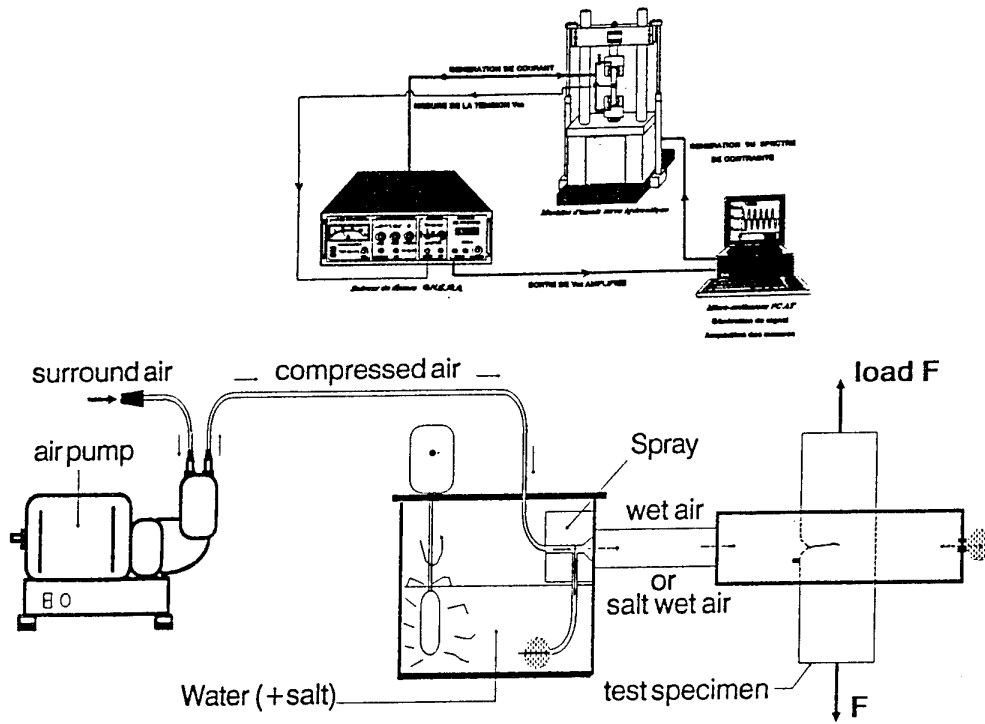


Fig.11 - Laboratory Test Facilities for Wet Air and Salt wet Air Generation

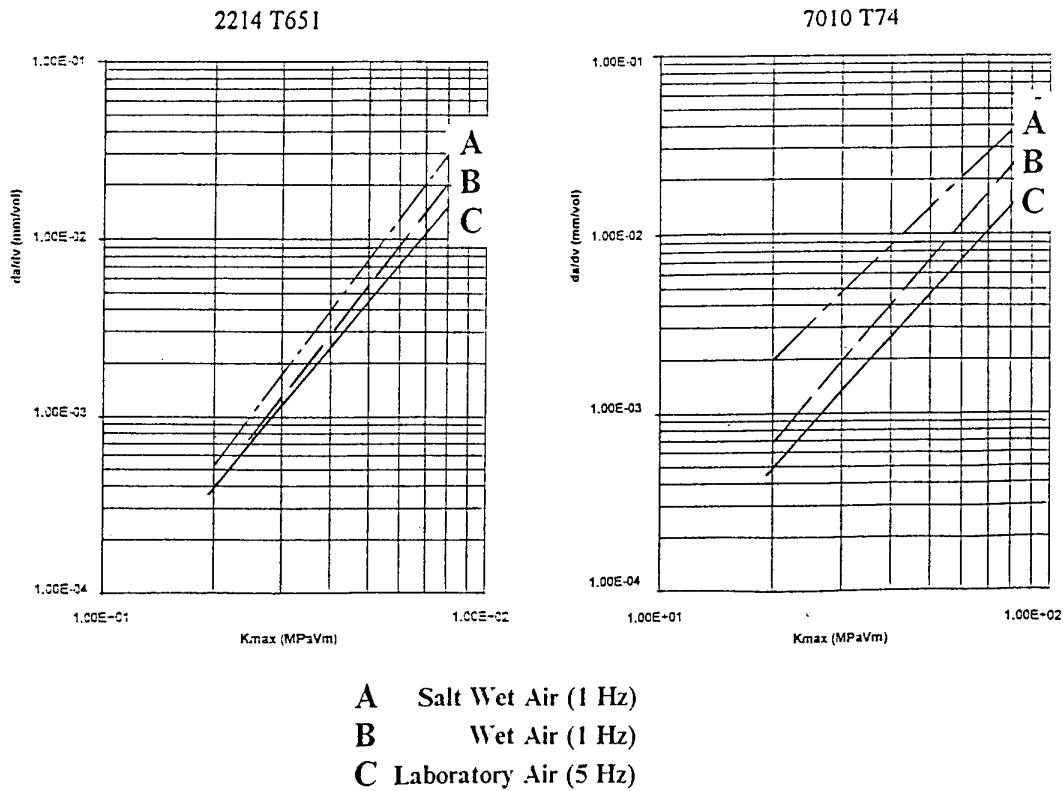


Fig.12 - Experimental Data : Crack Propagation Rates (Spectrum Loading)

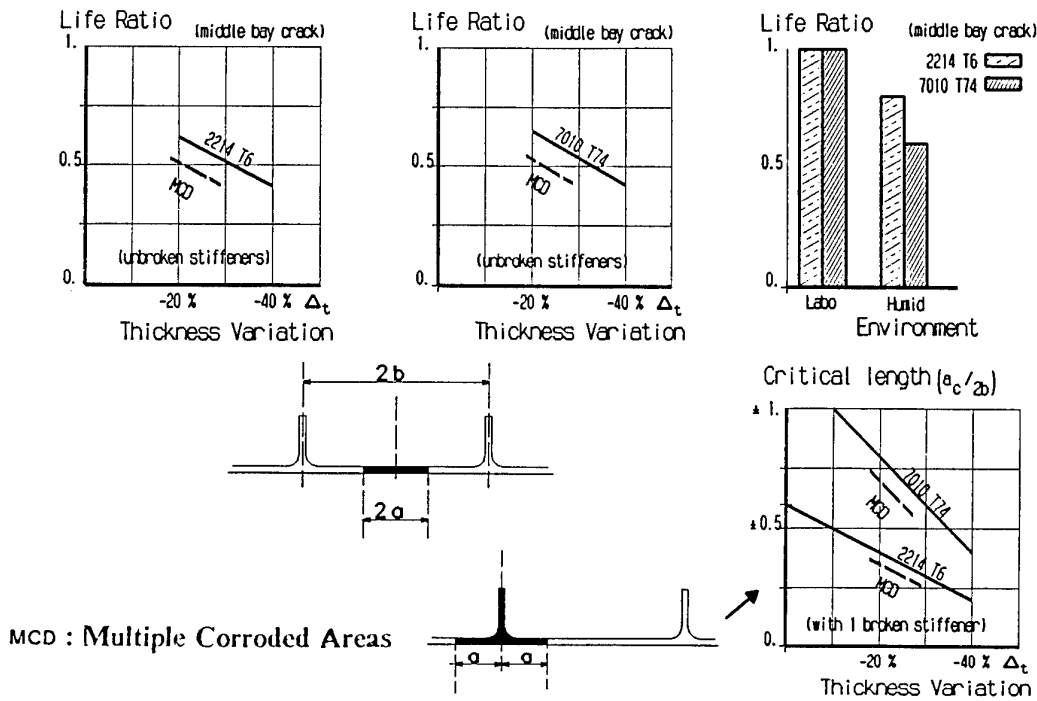


Fig.13 - Wing Lower Surface : Crack behaviour Study

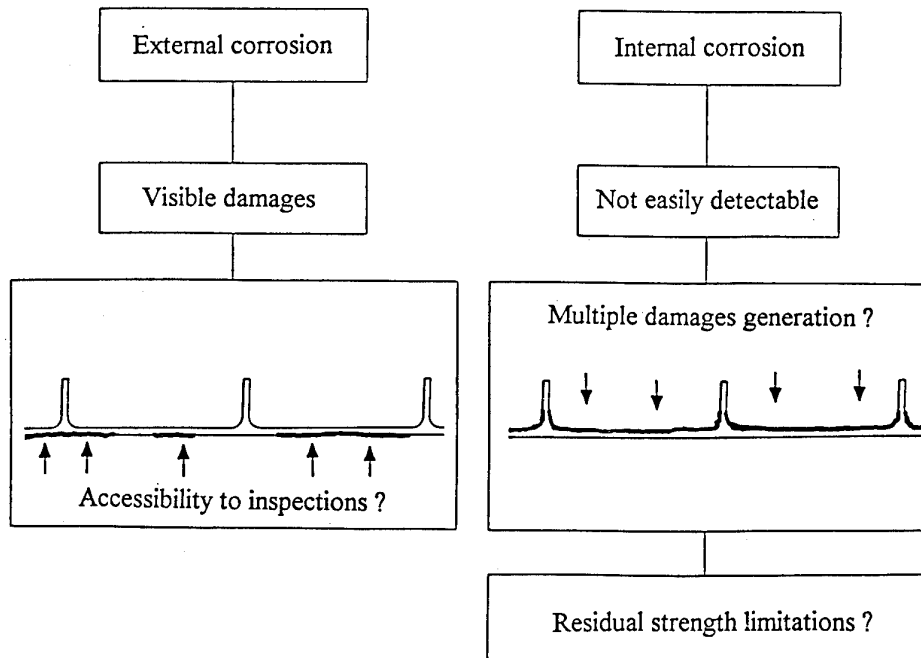


Fig.14 - Lower Wing Panel with WFD

Fatigue Damages During Tornado MAF Test

W. Bröcker

IABGmbH; Structure Tests and Technology TAS;
Einsteinstr. 20; D-85521 Ottobrunn, Germany

M. Buderath

Daimler-Benz Aerospace AG; Military Aircraft
Postfach 80 11 60; D-81663 München, Germany

SUMMARY

Some of the fatigue damages which have occurred during the major airframe fatigue test (MAF-Test) of TORNADO fighter aircraft seemed to be wide spread fatigue damages (WFD). These damages accompanied by results from coupon tests will be presented and analysed in this paper.

This paper will confirm that the load transmission in bolted splice sections is a rather complex phenomenon. The fatigue behaviour of a bolted joint/splice is dependent on many parameters, as there are different designs, materials and fastener types used. Because there is still not abundance of information available about the WFD problem, the inspections of bolted joints with respect to aging aircraft should be based on coupon tests or better still on full scale fatigue tests.

1 INTRODUCTION

The fatigue test on the complete airframe structure of the TORNADO-IDS-Version has been performed at IABG from March 1981 till March 1990. It was required to simulate a total of 16000 flight hours during this test time.

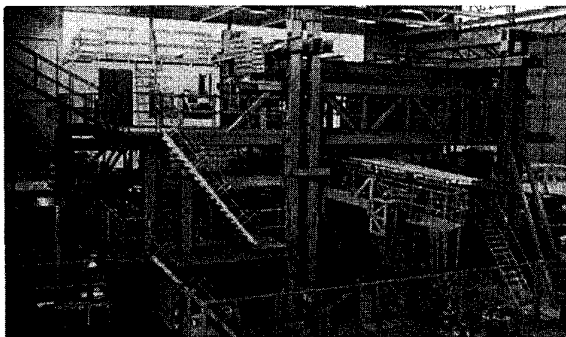


Fig. 1 Tornado MAF Test - Test Set-Up

WFD is defined as a group of small cracks that appear in an aircraft structure at about the same time, originating from similar design details located in a common area. The cracks influence each other so that the crack growth life of any crack at a specific hole may be considerably less than would be predicted by conventional damage tolerance

analysis which ignores the multiplicity of damages. The dominating phenomenon is apparently the stress level in the bolted lap joint and the design of the lap joint which is intended to show by using the results of the MAFT. Therefore fatigue damages which occurred in the structure during the fatigue test have been evaluated with respect to WFD. The results and experiences are presented in this paper.

2 TEST PERFORMANCE

The test article (IDS-Version) comprised the complete airframe structure without equipment and consisted of the front fuselage, the centre fuselage, the rear fuselage, the fin and the wings. Engines, airbrakes with actuators, tailerons with actuators, rudders, radom, nose and main landing gears, wing sweep actuators, subsonic ramps, outboard flaps, slats and wing pylons have been replaced by dummies.

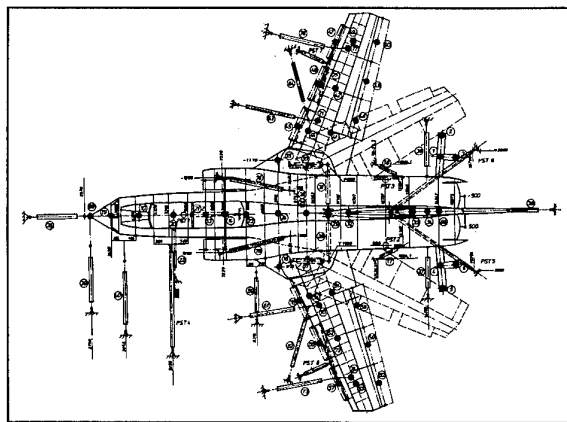


Fig. 2 Tornado Test Structure with Actuators (top view)

A loading rig was erected around the test article (see Fig. 1) to react the forces of the hydraulic actuators and struts and to permit the accessibility to the test article for the purpose of inspections. The loading rig had two movable platforms to take the wing loading actuators. These so called slave wings were attached to the centre frame of the rig with two large bearings, whose axis of rotation was coincident with the wing/fuselage pivot axis. The

slave wings were coupled with the wing via driving struts. So the original wings and the slave wings remain in the same location to each other during sweep.

A total of 79 servo-controlled hydraulic actuators, 6 struts and 6 different pneumatic systems served to simulate the required flight conditions (see Fig. 2). The test loads were introduced into the test specimen by several load introduction fittings fastened to the specimen and a large number of rubber loading pads bonded to the surfaces of fuselage, fin and wings. The fuselage fuel tanks and two air pressure seals (cockpit seal and wing slot seals) were incorporated into the test specimen and were pressurised by the test pneumatic system together with the cockpit and air bags, installed in the air intake ducts.

A total of 1095 load cases had been evaluated to simulate all aircraft loadings such as take-off, landing and ground operations including engine thrust, different flight manoeuvres (symmetrical and asymmetrical) with vertical and lateral gusts and the wing sweeping during the flight. The test article was loaded with these load cases in a randomised flight-by-flight programme. This program included 40 different flights with an average number of 200 load cycles. One flight corresponded to 1.11 flight hours an average and was simulated within 12 mins to 18 mins. The various flights were simulated in a random sequence within a period of 1000 flight hours.

During the progress of the fatigue test a very detailed and extensive inspection programme was performed. Superficial inspections of easily accessible areas were carried out daily with no or only short test stoppage. These walk around inspections consisted of a normal visual check as well as close examinations of suspected crack areas using visual aids (magnifying glass). On completion of every 1000 simulated flight hours (SFH) more detailed inspections were performed with approximately a 10 day test interruption. For these inspections some defined parts of the test set up and of the test article were removed. After every 2000 SFH a „major“ inspection was performed with an interruption of about four and a half weeks. Additional to the inspections made every 1000 SFH more substantial parts of the rig and dummy components were removed. Apart from visual inspection methods various non-destructive testing techniques were employed such as X-ray, ultrasonic, dye penetrant and eddy current. Additionally special inspections were carried out when parts of the specimen were dismantled during repairs and after request by the responsible partner companies.

3 TEST RESULTS

The damages found in the course of the MAF-Test consist of fatigue cracks in the structure, failure of fasteners (bolts, rivets e.a.), wear damages, static failures (in the course of the accompanying static tests), and others (for example failures of auxiliary structures as load introductions) as shown in Fig. 3. In a further investigation (see Fig. 4) all fatigue cracks were divided, corresponding to their position, into cracks due to the geometry (change of the stiffness etc.), cracks due to cut outs (open holes etc.), cracks with an initiation from holes for joints, fatigue failures in bolts and fasteners, and cracks in the lugs.

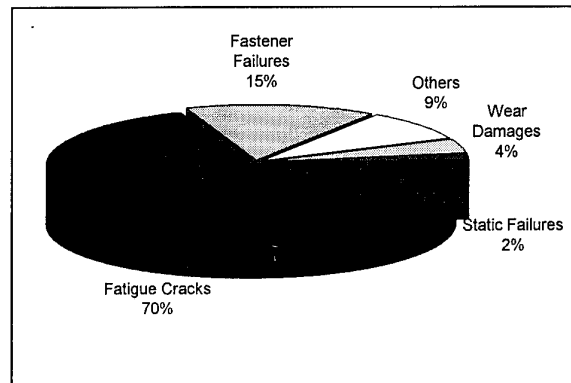


Fig. 3 Type of Damages

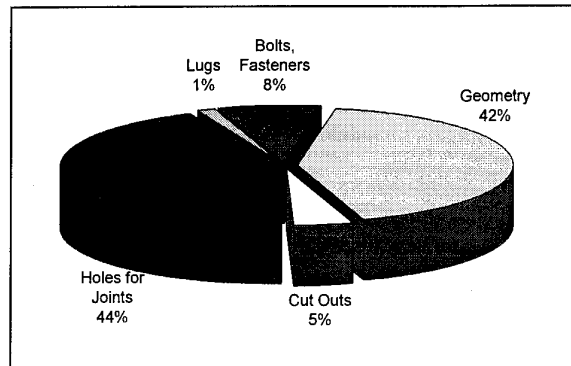


Fig. 4 Distribution of Fatigue Cracks

The damages in the centre fuselage corresponding to the group „cracks with an initiation from holes for joints“ have been checked, referring to the definition of WFD, with respect to groups of cracks which appeared in a common area at about the same time. They have been analysed with respect to the reasons for these damages to derive how far these damages might be classified as WFD. The following examples have been found:

- **Cracks in angles of the frames of the centre fuselage:**

In the angles that are mounted to the frames of the centre fuselage, fatigue cracks have been found between the rivet holes of a bracket (see Fig. 5). These cracks occurred in the left and right

hand sides of the structure. An analysis showed that the loads transferred by these angles were not too high, but caused by relatively high displacements in the structure. The brackets were bended up and down during the fatigue test what originated the fatigue cracks. Thus it makes no sense to classify this damage as WFD because it may not be attributed to a load transfer. This damage is not critical for the structure, so it will be tolerated within a certain scale and is defined as a life item.

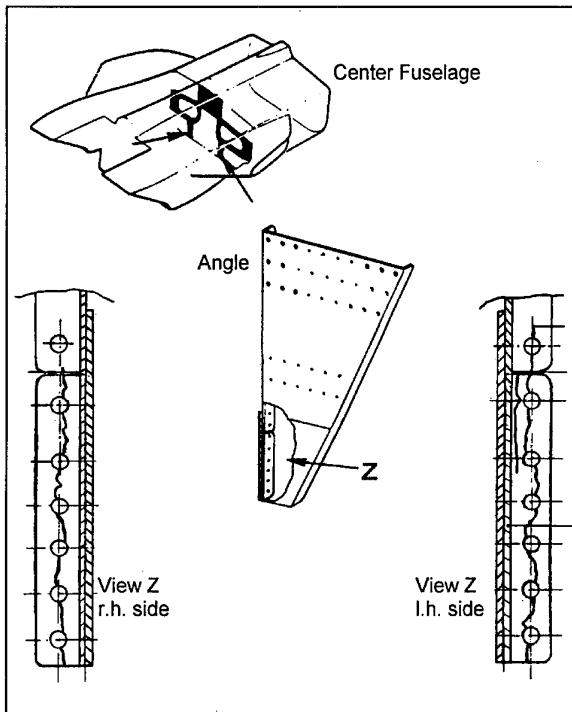


Fig. 5 Fatigue Cracks in the Angles of the Frames of the Centre Fuselage

- **Cracks in the panels of the air intake duct:** The panels of the air intake duct are connected via the flange of the frames. In the region of the transverse splices fatigue cracks occurred between the bolted holes (see Fig. 6). These cracks have been detected in the left hand duct and in the right hand duct of the structure of the IDS version. It was decided by the manufacturer that further investigations were necessary to set modifications (see chapter 4 „CRACKS IN THE DUCT PANELS“ and chapter 5 „FATIGUE TESTS ON SPECIMEN“)

4 CRACKS IN THE DUCT PANELS

After 2600 test hours the fatigue cracks in the splice of the air intake duct panels (see Fig. 6) on both sides were detected when the intake rubber bags were removed for leakage repair of the rubber bags. The panel No.1 is made from aluminium alloy 3.1364.7 (T81) and the panels No.3 and No.7/9 are made from aluminium alloy 3.1364.7 (T62). The

panels No.1 and No.3 lap over each other (see Fig. 7).

After removing the air intake duct panels the affected part of these panels were cut out for metallographic and microfractographic investigations. The crack situations in the panels of the left hand duct and right hand duct were similar (see Fig. 7).

The metallographic investigations have revealed a normal microstructure for the panels. The direction of grain was transverse to the flight direction which is easy to understand due to the fuselage bending and intake pressure loading. Brinell hardness measurements were carried out and compared to the data sheets. The results of the measurements confirmed that the material data were within the values presented by the data sheets.

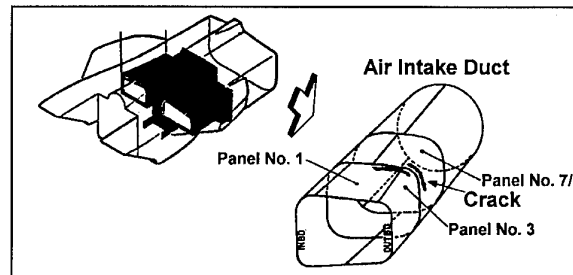


Fig. 6 Damages in the Air Intake Duct

A scanning electron microscope was used to investigate the fracture surface. Since the cracks were found with a relatively large crack length, the crack surface was worn and therefore not fully reproducible at each point of the fracture surface. Nevertheless, the most important areas of the damages could be investigated.

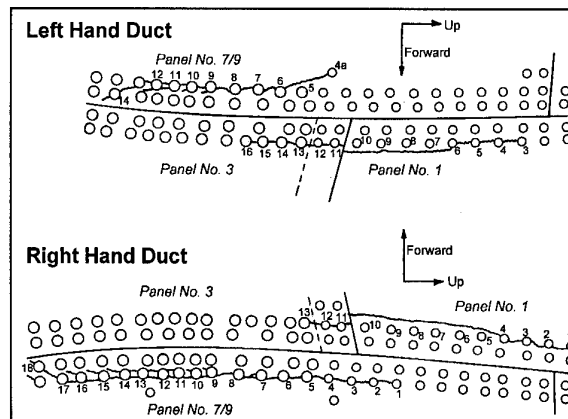


Fig. 7 Fatigue Cracks in the Panels of the Air Intake Ducts (view from inside duct)

- In the panels No.1 striations, starting from the outside duct surface (and not from the holes) of these panels, have been found in the region of holes No.8 to No.12. The cracks from hole No.1 (respectively No.3) to No.7 seemed to be static failures.

- The fracturgraphic analysis of panel No.3 revealed that the crack growth started from the outside of the panel at the holes. The residual area from one hole to the other failed statically.
- The panels No.7/9 showed in the regions of the holes No.1 (respectively 4a) to No. 8 small fatigue damages, also starting from the outside of the panels at the holes, and a static failure in the residual area. In the region of the holes No.9 to No.13 (respectively No.17) two crack surfaces exist. For the right hand side these cracks are shown in detail in Fig. 8. The cracks initiated at the outside duct edges of the holes and propagated in two different directions as shown in Fig. 8. The microfractographic examination showed typical sign of fatigue, but also indications of shear fracture (45°, intermixed regions of ductile tearing and striations).

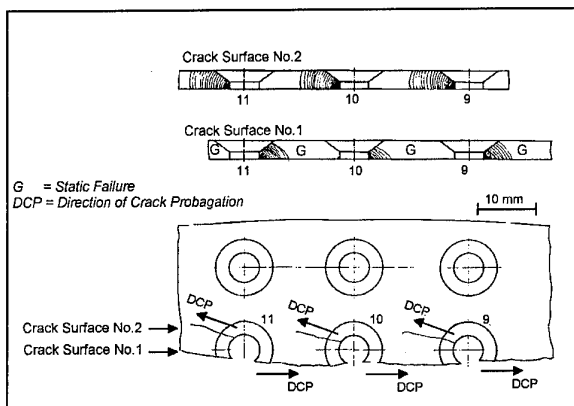


Fig. 8 Fatigue Cracks in the Right Hand Side Panel No.7/9

A comparison of the striations spacings and crack length lead to the supposition that the first fatigue crack possibly started from hole No.9 of panel No.7/9. Similar results have been found for the damages of the left hand side panel No.7/9.

The initial design of the splice section is sketched in Fig. 10 (section D-D). After carrying out fatigue tests on the specimen representing various modifications of the splice (see chapter 5 „FATIGUE TESTS ON SPECIMEN“), the splice section was modified corresponding to the results of these specimen tests. A 2mm steel doubler was introduced over the middle hole line of the splice and oversize fasteners were used (see Fig. 15, modification type 4). And although this modification did not change the design of the critical cross section and the loads being transferred by this cross section remained the same, this measure changed the fatigue behaviour of the splice significantly. The fatigue life of the air intake duct panels was improved by a factor >3 and the direction of the crack propagation was changed. The new fatigue damages are sketched in Fig. 9.

Unlike the initial damage mode, where the fatigue cracks run along the hole line of the splice from one hole to the other (see Fig. 7), in the modified splice the cracks run perpendicular to the splice and the cracks occurred in both hole lines. It can be assumed that the influence from one crack to the other is now negligible.

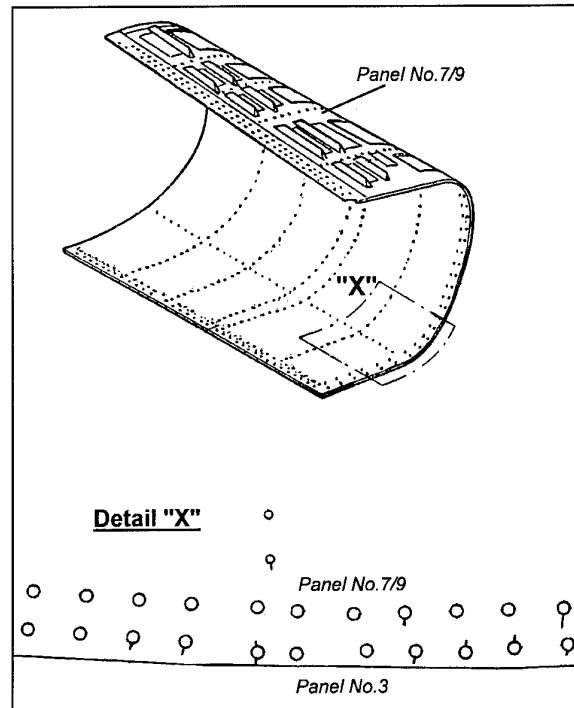


Fig. 9 Failure Mode after the Modification of the Air Intake Duct Splice

5 FATIGUE TESTS ON SPECIMEN

A Specimen representing a splice section D-D (see Fig. 10) of the air intake duct panel No.7/9 to No.3 was tested at MBB in a separate programme. Possible modifications of this splice section were investigated in order to improve the design and to reduce the stress level in the critical cross sections. The specimen tests did not exactly simulate the real conditions (e.g. curved splice, support of frame, shear loading). However, it was assumed that substantial fatigue behaviour from test specimen would give adequate knowledge about the final splice improvement.

The fatigue behaviour of the specimen was tested applying a flight-by-flight sequence of the TOR-NADO overall n_z -spectrum. The specimen was fixed to the rig perpendicular to the loading direction to simulate the support of the frame and prevent excessive buckling during the compression phase. For each type of modification the specimen were dynamically loaded with the flight-by-flight sequence at different load levels up to failure. The load level was within a range of 18 kN to 32 kN. To record the

interactions between the holes the specimen covered the width of two holes (see Fig. 11).

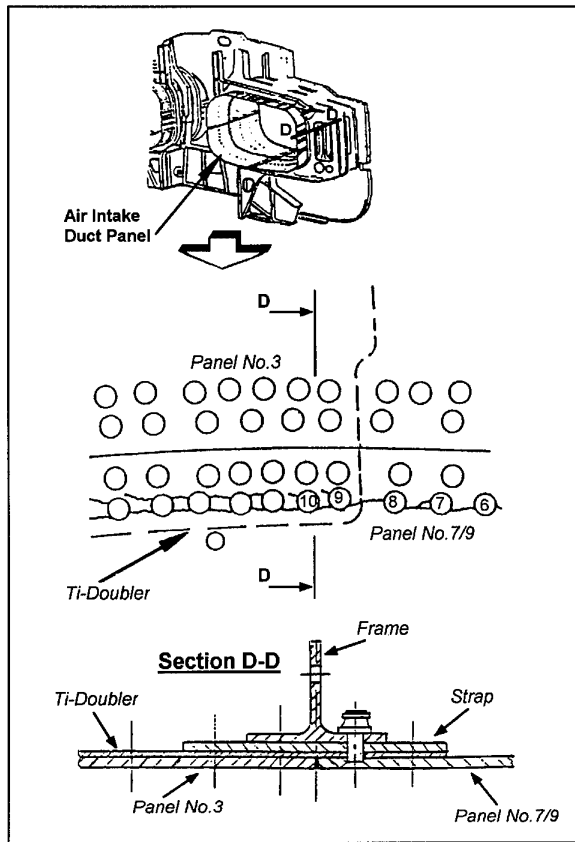


Fig. 10 Representing Splice Section

The following types of the splice have been considered in the test programme:

• **Type 1**

The specimen configuration is shown in Fig. 11. It represented the initial design and was tested to get comparative values for the change of the fatigue behaviour due to the modifications.

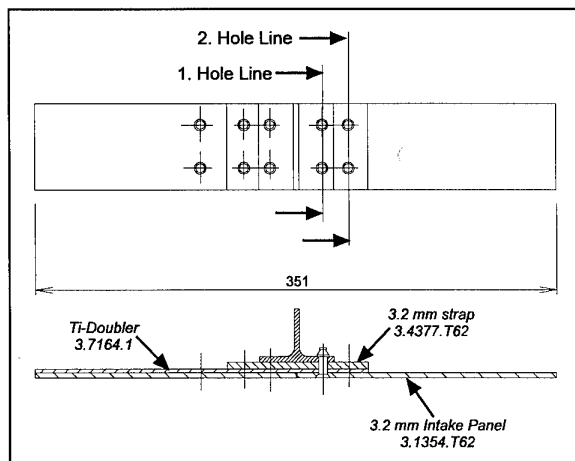


Fig. 11 Specimen Configuration for the Initial Splice

The test results are sketched in Fig. 12. The specimen 1-5, which was tested at the lowest load level, did not fail in the 2nd hole line but in the 1st hole line. At the other load levels the specimen failed, similar to the failure mode of the duct panels, in the 2nd hole line.

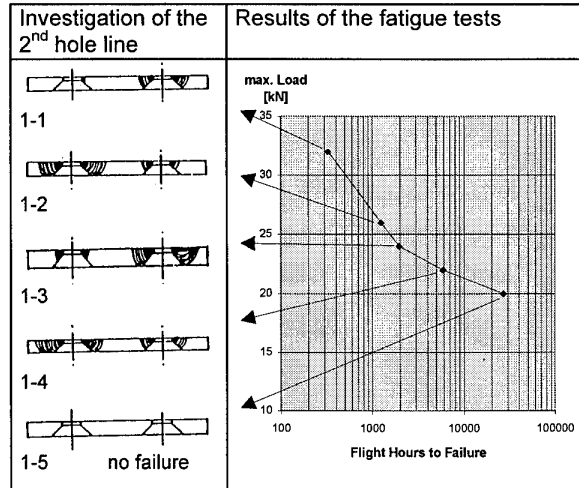


Fig. 12 Test Results of Splice Type 1

• **Typ 2**

The specimen was modified by a steel doubler with a thickness of 2 mm which was mounted over all holes of the splice. Thus the bolted joint was changed from a single shear type to a double shear type. (see Fig. 13).

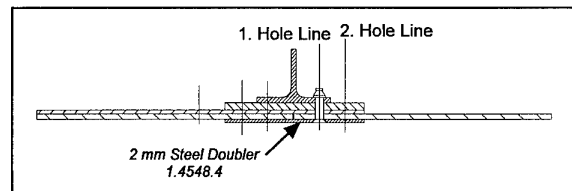


Fig. 13 Specimen Configuration of Splice Type 2

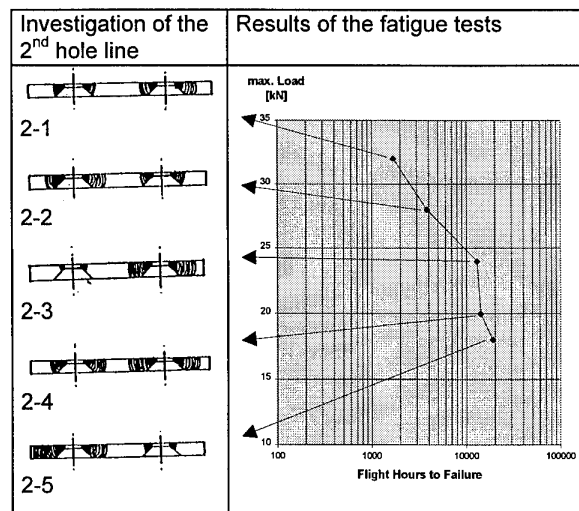


Fig. 14 Test Results of Splice Type 2

Specimen 2-3 failed after a relatively high number of flight hours compared to specimen 2-4 and 2-5 although the stress levels of these specimen are significantly reduced. It is supposed, this is because of one unfailed hole in the hole line and hence the crack tip is not influenced by another one (see Fig. 14). All specimen of this splice type failed in the 2nd hole line, thus it can be concluded, that the stress level in this section was too high compared with the stress level in the 1st hole line.

• **Type 3**

For the modification of splice type 3 specimen, the steel doubler was shortened to 43 mm so that it covered only the 1st hole line (see Fig. 15).

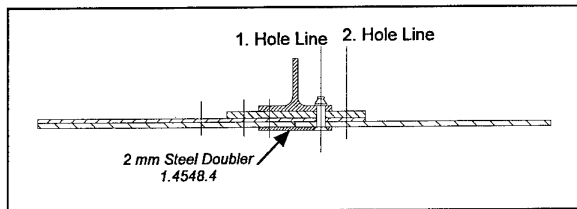


Fig. 15 Specimen Configuration of Splice Type 3 and Type 4

Specimen 3-1 and 3-4 failed in the 1st hole line after a relatively high number of flight hours compared with the specimen 3-2 and 3-5 that failed in the 2nd hole line.

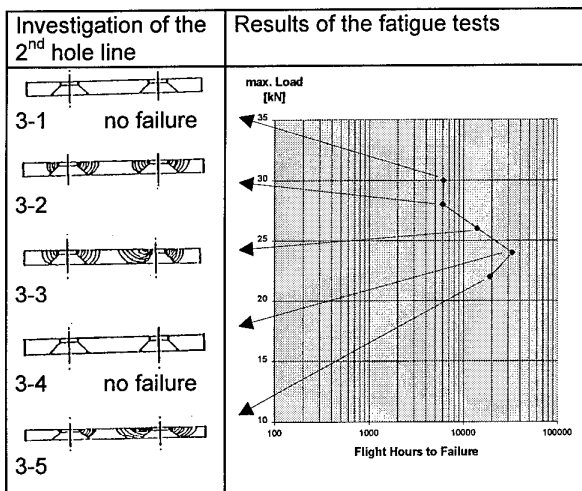


Fig. 16 Test Results of Splice Type 3

• **Type 4**

The configuration of this specimen is equal to the configuration of splice type 3 specimen (see Fig. 15), but oversized fasteners have been used.

All specimen failed in the 2nd hole line. The specimen 4-1 and 4-3 failed after a relatively high number of flight hours. The investigation of the failure section of these specimen showed fatigue cracks at one hole only (see Fig. 17).

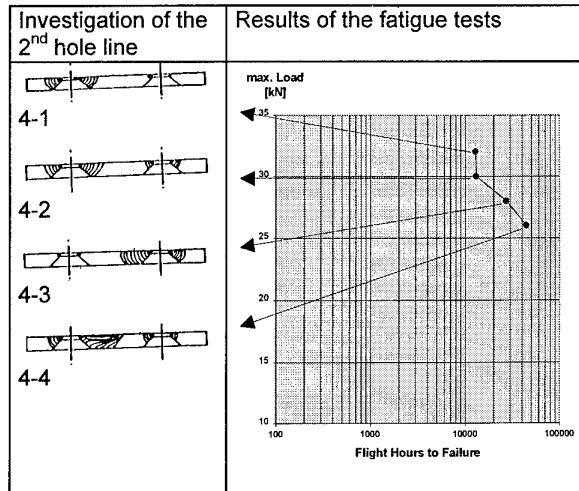


Fig. 17 Test Results of Splice Type 4

Summary of the specimen test results:

All test results are summarised in Fig. 18.

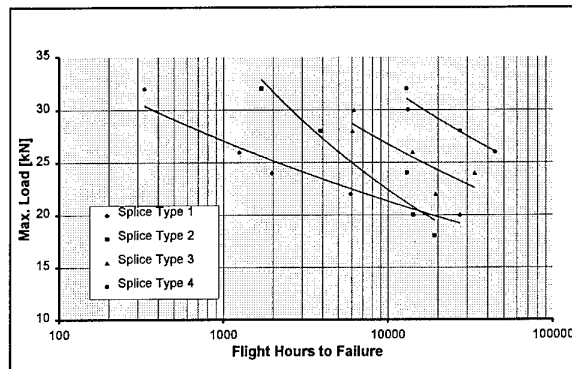


Fig. 18 Results of Fatigue Tests on Specimen

A life improvement was obtained by the change in design from a single shear type to a double shear type (type 1 to type 2). But the results of the double shear specimen having a steel doubler over both hole lines (specimen type 2) revealed that the fatigue life improvement was still unsatisfactory.

Mainly two reasons were considered to be responsible for the poor fatigue behaviour:

- The poor filling of the countersunk of the load carrying 3.2 mm strap (see Fig. 11), so that only the cylindrical part of the hole carried the load.
- The large load transfer through the 2nd hole line (see Fig. 13).

The next design of the specimen was significantly dominated from the intention to reduce the loading of the 2nd hole line. Therefore, the 3.2 mm steel doubler was shortened to transfer more loading in the 1st hole line (specimen type 3).

Fig. 18 shows, that with specimen type 3 a considerable life improvement was obtained although the critical cross section (2nd hole line) of this specimen is the same as of the specimen type 1. It appears

that by using the short steel doubler stress concentrations in the region of the holes could be reduced (the ratio between the bypass loads and the loads to be transferred by the bolt have been changed) and thus a better load transmission was achieved. Furthermore, the test results of specimen type 4 indicate an additional improvement which was probably based on a higher clamping force of the oversized fasteners.

From the observation of the fracture surfaces it can be derived, that the crack initiation always occurred in the countersunk of the fastener holes.

When the fatigue cracks occurred at both holes of a hole line, the number of flight hours to failure decreased. Thus it may be concluded, that cracks originating from adjacent holes at almost the same time lead to a crack growth life that was less than would be predicted by conventional fracture mechanics.

Also a phenomenon of fretting corrosion was found in the surrounding of the holes.

The splices type 1 and type 3 did not show a clear trend about the crack initiation. The splices failed as well in the 1st hole line and in the 2nd hole line.

6 CONCLUSIONS

In this paper the authors have re-visited the damages of Tornado MAF-Test to analyse them with respect to WFD.

In particular on the example of the fatigue results of the intake duct panels it was demonstrated, how sensitive the fatigue behaviour reacts on changing the design and mechanical treatment.

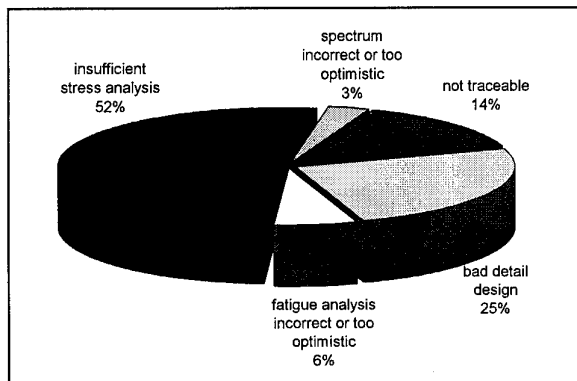


Fig. 19 Reasons for not Recognising the Fatigue Critical Sections
(Survey of Centre Fuselage Only)

WFD largely depends on probabilistic effects as for example loading, manufacturing, environment, material etc. The uncertainties in the probability of the crack originating from fastener holes have been confirmed by the specimen tests. Furthermore, an obviously interaction between multiple cracks and

the resulting influence on the crack growth life could be pointed out.

In addition the MAF-Test results of the centre fuselage have been re-considered with respect to the reasons for not recognising the fatigue critical sections. The results are sketched in Fig. 19. As it can be seen in this figure, the main reason is attributed to an insufficient stress analysis due to the fact that it is nearly impossible to detect and analyse all fatigue critical sections of a structure which has a complex design.

Considering all results it seems to be impossible to assess the widespread fatigue behaviour of aircraft structures in an analytical way only. Thus it is our opinion that in the near future verification of aircraft structures can not be done without fatigue tests on components or better still full scale fatigue tests.

7 REFERENCES

1. Tornado-IDS, Technical Report MBB SRR-TOR-0112, Fed. 1982
2. Tornado-IDS, Major Airframe Fatigue Test (Test Set-Up); IABG Report No. B-TF 2850; Feb. 1991
3. Tornado-IDS, Major Airframe Fatigue Test (Final Report); IABG Report No. B-TF 2860; May. 1991
4. Tornado MAFT Status Report at 8000 SFH; MBB Structural Test Report STR-TOR-0148 Oct. 1986
5. Tornado MAFT-IDS, Damage Documents up to 16000 SFH; DASA Report TN-TOR 2429; Nov. 1992
6. R. Bochmann and W. Weisgerber The Role of Fatigue Analysis For Design of Military Aircraft AGARD Report 797 Bordeaux, September 1993
7. Tornado-MAF-Test, Damage Investigation Duct Panel No. 1&3&7/9, L.H. Side IABG Technical Note TFS-T-53/82
8. J. Schijve Multiple-Site Damage Fatigue of Riveted Joints. Int. Workshop on Structural Integrity of Aging Airplanes, Atlanta, GA, March 1992
9. Thomas Johansson and Hans Ansell Structural Reliability in Fatigue Design - Applied to Riveted Joints and presence of Multiple Site Damage Int. Workshop on Structural Integrity of Aging Airplanes, Atlanta, GA, March 1992

10.A. Nathan and A. Brot
An Analytical Approach to Multiple-Site Damage
ICAF Stockholm, June 1992

11.D.Broek
The practical use of Fracture Mechanics
Kluwer Academic Publisher

Damage Tolerance Evaluation on the A7-P Aircraft Considering the PoAF Usage

Manuel de Freitas*
 Agostinho Fonseca*
 Humberto Gonçalo**
 Carvalho Pires**

*Instituto Superior Técnico, Dep.Engº. Mecânica, Av. Rovisco Pais, 1096 Lisboa, PORTUGAL

**Força Aérea Portuguesa, CLAF/DMA, Av. da Força Aérea - 2720 Alfragide, PORTUGAL

1. SUMMARY

An exploratory and preliminary damage tolerance evaluation on the A7-P Corsair is presented. The stress data was obtained through the data acquisition system installed in two aircraft in PoAF fleet.

Forman's law and Wheeler retardation model were used on a crack propagation simulation of cracks emanating from a hole in the wing lower skin.

The material fatigue data was originally generated by Vought Corporations, the aircraft manufacturer. The results show the influence of multiple crack initiation and propagation on the predicted fatigue life of the A7-P aircraft.

2. LIST OF SYMBOLS

a	- crack length
a_p	- crack length plus plastic zone at crack tip
ASIP	- Aircraft Structural Integrity Program
C	- constant of Forman's Law
C_p	- additional factor of retardation in the Wheeler's model
C_{ig}	- level counting of Gs (i=5 to 8)
$\frac{da}{dN}$	- crack growth rate
DI	- Damage Index
EBHF	- Equivalent Base Line Hours Flown
FH	- Flight Hours
K_{IC}	- critical stress intensity factor
M	- Mach number
m	- Wheeler's coefficient
n	- material constant of the Forman's Law
N_z	- vertical acceleration in the center of gravity of the aircraft
PFL_{BL}	- Potential Fatigue Life for Normalized Baseline Counts

PFL_{NC}	- Potential Fatigue Life for Normalized Counts
R	- stress ratio
R_Y	- plastic zone size at crack tip
WS	- wing station
ΔK	- stress intensity factor range
σ	- stress

3. INTRODUCTION

Safety and reliability of a structural component depend on factors that are initially associated to the design criteria and the quality requirements of the material and manufacturing processes.

During its operational usage, safety and reliability of the components depend on prompt detection and immediate damage repair before critical dimensions at which catastrophic failure occurs are reached.

In a military aircraft the fatigue life consumption of the structural components depend on different factors:

- severity of loads within each mission;
- mission sequence;
- usage by type of mission.

The fatigue life monitoring of the A7-P aircraft begun in PoAF in 1986. A g counter was installed in all aircraft. After each flight the g counter readings, the type of mission and the flight duration are recorded.

The damage index algorithm used by PoAF was developed by Vought for A7D. The g counter readings acquired in a given period, i.e. flight hours, after being normalized to 1000 flight hours, are used to calculate the potential fatigue life (PFL_{NC}) for a crack to grow from 1,27 mm to the critical crack size, 30,7 mm at WS 32.2. The damage equation obtained by

Vought through regression analysis is as follows:

$$\ln \text{PFL}_{\text{NC}} = -0,98253 \ln C_{5g} - 0,50445 \ln C_{6g} + 0,41444 \ln C_{7g} + 18,632$$

The calculation of the equivalent base line hours flown (EBHF) for the flight hours interval in evaluation is given by:

$$\text{EBHF} = \text{FH} \frac{\text{PFL}_{\text{BL}}}{\text{PFL}_{\text{NC}}}$$

For the A7-P the PFL_{BL} is equal to 21 141 flight hours.

The damage index is obtained dividing EBHF by the flight hours for a crack to grow from 0,127 mm to the critical size in the most fatigue critical location, WS 53.7 :

$$\text{DI} = \frac{\text{EBHF}}{18000}$$

In order to adapt this model to the operational usage of A7-P aircraft in PoAF, a whole work of instrumentation of two A7-P aircraft has been developed, since 1992, with the cooperation of National Aerospace Laboratory NLR, so that the following data could be registered in flight:

- stresses in the fatigue critical location: WS 53.7 and WS 24.6;
- vertical acceleration (Nz) measured in the aircraft center of gravity;
- speed and flight altitude.

Besides the usage characterization of the aircraft in the PoAF, this work also involves the following activities:

- definition of parametric equations which relate the vertical accelerations (Nz) to the stresses in the two fatigue critical locations: WS 53.7 and WS 24.6;
- cycle by cycle crack growth calculations in WS 53.7.

4. DATA ACQUISITION SYSTEM FOR THE A7-P CORSAIR

The multi-channel data acquisition system was manufactured by the German company "Swift" and is designated "Mas Micro-Box". This system shown schematically in figure 1, was specially developed to accomplish this kind of tests.

Apart from the typical elements of an ordinary data acquisition system, it also has the data storage and processing capacity, according to a previously defined algorithm.

The system has eight input channels that are sampled at a 2000 Hz frequency and converted into a digital shape through a 12 bits analogic digital converter. The information obtained in this way is internally processed according to a given algorithm and stored in a resident memory, with 512 Kb of capacity.

The data transfer to the ground station for processing and analysis is accomplished through an RS232 high speed connection to a personal computer. With this computer it is also possible to monitor the system's performance, enabling the possibility to realize calibration adjustments such as "gain" and "off set" associated to each input channel.

The eight parameters measured by the flight data acquisition system are:

- 1-Vertical acceleration in the aircraft center of gravity (Nz);
- 2-True air speed (TAS);
- 3-Altitude (H);
- 4-Micro strains in WS24.6;
- 5-Micro strains WS53.7;
- 6-Fuel flow (FF)
- 7-Engine rotation speed (N2);
- 8-Turbine inlet temperature (TIT).

Some of the acquired signals need a previous conditioning, before they are applied to the data acquisition system. For this purpose, an extra signal conversion unit was developed, named "SCULP", for conditioning signals corresponding to engine parameters (FF, N2 and TIT).

The signals corresponding to Nz, WS24.6 and WS53.7 have enclosed pre-amplifiers placed near the corresponding signal source.

Regarding data processing procedures, the implemented algorithm features six processes, that sequentially record peak and valley values of master and slave signals, as listed below:

Process 1:

Master:

-vertical acceleration(Nz)

Slaves:

-time

-true air speed(TAS)

-altitude(H)

-micro-strain in WS24.6

-micro-strain in WS53.7

Process 2 :

Master:

-micro-strain in WS24.6

Slaves:

-time

-micro-strain in WS53.7

Process 3:

Master:

-micro - strain in WS53.7

Slaves:

-time

-micro-strain in WS24.6

Process 4 :

Master:

-fuel flow (FF)

Slave:

-time

Process 5:

Master:

-engine rotation speed(N2)

Slaves:

-time

-fuel flow(FF)

-turbine inlet temperature (TIT)

Process 6:

Master:

-turbine inlet temperature (TIT)

Slaves:

-time

-fuel flow(FF)

-engine rotation speed(N2)

The added time information is generated by the data acquisition system itself and it is adjusted by "software". The time references corresponding to the beginning and end of each flight are always automatically registered as well as all the values of measured parameters.

The measuring process starts after an input signal incident, which in this case is the existence of electrical power in the aircraft battery bus. Figure 2 presents a segment of records for the following signals:

- Nz acceleration;
- micro strain in the WS53.7;
- altitude (H)
- true air speed (TAS)

5. CHARACTERIZATION OF PoAF USAGE

The flight hours associated with the existing ASIP g-counter program totals 20794 hours. These records include the exceedances readings of 5, 6, 7 and 8 g after each flight.

Comparing the average number of counts for each g level in the A7-P fleet with the A7-D reference counts an increase in the frequency of higher g levels has occurred.

Figure 3 presents four normalized 1000 flight hours load spectrum:

- A7-D baseline spectra;
- A7-P 1989 g counter readings;
- A7-P 1994 g counter readings;
- A7-P 1994 "Mas-microbox" data readings.

The parametric equations for the wing station 53.7 of the A7-P were obtained using the same procedures that were used by Vought on the structural integrity analysis of the A7-D.

Comparing the parametric equations of the present study with those determined by Vought based on different aircraft configuration and usage, there are important differences, table 1.

6. PRELIMINARY EVALUATION OF DAMAGE TOLERANCE

The amount of collected data demand a statistical treatment that enables a correct analysis.

Among the most used existing techniques for the counting of the number of loading cycles, there is the "Rainflow Counting Method", proposed in the sixties by Japanese researchers that was universally adopted, as it is based in the mechanical behavior of the materials. An algorithm was developed, that gathers the strains variations, according to the above mentioned technique, through cycles of equal amplitude and average value easily transformed into cycles of equal maximum and minimum value. A matrix of stresses range in WS 53.7 was generated, figure 4.

The exploratory and preliminary damage tolerance evaluation was based on the available flight data that was recorded in one of the two A7-P with the data acquisition system installed. The most severe recorded flight was selected.

An initial crack size of 1,2 mm was assumed in the damage tolerance evaluation on the A7-P. For the crack propagation calculation the Forman's Law was used:

$$\frac{da}{dN} = \frac{C(\Delta K)^n}{(1-R)K_{IC} - \Delta K}$$

To account the overloads effects the Wheeler model was adopted:

$$\frac{da}{dN} = C_p \frac{C(\Delta K)^n}{(1-R)K_{IC} - \Delta K}$$

in which

$$C_p = \left[R_y / (a_p - a) \right]^m$$

The Wheeler retardation exponent, m, for 7075-T651 attack aircraft spectrum was adopted (3).

One and two corner cracks emanating from a hole in the most critical identified fatigue localization of the A7-P, WS 53.7, as shown in figure 5, were considered in the crack propagation calculation.

The stress intensity factor for WS53.7 was calculated by Vought and a growth rate for 7075-T651 in severe environment was considered (3).

The integration of Forman's equation cycle by cycle for a loading corresponding to a mission, which represents 39,5% of the aircraft usage in PoAF, enable the calculation of the propagation curves presented in figure 6.

7. CONCLUSION

The analysis of the results point to a different operational usage of the A7-P in PoAF, in comparison with that one in USNAVY and USAF:

- a greater frequency of higher g levels, considering the g counters readings;

- different parametric equations coefficients from those determined by Vought in the damage tolerance analysis of the A7D .

The crack propagation data for the wing station 53.7, the most critical fatigue location, in relatively severe operation conditions, shows how much the multiple initiation and crack propagation influences the fatigue life of A7-P.

8. ACKNOWLEDGMENTS

The flight data acquisition system design and installation was performed in a cooperative DDI - project between NLR and PoAF "Monitoring and Fatigue Life Assessment of Fighter Aircraft Critical Airframe and Engine Components". The participation of A. A. Ten Have, J. Dominicus and A.J.M. Gijssels from NLR and Manuel dos Santos from OGMA, SA is gratefully acknowledged.

9. BIBLIOGRAPHY

(1)Dominicus, J. A. and Ten Have, A. A., "Description of the PoAF/NLR A-7P Load/ Usage Monitoring System", report NLR CR 93503L, National Aerospace Laboratory NLR, The Netherlands, 1993.

(2)Vought Corporation, Report n° 2 - 53440 /7R - 59

(3)Vought Corporation, Report n° 9 - 51220 / 9R - 114

Table I - Fatigue critical location WS 53.7 parametric equations

A7-P 15515

$N_z > 0$

$$\sigma = 1853,76 + 874,015N_z + 1937,37N_zM^2 - 0,0894H$$

$N_z \leq 0$

$$\sigma = 299,90 + 1,227N_zH - 0,0247H + 5087,1M^2 - 0,000063N_zH^2$$

A7-D(3)

$N_z > 0$

$$\sigma = 950,6 + 2556,37N_z + 674,63N_zM^2 - 0,0405H$$

$N_z \leq 0$

$$\sigma = 172,15 + 0,32346N_zH - 0,026H + 1241,5M^2 - 0,0000092N_zH^2$$

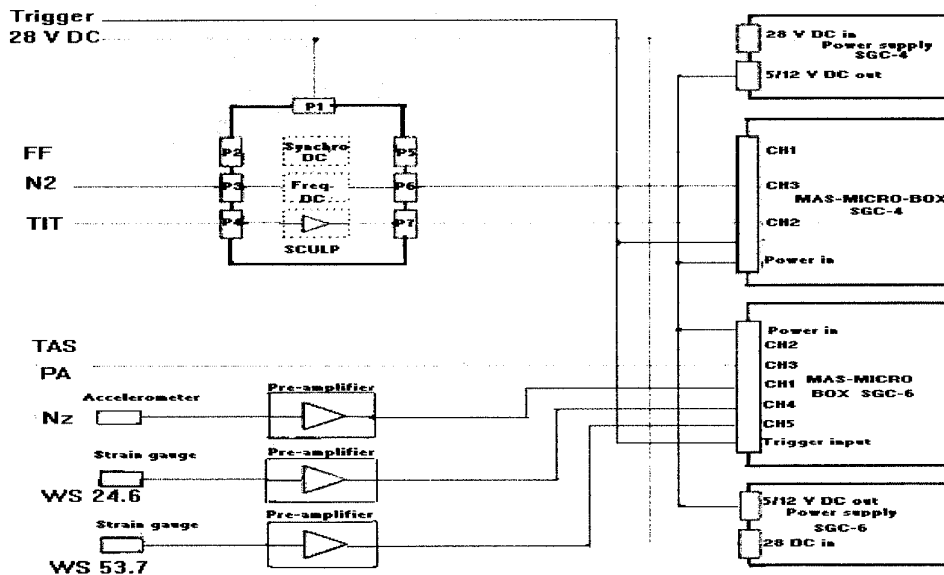


Figure 1- Flight data acquisition system

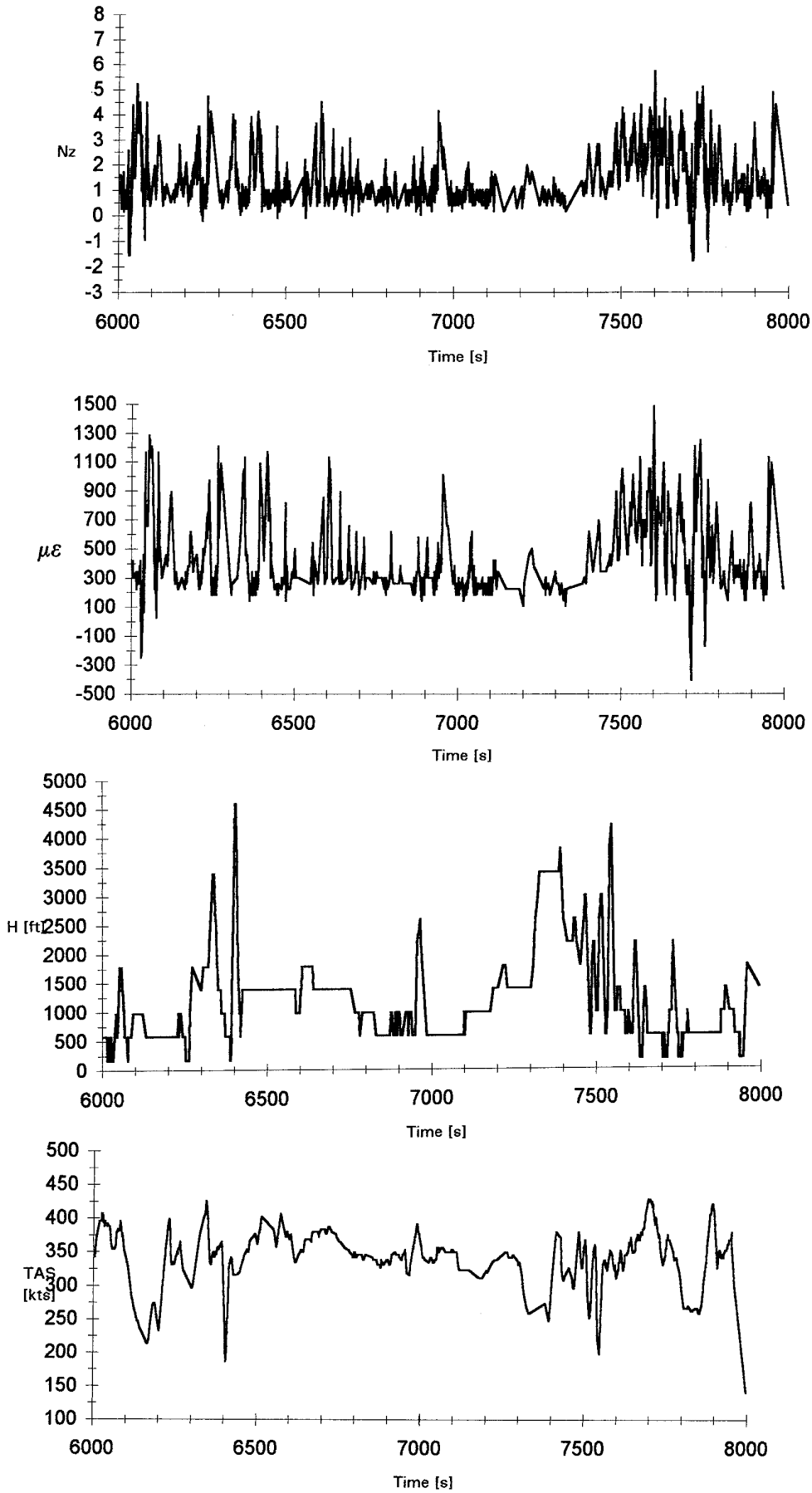


Figure 2 - Flight data measurements

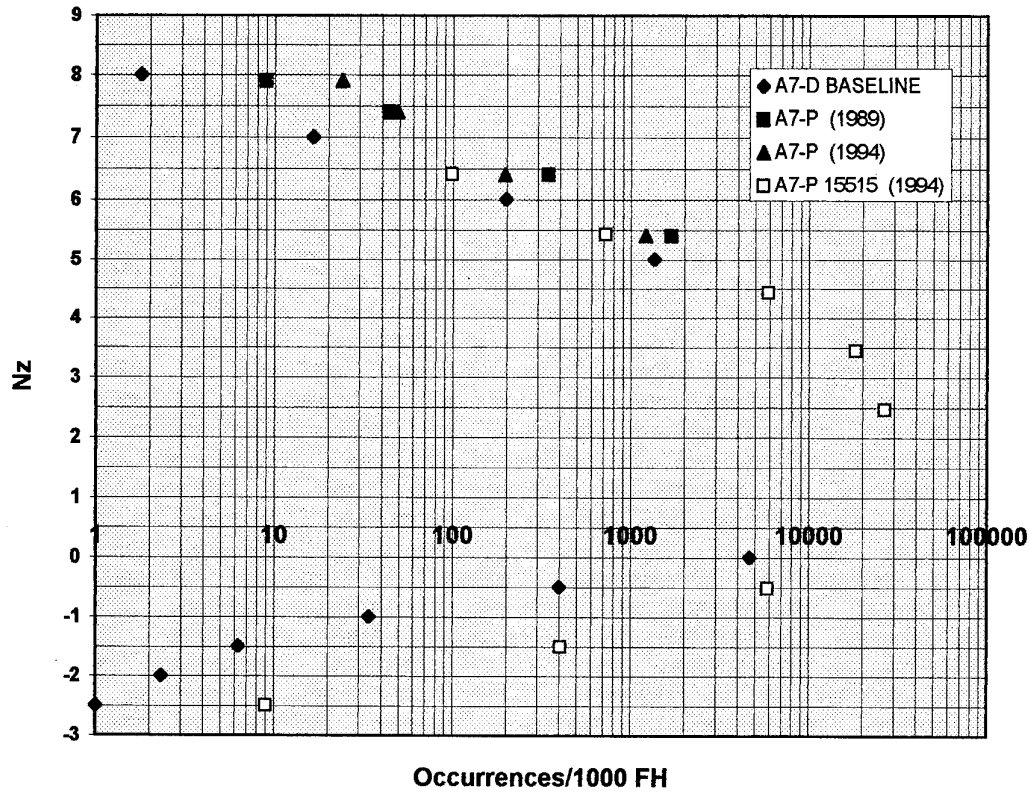


Figure 3 - A7-P load spectrum

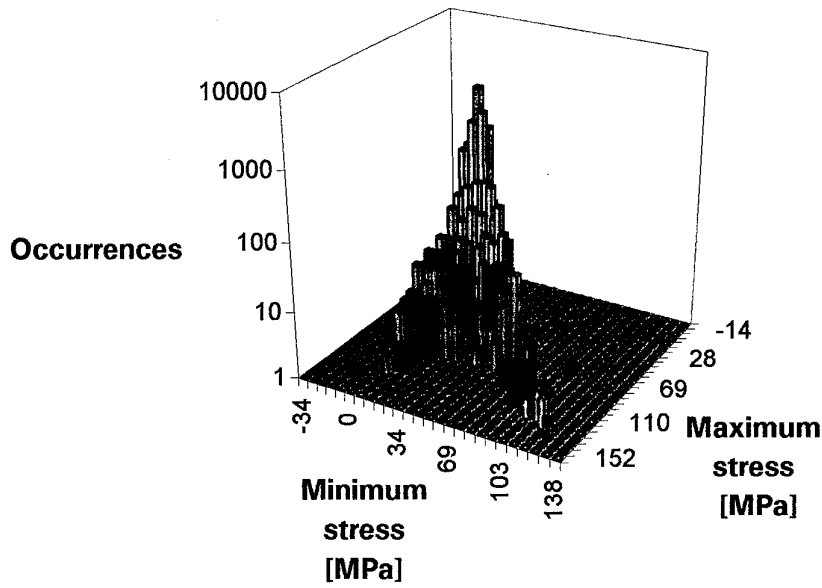


Figure 4 - Measured stresses range in location AE WS 53.7

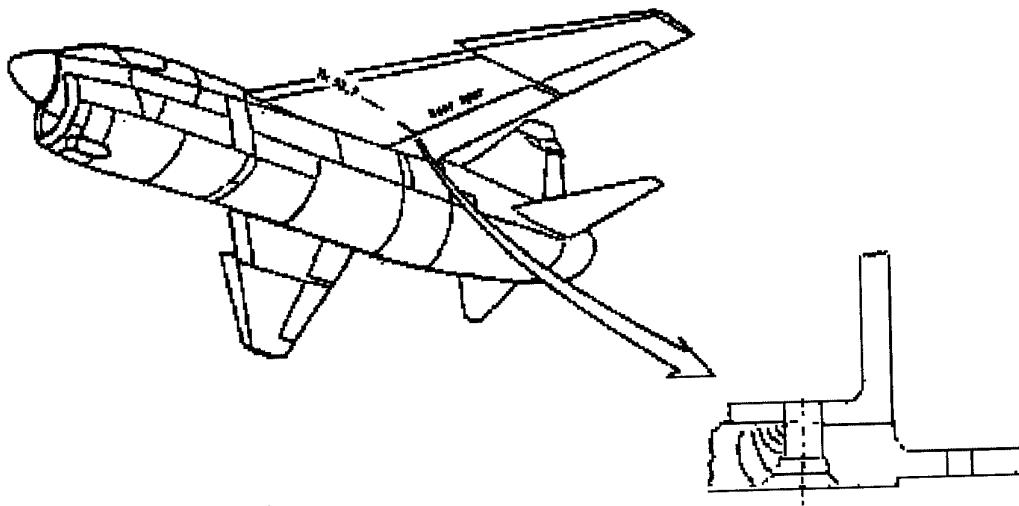


Figure 5 - A7-P fatigue critical location AE WS 53.7 (3)

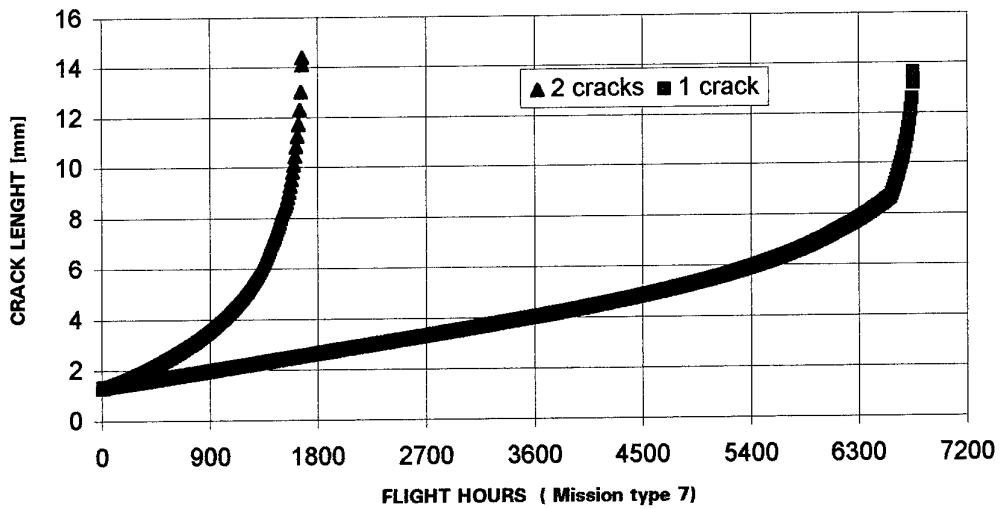


Figure 6 - Fatigue critical location AE Ws 53.7 crack propagation curves.

WIDESPREAD FATIGUE DAMAGE IN COMBAT AIRCRAFT

by

Hans Ansell and Thomas Johansson
Saab Military Aircraft
S-58188 Linköping
Sweden

ABSTRACT

Most attention to Widespread Fatigue Damage (WFD) has for obvious reasons been focused on the transport aircraft category. For such aircraft many of the prerequisite for WFD to occur are present. Colinear structure, stress field close to uniform, thin sheet sections and almost constant amplitude loading are all conditions that make some primary transport aircraft structures prone to develop WFD. In combat aircraft, these conditions are not so easily identified and not always present all together at the same time.

An inventory has been done of combat aircraft wing-structure that may have the potential to develop WFD. Saab combat aircraft designed during the 50:ies and 60:ies have been studied. Structures have been selected according to a set of conditions that may be important for WFD to develop. The design and stresses of such structure are discussed in view of available full-scale test results of presence or non-presence WFD.

INTRODUCTION

The role of damage tolerance is to assure structural integrity through in-service directed inspections of critical structures. The aircraft should be designed not to crack within one lifetime but may crack due to damage caused during manufacture or during service.

Specialists on the philosophy of Damage Tolerance have during a long period of years expressed concerns to the issue of Widespread Fatigue Damage in aging airframes. The studied designs are often representative of skin splices in pressurized fuselage panels. Some of the specialists, e.g. Swift [1], strongly recommend that "research for Multiple Site Damage (MSD) should be concentrated on the effects of MSD on lead crack strength rather than on crack growth investigations with a view to establishing inspection programs to manage the safety of aircraft in the presence of MSD".

Schijve [2] strongly advise for more realistic testing programs to find the locations where the fatigue resistance is insufficient and where it is likely that an MSD situation can arise. From [2] the following important statements are adopted:

- The real solution is a full-scale fatigue test until a life time which is a multiple of the target life. The frequently suggested twice the target life should be regarded as a bare minimum. Obviously, full-scale fatigue testing of new aircraft fuselage does not cover the deterioration of fatigue strength of lap joints due to corrosion effects. It is partly covered by continuing the full-scale test until a sufficient multiple of the target life.
- A pressurized fuselage should not be designed to prevent a catastrophic failure if MSD occurs. It should be designed for the non-occurrence of MSD. The fatigue life, although it will be finite, should be sufficient to have no significant

cracks in the fuselage lap joints. If the fatigue life is not sufficient, there will be an MSD problem.

Since fracture mechanics became the main tool for satisfying that primary structure are damage tolerant, i.e. that the structure should maintain sufficient residual strength until any cracks or defects are detected during scheduled inspections, demands on the traditional classical fatigue approach for satisfying durability are in more free hands. The following two main tasks for the use of classical fatigue were defined by Ansell, Johansson [3]:

- To satisfy durability, i.e. to design for good fatigue quality with moderate demands on risk levels for damage tolerant primary structure and for structure which is secondary in terms of safety.
- To satisfy safety for safe-life primary structure by design at remotely low failure risk levels, e.g. the landing gear.

A simple approach to handle the problem of MSD was outlined in [3] and the following were stated:

- Fatigue critical areas and areas expensive to repair should be designed for damage tolerance and with respect to fatigue.
- Areas of the structure which is prone to MSD should be fatigue designed with an extra margin of about 10-15% based on stress.

It is worth noticing that none of the presented airframes within this paper has been designed to meet any damage tolerance requirements. Further, at the present time the selected examples have not been analysed in accordance with the concept of damage tolerance, i.e. the authors do not answer the question if the structure will meet a residual strength criteria such as 120% of Limit Load.

Structure potentially susceptible to WFD is defined by the Industry Committee on Widespread Fatigue Damage, [4], as structure which has the characteristics of similar details operating at similar stresses where structural capability could be affected by similar cracking.

In general MSD occurs within a single cross section although it is also possible for MSD to occur in multiple cross sections. The latter type of damage occurs in a few locations where multiple cracks are parallel to each other and do not have the potential to link up. This type of damage will not increase the crack growth, but may reduce the residual strength.

To select areas susceptible to WFD the following two criteria have been used:

- Close to Uniform Stress Field.
- Similar Closely Spaced Stress Concentrations.

DEFINITIONS

A number of different definitions of Widespread Fatigue Damage (WFD) and its subsets Multiple Site Damage (MSD) and Multiple Element Damage (MED) are given in the literature. The phenomenon is strongly related to damage tolerance i.e. the attribute of a structure that permits it to retain its required residual strength for a period of usage after the structure has sustained specific levels of fatigue, corrosion, accidental or discrete source damage. Below is a set of necessary keywords adopted from [4]. Some of these are illustrated in Figure 1.

Widespread Fatigue Damage

Widespread fatigue damage in a structure is characterized by the simultaneous presence of cracks at multiple structural details that are of sufficient size and density whereby the structure will no longer meet its damage tolerance requirement.

Multiple Site Damage

Multiple site damage is a source of WFD characterized by simultaneous presence of fatigue cracks in the same structural element (e.g. fatigue cracks that may coalesce with or without other damage leading to a loss of required residual strength).

Multiple Element Damage

Multiple element damage is a source of WFD characterized by simultaneous presence of fatigue cracks in the similar adjacent structural elements.

Fatigue Crack Initiation

That point in time when a finite fatigue crack is first expected in a group of details where WFD is likely.

Occurrence of WFD

That point in time when the damage has grown such that the required residual strength can just be sustained.

Monitoring Period

The period of time between fatigue crack initiation and occurrence of WFD.

Design Service Goal

The period of time established at design and/or certification during which the principal structure will be reasonable free from significant cracking.

OBJECTIVE

The paper is intended to highlight and to discuss design and stresses for some chordwise wing-structure splices in the Saab aircraft designed during the 50:ies and 60:ies which may have the potential to develop Widespread Fatigue Damage. The presence or non-presence of cracks at multiple structural details will be discussed in view of full-scale test results, stress levels and stress distributions. The presentation is based on experiences from:

- A full-scale fatigue test of the wing of the 32 Lansen aircraft.
- Fatigue analysis on the lower skin joint of the outer wing of the 35 Draken aircraft.
- A full-scale fatigue test of the wing of the SK60 aircraft.
- A full-scale fatigue test of the complete airframe of the 37 Viggen aircraft.

BACKGROUND

Since World War II and the onset of the Cold War, Saab has developed and produced several generations of combat aircraft. The Saab 17 single-engined bombers were the company's first products, to be followed by the J21 twin-boom fighter and its jet successor the J21R. The next following jet fighters were the J29 Flying Barrel and the 32 Lansen aircraft but it was really the appearance of the Draken and Viggen which established Saab's reputation as a qualified developer and manufacturer of advanced fighters.

Today, Saab is the market leader for commuter aircraft in the 30 to 40 passenger range (Saab 340) and is presently delivering the new high-speed jetprop commuter aircraft in the 50 passenger range (Saab 2000) to airlines. On the military side, deliveries are ongoing to the Swedish airforce of the first fighter aircraft of the fourth generation (JAS39 Gripen). Manufacturing of the twin-seated version (JAS39B) is ongoing.

The present investigation deals with some wing structure splices from Saab 32, Saab 35, Saab 105 and Saab 37, Figure 2. Some general (brief) information about these four aircraft is given at the opening of each aircraft chapter. This information can be found in [5].

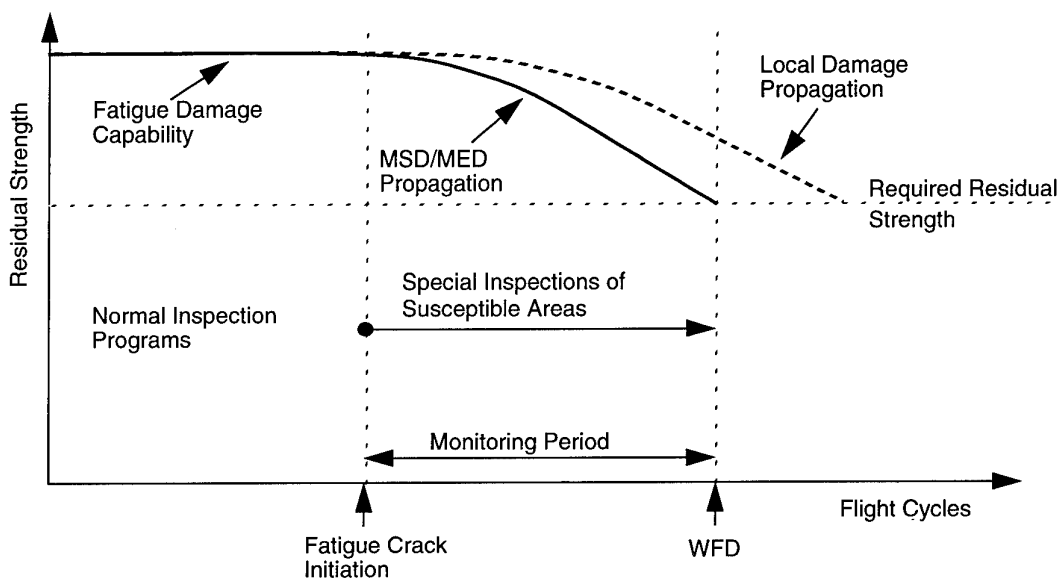


Figure 1. Residual Strength Capability and Resulting Inspections/Actions.

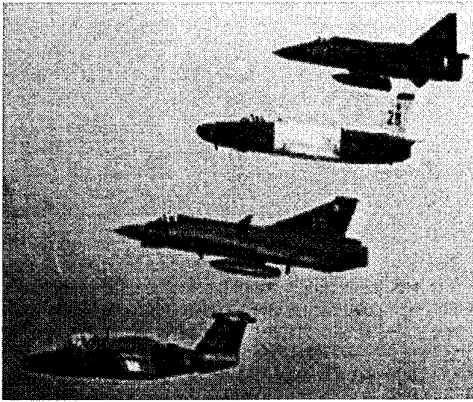


Figure 2. Four generations of Saab aircraft: Saab 105, Saab 35, Saab 32 and Saab 37.

The engineering design tools and requirements have been changed dramatically from the early fifties until now. It implies that the design criteria are different for different generations of aircraft. The stress-strength criteria used for the studied aircraft are summarized in Table 1 which also highlight some general information such as the maiden flight year, number of produced aircraft and production year.

Static Clearance

In the sizing process for static clearance of structurally significant items, a safety factor against failure of minimum $j=1.5$ is applied. For joints, such as wing-to-fuselage and fin-to-fuselage as well as hinges for all control surfaces etc. an extra factor $j_x \geq 1.15$ is applied bringing the total factor against failure up to a value $j \geq 1.725$.

Functionality and safety issues are covered by requiring that no detrimental deformations or lack of function will occur at the Limit Load.

Allowable strength for all materials is set to the Minimum Specification value or a statistical stringent value such as A- or B-values.

Fatigue Clearance

Fatigue life calculations are based on the application of the "Relative Palmgren-Miners Rule". The word relative implies that the failure criterion is adjusted to past experience from realistic spectrum tests by setting the critical damage sum somewhere between 0.5 and 1.0 depending on type of structure

and spectrum.

Fatigue design is based on a safe life approach. Experimental constant amplitude fatigue strength is adjusted to account for differences in geometry, surface finish and other material and structural parameter differences where the test data is not representative. The fatigue strength data thereafter are reduced to account for batch-to-batch variation and to produce "Safe Curves".

Damage Tolerance

Critical parts, i.e. parts which if failing, alone may cause the loss of an aircraft, are designed to comply with a damage tolerance requirement, such as the USAF specification MIL-A-83444.

Crack like flaws are from the damage tolerance point of view, assumed to be present at any location already when delivering the aircraft. Using fracture mechanics the growth of such flaws are predicted and inspection intervals are established.

SAAB 32 - LANSEN

The aircraft

During the fifties a replacement for existing Swedish Air Force attack, reconnaissance and night-fighter aircraft had to be initiated. The first project studies began in late 1946. After investigating several interesting projects the Air Force decided to go ahead with a single-engined transonic two-seater of fairly conventional layout. As had been the case with the Saab 29, the swept wing (39 degrees) was first tested in reduced scale on a Saab Safir trainer. Lansen was the first two-seat Swedish jet aircraft and the first equipped with a built-in search radar.

The Air Force requirements were very demanding at the time referred to: the aircraft was to be able to attack from a central base any part of Sweden's long coast in less than one hour with its armament and in all kinds of weather, day and night. Special development effort went into the integration of the electronic and weapons systems - Lansen was Sweden's first true systems aircraft - and also into the aerodynamic configuration. Particular problem areas were the large Fowler flaps and the shape of the rear fuselage, more precisely its integration with the movable tailplane.

The first Lansen version to be developed was the A32A attack aircraft and it made its first flight on November 3rd, 1952. Saab delivered a total of 287 A32As between December 1955 and June 1957 and the aircraft served all five attack Wings. The second Lansen version to be developed was the S32C reconnaissance aircraft. It made its first flight on March 26th, 1957.

Table 1 History of the presented Saab aircraft: Saab 32, Saab 35, Saab 105 and Saab 37.

	Saab 32 Lansen	Saab 35 Draken	Saab 105 SK60	Saab 37 Viggen
Maiden Flight	1952	1955	1963	1967
Aircraft Produced	447	604	190	329
Production Year	1955-60	1960-75	1965-72	1971-90
Design Service Goal (FLH)	1500	1500	3500	2800
Static Clearance	Yes	Yes	Yes	Yes
Fatigue Clearance	-	Life Ext.	Life Ext.	Yes
Damage Tolerance	-	-	-	Life Ext.
Full-scale Fatigue Test ^a	Yes	-	Yes	Yes

a. Complete airframe or complete wing

During 1955 development began of a night and all-weather fighter version of Lansen. Designated J32B, it made its first flight on January 7th, 1957. It had 50 percent more engine power and, consequently, true fighter performance. Including the two prototypes, a total of 120 J32Bs were delivered between July 1958 and May 1960.

During seven years, a total of 449 Lansen aircraft were produced in addition to seven prototypes.

Potential WFD-areas

A potential widespread fatigue damage item may be the lower wing chordwise skin splice at $Y_{34}=2140$. The splice joins the inner skin, $t=4$ mm, to the outer skin, $t=3$ mm, by way of a shaped splice plate and 8 mm rivets. The skin is made of AA2024 and the local geometry is illustrated in Figure 3.

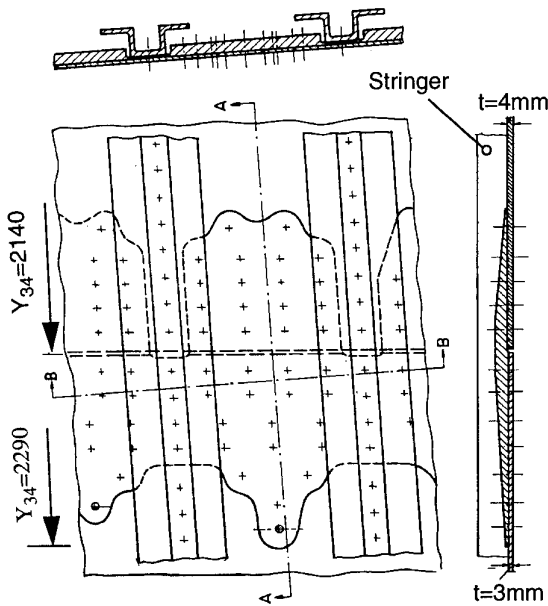


Figure 3. Wing: Lower skin splice at $Y_{34}=2140$.

Stress distribution and stress levels

The aircraft was originally designed for static clearance. Evaluated stresses from strain gauge measurements, on the wing fatigue test, at the maximum peak spectrum load (<LL) are presented in Table 2. The location of the strain gauges is given with reference to the stringer designation shown in Figure 4.

Location	$\sigma_{peak, Y34}$ (MPa)
Left side of 201	107
Left side of 205	126
Right side of 205	135
Right side of 206	131
Between 207/208	138
Left side of 208	133
Right side of 208	142
Rear Spar	133

Table 2. Lower skin stresses at $Y_{34}=2290$. Stresses at maximum peak spectrum load.

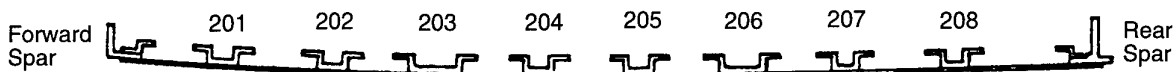


Figure 4. Definition of the stringer locations.

Full-scale fatigue testing

During the period March 1968 to November 1969 a complete wing fatigue test, flight-by-flight, was performed. The tested wing, taken from an A32A aircraft, had been used in service for almost 1500 flight hours, June 1956 to September 1966.

The main target with the test was to get knowledge about "if-when-where" fatigue cracks will appear and the damage sizes when the structure must be repaired.

The randomized test load sequence represented 100 flight hours and was based on available load statistics from the aircraft usage. This load sequence was repeated until the test was interrupted. No residual strength test was performed at the end of the fatigue test.

Several fatigue cracks were reported during the test, both primary cracks and secondary cracks. The positions of the cracks are noted in Figure 5 and 6. A general outline of all types of cracks are shown on one wing-half, in spite of the fact that some of those only appeared on one of the two wing-halves.

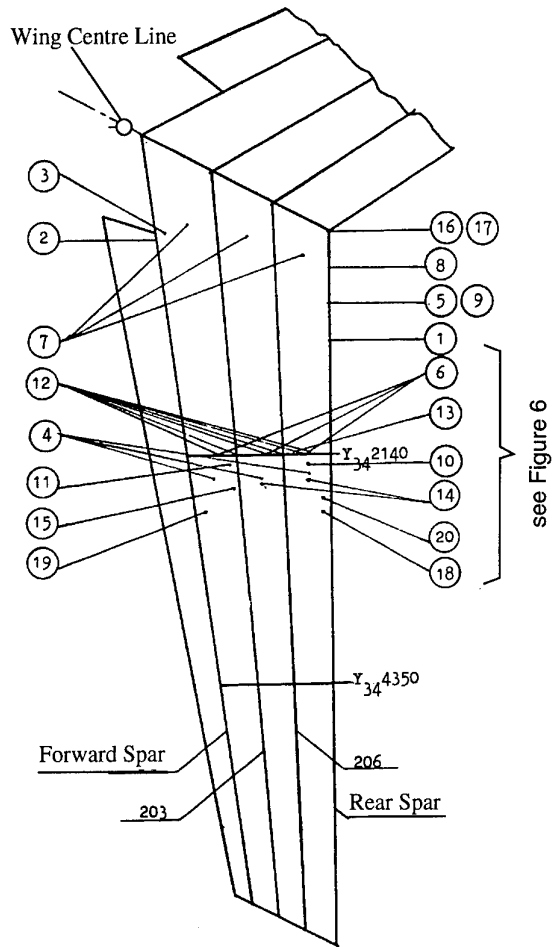


Figure 5. Type of fatigue cracks at the end of the fatigue test.

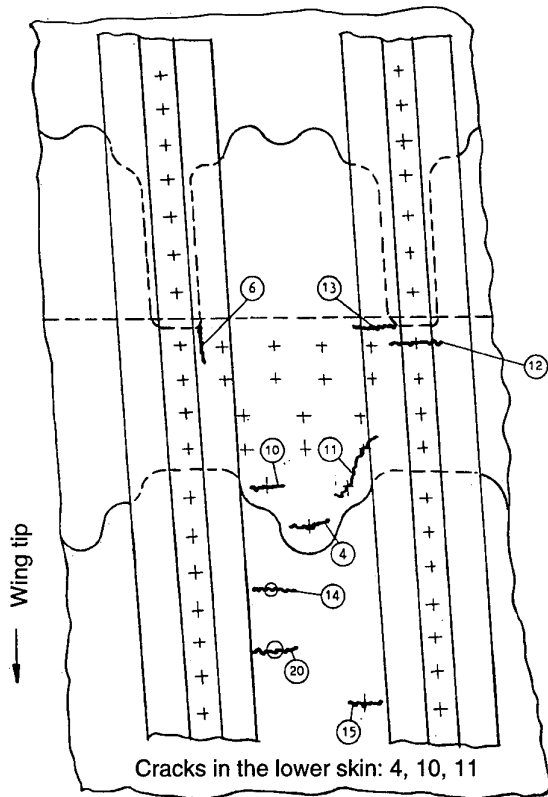


Figure 6. Type of fatigue cracks close to the $Y_{34}2140$ skin joint at the end of the fatigue test.

Radiographical and visual methods were used for inspection. The wing was loaded during the inspection periods to approximately 46% of the maximum peak spectrum load.

In this paper we have been focused on the crack with the designation 4, see Figure 6, i.e. a crack in the lower skin which can be looked upon as a fatigue critical crack.

The crack growth of several types of cracks were recorded during the test. The results for our crack-type No 4 at different locations are outlined in Figure 7. The curves have been extrapolated down to the size of the hole L_0 .

The first observation of type 4 cracks was indicated by X-ray at $1500+2400 = 3900$ simulated flight hours. The cracks were located between the stringers 203-204, 205-206 and 206-207.

The fatigue crack 4f, between the stringers 205-206, was stopped by ball thrust (backward directed crack front) after $1500+3800=5300$ simulated flight hours.

Conclusions

The stress level in the lower skin for the 32 aircraft is high and the stress distribution can be classified as uniform. At the selected joint similar stress concentrations are present. Testing indicate that:

- Fatigue crack initiation should not be expected but may occur close to the design service goal.
- It is likely that an MSD-situation can arise after a service period not so much longer than the design service goal.

Early fatigue crack initiation occurred in the "front" rivet holes where the pitch distance is large i.e. it is likely that the fatigue cracks can be detected during scheduled inspection before the structural capability is strongly affected by similar cracking. The simultaneous cracking of the type 4 cracks initiated scheduled in-service inspections. Nowadays, the aircraft is no longer used in advanced flying missions.

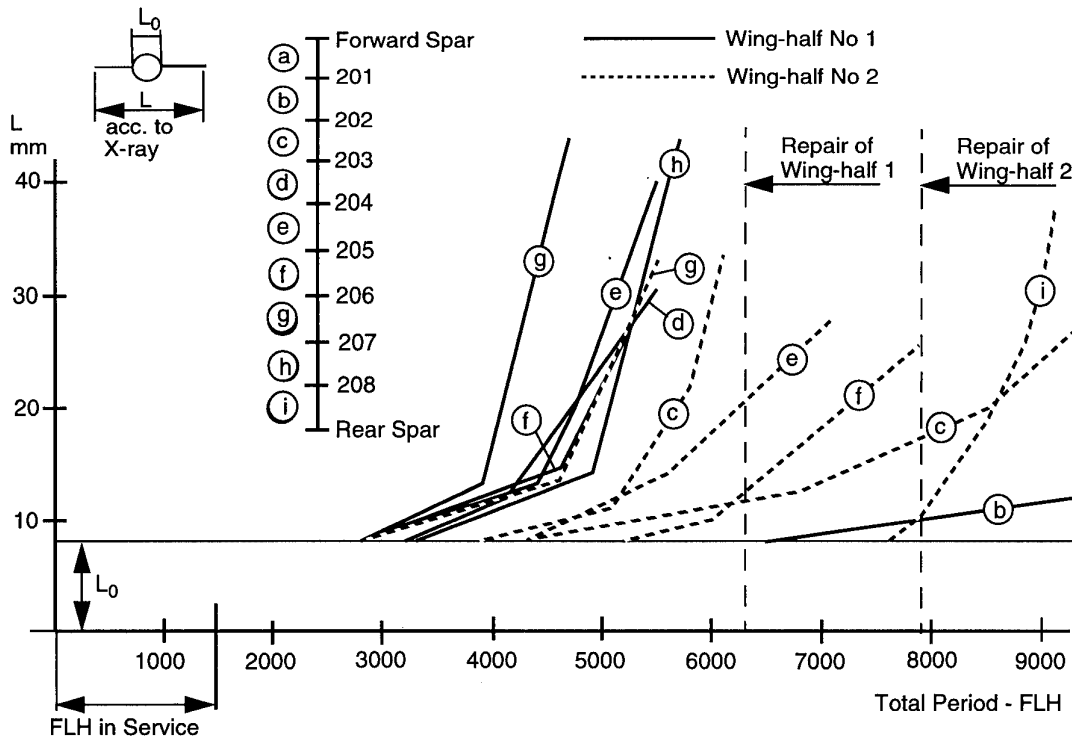


Figure 7. Crack growth of the crack type No 4 at the wing station $Y_{34}2140$.

SAAB 35 - DRAKEN

The aircraft

The Swedish Air Force accepted the project for full-scale development at the beginning of 1952 and in April three prototypes were ordered under the Air Force designation J 35. Later the name Draken was added. Draken was not a pure delta-winged aircraft; instead an extraordinary "double delta" configuration was chosen, see Figure 8. This configuration was selected in order to meet both the high-speed and low-speed requirements and short-take off and landing distance. The inner wing featured low drag but was broad and thick, permitting ample space for air-intakes, main undercarriage, fuel and gun armament. The inner wing was integral with the fuselage which gave many advantages from a stress point of view.

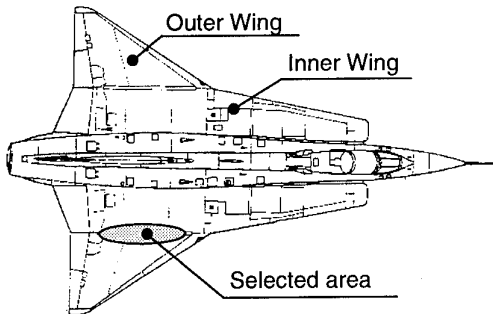


Figure 8. Saab J35F Draken.

Potential WFD-areas

A potential widespread fatigue damage item may be the lower skin splice to the chordwise extrusion in the outer wing, identified in Figure 8. The local geometry of the riveted joint is illustrated in Figure 9. Some important joint parameters are:

- Rivet size: $\varnothing 6$ mm
- Skin material: 2024-T4

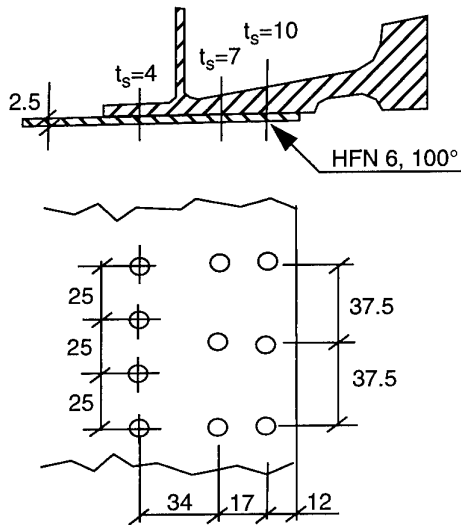


Figure 9. Outer wing: Lower skin to the chordwise extrusion.

Stress distribution and stress levels

The aircraft structure was designed to give rather low stress levels at Limit Load. It was also designed with redundant load paths, which give Fail-Safe qualities. No full-scale fatigue test to verify the structural integrity was carried out. The demand of

service life was not very high at the time referred to.

Calculated stresses by FE-analysis are shown in Figure 10 for two symmetrical flight load cases, LC213d and LC216. The lower skin stresses (σ_{Y7}) in the Y_7 -direction are moderate, below 90 MPa, however the stress distribution might be looked upon as more or less uniform between the two stations $X_7=10474$ and $X_7=12066$. It is worth noticing that the aircraft was originally designed (static clearance) to resist more severe stresses than those presented in Figure 10.

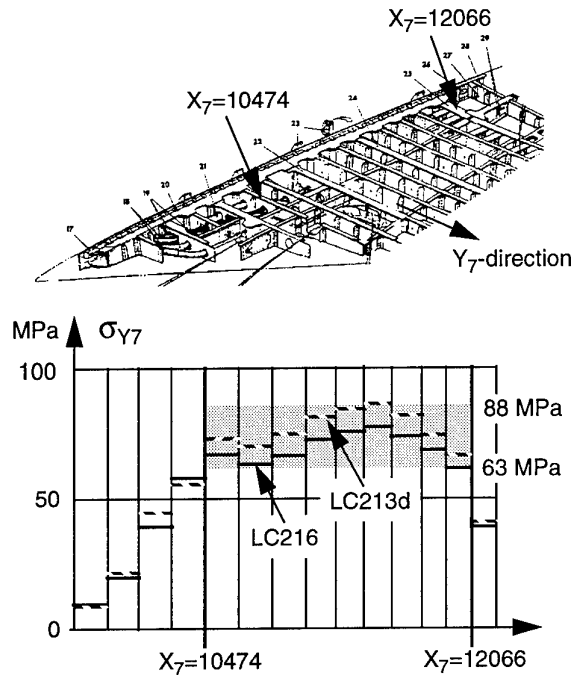


Figure 10. Outer wing structure Saab 35 and skin stresses for two symmetrical load cases.

Fatigue calculation

The use and handling of the aircraft in service became slightly different from what was originally anticipated, and the extension of service life was reconsidered in steps. A limited number of aircraft has been equipped with counting accelerometers near the centre of gravity in order to give load statistics.

The design of aircraft Saab 35 is from stress-strength point of view based on static clearance. During a number of life extension programmes the goodness of the existing design has been assessed by classical fatigue calculations. The outcome of the latest life extension programme for the J35F a/c-version was reported 1988 and was supported by e.g.:

- Mission analysis and operating profile of the aircraft.
- Pressure measurements in new wind tunnel tests.
- Updating of the aerodynamic loading and establishing of the load basis for a new FE-calculation.
- Checking the internal static load distribution and the calculated fatigue status.
- An extensive FE-model of the airframe.

The results of the life extension programme show that some joints and splices, such as the joining of inner wing spar caps to fuselage frames, splices in frames and the joining of outer wing to inner wing are potentially fatigue critical areas.

Classical fatigue calculations have been done, based on con-

stant amplitude safe life fatigue data, to study the goodness of fatigue resistance. The results for our joint are presented in Table 3. In the third column the calculated cumulative damage sums have been corrected to account for an increase of the actual stress levels by 15% in accordance with the proposed MSD-criteria from [3]. The correction is in this paper simplified by use of a damage factor equal to 1.15^q where $q=5$ is chosen. The allowable cumulative damage sum is normally set to 0.7.

X_7	$\Sigma n/N$	$\Sigma n/N$ at 15% stress increase
10562	0.03	0.06
11159	0.06	0.12
11499	0.12	0.24
11985	0.05	0.10

Table 3. Calculated cumulative damage sums based on safe life fatigue curves. Reference period $T_0=2500$ fh.

Conclusions

In spite of the fact that the stress distribution is more or less uniform over a large area and the presence of closely spaced stress concentrations, MSD should not be expected in this lower skin area since the stress level is low. Furthermore, the outcome of classical fatigue calculations indicate that the fatigue resistance is good enough to withstand a 15% stress increase i.e. the above statement about MSD is supported.

SAAB 105 - SK60

The aircraft

The Saab 105 aircraft was initially a private-venture project, it was adopted by the Swedish Air Force in 1961. It was a high-winged, moderately swept, twin-engine monoplane with instructor and pupil seated side by side.

On December 16th, 1961, the Government authorized Saab to "continue the development of Saab 105 twin-jet trainer which also include attack capability" and in April 1962 a preliminary contract was signed between the Air Board and Saab for procurement of 130 aircraft on the condition that "the coming flight testing showed that the aircraft could meet the requirements". A Government decision in March 1964 formally authorized the Air Board to go ahead with the acquisition of the new SK 60, as the aircraft had been designated.

Manufacture of the two prototypes began in 1962 and on July 1st 1963 it was ready to go. The early flight testing showed that both the air intakes and outlets had to be considerably modified, including the wing root beneath where the intakes were situated. The second prototype flew for the first time in June 1964. The third aircraft produced, which was the first production aircraft, made its first flight in August 1965. At this point, the Air Board had increased its order from 130 to 150 aircraft.

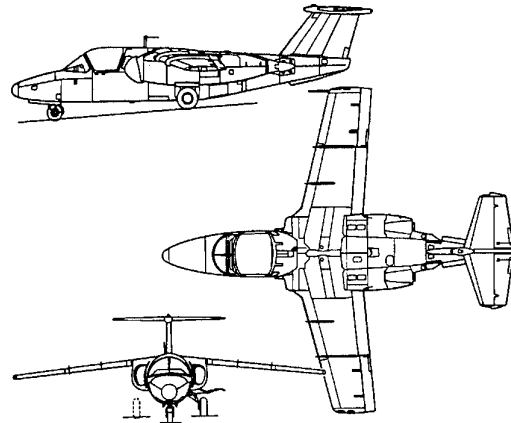


Figure 11. The Aircraft Saab 105 - SK 60

The SK 60 has continuously served with a total of five Wings and will continue to serve for many years to come as a result of a structural modification programme started in 1988 and involving as many as 135 aircraft. The fact that so many aircraft still serve in the Swedish Air Force after 20-25 years of service as a trainer and low-level strike aircraft of the original 150 produced is proof of the inherent flight safety of this design.

Potential WFD-areas

Three chordwise wing sections with pronounced fatigue cracking at the end of a wing fatigue test are noted in Figure 12. In this paper the lower skin joint at $Y_{308}=0$ is discussed. The local joint configurations "at and between" the stringers are shown in Figure 13. Some joint parameters are:

- Steel Bolt: $\varnothing 6$ mm and $\varnothing 8$ mm
- Skin material: 2024-T4

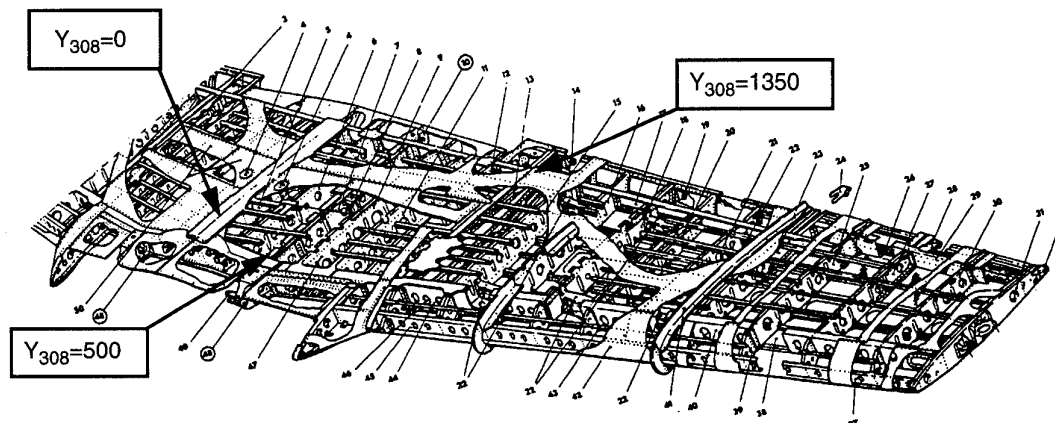


Figure 12. Wing structure SK 60 aircraft. Wing sections with pronounced fatigue cracking at the end of a fatigue test were $Y_{308}=0$, $Y_{308}=500$ and $Y_{308}=1350$.

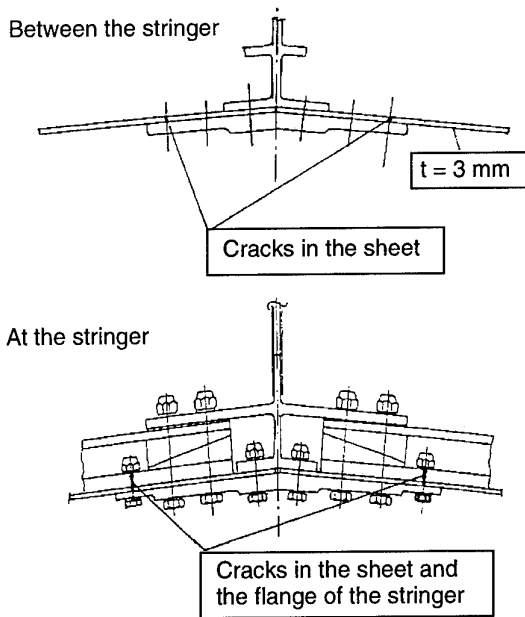


Figure 13. Local joint configuration at $Y_{308}=0$. Location of cracks are shown.

Stress distribution and stress levels

The aircraft was originally designed for static clearance. Evaluated stresses from strain gauge measurements at a symmetrical limit load case (extrapolated values) are illustrated in Figure 14 for the wing section $Y_{308}=100$. The lower skin stresses (σ_{Y308}) in the Y_{308} -direction are classified as severe and the stress distribution might be looked upon as uniform.

Full-scale fatigue testing

A complete wing fatigue test started in September 1986 and ended with a residual strength test in December 1989. The test was performed on a new wing and the loads were based on a mission profile corresponding to the aircraft usage until 1984/1985 in the Swedish Air Force. The flight-by-flight fatigue test was continued during approximately 19500 simulated flight hours. Unfortunately there was a minor error in the applied load distribution during the first half of the test, the forward spar was loaded too severe in some sections.

The main target with the programme was to study if the wing was able to withstand a life extension. Also coupon test was performed on a simple riveted joint to study the effect of Cold Expansion on the fatigue strength in a "three layer bonded sheet configuration" which is the design on the lower skin.

Several cracks were reported in a number of wing areas however, the crack growth rates were classified as slow and the wing design demonstrated good damage tolerance capability. The residual strength was larger than 120% limit load (136%LL) in the presence of several fatigue cracks in the fracture section, $Y_{308}=0$. The inspection methods used to establish crack sizes were penetrant testing, inductive testing and X-ray testing.

The occurrence of fatigue cracks at the end of the fatigue test is illustrated in Figure 15 for the wing section $Y_{308}=0$. Fatigue cracks in the lower skin are frequently occurring at the stringer locations.

In Figure 16 the skin fracture section is illustrated after the residual strength test. The fracture went through the "front" fastener holes at the stringer locations where fatigue cracking was present.

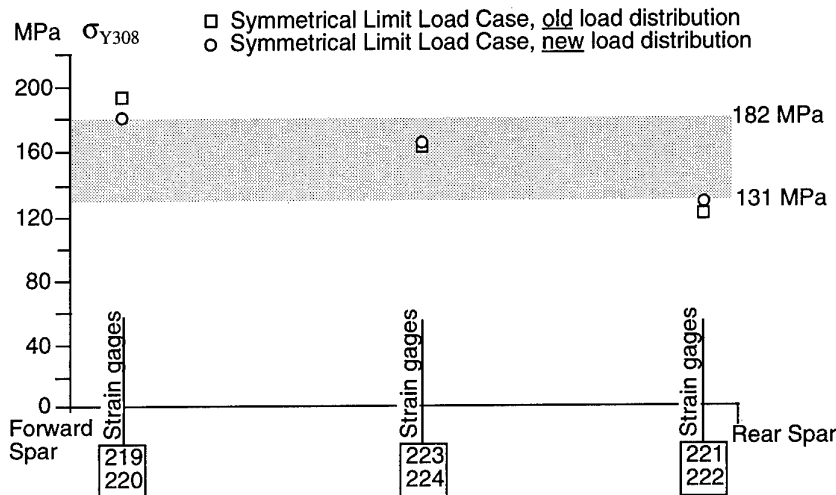


Figure 14. Stress levels in the lower skin at the chordwise section $Y_{308}=100$.

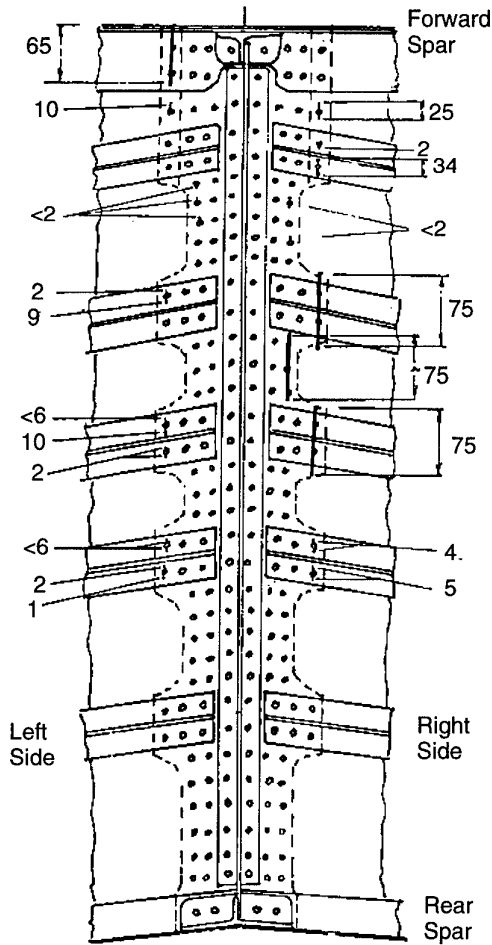


Figure 15. Locations of skin fatigue cracks at the end of the fatigue test, $Y_{308}=0$.

Conclusions

An MSD-situation can arise in this selected area since the stress level is severe, the stress distribution can be classified as uniform and similar stress concentrations are present. It is only a matter of time. The outcome from the full scale fatigue test supports the statement. The testing indicate that:

- Fatigue crack initiation can be expected to occur beyond the design service goal.
- It is likely that an MSD-situation will arise after a service period much longer than the design service goal.

The crack growth rate was classified as slow and the residual strength was demonstrated to be higher than 120% Limit Load in the presence of large fatigue cracks at several locations i.e. a moderate life extension can be accepted without hazard the structural safety.

SAAB 37 - VIGGEN

The aircraft

Preliminary studies of designs intended to replace the Swedish Air Force's existing attack, reconnaissance and fighter aircraft begun in the early 1950's. In February 1961, the Air Board submitted its detailed requirements to the industry and in December 1961 a Government decision to develop Aircraft System 37 was taken. The system would include the AJ 37 attack aircraft forming the multi-role "platform" to be followed by the S 37 reconnaissance version and the JA 37 fighter version.

The new aircraft had an outstandingly novel aerodynamic configuration. This advanced configuration used a fore-plane fitted with flaps, in combination with a main delta wing. The delta-shaped fore-plane is placed in front of and slightly above the main wing, and thus serves as a lift generator, making possible very low landing-speeds.

In April 1965, a very detailed mock-up was completed for a first checking of the design drawings. In the mean time the new aircraft had been given the name Viggen.

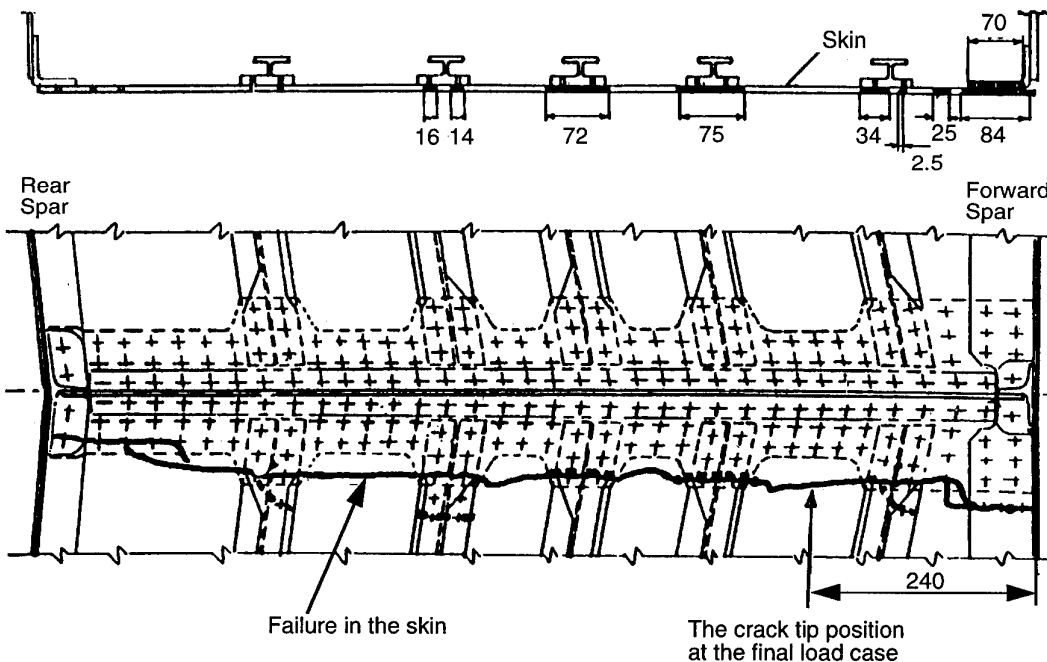


Figure 16. Fracture in the skin joint $Y_{308}=0$ at the residual strength test.

Preceded by extensive ground testing in Saab's new simulation centre, the first Viggen prototype made its first flight on February 8th, 1967. In April 1968 the Government authorized a first production order for 175 Viggen aircraft in the attack (AJ 37) and two-seat trainer version (SK 37). The order was later amended to include an additional five AJ 37s and two reconnaissance versions. The first production of AJ 37s was delivered in 1971 with the production of the first Viggen generation continuing until 1979 with delivery of the 180th aircraft.

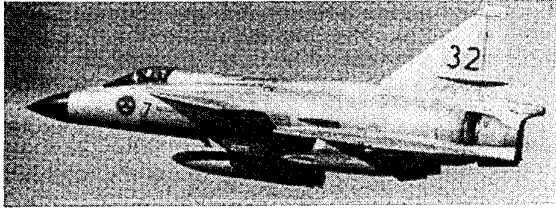


Figure 18. The AJ 37 was the first Viggen version to go into service.

Most new aircraft invariably suffer from teething troubles, but in 1974-75 Viggen had more than its fair share. Three aircraft were lost in flight under unexplained circumstances, fortunately without loss of aircrew. After extensive investigations, it became clear that the main wing spar - a heavy light metal forging - had developed cracks partly initiated by faulty drilling. Cracks could only be found in the wing spar design used in the first 28 production aircraft, after which another spar design had been introduced to allow for a longer service life. Contributing to the problem was that the high performance of the Viggen platform was used more severe by the pilots than originally specified for the attack and reconnaissance versions. The heavier spar design was retrofitted in more than 20 aircraft. For later aircraft no modification was required.

The first JA37 prototype made its first flight on September 27th, 1974. Six development aircraft were used for the JA37 programme accumulating nearly 3000 test flights to verify the system. The first production aircraft flew on November 4th, 1977. Eventually a total of 149 JA 37s were ordered, with deliveries starting in 1979. The JA 37 series brought Viggen up to a total of 329 aircraft.

Potential WFD-areas

The selected joint is located at the wing rib Y₃₁₉ 2550 and is pointed out in Figure 19. The local joint design is illustrated in Figure 20 and indicate the use of honey-comb panels. There is an extensive use of bounded honey-comb panels on the Viggen

aircraft, see Figure 21. Some joint parameters in the tested airframe are:

- Cold expanded holes.
- Titanium bolts: Ø8 mm
- Sheet materials: 7075-T6 Clad.

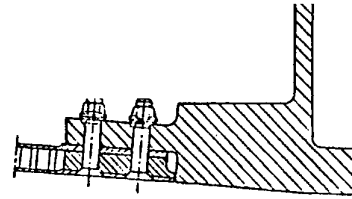


Figure 20. The local joint design at Y₃₁₉2550.

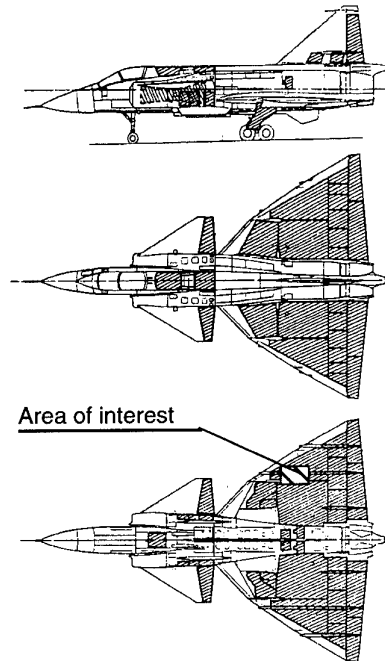


Figure 21. Illustration of the extensive use of bounded honey-comb panels on the Viggen aircraft.

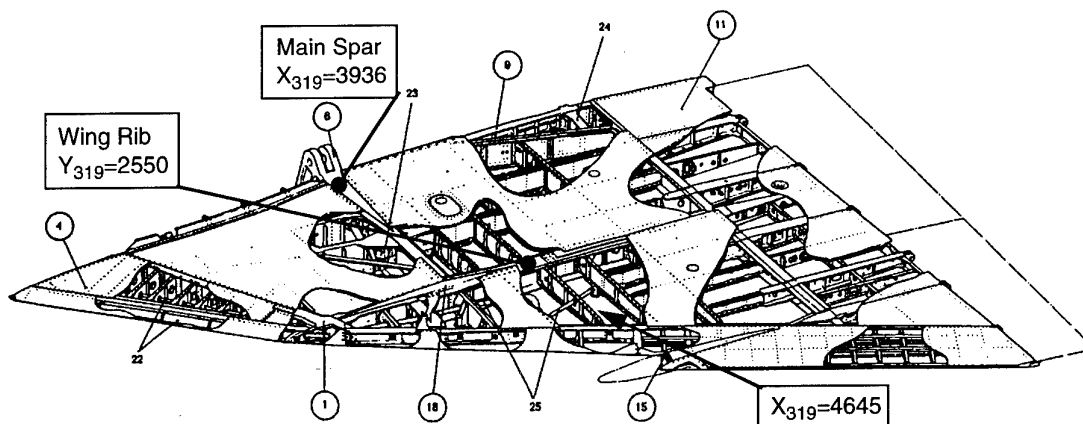


Figure 19. Wing structure of the Viggen aircraft.

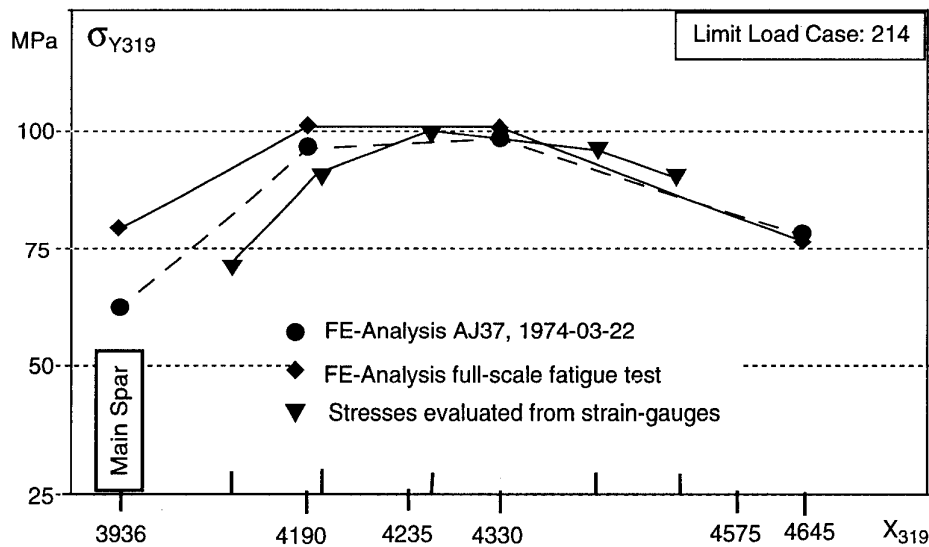


Figure 22. Stress levels in the lower skin at the chordwise section $Y_{319}2550$.

Stress distribution and stress levels

The design of the Viggen aircraft is from stress-strength point of view based on static clearance and fatigue clearance. Evaluated stresses from strain gauge measurements and calculated stresses by FE-analysis for a symmetrical limit load case, LLC214, are outlined in Figure 22. The stress level ($\sigma_{Y_{319}}$) in the Y_{319} -direction is moderate, at or below 100 MPa, and there is some doubt to classify the stress distribution as uniform.

Full-scale fatigue testing

The full-scale fatigue test of the airframe of the attack version of the Viggen aircraft has earlier been described in e.g. the Swedish ICAF Reviews 1979, 1981 and 1983. The real flight by flight testing was finished after 16 800 fh without damaging fracture. The first 14 000 fh were carried out in a regular way and the last 2 800 fh with all load levels increased 15%.

Several cracks were reported but most of them were small, only a few cracks have been looked upon as a potential failure risk. The final inspection at the end of the test consists of two steps. The first level was a regular after-testing-procedure and the second one included more dismounting work than normally. The most frequently used inspection method was penetrant testing. Inductive testing has been used on fastener holes with diameter $\varnothing 6$ mm - $\varnothing 10$ mm.

The inspections did not report any cracks at all at our selected chordwise joint at the wing rib $Y_{319}2550$.

Conclusions

An MSD-situation should not be expected in the studied area since the stress level is low and the stress distribution hardly can be classified as uniform. Furthermore, the fatigue resistance has been increased by the use of cold expansion. The outcome from the full-scale fatigue test strongly supports the statement.

CONCLUSIONS

The current review of WFD potential areas of older but still operative Saab aircraft have, for the selected areas, indicated that:

- The stress levels for the 35 and 37 aircraft are much lower than the stress levels that must be present if WFD should occur within the design life or after a moderate life extension.

- Stress levels for the 32 aircraft are higher than the stress levels for a/c 35 and 37. Testing indicate that a WFD-situation may occur after a service period not so much longer than the design service goal. However, the fastener pitch is large (equal to the stringer pitch) at the section where the most severe primary fatigue crack occurred. This type of fatigue crack can be allowed to grow to a large size before some interaction effects can be expected i.e. it can easily be detected during scheduled inspections.
- Stress levels for the 105 aircraft are higher than the stress levels for a/c 35 and 37. Testing indicate that a WFD-situation may occur beyond the design service goal. However, the fastener pitch is large (equal to the stringer pitch) at the fracture section. The crack growth rate was classified as slow and the residual strength was demonstrated to be high in the presence of large cracks at several locations i.e. a moderate life extension can be accepted without hazard the structural safety.

REFERENCES

- [1] Swift, T; Widespread Fatigue Damage Monitoring - Issues and Concerns. Presented at the 5th International Conference on Structural Airworthiness of New and Aging Aircraft, June 16 - 18, 1993.
- [2] Schijve, J; Comments on the problem of Multiple-Site-Damage. ICAF Doc. No. 1827.
- [3] Ansell, H - Johansson, T; Structural Reliability in Fatigue Design - Application to Riveted Joints and the Presence of Multiple Site Cracking. Presented at the International Workshop on Structural Integrity of Aging Airplanes, Atlanta Georgia, March 31 - April 2, 1992.
- [4] Industry Committee on Widespread Fatigue Damage. Final Report; A Report of the Airworthiness Assurance Working Group Industry Committee on Widespread Fatigue Damage, July, 1993.
- [5] Andersson, Hans G; Saab Aircraft since 1937. First published 1989.

THE EFFECT OF PROOF PRESSURE TESTING ON THE RETARDATION
OF MULTI-SITE DAMAGE

Squadron Leader E. Bittel
Headquarters Logistics Command
Royal Air Force Wyton
Huntingdon, Cambs, PE17 2DL
UNITED KINGDOM

SUMMARY

A range of laboratory specimens, representative of pressurized fuselage structures, were tested under constant amplitude loading to provide data for comparison with theoretical predictions. A proportion of specimens were subjected to single overload cycles. The theoretical model was based on recognised methods of contemporary fracture mechanics, allied to a simple but effective technique for modelling the growth behaviour of a fatigue crack following an overload cycle. Good agreement was noted between predictions and experimental results, and recommendations for further development of the model are being formulated.

INTRODUCTION

The well-publicised 1988 incident of the Aloha Airlines Boeing 737, which lost a large section of fuselage structure in flight, ushered in the era of research into ageing aircraft. This incident had been caused by a collinear series of fatigue cracks which had suddenly linked to form a single critical crack, leading to the catastrophic failure. At the time of the Aloha incident, the RAF was operating a number of relatively high-life VC10 aircraft. Concerns about the structural integrity policy for this type, based on a number of factors, prompted a change to a wholly damage-tolerant system, and a structural assurance policy was instigated which included a fuselage proof testing programme. As a further refinement to the process of proof testing on the VC10, this research project was instigated with the aim of assessing the potential benefits of overloads in retarding crack growth, particularly in the context of Multi-Site Damage.

The Royal Air Force Perspective

At the time of the Aloha incident, the RAF was operating a large number of relatively high-life aircraft, mainly in the roles of air transport (AT), air-to-air refuelling (AAR) and maritime reconnaissance (MR). Of the various types involved, the aircraft receiving most attention from a structural integrity aspect was the VC10, which was operating in both AT and AAR roles (Ref 1). The design of the VC10 is an early example of the 'fail-safe' philosophy and

incorporates appropriate design features. In addition to the declared design features, the then Civil Air Regulations Board required additional demonstrations of the damage tolerance of the VC10 structure. These tests, and others on the wing, fin, control surfaces and undercarriage were used to develop additional safe-life limits for the aircraft. However, in 1988 and 1989, several factors combined to prompt a review by the RAF of VC10 structural integrity and, in May 1989, it was decided that the VC10 inspection philosophy should disregard the supplementary safe-life limits and revert to a wholly damage-tolerant system.

For the longer term, a complete re-analysis of the fatigue and damage data was initiated and, while awaiting the results of the re-analysis, a programme of fuselage structural assurance was devised to fill this knowledge gap. The programme comprised proof pressure testing with acoustic emission monitoring. The principle is that a successful proof pressure test, at a cabin differential of 1.33 times the maximum in-service cabin differential pressure, demonstrates that any cracks which are present in the structure under test are less than the critical length at the proof load. If the post-proof test inspection then reveals no cracking, it can be assumed that any cracks which are present are, at worst, just about to become detectable. It can then be assumed that these cracks propagate under normal service loads. In the case of the VC10, acoustic emission testing was to be used during the proof test, both as a safety measure and as an aid to crack detection. There was also the prospect of a degree of retardation of fatigue crack growth, albeit unquantified, subsequent to the proof test. As a further refinement to the process of proof testing on the VC10, the structural integrity specialist branch of the RAF sponsored this research project with the aim of assessing the potential benefits of overloads in retarding crack growth, particularly in the context of Multi-Site Damage.

THE EFFECTS OF OVERLOAD AND
THEORETICAL MODELS

Although the subject of overloads has most recently been studied in the specific context of proof testing, the early investigations were centred on

improving the accuracy of fatigue calculation methods such as the Miner-Palmgren cumulative damage technique. However, the first attempt to produce a simple computational technique was by Wheeler (Ref 2). Subsequently, various attempts have been made to derive different models of the crack retardation phenomenon, notably that by Willenborg. For this research, the Wheeler model was selected for simplicity and ease of coding into a computer program.

Wheeler Crack Growth Retardation Model.

From an examination of experimental data, Wheeler proposes a relationship of the form:

$$a_r = a_0 + \sum_{i=1}^r C_{pi} \cdot f(\Delta K_i)$$

...where C_{pi} = retardation parameter.

a_0 = initial crack length

a_r = crack length after r cycles

The experimental data implied that this parameter should lie between zero and one, and should increase from its smallest value immediately after the peak load to unity at some later time. These requirements can be satisfied if the parameter is given the following form:

$$C_p = \left(\frac{R_y}{a_p - a} \right)^m ; a + R_y < a_p$$

... where R_y = extent of current yield zone

$a_p - a$ = distance from crack tip to elastic-plastic interface

m = shaping exponent

Thus, using this model, the crack growth rate is retarded until such time as the yield zone for the current load cycle moves out of the prior yield zone, at which point the crack growth returns to 'normal'. The exponent m gives the facility to shape the scaling parameter to accord with experimental data, so as to take account of different material properties and different loading spectra for the same material. The exponent m , just like the Paris constants C and n , must be determined experimentally. There is only a very limited amount of data available on this factor. In fact, this is probably the major shortcoming of the Wheeler method, namely that it requires a

significant level of calibration, specific to the particular problem being studied, before work can proceed to a prediction of crack growth.

MULTI-SITE DAMAGE (MSD)

The basis for this research was taken from the paper by Partl and Schijve (Ref 3), in which the aim was to produce a simple computational technique for the prediction of fatigue crack growth in a MSD configuration. A series of fatigue crack growth tests were carried out on specimens fabricated in 2024-T3 alloy, using the centre-cracked tension (CCT) and multiple open-hole (MOH) configurations only. The prediction method incorporated the effects of mutual interactions between cracks, as well as between cracks, holes and the panel boundaries. The basic CCT specimens were precracked with a central saw cut of tip-to-tip length 10mm, and then subjected to cyclic loading ($R = 0.03$, $\Delta\sigma = 65$ MPa). The objectives of this phase were to obtain the constants for the Paris crack growth equation, and to evaluate the effectiveness of a 'marker-load' technique for measuring crack growth compared to the 'potential drop' method.

The MOH specimens were prepared in three different configurations, as shown in Fig 1. The predictions of the fatigue lives of these MSD specimens agreed well with the experimental results, but there was a significant loss in accuracy if the prediction was made without regard for crack/boundary interaction. The authors noted that the interaction effect was relatively small for the major part of the fatigue life, but increased noticeably when the inter-crack ligaments became smaller than half the pitch between holes, but by that stage the life remaining was relatively short. The prediction technique revealed the same trend. The main conclusion drawn from this was that there was little to be gained from applying more sophisticated prediction techniques to the study of MSD.

DERIVATION OF COMPUTER-BASED MODEL

The intention from the outset was to keep the model as simple as possible. This was partly because of the limitation on time for development and also an acknowledgement of the findings in Ref 3, namely that increasing the sophistication of prediction techniques for MSD was unlikely to bring any real benefit.

Implementation.

It was first necessary to select a MSD configuration for the experimental phase which

would also be modelled. Obviously, an almost infinite range of possibilities was available, but it was decided to devise a small elemental configuration which, when repeated in a periodic array, would be representative of actual MSD. The type 1 configuration from Ref 3 was selected for the following reasons:

- a. It would lend itself readily to both theoretical and experimental work
- b. It would, by inclusion of the appropriate geometry correction factors, allow analysis of configurations which included both equal and unequal crack lengths. In this way, it would be possible to simulate both uniform and non-uniform MSD cracking with a relatively simple model, albeit one which would not represent a true random distribution of crack sizes. Although it is possible, using the appropriate geometry correction factors, to develop a model in which all cracks are of different lengths, the development was restricted initially to a configuration of partial symmetry in which outer crack A = outer crack D and inner crack B = inner crack C, but the outer cracks A and D were not equal to the inner cracks B and C.

EXPERIMENTAL METHODS AND RESULTS

The experimental program consisted of two main parts:

- a. Basic fatigue tests on CCT specimens to determine constants for the Paris crack growth equation, and also to determine a value for the Wheeler retardation exponent.
- b. Fatigue testing on MOH specimens, both with and without overloads, to provide data for the verification of the theoretical model.

The material chosen for the experimental work was 17swg (1.42mm) L163 (L72) aluminium alloy which is used extensively in the fuselage skins of the VC10. All specimens were cut from two sheets of L163 taken from the same batch, and the loading direction of the specimens was transverse to the rolling direction of the sheet.

In the basic tests (specimens CCT1 - 12), the panels were notched from a central hole using a saw blade. The first five specimens were loaded cyclically until failure, and the crack growth data was used to obtain the constants C and n for the

Paris crack growth equation. Specimens CCT6 - 12 were subjected to the same loading, but with the inclusion of single overload cycles to a variety of overload factors from 1.33 up to 2. This data was used to derive a value for the Wheeler retardation exponent m. Recalling that the exponent may require recalibration for different loading parameters, the range of overload factors for CCT6 - 12 was deemed necessary to ensure that the derived value of m was valid for overload factors which would be relevant to proof pressure testing of aircraft fuselages.

In the MSD tests, MOH specimens (MOH1 - 6) were subjected to the same basic loading as the CCT specimens to give a basis for comparison with the computer model. The remaining specimens (MOH 7 -12) were subjected to single overload cycles ranging from 1.33 to 1.7. The hole size and the hole pitch were all chosen to be broadly representative of the fuselage skin assembly of the VC10.

Experimental Equipment and Conditions

All specimens were tested in laboratory conditions at normal room ambient temperatures. All tests were carried out on an Instron Model 8032 servohydraulic loading machine with a maximum capacity of 10 tons. Cyclic loading was carried out under computer control, with fixed blocks of 10,000 cycles for the CCT specimens and 5000 cycles for the MOH and riveted specimens. However, it was possible to pause the loading at intermediate points if this was deemed necessary, such as during the latter stages of high rate crack growth. A sinusoidal waveform was used, and the constant amplitude loading was applied between the stress limits of $\sigma_{\max} = 75\text{MPa}$ and $\sigma_{\min} = 5\text{MPa}$, which gave the stress ratio $R = 0.06$, and $\Delta\sigma = 70\text{MPa}$. The frequency f of load application was 10Hz for CCT, and MOH specimens.

Crack length measurement was carried out using a Baker optical travelling microscope with 10x magnification mounted on a support beam rigidly fixed to the vertical pillars of the Instron test machine. The vernier scale mounted on the beam permitted readings to an accuracy of 0.02mm.

Analysis of Experimental Data.

All data derived from the experimental specimens is presented at the end of the report. The crack labelling conforms to the earlier convention. For the basic CCT specimens, the data was reduced to a plot of da/dN vs. ΔK . For

the MOH specimens, the measurements of crack half-length a and cycles N were used to produce the standard crack growth curves.

In the time which was available for experimental work, it was not possible to build up the comprehensive amount of data for each configuration of specimen, crack pattern and overload factor which is desirable for detailed comparison. Rather, the aim was to obtain a basic understanding of the potential scope of the theoretical model by reference to a limited number of specimens representing the boundaries within which the model would be expected to show applicability.

Basic CCT Specimens. The testing of the basic CCT specimens was necessary to obtain values for the coefficients to be inserted into the crack growth equations. The data from the CCT specimens without overload, when plotted as da/dN vs ΔK , conformed to the recognised pattern of three distinct crack growth phases. However, there was a relative lack of data for the early stages of crack growth. The lack of data in the initial growth phase was largely due to the difficulty experienced with the optical equipment in identifying the existence of early cracking. This problem was encountered to a greater or lesser extent throughout the practical work, and was particularly evident when testing MOH and riveted specimens, where the crack lengths were considerably smaller than those in the CCT specimens.

Basic CCT Specimens with Overload. In the case of the specimens subjected to overload, the data from specimens CCT 7 and 12, subjected to single overloads, showed that a value of 2.7 for the Wheeler retardation exponent would give good correlation between theoretical and experimental results. There is very little reference data available for this constant, but the treatment of the retardation phenomenon in Ref 4 indicates that this value is of the correct order. Subsequent application of this exponent to the prediction of crack growth with other overload factors showed generally very good agreement, although experimental data for the specimens with a 1.5 factor overload diverged from prediction at a noticeably earlier stage than for the other overload factors. Additional experimental data would be required before this could be confirmed as a definitive feature in the comparison between theory and experiment. In addition to the above, the model showed good agreement with the experimental data in predicting only very modest fatigue life increases from the lowest value of overload, but much greater life increases for the

highest overload factors (1.7 and 2). In all cases, it is also considered that some improvement in prediction accuracy might be obtained for the latter stages of crack growth if the Paris crack growth equation were replaced by the Forman method of calculation.

MOH Specimens. The theoretical predictions were compared with cycles to crack link-up, although in some cases the link-up showed a complex type of inter-crack ligament, and in other cases the crack growth paths departed so far from the initial direct lines that no join-up occurred and the cracks overlapped. Overlap was also taken as a failure criterion, since crack growth subsequent to overlap was virtually zero. There was generally good agreement between theoretical predictions and experimental results. The most significant problem was the non-simultaneous crack initiation evident on all specimens. This immediately introduced differences between experiment and the prediction model which contains the implicit assumption that crack growth proceeds according to the Paris law from the first cycle. Clearly, crack initiation from a saw cut requires some crack extension before a well-defined through-crack has developed. This can delay one crack more than another and thus deviate from the ideal of simultaneous growth for all cracks.

All predictions were made for equal size cracks of half-length 7.5mm, since this was the nominal size of the cracks introduced into the specimens by saw-cuts. In practice, small variations in this size were impossible to avoid, and this would provide a further reason for differences between theory and experiment. There was no intention of carrying out separate computer runs and analyses to simulate all the actual crack pairs observed during the experimental work, and indeed the problem of non-simultaneous crack initiation would have rendered this effort largely nugatory. However, it was found that small changes in initial crack sizes input into the computer program would produce significant differences in predicted lives, as defined by the first crack link-up. In particular, it was possible to achieve much better agreement with experimental results by input of slightly increased values of initial crack length.

In the absence of any changes to the input data, however, the model tended to produce modest over-estimates of the actual fatigue life of the specimens before link-up. Crack growth rates for the model were comparable to those observed in the specimens, although a separate analysis of the experimental data into da/dN vs ΔK curves would give a more detailed basis for comparative

comment. The model correctly predicted the growth of the cracks from the centre hole to be ahead of the outer hole cracks, although this was exaggerated in most experimental cases by the non-simultaneous initiation. In general, the experimental data indicated that the stress intensity factor values obtained from the compounding process were satisfactory.

MOH Specimens with Overload. The MOH specimens which were subjected to overloads again showed good general agreement with the theoretical model, but the scatter of experimental data was significant and more noticeable than for specimens MOH 1-6 without overload. Once again, the problem of achieving simultaneous crack initiation tended to reduce the value of the comparison, particularly on the subject of fatigue life to first crack-link-up. Nevertheless, the model again correctly predicted the dissimilar crack growth rates between the inner and outer holes, and showed good correlation with the actual crack retardation effects which were observed on the experimental specimens. As was noted on the CCT specimens, the lowest level of overload produced only a small increase in overall fatigue life, whereas the effect for the highest overload factor (1.7) was much more pronounced. In this respect, the agreement between the model and specimen MOH 12 was particularly encouraging.

Retardation Model

The good agreement between predictions and experimental results indicates that the choice of the Wheeler crack retardation model was justified. These results were achieved with a single value for the retardation exponent for a range of overload factors between 1.33 and 2. Thus, despite its acknowledged lack of a rigorous theoretical basis, the Wheeler model is recommended as a practical means of representing retarded fatigue crack growth in CCT and MOH specimens of the types investigated in this research. Its use for riveted specimens requires further investigation.

Application to a Real Problem

The work described in this paper covers the derivation of mathematical models of simple physical specimens, the configurations of which were based broadly on materials and loading criteria representative of those existing in the fuselage structures of transport aircraft. Despite the encouraging level of agreement which has been achieved between theoretical and experimental results, a great deal of development

work would be required on the model before it could be applied directly to actual aircraft structures. Nevertheless, the objectives of this thesis include the requirement to assess the effectiveness of proof pressure testing in the retardation of MSD. Accordingly, the model was run using data representative of the VC10 where available, and assuming other data (such as the value of the Wheeler retardation exponent) where better information was not readily available.

The first run assumed uniform MSD at the outer row of rivets (pitch 30mm) in the VC10 fuselage lap-splice joint, such that the visible part of each crack extended 1.5mm beyond the edge of the head of the countersunk rivet. Using the same maximum and minimum stress levels as in the CCT and MOH modelling, which were based on VC10 cabin pressure levels, the model predicted a fatigue life of 80900 cycles before crack link-up would occur. A second run was then carried out, with the imposition of a single overload of factor 1.33 at 40000 cycles. The model forecast a new fatigue life of 81100 cycles. This small increase was in keeping with the observed experimental results for all CCT and MOH specimens with overload i.e. that the normal pressure proof factor of 1.33 produced only very small improvements in fatigue life, whereas the higher levels of proof load were much more effective in retarding crack growth. However, the decision to apply higher proof pressures would demand careful consideration of the likelihood of a structural failure under the proof load, but this question is beyond the scope of this paper.

CONCLUSIONS

A simple computer model of MSD was produced from existing crack growth prediction methods, using the compounding method to obtain values for the stress intensity factors. The model configuration was an elemental representation of a periodic array of MSD cracks, but was capable of allowing a limited degree of non-uniformity in crack sizes. The model was developed to incorporate a facility for introducing crack retardation after a proof load. This facility was based on a recognised mathematical model. Predictions produced by the model were verified against experimental data obtained from a range of laboratory specimens subjected to cyclic constant amplitude loading representative of loads imposed on transport aircraft fuselages; a proportion of the specimens were also subjected to single overload cycles.

REFERENCES

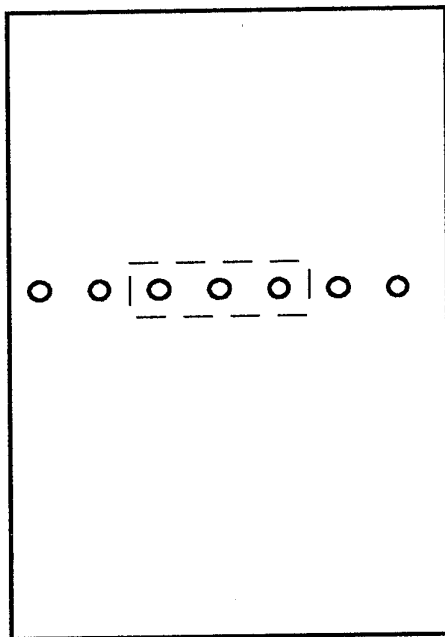
1. Gp Capt G M Skinner Management of the VC10 Structural Integrity Programme.
Unpublished Article - February 1992
2. Wheeler, O E Spectrum Loading and Crack Growth.
J Basic Eng, March 1972.3. Cartwright, D J
3. Partl, O Multiple Site Damage in 2024-T3 Alloy Sheet.
Schijve, J Delft University Report LR-660, January 1992
4. Broek, D Elementary Engineering Fracture Mechanics (4th Ed)

(c) British Crown Copyright 1993 /MOD

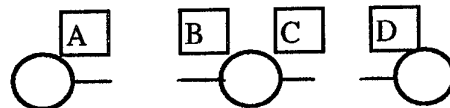
Reproduced with the permission of the Controller of Her Britannic Majesty's Stationery Office.

Acknowledgement is given to EMAS Publications Ltd, Warley, West Midlands, UK.

ILLUSTRATIONS AND GRAPHS



Three central holes



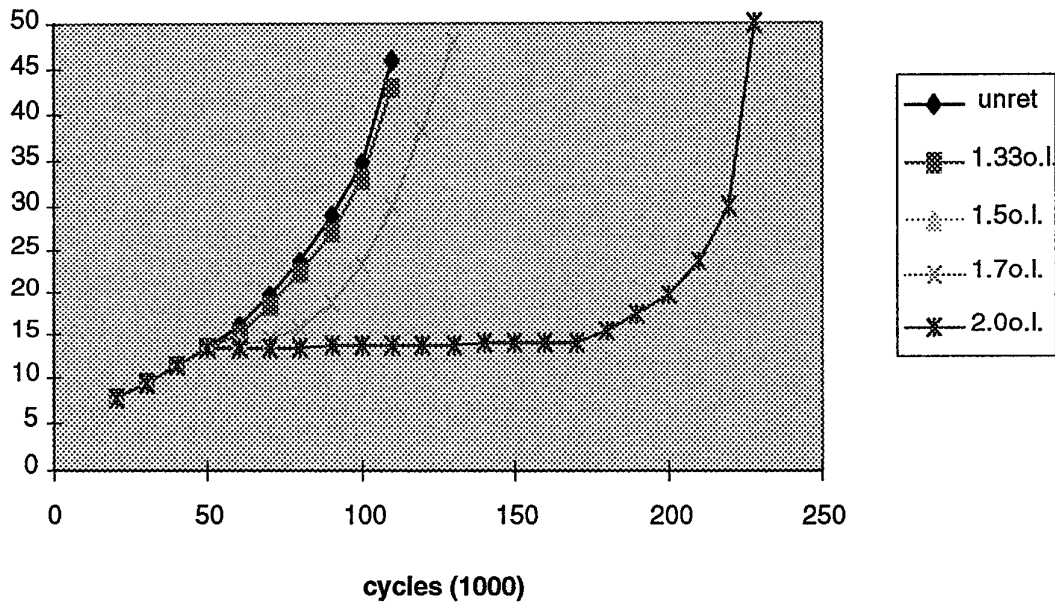
Hole Pitch 40mm

Hole dia. 4mm

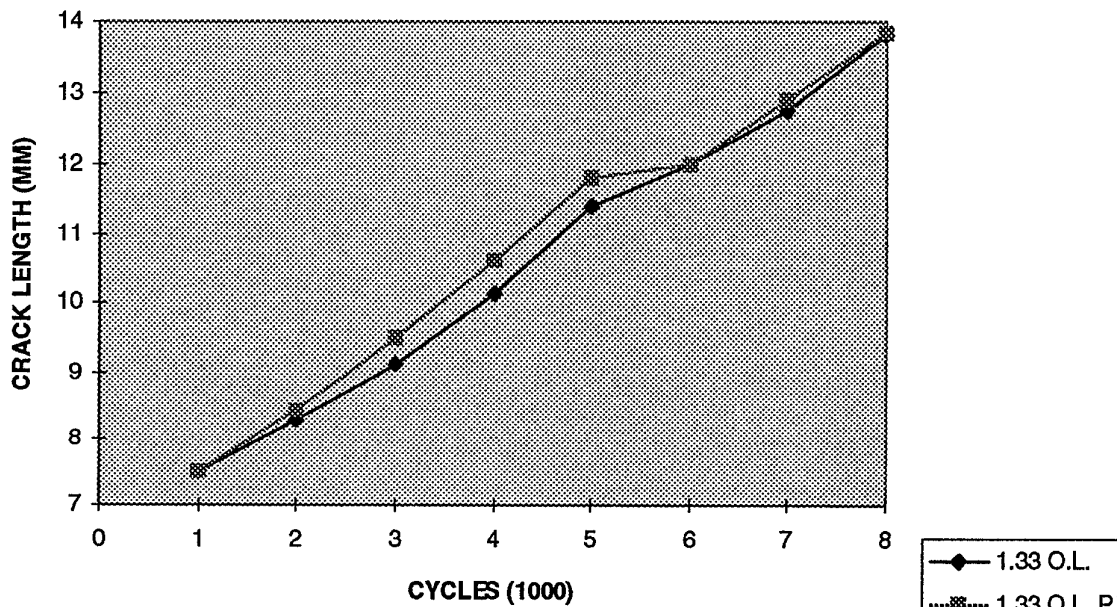
MSD Configuration for MOH Specimens

Crack Growth in Centre Cracked Specimens with Various Overloads

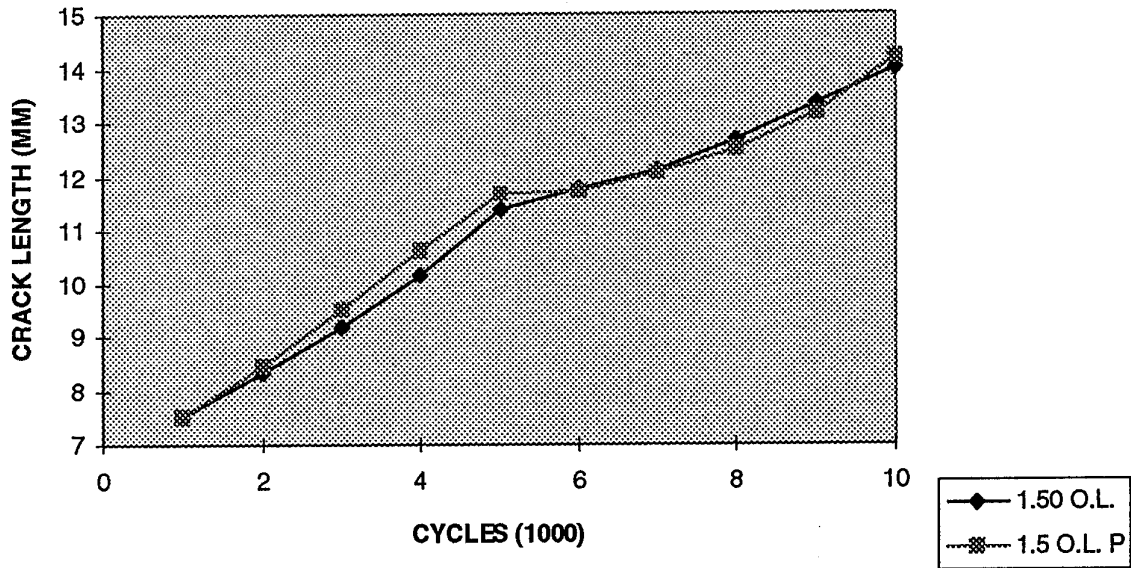
crack length (mm)



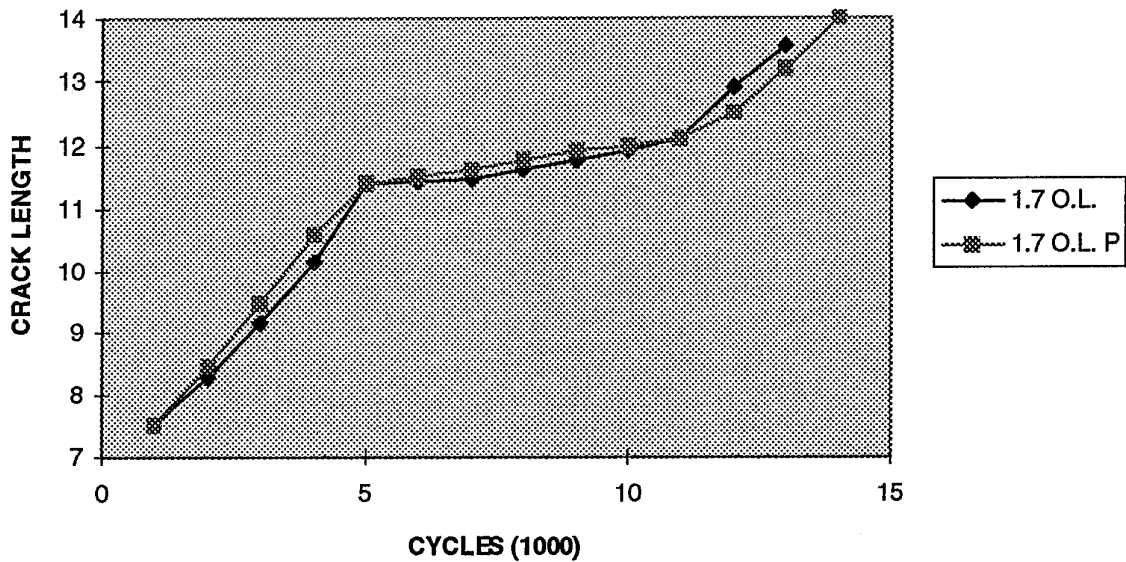
COMPARISON OF EXPERIMENTAL AND PREDICTED CRACK GROWTH FOR M.O.H. SPECIMEN (O.L.=1.33)



COMPARISON OF EXPERIMENTAL AND PREDICTED CRACK GROWTH FOR M.O.H. SPECIMEN (O.L.= 1.5)



COMPARISON OF EXPERIMENTAL AND PREDICTED CRACK GROWTH FOR M.O.H. SPECIMEN (O.L.= 1.7)



REPORT DOCUMENTATION PAGE

1. Recipient's Reference	2. Originator's Reference	3. Further Reference	4. Security Classification of Document
	AGARD-CP-568	ISBN 92-836-1021-0	UNCLASSIFIED/ UNLIMITED
5. Originator Advisory Group for Aerospace Research and Development North Atlantic Treaty Organization 7 rue Ancelle, 92200 Neuilly-sur-Seine, France			
6. Title Widespread Fatigue Damage in Military Aircraft			
7. Presented at/sponsored by The 80th Meeting of the AGARD Structures and Materials Panel, held in Rotterdam, The Netherlands, 10-11 May 1995			
8. Author(s)/Editor(s) Multiple			9. Date December 1995
10. Author's/Editor's Address Multiple			11. Pages 222
12. Distribution Statement There are no restrictions on the distribution of this document. Information about the availability of this and other AGARD unclassified publications is given on the back cover.			
13. Keywords/Descriptors			
Military aircraft		Degradation	
Transport aircraft		Aircraft maintenance	
Fatigue (materials)		Widespread fatigue damage	
Fatigue limit		Damage tolerance	
Structural analysis		Service life	
14. Abstract			
<p>Several countries have been experiencing aging aircraft related problems in their military fleets, particularly among their military transport aircraft. The most troubling aging aircraft structure-related issue is widespread fatigue damage (WFD), sometimes termed as multiple site damage, whose onset due to fatigue causes a dramatic structural strength reduction. Invariably, when WFD occurs, the affected model in the fleet is subjected to an extensive modification program which is almost always expensive and time-consuming.</p> <p>A Specialists' Meeting on the subject was held in order to explore ways and means to quantitatively predict structural degradation on account of WFD as a function of usage and when WFD is likely to occur.</p>			

Aucun stock de publications n'a existé à AGARD. A partir de 1993, AGARD détiendra un stock limité des publications associées aux cycles de conférences et cours spéciaux ainsi que les AGARDographies et les rapports des groupes de travail, organisés et publiés à partir de 1993 inclus. Les demandes de renseignements doivent être adressées à AGARD par lettre ou par fax à l'adresse indiquée ci-dessus. *Veillez ne pas téléphoner.* La diffusion initiale de toutes les publications de l'AGARD est effectuée auprès des pays membres de l'OTAN par l'intermédiaire des centres de distribution nationaux indiqués ci-dessous. Des exemplaires supplémentaires peuvent parfois être obtenus auprès de ces centres (à l'exception des Etats-Unis). Si vous souhaitez recevoir toutes les publications de l'AGARD, ou simplement celles qui concernent certains Panels, vous pouvez demander à être inclu sur la liste d'envoi de l'un de ces centres. Les publications de l'AGARD sont en vente auprès des agences indiquées ci-dessous, sous forme de photocopie ou de microfiche.

CENTRES DE DIFFUSION NATIONAUX

ALLEMAGNE

Fachinformationszentrum Karlsruhe
D-76344 Eggenstein-Leopoldshafen 2

BELGIQUE

Coordonnateur AGARD-VSL
Etat-major de la Force aérienne
Quartier Reine Elisabeth
Rue d'Evere, 1140 Bruxelles

CANADA

Directeur, Services d'information scientifique
Ministère de la Défense nationale
Ottawa, Ontario K1A 0K2

DANEMARK

Danish Defence Research Establishment
Ryvangs Allé 1
P.O. Box 2715
DK-2100 Copenhagen Ø

ESPAGNE

INTA (AGARD Publications)
Pintor Rosales 34
28008 Madrid

ETATS-UNIS

NASA Headquarters
Code JOB-1
Washington, D.C. 20546

FRANCE

O.N.E.R.A. (Direction)
29, Avenue de la Division Leclerc
92322 Châtillon Cedex

GRECE

Hellenic Air Force
Air War College
Scientific and Technical Library
Dekelia Air Force Base
Dekelia, Athens TGA 1010

ISLANDE

Director of Aviation
c/o Flugrad
Reykjavik

ITALIE

Aeronautica Militare
Ufficio del Delegato Nazionale all'AGARD
Aeroporto Pratica di Mare
00040 Pomezia (Roma)

LUXEMBOURG

Voir Belgique

NORVEGE

Norwegian Defence Research Establishment
Attn: Biblioteket
P.O. Box 25
N-2007 Kjeller

PAYS-BAS

Netherlands Delegation to AGARD
National Aerospace Laboratory NLR
P.O. Box 90502
1006 BM Amsterdam

PORTUGAL

Força Aérea Portuguesa
Centro de Documentação e Informação
Alfragide
2700 Amadora

ROYAUME-UNI

Defence Research Information Centre
Kentigern House
65 Brown Street
Glasgow G2 8EX

TURQUIE

Millî Savunma Başkanlığı (MSB)
ARGE Dairesi Başkanlığı (MSB)
06650 Bakanlıklar-Ankara

Le centre de distribution national des Etats-Unis ne détient PAS de stocks des publications de l'AGARD.

D'éventuelles demandes de photocopies doivent être formulées directement auprès du NASA Center for AeroSpace Information (CASI) à l'adresse ci-dessous. Toute notification de changement d'adresse doit être fait également auprès de CASI.

AGENCES DE VENTE

NASA Center for
AeroSpace Information (CASI)
800 Elkridge Landing Road
Linthicum Heights, MD 21090-2934
Etats-Unis

ESA/Information Retrieval Service
European Space Agency
10, rue Mario Nikis
75015 Paris
France

The British Library
Document Supply Division
Boston Spa, Wetherby
West Yorkshire LS23 7BQ
Royaume-Uni

Les demandes de microfiches ou de photocopies de documents AGARD (y compris les demandes faites auprès du CASI) doivent comporter la dénomination AGARD, ainsi que le numéro de série d'AGARD (par exemple AGARD-AG-315). Des informations analogues, telles que le titre et la date de publication sont souhaitables. Veuillez noter qu'il y a lieu de spécifier AGARD-R-nnn et AGARD-AR-nnn lors de la commande des rapports AGARD et des rapports consultatifs AGARD respectivement. Des références bibliographiques complètes ainsi que des résumés des publications AGARD figurent dans les journaux suivants:

Scientific and Technical Aerospace Reports (STAR)
publié par la NASA Scientific and Technical
Information Division
NASA Headquarters (JTT)
Washington D.C. 20546
Etats-Unis

Government Reports Announcements and Index (GRA&I)
publié par le National Technical Information Service
Springfield
Virginia 22161
Etats-Unis
(accessible également en mode interactif dans la base de
données bibliographiques en ligne du NTIS, et sur CD-ROM)



AGARD holds limited quantities of the publications that accompanied Lecture Series and Special Courses held in 1993 or later, and of AGARDographs and Working Group reports published from 1993 onward. For details, write or send a telefax to the address given above. *Please do not telephone.*

AGARD does not hold stocks of publications that accompanied earlier Lecture Series or Courses or of any other publications. Initial distribution of all AGARD publications is made to NATO nations through the National Distribution Centres listed below. Further copies are sometimes available from these centres (except in the United States). If you have a need to receive all AGARD publications, or just those relating to one or more specific AGARD Panels, they may be willing to include you (or your organisation) on their distribution list. AGARD publications may be purchased from the Sales Agencies listed below, in photocopy or microfiche form.

NATIONAL DISTRIBUTION CENTRES

BELGIUM

Coordonnateur AGARD — VSL
Etat-major de la Force aérienne
Quartier Reine Elisabeth
Rue d'Evere, 1140 Bruxelles

CANADA

Director Scientific Information Services
Dept of National Defence
Ottawa, Ontario K1A 0K2

DENMARK

Danish Defence Research Establishment
Ryvangs Allé 1
P.O. Box 2715
DK-2100 Copenhagen Ø

FRANCE

O.N.E.R.A. (Direction)
29 Avenue de la Division Leclerc
92322 Châtillon Cedex

GERMANY

Fachinformationszentrum Karlsruhe
D-76344 Eggenstein-Leopoldshafen 2

GREECE

Hellenic Air Force
Air War College
Scientific and Technical Library
Dekelia Air Force Base
Dekelia, Athens TGA 1010

ICELAND

Director of Aviation
c/o Flugrad
Reykjavik

ITALY

Aeronautica Militare
Ufficio del Delegato Nazionale all'AGARD
Aeroporto Pratica di Mare
00040 Pomezia (Roma)

LUXEMBOURG

See Belgium

NETHERLANDS

Netherlands Delegation to AGARD
National Aerospace Laboratory, NLR
P.O. Box 90502
1006 BM Amsterdam

NORWAY

Norwegian Defence Research Establishment
Attn: Biblioteket
P.O. Box 25
N-2007 Kjeller

PORTUGAL

Força Aérea Portuguesa
Centro de Documentação e Informação
Alfragide
2700 Amadora

SPAIN

INTA (AGARD Publications)
Pintor Rosales 34
28008 Madrid

TURKEY

Millî Savunma Başkanlığı (MSB)
ARGE Dairesi Başkanlığı (MSB)
06650 Bakanlıklar-Ankara

UNITED KINGDOM

Defence Research Information Centre
Kentigern House
65 Brown Street
Glasgow G2 8EX

UNITED STATES

NASA Headquarters
Code JOB-1
Washington, D.C. 20546

The United States National Distribution Centre does NOT hold stocks of AGARD publications.

Applications for copies should be made direct to the NASA Center for AeroSpace Information (CASI) at the address below. Change of address requests should also go to CASI.

SALES AGENCIES

NASA Center for
AeroSpace Information (CASI)
800 Elkridge Landing Road
Linthicum Heights, MD 21090-2934
United States

ESA/Information Retrieval Service
European Space Agency
10, rue Mario Nikis
75015 Paris
France

The British Library
Document Supply Centre
Boston Spa, Wetherby
West Yorkshire LS23 7BQ
United Kingdom

Requests for microfiches or photocopies of AGARD documents (including requests to CASI) should include the word 'AGARD' and the AGARD serial number (for example AGARD-AG-315). Collateral information such as title and publication date is desirable. Note that AGARD Reports and Advisory Reports should be specified as AGARD-R-nnn and AGARD-AR-nnn, respectively. Full bibliographical references and abstracts of AGARD publications are given in the following journals:

Scientific and Technical Aerospace Reports (STAR)
published by NASA Scientific and Technical
Information Division
NASA Headquarters (JTT)
Washington D.C. 20546
United States

Government Reports Announcements and Index (GRA&I)
published by the National Technical Information Service
Springfield
Virginia 22161
United States
(also available online in the NTIS Bibliographic
Database or on CD-ROM)

